

NEW SCHEMES FOR PROCESSING ACCELEROGRAMS

A THESIS

submitted in fulfilment of the
requirements for the award of the degree
of
DOCTOR OF PHILOSOPHY
in
EARTHQUAKE ENGINEERING

By

ASHOK KUMAR



DEPARTMENT OF EARTHQUAKE ENGINEERING
UNIVERSITY OF ROORKEE
ROORKEE-247 667 (INDIA)

February, 1993



CANDIDATE'S DECLARATION

I hereby certify that the work which is being presented in the thesis entitled '*New Schemes for Processing Accelerograms*' in fulfilment of the requirement for the award of the Degree of Doctor of Philosophy and submitted in the Department of Earthquake Engineering of the University is an authentic record of my own work carried out during a period from February, 1990 to February, 1993 under the supervision of Dr. Brijesh Chandra, Professor, Department of Earthquake Engineering and Dr. Susanta Basu, Professor, Department of Earthquake Engineering.

The matter presented in this thesis has not been submitted by me for the award of any other degree of this or any other University.


15/2/93
(ASHOK KUMAR)

This is to certify that the above statement made by the candidate is correct to the best of our knowledge.

Date: 15.2.1993


(SUSANTA BASU)


(BRIJESH CHANDRA)

The Ph.D. Viva-Voce examination of Ashok Kumar, Research Scholar has been held on _____

Signature of Supervisors

Signature of H.O.D.

Signature of External Examiner

Abstract

Strong ground motion data is the primary input for earthquake response analysis and design of structures, equipments and other life line systems. The best description of strong earthquakes is provided by accelerographs which produce time history of the three orthogonal translational components of ground acceleration at the location where it is installed. It is, therefore, essential that the information is extracted as accurately as possible from accelerograph records (known as accelerograms) and this be interpreted carefully.

In work presented herein, studies have been carried out on various aspects of processing and interpretation of strong motion data including survey of literature available on the subject. The work done by different investigators is reviewed to understand the causes and characteristics of the noise and other transformations in the records. About a dozen schemes are discussed for correction of data obtained from accelerographs. Literature related to characteristics of digital accelerographs and correction schemes for their records is also reviewed. Based on this literature survey, gaps and shortcomings are identified in the prevailing practices of strong motion data processing. In the present work an attempt is made to fill these gaps and find solutions for some of these problems.

For RESA V which is an analog accelerograph developed in India, detailed noise characteristics have not been studied. This has been done through a study of straight line traces of RESA V for 10, 20 and 30 seconds duration, digitized by three different operators with each trace being digitized three times by each operator. Fourier transformation spectra and velocity response spectra for zero damping for all the 27 digitized records of noise are determined. A comparison with other standard analog accelerographs indicated that the level of noise present in records of RESA V is more, in low as well as high frequency ranges. This is attributed mainly due to the thickness of trace of RESA V which suggests that the optics of the instrument needs improvement. The average and standard deviation of maximum acceleration, velocity and displacement of noise history of RESA V has also been worked out.

The digitized uncorrected accelerograms which are usually available at unequal sample interval (nonuniform samples) are conventionally converted into data with constant time interval through linear interpolation. It is a well recognized that linear interpolation introduces frequencies from zero to infinity. In the digital data which is ought to be band limited, linear interpolation distorts the entire band upto Nyquist frequency due to effect of aliasing. In the work reported herein, a concept of stable sampling set is presented and guidelines are provided for operators who perform digitizations

on semi-automatic digitizers. Based on this study, some of the published uncorrected accelerograms are reviewed and limitations of these accelerograms in regard to highest frequency that can be retrieved from such data is pointed out. An iterative algorithm is discussed to recover band limited signal from nonuniform samples. Based on this algorithm, a scheme is developed for band limited interpolation of nonuniform samples of uncorrected accelerogram to obtain the same at a uniform interval of 200 samples per second. Deficiencies in linear interpolation are highlighted through comparison with different types of sequences obtained through band limited interpolation.

For several numerical compulsions, it often becomes necessary for the users of corrected accelerogram to reduce its time steps which are generally made available to them at equal intervals of 0.02 second. The prevailing practice, again, is to linearly interpolate the signal to get the desired sampling rate. However, as the original accelerogram is essentially a band limited signal, linear interpolation modifies the frequency contents of the data and introduces spurious high frequency components at the cost of reducing power in the low frequency range. This work highlights the inadequacy of linear interpolation of uniform samples and suggests the use of an interpolation technique by virtue of which the band limited property is maintained. To illustrate the usefulness of the scheme, simple structural systems are analysed using both conventional linear interpolation and with the aid of the proposed band limited interpolation technique.

With the above background work, a scheme for correction of records obtained from analog accelerograph is developed. The proposed scheme first performs band limited interpolation from nonuniform samples to obtain the uncorrected accelerogram at 200 samples per second. The process of decimation, instrument correction and band pass filtering is done in frequency domain and the scheme controls the frequency contents of the data during the processing. If the data is required at higher sampling rate then band limited interpolation is recommended. The integration to obtain velocity and displacement is also performed in frequency domain.

The proposed correction scheme is compared with three other correction schemes namely those of Lee and Trifunac [56], of Erdik and Kubin [32] and of Khemici and Chiang [50]. Response of different sections of the four processing schemes with white noise as input is first compared and then comparison of overall response of the schemes to white noise input is done. Advantages of the proposed processing technique is established by comparing it to the ideal case. Illustrative examples are taken by processing four uncorrected accelerograms of different earthquakes by all the four processing techniques and a comparison in a tabular form is presented.

Although it is established that the noise content in the data recorded from digital accelerographs is far less than the analog accelerographs yet the record of digital accelerograph does get transformed at various stages and in the process noise does creep in which suggests that it is essential to understand these transformations and noise so that true signal can be retrieved. In this work transformations of the signal which take place in the accelerometer and anti aliasing filter are studied and their solution presented.

In addition to above transformations, the system continuously records instrumental or environmental noise. This pre event portion of the record of digital accelerograph represents the characteristics of this noise which is modelled as coloured noise. An adaptive filter is then developed to cancel noise from the recorded event.

In the end of the thesis, conclusions of the various aspects of the studies are summarized.

Acknowledgements

This thesis is the outcome of more than three years of my research efforts. I am deeply indebted to many people for professional, intellectually stimulating and enjoyable research and educational experience gained by me during this period.

I would like to express my deep gratitude to my thesis guides Professor Brijesh Chandra and Professor Susanta Basu, for their continued support over the last several years due to which this work could take this shape. Their wide research experience and foresight was a major guiding force in my professional development. But more than that it is their personal warmth and concern for my work which has made our relationship so very valuable to me.

I am unable to pick the right words to thank Professor S. Basu for the work culture enthused by him amongst his co-workers. His great motivation for the work has always been a guiding spirit for me and I am proud of being a member of a truly professional shake table team led by him. It is in this professional and research oriented atmosphere that I did all the work presented in this thesis.

Graphics software and FFT subroutines developed by Professor Basu and made available to all the users of HP9000 system were widely used in this work which is thankfully acknowledged.

I am thankful to my colleague Dr. Pankaj who played very important role by patiently listening to me on my work and providing useful suggestions on several occasions. He went through my manuscript with great care and provided the required help to me when I needed it most.

I am thankful to the Head, Department of Earthquake Engineering for providing me all the necessary facilities during the course of this work.

I must express my gratitude to Prof. D.K. Mehra of Department of Electronics and Computer Engineering, who provided me important references on digital signal processing and has given useful suggestions during the course of this work.

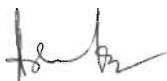
I am grateful to Prof. V.K. Verma of Department of Electrical Engineering whose deep knowledge on microprocessors was the key to the development of digital accelerograph. Thanks are due to Mr. A.D. Pandey, Mr. M.K. Bansal and Mr. N.C. Gupta of my department for their contributions in the development of digital accelerograph.

I am also thankful to Mr. M.K. Bansal, Mr. K.K. Lawania, Mr. Babu Ram, Mr. Ramesh Chand, Mr. Prem Chand and Mr. Satish Kumar, the members of the shake table team, who were ever ready to help me in my work.

I am also thankful to Mr. S.C. Sharma, Mr. Laxman Singh, Mr. Jagdish Prasad and Mr. Chabil Das for help in finalizing the figures of this thesis.

Last but not the least I am thankful to my wife Renu, daughter Niha and son Nitesh whose support and encouragement gave me the necessary strength to complete this work.

I dedicate this thesis to my mother Mrs. Dhanwanti Mathur who is a constant source of inspiration to me.



(Ashok Kumar)

Department of Earthquake Engineering,
University of Roorkee,
ROORKEE-247 667.

Date: February 15 , 1993.

Contents

Candidate's declaration	i
Abstract	iii
Acknowledgement	vii
1 Introduction	1
1.1 Noise characteristics of RESA V	2
1.2 Band limited interpolation	2
1.3 Band limited interpolation of uniformly spaced samples	3
1.4 Suggested correction scheme for analog records	4
1.5 Comparison of proposed and other schemes	4
1.6 Problems of analog accelerograph and specification of an ideal accelerograph	5
1.7 Development of a digital accelerograph	5
1.8 Processing of records of digital accelerograph	5
2 Literature review	7
2.1 Noise in analog accelerograph	7
2.2 Correction of records of analog accelerograph	8
2.3 Digital accelerographs and their characteristics	12
2.4 Identified gaps in the literature	14
3 Noise characteristics of RESA V	17
3.1 Brief description of RESA V	17
3.2 Why noise characteristics ?	18
3.3 Classification of noise	19
3.4 Methodology	19
3.5 Discussion on results	22

4	Band limited interpolation of nonuniform samples	27
4.1	Digitization of analog records and stable sampling set	28
4.2	Method of interpolation	29
4.2.1	The <i>S</i> Operator	30
4.2.2	The <i>P</i> Operator	30
4.2.3	Iteration	32
4.3	Examples on recovery of sine waves	34
4.3.1	With Stable Sample Set	34
4.3.2	With Random Sample Set	39
4.4	Examples on recovery of earthquake data	44
4.5	Effect of convergence constant λ on recovery of earthquake data	52
4.6	Discussion on interpolation of nonuniform samples	52
5	Band limited interpolation of uniform samples	55
5.1	The need to interpolate	56
5.2	Interpolation schemes	57
5.2.1	Linear Interpolation	57
5.2.2	Band Limited Interpolation	59
5.3	Details of band limited interpolation	62
5.4	Illustrative examples on interpolation	63
5.4.1	Sine Waves	63
5.4.2	Earthquake accelerograms	66
5.5	Effect of interpolation on SDF systems	68
5.5.1	Sinusoidal excitation	68
5.5.2	Parkfield Earthquake	69
6	Proposed correction scheme for records of analog accelerograph	71
6.1	The uncorrected accelerogram	73
6.2	Recovery of signal from nonuniform samples	75
6.3	Decimation	75

6.4	Instrument correction	76
6.4.1	Response to White Noise	78
6.5	Bandpass filter	80
6.6	Band limited interpolation to increase sampling rate	81
6.7	Integration for velocity and displacement	83
6.8	The computer program	84
7	Comparison of proposed scheme with other schemes	86
7.1	Scheme of Trifunac and Lee	87
7.2	Scheme of Erdik and Kubin	89
7.3	Scheme of Khemici and Chiang	92
7.4	Comparative study of schemes to white noise	93
7.5	Comparative study of schemes to earthquake signal	95
7.5.1	Comparison of Maximum Motion	98
7.5.2	Comparison in Frequency Domain	98
7.5.3	Comparison of Response Spectra	105
8	Problems of analog accelerograph & an ideal accelerograph	108
8.1	Design, operation & maintenance	108
8.2	Development & digitization of records of analog accelerograph	110
8.3	Processing of accelerograms	111
8.4	An ideal accelerograph	112
8.4.1	Range of Recording	112
8.4.2	Sensor	113
8.4.3	Other Specifications	116
9	Details of a digital accelerograph	118
9.1	Transducer	120
9.2	Signal conditioner	121
9.2.1	Design of Antialiasing Filter	121

9.3	Digital recorder	123
9.3.1	Brief Description of Hardware	123
9.3.2	Digital Accelerograph Software	128
9.4	Post processing	129
10	Correction of data recorded from digital accelerographs	136
10.1	Transformations and noise in digital accelerographs	136
10.2	Analysis of noise and algorithm for noise cancellation	138
10.2.1	Noise analysis	139
10.2.2	Model of pre-event data	142
10.2.3	Time domain analysis of adaptive filter	145
10.2.4	Adaptive algorithm	149
10.2.5	Noise cancellation using adaptive algorithm	153
10.3	Low pass filter for phase correction	159
11	Conclusions	169
	Bibliography	174

Chapter 1

Introduction

For aseismic design of engineering structures, understanding the nature of earthquake ground motion and the resulting response of the structures is of prime importance. This can only be achieved by actually measuring the ground motion and computing the response of structures during a strong earthquake. The best description of strong earthquakes is provided by accelerographs which give time history of three orthogonal translational components of acceleration at the location where it is installed. It is, therefore, essential that information be extracted as accurately as possible from accelerograph records (known as accelerograms) and this be interpreted carefully.

There are two different types of accelerographs that are currently in use. The first type is the conventional analog accelerograph which produces record of acceleration history as an analog trace generally, on a photographic paper or film. Such analog accelerographs however miss some of the initial portion of the earthquake record due to the triggering mechanism. The second type of instruments are digital accelerographs which use digital technology and the records are obtained on solid state memory chips in a digital form at a prescribed sampling rate. This category of accelerographs have a pre-event memory which enable recording the motion from beginning of the earthquake and in most cases even few seconds before the start of the earthquake.

Unfortunately, during the recording, digitization and processing of records, signal gets transformed and noise creeps into the signal in case of both analog and digital accelerographs. This transformation of signal and introduction of noise, significantly affects the reliability of high and low frequency components. Considerable research has been directed towards understanding and analysing this problem so that the best possible information could be obtained from such records. Since analog accelerographs have been in use for last few decades, most of the published work relates to interpretation

of records of analog accelerographs. Digital accelerograph being a recent development, only few publications are available relevant to processing of its record. A detailed literature survey on the subject is dealt with in Chapter II of the present thesis.

The work presented herein tries to fill up the gaps in the available knowhow with regard to processing of records of analog accelerographs and suggests a correction scheme in frequency domain. With regard to processing of data obtained from digital accelerographs, studies were performed on one such instrument developed under a project of which the author was the Principal Investigator. Based on these studies a correction scheme is proposed for processing records of digital accelerographs also. The efficacy of developed correction schemes is checked through shake table tests on the accelerographs developed at the Department of Earthquake Engineering, University of Roorkee.

A brief description of the contents of each chapter is discussed in the following sections.

1.1 Noise characteristics of RESA V

RESA V is the analog accelerograph which has been developed in India and about 100 of these are installed all over the country. This instrument has been giving useful strong motion data and several of them triggered in North-East India earthquake of August 1988, Bihar-Nepal earthquake of August 1988 and the Garhwal earthquake of October 1991. Till now no systematic studies about noise characteristics of this instrument had been done. As a part of the present work a systematic determination of noise characteristics is done almost on the same lines as was done by Trifunac [91] for SMA 1. In this study, in addition to pseudo spectral velocity spectra of the noise, Fourier spectra of noise is also studied. This study gave an indication of cut off frequency particularly for low frequency removal, for the earthquake records obtained from RESA V and an estimate of errors in acceleration and derived velocity and displacement histories.

1.2 Band limited interpolation

The analog traces of accelerographs recorded during the past earthquakes were mostly digitized on semi automatic type digitizers. It is, therefore, obvious that such data can

not be obtained at constant time interval and hence are called nonuniform samples. All presently available methods of processing strong motion data convert these nonuniform samples into data at constant time interval through linear interpolation. It is a well known fact that linear interpolation introduces frequencies from zero to infinity. In the digital data which is ought to be band limited this method will distort the entire band upto Nyquist frequency due to effect of aliasing. Another question of interest is as what should be the maximum interval which should not be exceeded during digitization so that mathematically sound information can be obtained in a desired band.

Based on the method suggested by Marvasti *et al.* [60] an iterative procedure is used to recover band limited signal from nonuniform samples as are commonly obtained from semi-automatic digitizers. Several combinations of nonuniformly sampled sine waves are recovered through proposed scheme and compared with linearly interpolated as well as exact signal to establish the superiority of the band limited interpolation over linear interpolation. The comparison is done in time domain as well as in frequency domain for this purpose. This procedure is then used to recover nonuniformly sampled uncorrected accelerograms and the results are compared with linearly interpolated data. Based on this study, some of the nonuniformly sampled uncorrected accelerograms which are frequently used for analysis are reviewed and their shortcomings presented.

This work of Marvasti *et al.* [60] has also given definition of stable sampling set for nonuniform samples and this definition is used to determine the maximum interval which should not be exceeded while digitizing an accelerogram so that a desired band limited data could be obtained.

1.3 Band limited interpolation of uniformly spaced samples

Interpolation of uniformly spaced data to reduce the sampling interval is frequently required due to several numerical compulsions during processing of data or during use of the data for analysis. In this study a method for band limited interpolation is presented in which frequency contents of the data do not change after the interpolation. To achieve this, the data is first packed with required number of zeros in between samples and then low pass filtered with cut off frequency as Nyquist frequency of uninterpolated data. Again a comparison through Fourier spectra is made for data obtained from linear and band limited interpolation techniques. A comparison is also done on the effect

of response of single degree of freedom system to band limited sequence and linearly interpolated sequence.

1.4 Suggested correction scheme for analog records

The effectiveness, simplicity and popularity of fast Fourier transformation algorithm make frequency domain data processing simpler, easy to understand and perhaps more accurate than its time domain counterpart. Therefore, a data processing scheme in frequency domain is proposed. The scheme consists of an iterative band limited interpolation of nonuniform samples to obtain data at 200 samples per second (*SPS*). A band limited decimation is done to reduce the sampling rate to 100 *SPS*. A transfer function based on $|H(jw)|^2$ of Butterworth filter and single degree of freedom system for instrument correction is used for processing in frequency domain. Velocity and displacement sequence is also obtained through frequency domain integration. A band limited interpolation is performed to increase the sampling rate of the corrected accelerogram to 200 *SPS*. The performance of the correction scheme is studied by determining response of different sections of the scheme as well as overall scheme for white noise input.

1.5 Comparison of proposed and other schemes

Although, large number of correction procedures for obtaining corrected accelerograms have been developed but correction schemes of Trifunac and Lee jointly and independently [56,88,89,92,93,95] Erdik and Kubin [32] and Khemici and Chiang [50] have been selected for assessment and comparison. The first two of the above schemes are in time domain whereas third is in frequency domain. Computer programs are developed for correction of accelerogram for these schemes. Firstly, assessment of these schemes is done by determining performance of each step of schemes as well as overall performance for white noise input. A comparative study is then done for these schemes with the proposed scheme for white noise input. The advantages of the proposed scheme is then established through this comparison by demonstrating the perfect band limited performance of the proposed scheme with that of jittery response of other schemes. Few uncorrected accelerograms are then corrected by all the four schemes and a frequency domain comparison of corrected accelerogram as well as response spectra is obtained and presented. Peak acceleration, velocity, displacement and the time of their occurrence are determined through the four schemes are also compared for these accelerograms.

1.6 Problems of analog accelerograph and specification of an ideal accelerograph

This part of the work discusses in detail, various aspects of analog accelerographs including its operation, maintenance, data retrieval and data processing and problems associated with each of these aspects are presented. Various limitations of processing methods for correcting accelerograms recorded from analog accelerographs are elaborated. In view of these discussions a set of specifications of an ideal accelerograph are discussed.

1.7 Development of a digital accelerograph

This chapter presents details of a microprocessor based digital accelerograph [53,111] developed under a separate research scheme of which the author of this thesis was the Principal Investigator. This instrument uses a force balance accelerometer (FBA) and a variable amplification signal conditioner with four pole Butterworth anti-aliasing filter. This digital accelerograph has an INTEL 8085 CMOS microprocessor and a 12 bit analog to digital converter (ADC). It has 512 KByte RAM which is sufficient to have a record of about 15 minutes at 100 *SPS*. Various parameters like sampling rate, pre-event time, post-event time, trigger threshold and end of event threshold are menu selectable. Data retrieval is done on an IBM compatible PC through a serial port. The communication between PC and digital accelerograph is done through a commercially available software. Two files are retrieved from digital accelerograph to PC. The first file named as the flag file has important information about the event to be processed, like trigger time, addresses of some important memory locations etc. and the second contains the data. An interactive software is developed in FORTRAN which reads the acquired files and give an output for the three components of time histories of recorded acceleration. The description of the instrument, its system software and hardware as well as post processing software is presented.

1.8 Processing of records of digital accelerograph

The noise characteristics of the indigenously developed digital accelerograph is determined by analysing the initial portion of the pre event record before the start of the

earthquake. This part of the record represents characteristics of the noise present in the earthquake record. It is shown in this work that the noise of the pre event can be modelled as coloured noise. An adaptive filter is then developed to cancel noise from the recorded event. This type of adaptive filter algorithm is realizable and can be used for future inclusion in the hardware through DSP chips.

Digital accelerographs generally use FBAs as transducers. This digital accelerograph uses a Columbia make SA-327TX FBA. Such accelerometers have been studied in detail by Amini and Trifunac [4,5] who have deduced its transfer function. The same is used in performing the instrument correction. The signal of the digital accelerographs gets transformed while getting through anti-aliasing filter. In the digital accelerograph which was studied, a four pole Butterworth filter is used as anti-aliasing filter. The transfer functions of these filters are well known [54] and the same is used to get rid of nonlinear phase shift introduced by the anti aliasing filter and to get the corrected accelerogram.

Chapter 2

Literature review

2.1 Noise in analog accelerograph

In analog accelerographs, it is essential that the trace of the record be converted into a digital form before it can be put to any effective use in seismic analysis. In the process of recording and digitization, the original ground signal is distorted with noise and undergoes several transformations. It is important that these noise and transformations are understood and identified in order to derive the true ground motion from the digitized record. Trifunac *et al.* [97] presented a comprehensive list of causes of transformations and noise in the recording and digitization of records from analog accelerographs. They discussed the effect of higher modes and cross-axis sensitivity in transduction error and concluded that the effect of cross-axis sensitivity of accelerometers was negligible and for the usually adopted rate of sampling (about 25 to 30 samples per second) the effect of higher modes was negligible and the transducer could be considered to be a single degree of freedom spring-mass-dashpot system. They also discussed and analysed errors caused by the transversal play of recording paper, nonuniform speed of film and/or inaccurate time mark, misalignment of three transducers, errors due to clipping of large signals, variable trace thickness, warping of film negatives and other errors. They also analysed in detail, the digitization errors which is an important source of low as well as high frequency noise.

To determine signal to noise ratio of corrected accelerograms which were processed earlier, Trifunac [91] examined 13 straight line traces for which the digitization was done by seven different persons. He found acceleration, velocity and displacement history of noise for each of these records and conducted a statistical analysis. A pseudo spectral velocity (PSV) spectra of identified noise and PSV spectra of accelerogram

were used to estimate signal to noise ratio for different periods. PSV spectra of large number of corrected accelerograms and noise were studied and it was concluded that the earthquake PSV spectra tends towards a slope of -1 at higher period end whereas PSV spectra of noise are mostly pink noise *ie.* spectral velocity of noise increases with the increase in periods. He used this property of signal and noise to appropriately select lower cutoff frequencies for the purpose of correction.

Shakal and Ragsdale [80] conducted a series of tests to establish the level and characteristics of processing noise associated with a scanning digitizer used in the California Strong Motion Instrumentation Program. An average PSV spectra of noise for 20% damping was determined by digitizing eight straight line records of 60 seconds length. This was compared with the noise spectra determined by Lee and Trifunac [56] and the noise spectra for manual digitization as determined by Trifunac [91]. They indicated that noise spectra for manual digitization was not strictly comparable as it was done using a single straight line. Stating the importance of these noise spectra it was concluded that if any part of strong motion spectrum is low enough so as to approach the noise spectrum, the indication is that the true signal, if present, is not recoverable. The noise time history was processed in the usual manner and velocity and displacement histories of noise were obtained. The processing was done with a number of lower cutoff frequencies and maximum uncertainties in velocity and displacement for each case obtained. As can be expected for smaller cutoff frequency the uncertainties were larger.

Iai [45] classified different types of noise that can be present in an analog accelerograph. He presented a table containing sources of the noise in SMAC-B2 accelerographs.

2.2 Correction of records of analog accelerograph

Basili and Brady [6] gave in a tabular form the value of low cutoff frequency that should be used in bandpass filtering. Their conclusions were based on the study of low frequency contents in San Fernando Earthquake records analysed by Hanks [36,37].

Trifunac and Lee jointly and independently [56,88,89,91,92,93,95] presented a series of papers and reports in which a correction scheme to process the records obtained from accelerographs were discussed. This scheme was used as standard strong motion data processing scheme during the seventies. In this scheme the unequally sampled digitized data is first converted into time *vs.* acceleration values by using time mark traces and tilt calibration of accelerometers. These values were linearly interpolated

to get acceleration values at a uniform sampling period of 0.005 seconds. The scheme used a FIR (non recursive) Ormsby filter [72] which was applied in the time domain to remove the undesired frequencies. For low pass filtering, the scheme used accelerogram with a sampling period of 0.005 sec whereas for highpass filtering the accelerogram was decimated to a sampling period of 0.2 sec. A cutoff frequency of 25 Hz with a roll off of 2 Hz for low pass filtering and a cutoff frequency of 0.07 Hz with a roll off of 0.02 Hz for high pass filtering were used. Prior to high pass filtering, the scheme passed the signal through a lowpass rectangular window. Instrument correction was performed by solving the equation of motion of a single degree of freedom (SDF) spring mass dashpot system using second order central difference approximation with a sampling period of 0.02 seconds.

Shyam Sunder and Connors [81,82] demonstrated the shortcomings of the scheme developed by Trifunac and Lee and suggested a new processing technique. They showed that for the instrument correction, the second order central difference approximation with a sampling period of 0.02 seconds has a transfer function which differs considerably from the exact frequency response of SDF systems at frequencies more than 5 Hz . They also showed that decimation done to reduce the computation effort, introduces marked distortion in the processed signal due to aliasing and that an undecimated signal using an Ormsby filter will require enormous amount of computational effort for high pass filtering. It was concluded that transients that legitimately arise from the filtering process should not be ignored. They also stated that it should not be necessary to filter the ground velocities and displacements as done by Trifunac and Lee. Shyam Sunder and Connors suggested a new processing scheme. The scheme used a method presented by Rabiner et al. [77] for designing an optimal finite impulse response differentiator for instrument correction. An odd length differentiator was used to avoid introducing half sample delay. The instrument correction filter was implemented as a cascade parallel combinations of differentiators. For band pass filtering they used an IIR (recursive) elliptic filter with a filter order of 10. They proposed use of an elliptic filter as these are optimal in the sense that for a given order and ripple specifications in both the pass and stop bands, no other filter achieves a faster transition between the pass and stop bands. They also used 0.07 Hz as lower cutoff frequency and 25 Hz as upper cutoff frequency for filtering. For designing digital filters they used the computer program of Gray and Markel [35]. The integration method of Schuessler and Ibler [79] for getting velocity and displacement signal was used. Zero initial conditions of velocity and displacements were assumed to apply at the beginning of a sequence lengthened band pass filtered signal.

Lee [55] in a rejoinder to the work of Shyam Sunder and Connors, defended the use of Ormsby filter instead of elliptic filter. It was argued that elliptic filters have nonlinear phase and in earthquake engineering nonlinear phase distortion in the processed signal cannot be accepted. To avoid phase distortion, the signal will have to be filtered again with reverse time. The optimality of the resulting filter is thus lost. Whereas in case of Ormsby filter the filter weights are symmetric about $t = 0$ and, therefore, the filter performs with perfect phase distortionless transmissions. In this regard he concluded that the comparison of performance of Ormsby and elliptic filters is the same as comparing two general type of filters: recursive *vs.* non-recursive. Lee also discussed superiority of Ormsby filter over elliptic filter in terms of smaller transient response. With regard to instrument correction using central difference, he conceded that using a sampling period of 0.02 seconds will be inaccurate. He, however, suggested that in view of automatic sampling of data done at 200 samples per seconds and automatic determination of cutoff frequencies for bandpass filtering there is a need to have an algorithm which should be accurate upto the cutoff frequency for lowpass filter. He suggested using a higher order central difference type formula with coefficients determined through Chebyshev minimax criterion. He strongly criticised the use of Schussler-Ibler formulae for integration for obtaining velocity and displacement because they give phase distorted output which is not acceptable in earthquake engineering. As in the case of differentiation he proposed the use of integration filter that is accurate upto the cutoff frequency of a low pass filter obtained by using the Chebyshev minimax criterion.

Erdik and Kubin [32] modified the processing method of Trifunac and Lee. They used Ormsby filter as low pass filter and performed the instrument correction at a sampling period of 0.005 sec. The instrument corrected data was least square fitted with a straight line and was integrated with zero initial velocity to get the velocity trace. This velocity trace was then high pass filtered. They determined the low frequency limit for high pass filtering by using the near field Fourier amplitude spectrum of the ground motion as proposed by Brune [20]. They used Butterworth type recursive filter for high pass filtering and argued that such filters do not incorporate Gibbs phenomena near the cutoff frequencies as exist in the Ormsby type FIR filters. As Butterworth filters have nonlinear phase spectra, input data was first filtered in a normal manner, then it was reversed in time and filtered again and this output reversed in time gave high pass filtered data with no phase distortion. This high pass filtered velocity was then fitted with a least square line and was integrated to get the displacement. A straight line was again least square fitted on the displacement trace to get the corrected displacement. The slope of the least square fitted straight line of the displacement trace was added

to the velocity to get the corrected velocity data. The velocity history so obtained was then differentiated to get the acceleration. This again went through a low pass Ormsby filter to remove the aliasing effect and this was called as the corrected accelerogram. Erdik and Kubin also found effect of the cutoff frequency for low pass filter on the displacement trace and also the effect of the cutoff frequency of the low pass filter on the acceleration response spectra.

Khemici and Chiang [50] suggested a frequency domain equivalent of scheme proposed by Trifunac and Lee (also called as the Caltech scheme). They determined the transfer function of the Caltech scheme by determining its response in the time domain for a time history which has only one impulse of any magnitude. They found discrete Fourier transform (DFT) of the response which when divided by DFT of input impulse yielded the transfer function of the Caltech scheme. This transfer function when multiplied by DFT of input signal yielded DFT of corrected accelerogram which by inverse Fourier transformation produced the corrected accelerogram. They argued that introduction of FFT algorithms has made convolution in the frequency domain much faster than the time domain convolution. A scheme called the Stanford scheme [50] was proposed whose transfer function incorporated instrument correction and band pass filter with transition band tapered with half cosine wave on each side. The values of the rolloff and cutoff frequencies as used in the Caltech scheme were maintained. The integration of accelerogram to obtain velocity and displacement was also done in frequency domain. The authors compared the results of the Stanford scheme with the time and frequency domain results of the Caltech scheme by applying them on four different earthquake records. The peak acceleration, velocity and displacement and the time of their occurrence was compared and the match was found to be fairly good.

Allessandrini *et al.* [3] proposed a methodology which was based on the exact deconvolution method. They felt that their method did not contaminate the impulsive shape of the initial ground displacement and provided an objective displacement time history. The proposed method was in time domain and directly yielded the ground displacements after instrument deconvolution. Corrected velocity and accelerations were then obtained by numerical differentiations.

Several papers were presented in the Workshop on Processing of records of strong motion instruments held in Tokyo, Japan in August, 1988 [109]. The organisers provided five uncorrected digitized accelerograms numbered 1 to 5 to the participants. The participants in turn processed these accelerograms and presented their results along with the details of their schemes. Some of the presentations of the workshop are discussed below.

Ohta [68] analysed File no. 5 of the distributed uncorrected accelerogram. He informed that velocity as well as displacement time history was also recorded at the same site. He compared the Fourier spectra of the original velocity record $V(\omega)$ with the Fourier spectra of velocity derived from Fourier spectra of recorded acceleration $F_a(\omega)$ and Fourier spectra of recorded displacement $F_d(\omega)$. Noise and cutoff frequencies were recognized for $V(\omega)$ and $F_d(\omega)$ on the short period side and for $F_a(\omega)$ on the long period side from the above comparison. He then corrected the acceleration, velocity and displacement history using characteristics of respective transducer. This was the first time that this type of field recording had been reported.

Iai *et al.* [47] used two frequency domain methods for processing and analysed only those records which had a peak acceleration greater than 50 gals. Their first method employed a lower cutoff frequency of 0.154 Hz while the second method required information on the level of noise contained in the accelerogram. Fourier spectra of instrument corrected accelerogram was smoothened and the lower cutoff frequency was selected accordingly.

Katukura *et al.* [49] processed the accelerogram after DC elimination by dividing it in three parts. For each part they calculated displacement in frequency domain, after selecting a proper cutoff frequency based on the information on the meaningless displacements under the law of causality.

Omote *et al.* [70] found pseudo-velocity spectra of the record and then assuming noise to be inversely proportional to the frequency (pink noise), estimated the lower cutoff frequency for the band pass filter.

Toki and Sawada [85] also assumed that all records contain pink noise. They used $1/f$ filter to remove this noise. However, to determine the filter level they used an iterative method by comparing the Fourier spectra of two accelerograms recorded from similar accelerographs installed nearby.

2.3 Digital accelerographs and their characteristics

The advancement of technology and requirement of getting record with pre-event memory and higher signal to noise ratio led to development of digital accelerographs.

Force balance accelerometers (FBA) were mostly used as transducers in digital accelerographs. Amini and Trifunac [4,5] derived equation of motion of FBA and

analysed its various segments. They found transfer function of each of the segment as well as overall transfer function of FBA. They derived value of natural frequency and damping of FBA and showed that natural frequency and damping in FBA are almost completely controlled by values of electronic components and therefore can be accurately adjusted unlike in conventional accelerometers where natural frequency and damping are dependent on mechanical properties like spring stiffness, viscosity of oil etc.

Iwan *et al.* [48] studied characteristics of a digital accelerograph in laboratory as well as in the field. They performed a noise test on a 20 second record which was obtained by operating the instrument in a quiet environment. This record was analysed to evaluate the pseudo-velocity response spectra. This was compared with that of noise of hand digitized and optically digitized analog records. This study showed that spectral displacement due to noise of the order of 0.02 inches for a period of 10 second was present in digital accelerograph whereas it was of the order of 2 inches for analog accelerographs. To test the accuracy of derived velocity and displacements from the recorded accelerations, laboratory tests were performed on digital accelerographs by applying known displacements. The results were reported to be quite accurate. During these tests authors found some anomalies of shift of zero acceleration output in FBA particularly after it was subjected to larger acceleration values. Authors also presented a comparative study of analog and digital accelerographs from the record obtained from after shock of Coalinga Earthquake of May, 1983. The records of analog accelerographs were bandpass filtered with a low frequency cut off of 0.2 to 0.4 *Hz* and high frequency cutoff of 23 to 25 *Hz*. They reported that in general there was a rather close agreement between the results of response spectra and Fourier spectra obtained from analog and digital accelerographs and the greatest difference was, as expected in the displacement.

Diehl [28] discussed about standard requirements of analog and digital accelerographs. He discussed comparative performance of analog accelerographs, digital accelerographs with magnetic tape recording and digital accelerographs with solid state recording.

Okada *et al.* [69] suggested an algorithm based on which they evaluated the recording performance of accelerographs. They presented in a tabular form the relationship between accelerograph specifications and noise controlling factors.

Hudson [43] presented a brief history, current status and future prospects of strong motion instruments and data processing. He discussed, in brief, the advantages of using digital accelerographs.

Brady [19] discussed advantages of digital accelerographs along with their capabilities that affect processing of recorded data. He stated that the presence of pre-event helps in accurate placement of the zero line for acceleration, velocity and displacement time histories. This may lead to a situation where long period contents may not be required to be removed and the acceleration record on integration may permit accurate displacement including value of final displacement offset. He discussed in detail other capabilities of digital accelerograph like fast data recovery, ease in placement of transducers at different locations in a building and recording on a common time base, accurate sampling rate, high resolution and dynamic range, choice of triggering algorithm etc. Some problems in digital accelerographs with magnetic tape recording were also mentioned. With regard to the processing of record obtained from digital accelerograph he discussed about the cutoff frequency of anti-aliasing analog filter which should be less than Nyquist frequency (half of sampling frequency) and stated that it could vary from 25 to 300 Hz depending on recording sampling rate. With regard to high frequency noise removal he argued that if high frequency motion of earthquake is to be studied accurately then at least eight samples per cycle would be necessary and thus 25 Hz frequency requires 200 SPS. The sampling rate should, therefore, be the consideration in selection of cutoff frequency for high frequency removal. He stated that instrument correction will be similar to that of an analog accelerograph if FBA is a SDF second order oscillator. Otherwise, manufacturer's description of the instrument should govern the correction required. Further, in order to obtain the final displacement, low frequency noise removal should be avoided. However, Brady discussed several criteria, on the basis of which the cutoff frequency for low frequency noise removal could be selected, in case final displacement offset was not required.

2.4 Identified gaps in the literature

RESA V is an analog accelerograph developed in India which has not been studied in detail in regard to its noise characteristics. The instrument has optics which is certainly inferior to American accelerographs causing thicker trace. This instrument has started giving several strong motion records for the last few years. It is, therefore, essential that the noise characteristics of this instrument are studied in detail so that the records obtained from it can be interpreted with greater confidence.

In the entire literature available for processing of accelerograms, linear interpolation is invariably used every where. From the raw nonuniformly sampled uncorrected

accelerograms, the uniformly sampled uncorrected accelerograms are recovered consistently by every author through linear interpolation. Similarly, for increasing the sampling rate of a given uniformly sampled accelerogram (generally corrected) linear interpolation is commonly used. It is well known fact that linear interpolation introduces frequencies from zero to infinity and digital data which is always band limited (information is available only upto Nyquist frequency) is bound to be corrupted due to aliasing. This effect has not been studied so far and as such no attempts have been made to interpolate the data so as to preserve its frequency contents after the interpolation.

Similarly, during the processing of records, decimation is required to be performed to reduce the sampling rate. The decimation is commonly done by dropping samples. For example if a sequence is defined at 200 *SPS* which is required to be decimated to 50 *SPS* then first, fifth, ninth, thirteenth etc. samples are taken as signal and the remaining samples are dropped. The effect of such decimation again will be to change the frequency content of the original data. Thus there is a need to perform the decimation also in such a way as to maintain the frequency content of the original data.

The performance of different correction schemes have been studied and compared in the literature by comparing peak values of motion and its instant of the corrected accelerograms. With such comparisons it is not possible to really understand the details of the transformations which are taking place in the processing schemes. Khemici and Chiang [50] have suggested to study the performance of Trifunac's scheme by finding response of the scheme for a sequence which has all zeros except a single unity at the initial portion of the sequence. This yielded the unit impulse response function or the ideal transfer function of the whole scheme. However, such determination of transfer function eliminates the computational errors as most of the computations are performed with zeros and thus does not indicate the true performance of a scheme. Perhaps the right approach to assess the performance of a scheme is to find the response of the scheme for a white noise input. Such assessments of performance of the schemes have not been reported in the literature.

The available literature on processing of records of digital accelerographs is scanty. In fact the presently available literature does not differentiate much between the records of analog and digital accelerographs as far as processing is concerned. No attempts have been made to use the pre event part of the digital accelerograph to be used to determine the exact noise characteristics of the noise present in the record. With this background an adaptive filter can be designed to perform the noise cancellation and to obtain noise free record. Such type of algorithms are quite commonly used in speech and image processing. Similarly in digital accelerographs, anti aliasing filter results

into nonlinear phase shift of the record. As the transfer function of anti aliasing filter is known, the same can be used to design a digital filter so as to neutralize this phase shift.

Chapter 3

Noise characteristics of RESA V

There are several thousand analog accelerographs installed all over the world for recording strong ground motion. One of the most popular analog accelerograph is SMA 1 manufactured by Kinematics. SMA 1 has been studied in detail by several authors who have determined its characteristics including noise characteristics. In India, RESA V accelerographs developed at the Department of Earthquake Engineering, University of Roorkee have been installed at more than 100 sites (Chandra and Kumar [23]). However, as mentioned in Chapter 2, a detailed study of the noise characteristics of RESA V had not been done conducted. This chapter is devoted to the study of the noise characteristics of RESA V.

3.1 Brief description of RESA V

The working principle of RESA V is similar to other commonly used analog accelerographs like SMA 1. This instrument has mechanical starting pendulums of natural period of about 0.8 second and damping of around 30% of critical. The instrument is triggered when any one of these pendulums makes contact with a contact screw. The gap between pendulums and contact screws is so adjusted as to get contact at approximately 30 gals. The three accelerometers of RESA V use torsional pendulums and have a natural frequency ranging from 22 to 25 Hz and a damping of around 60% to 65% of critical. Each accelerometer pendulum has a concave mirror fixed to it which reflects the image of filament of the light source as a sharp spot on the moving photographic paper with the help of suitable optics. The deflections of the mirror of pendulums are amplified using an optical lever and have a sensitivity of about 30 mm for unit acceleration due to gravity (g). The record of the instrument is obtained on 22.5 cm

wide photographic paper which moves inside the camera at a speed of 2 *cm/sec*. The time mark of the instrument provides quarter second OFF and quarter ON spots on the moving photographic paper. The instrument operates for about 10 *seconds* after the last contact of any one of the triggering pendulum. The instrument is controlled electronically and the entire circuit is in a 14*cm*×9*cm* PCB which is mounted on a control panel. This instrument has given useful strong motion data in recent past and several of them triggered in North-East India earthquake of August 1988, Bihar-Nepal earthquake of August 1988 and the Garhwal Earthquake of October 1991.

3.2 Why noise characteristics ?

It is well known that during recording and digitization of records of analog accelerographs like RESA V, noise creeps in due to a number of reasons (Trifunac et al. [97]). Three specific reasons that necessitate detailed analysis of noise are as follows:

1. Choice of frequency band for the processing of the record which should ideally be noise free and in actual practice with an acceptable signal to noise ratio. This implies that for an acceptable signal to noise ratio, suitable cutoff frequencies of the band pass filter for processing the record can be estimated by comparing the noise characteristics with that of characteristics of the uncorrected accelerogram.
2. Estimation of the level of error in time domain which is present in the corrected accelerogram. This is done to apprise the users of the data about the estimate of inherent error that is present even in corrected data and in derived velocity and displacement.
3. Understanding of the complete process of recording, digitization and correction schemes. This, not only provides confidence in our processing methods but also gives an insight that helps in formulating specifications for use in the design of a better instrumentation system for the future.

It may be mentioned here that noise characteristics so determined, consist of several uncertainties due to characteristics of each instrument, thickness of the trace, judgement of operator performing the digitization, level of signal and resolution of the digitizer. It may also be mentioned that it will be impractical to study the noise characteristics for each installed instrument and determine signal to noise ratio for each record. Therefore, the parameters determined by such a study *viz.* cutoff frequencies

of band pass filter for a required signal to noise ratio and level of error in the corrected data are not the exact and absolute values but can at best be considered as an estimate.

3.3 Classification of noise

Iai [45] classified noise according to the nature of its time history which can be periodic or random or of limited duration.

In case the noise is assumed to be periodic then the Fourier transform of the noise will be proportional to the duration of the record (T) and the Fourier spectrum will be independent of duration. This assumption is not applicable in this case where the noise cannot be treated as a periodic function.

If the noise is assumed to be a random infinite sequence then Fourier transform of the noise for a duration of the record T will be proportional to square root of the duration (\sqrt{T}). Iai *et al.* [46] and Iai *at al.* [47] consider noise in this fashion. However, the recorded noise is not the background noise which can be assumed to be an infinite sequence but it is instrumental noise which creeps in due to various physical reasons during the process of recording and digitization and has a finite duration equal to that of the record.

In this study the noise is assumed to be of finite duration and therefore the Fourier transformation of this noise will be independent of T and Fourier spectrum will be inversely proportional to the duration. For such a case Fourier transformation of the noise will be approximately same as the velocity response spectra for zero damping or for very small damping. Trifunac [90,91] and Trifunac and Lee [95] also treat noise in this fashion.

3.4 Methodology

Experiments were conducted for determining the noise characteristics on a RESA V accelerograph which has specifications similar to most other instruments installed at various locations in India. Table 3.1 gives the calibration constants of the instrument used for the purpose. This instrument was made to trigger several times in a peaceful environment and records for 10, 20 and 30 *seconds* trigger were obtained. One of the accelerometer trace of each of these records were digitized by three operators. Each

operator digitized each trace three times. Thus, each record (10, 20 sec and 30 seconds trigger) was digitized nine times. The digitization was performed on a semi-automatic digitizing table which had a resolution of 1/1000 of an inch.

Table 3.1: Calibration Constants of RESA V

Natural frequency (<i>Hz</i>)	% of critical damping	Tilt sensitivity (<i>mm/g</i>)	Time for 20 ON of time mark (<i>second</i>)
22.5	63.6	29.8	19

Using the calibration constants of the instrument, all the 27 digitized records (files) were converted into unequally sampled uncorrected accelerograms with base line being taken as the least square line of the record. A linear interpolation was done to get 27 uncorrected accelerograms at an equal sample interval of 0.005 *second*. Fourier transformation spectra and velocity response spectra for zero damping of all the 27 files were determined. The average Fourier transformation spectra of 9 files each of 10,20,30 *seconds* records and average Fourier transformation spectra of all the 27 files are plotted one over the other for frequencies upto 25 *Hz* and are shown in Fig. 3.1. Similarly 3 sets of velocity response spectra for zero percent damping was determined using algorithm of Nigam and Jennings [65,66]. Figure 3.2 shows above 3 sets of velocity response spectra alongwith average velocity response spectrum of all the 27 files.

The velocity response spectra for zero damping and the Fourier transformation spectra should be almost same for a particular excitation and Velocity response spectra should be above Fourier response spectra at each point (Hudson 1970). However, this is not getting reflected in Figs. 3.1 and 3.2. This is due to the fact that averaging of large number of files have been done to obtain these figures. However, a doubt gets created about the validity of the softwares used for determining velocity response spectra and Fourier transformation spectra. For the determination of velocity response spectra, the software developed by Nigam and Jennings [65] was used, which is well established and commonly used software. For the computation of the Fourier transformation spectra, a software comprising fast Fourier transform using Radix-2 algorithm (with decimation in frequency) is used (Burrus and Park [22]). To compare the results from the two programs, first of all Fourier transformation spectra of an earthquake motion was determined. The velocity response spectra for zero percent damping for the same earthquake

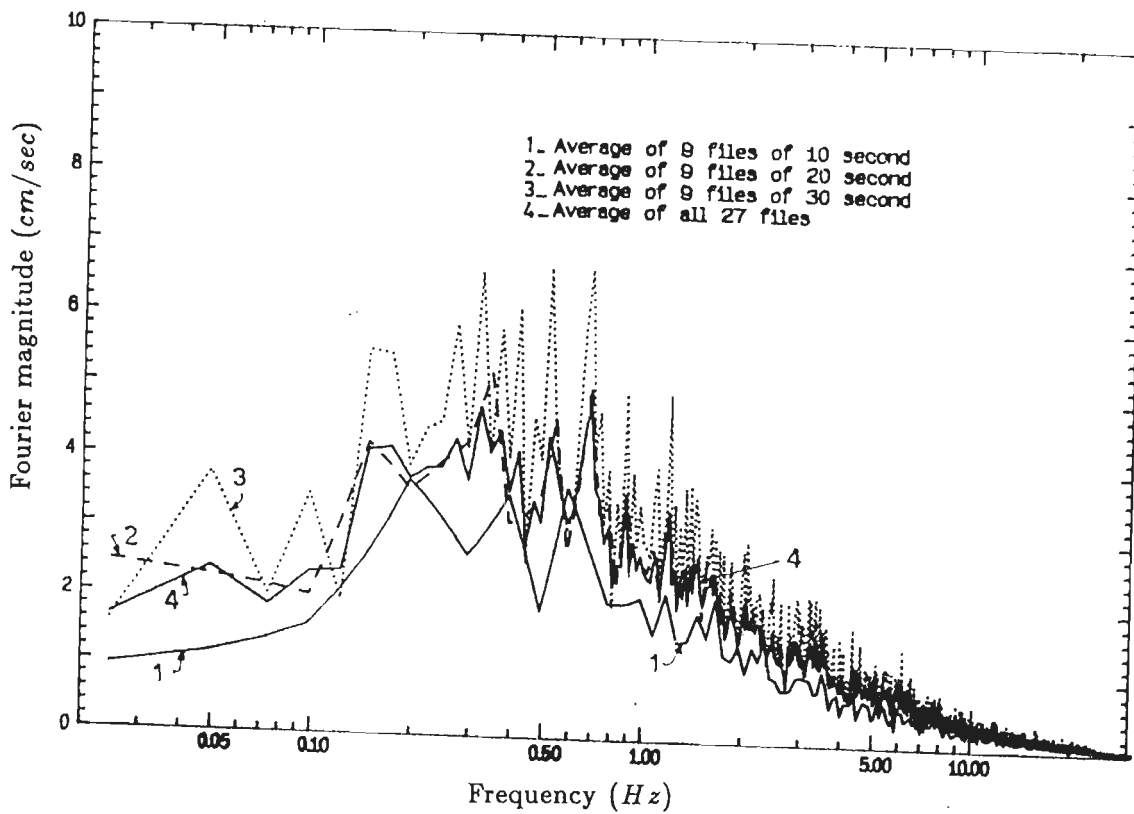


Figure 3.1: Average Fourier magnitude of noise of RESA V

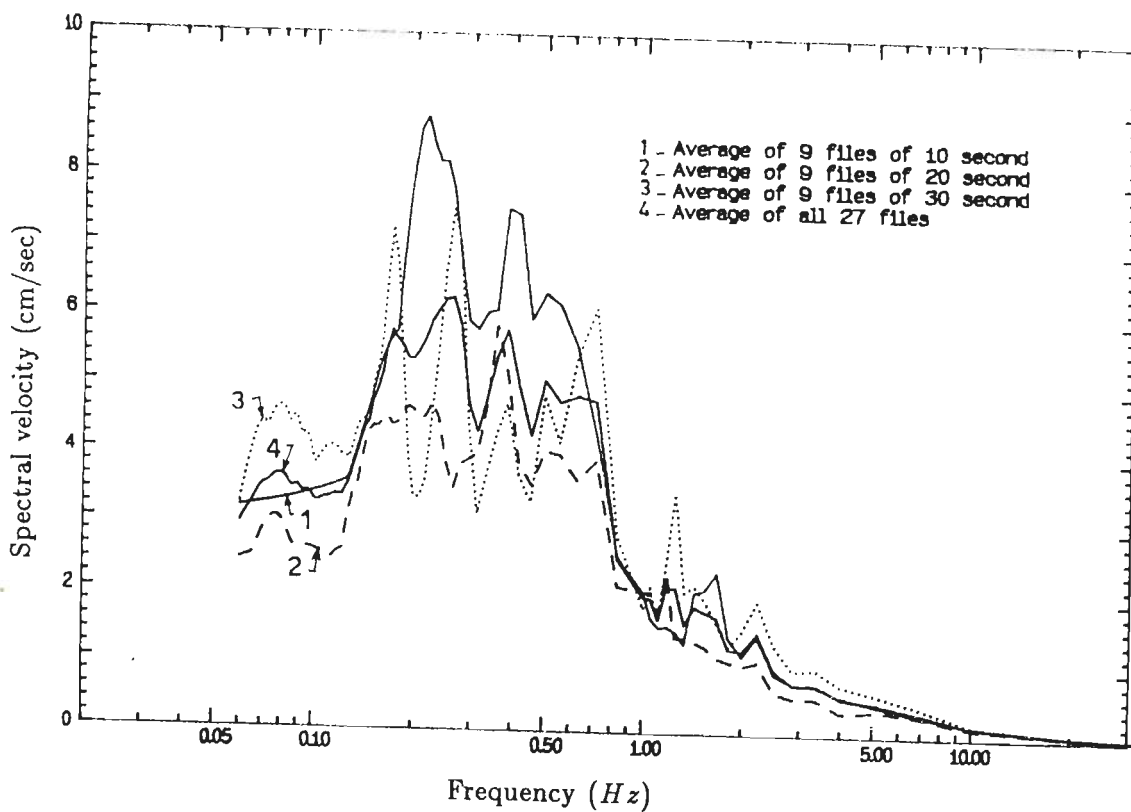


Figure 3.2: Average velocity response spectra of noise

was determined for 50 frequencies between 1 *Hz* and 2.2 *Hz*. These 50 frequencies were the same as the bin frequencies of Fourier transformation spectra. The two spectra were plotted one over the other as shown in Fig. 3.3. The results are as expected and it can be seen that the nature of the two spectra is almost the same and velocity response spectra is above Fourier transformation spectra at all the frequency points (Hudson [40]).

To demonstrate the use of Fourier transformation spectrum of noise in selecting the appropriate cut off frequency, a record obtained at Uttarkashi on RESA V during Garhwal earthquake of October 20, 1991 was used. Fourier transformation spectrum of uncorrected accelerogram of earthquake record which was interpolated at .005 *second* was obtained. This spectrum was plotted alongwith average Fourier transformation spectrum of the noise upto a frequency of 25 *Hz* as shown in Fig. 3.4. The signal to noise ratio of this record was determined by dividing the two spectra of Fig. 3.4 at each frequency point, keeping the bin frequency of two spectra same. Figure 3.5 gives a curve of signal to noise ratio at each frequency point. This curve was smoothed with a running mean filter. Figure 3.6 show smoothed signal to noise ratio of the record. If a signal to noise ratio of 10 is required then a cut off frequency of 0.5 *Hz* is essential. For lowpass filter a cutoff frequency of 25 *Hz* is ideal because the level of signal at higher frequencies is very small as can be seen from Fig. 3.4.

To estimate the noise in time domain, the uncorrected time histories of the noise were processed by Trifunac's scheme [56,93] with a cutoff frequency for high pass filter as 0.1 *Hz* with a roll-off of 0.02 *Hz* and a cutoff frequency for low pass filter as 25 *Hz* with a roll-off of 2 *Hz*. The maximum acceleration of the noise history of the 27 files had an average of 5.791 *gals* with a standard deviation of 2.106 *gals*. The maximum derived velocity of the noise history of the 27 files had an average of 2.043 *cm/sec* and a standard deviation of 0.925 *cm/sec*. The maximum derived displacement of the noise history of the 27 files had an average of 2.48 *cm* and a standard deviation of 1.46 *cm*. Table 3.2 summerizes the above results. Figure 3.7 shows one of the noise acceleration, velocity and displacement history.

3.5 Discussion on results

Study of noise characteristics of RESA V is done in this part of the work. The following are the conclusions of this work:

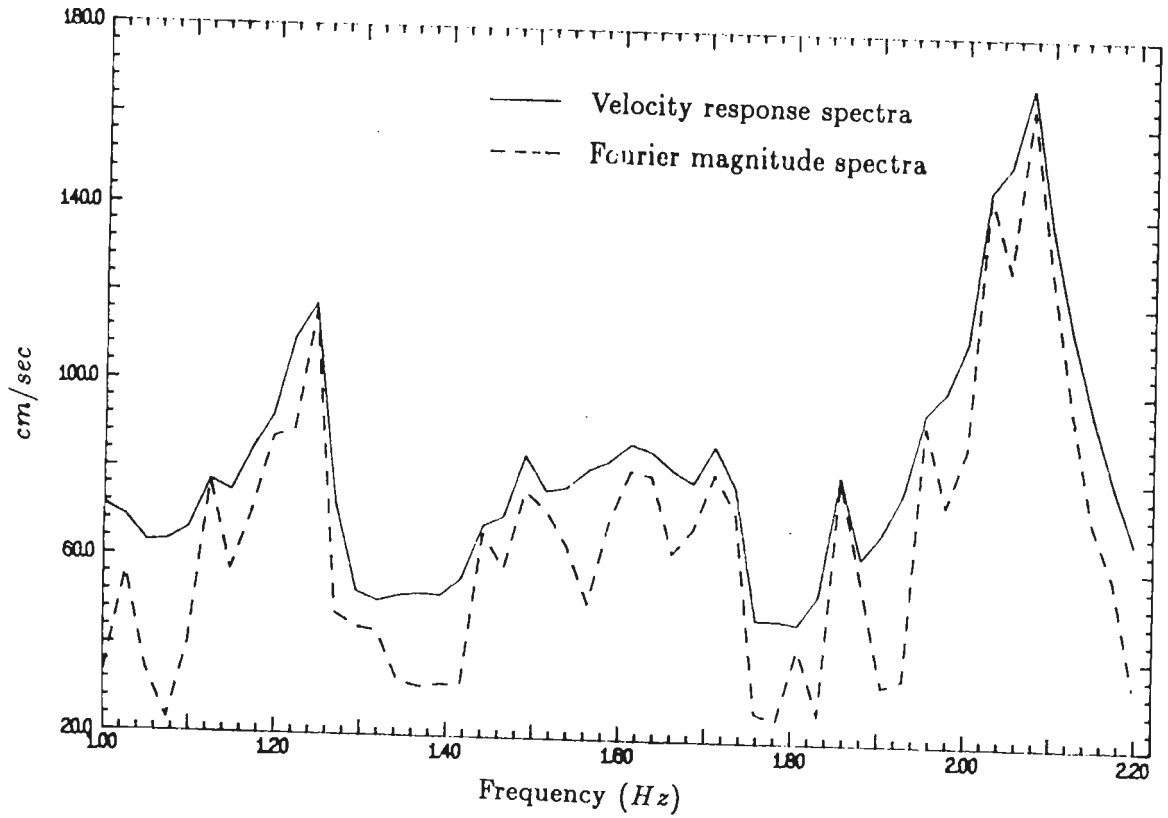


Figure 3.3: Comparison of velocity response spectra and Fourier magnitude spectra for validation of computer programs.

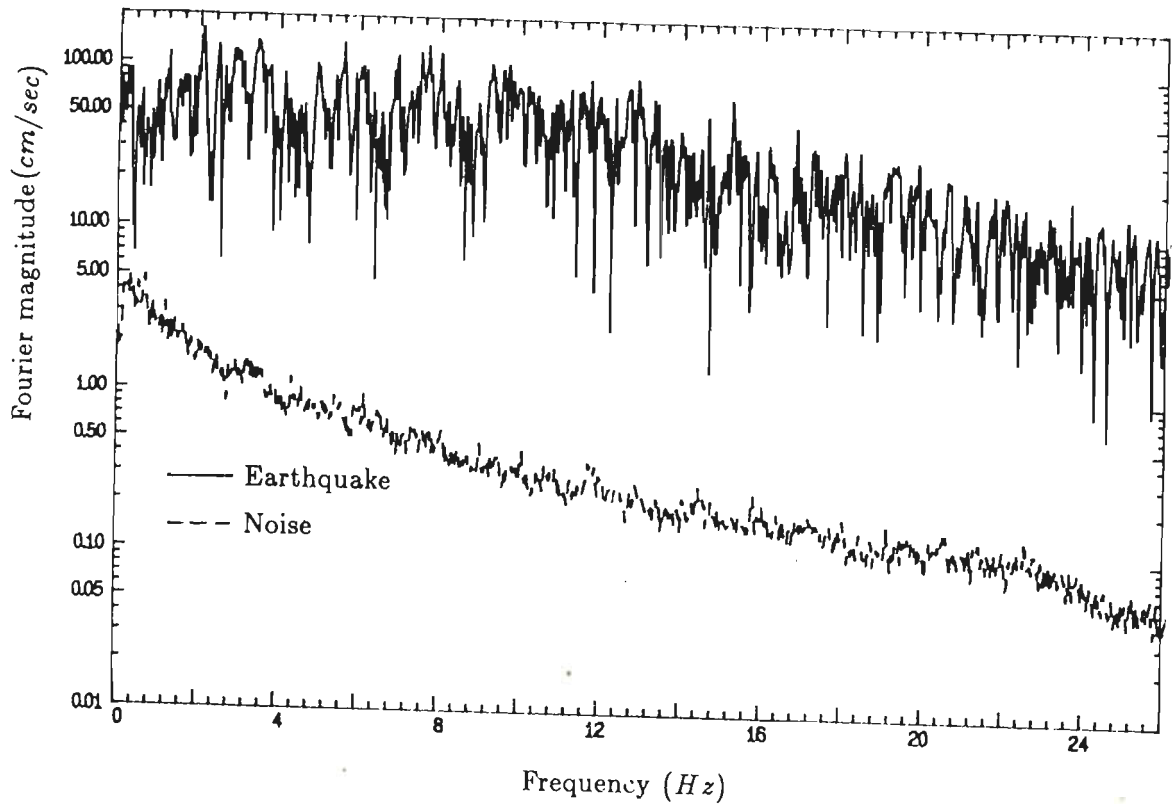


Figure 3.4: Fourier magnitude spectra of uncorrected Uttarkashi accelerogram and noise.

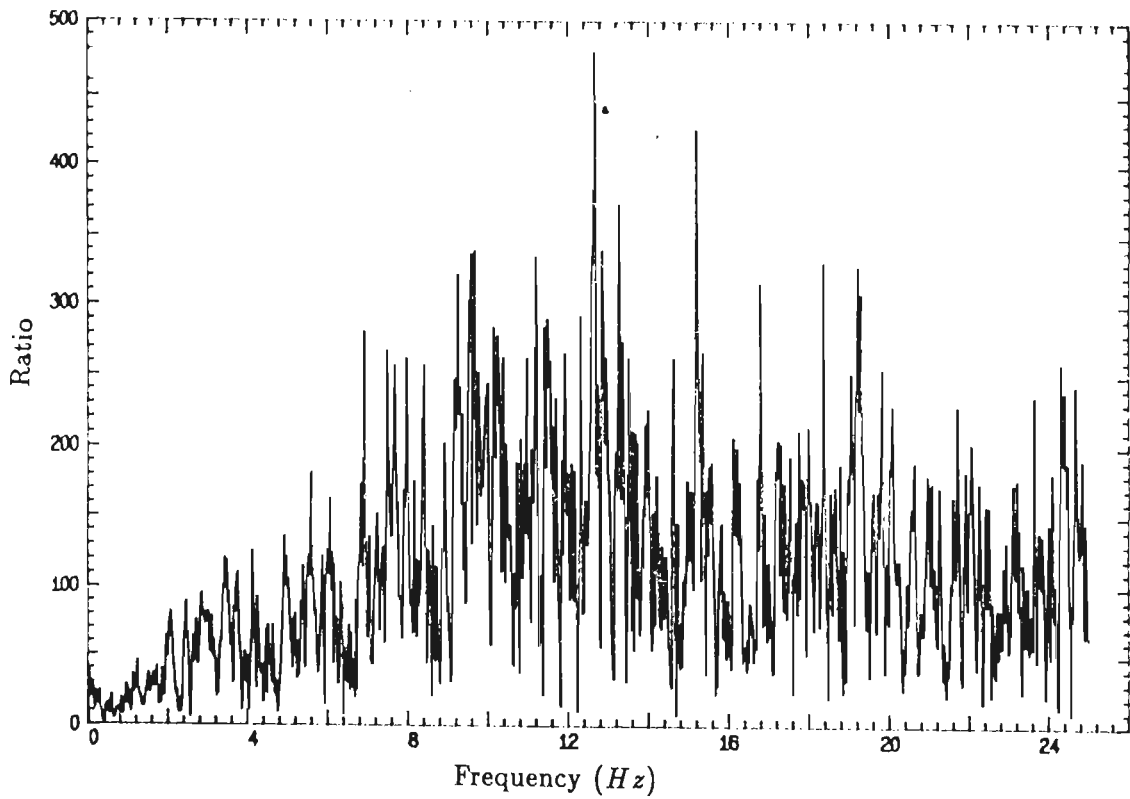


Figure 3.5: Earthquake signal (Uttarkashi accelerogram) to noise ratio

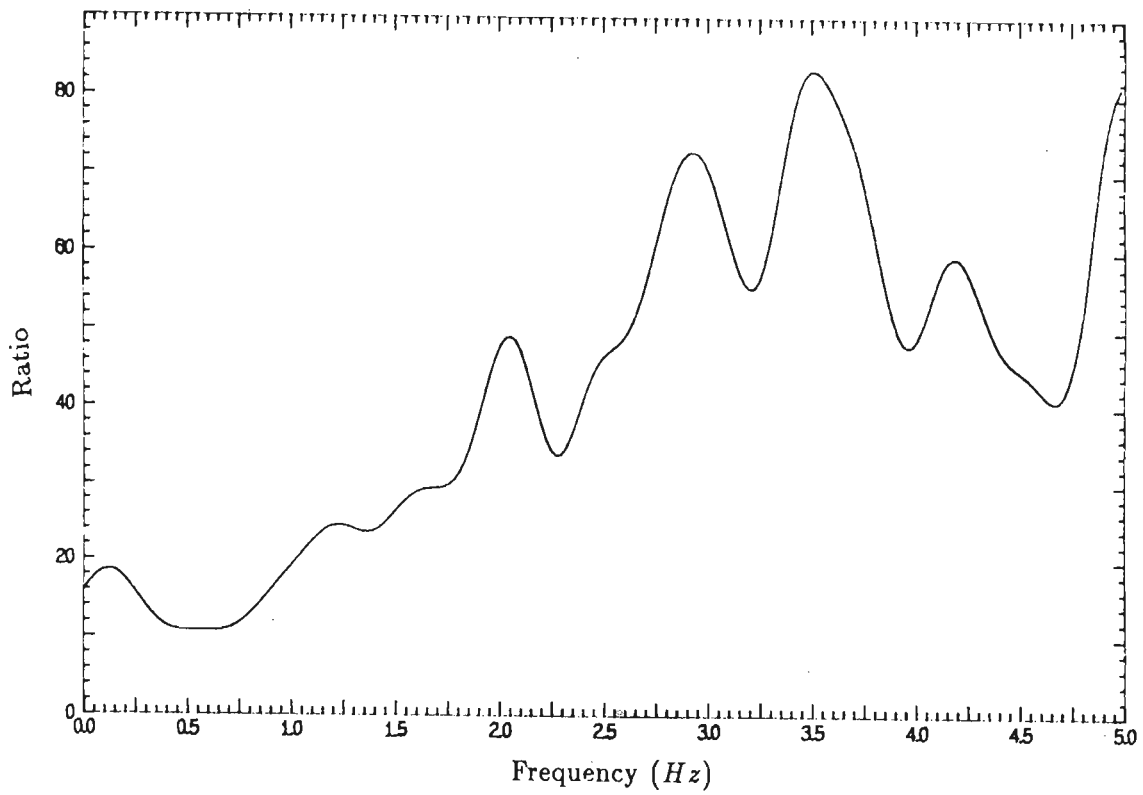


Figure 3.6: Smoothed earthquake signal to noise ratio (for frequencies up to 5 Hz)

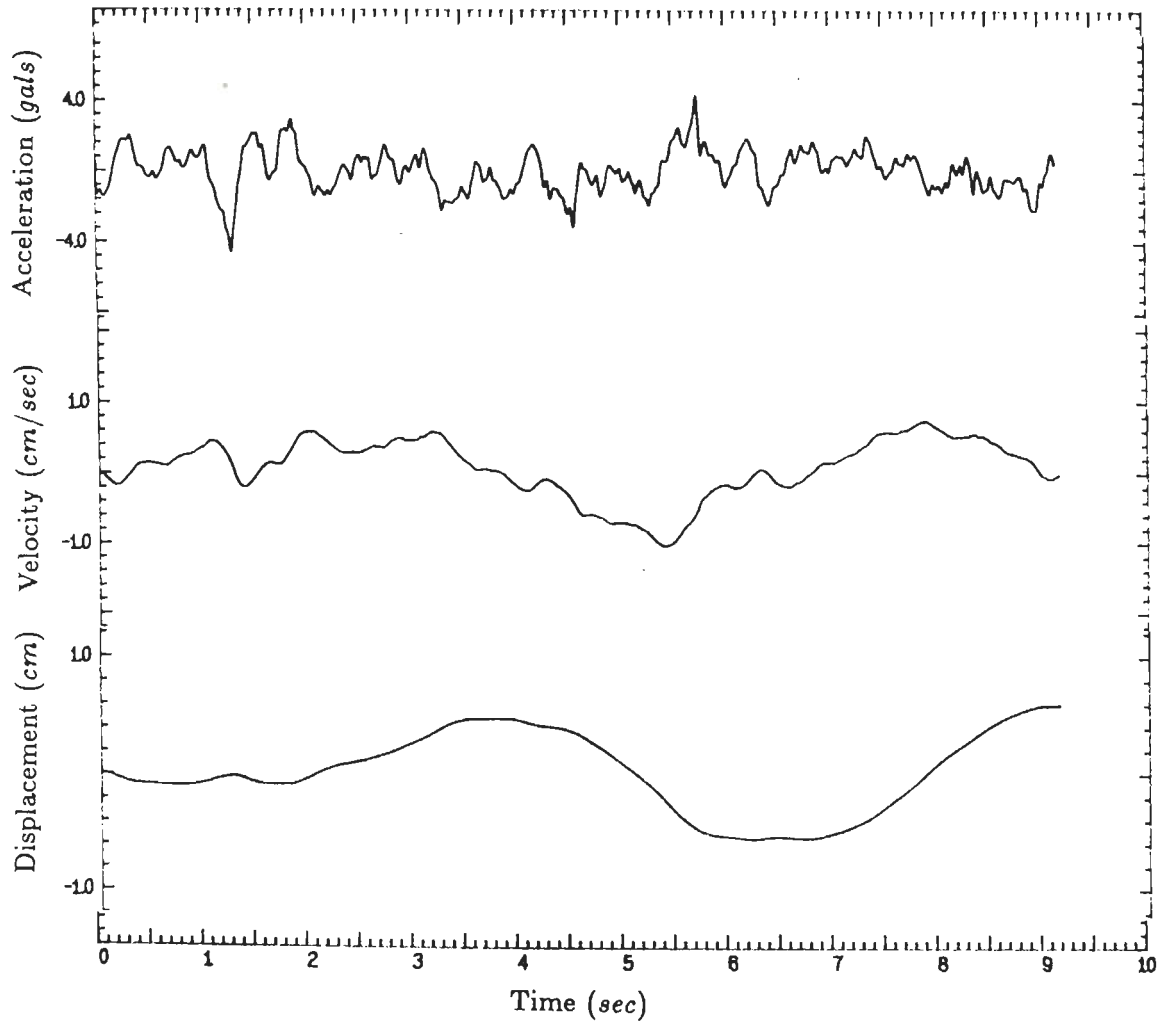


Figure 3.7: A typical corrected noise acceleration, velocity and displacement history

Table 3.2: Noise of RESA V

Duration <i>sec</i>	Acceleration <i>gals</i>		Velocity <i>cm/sec</i>		Displacement <i>cm</i>	
	Mean	σ	Mean	σ	Mean	σ
10	5.801	2.126	1.758	0.843	1.310	0.621
20	5.812	2.118	1.938	0.842	3.015	1.450
30	5.760	2.070	2.353	1.017	3.124	1.361
Overall	5.791	2.106	2.043	0.925	2.480	1.460

1. The noise in an accelerograph is of finite duration. This is amply demonstrated in Fig. 3.1 where average Fourier Transformation amplitude of 10, 20 and 30 *seconds* records are plotted one over the other and which shows that Fourier Transformation is independent of duration T .
2. The level of noise in low as well as in high frequency range in the system (RESA V and digitizer used) is more than the noise reported by American systems. This is attributed to the trace thickness of RESA V which is substantially more than American accelerographs like SMA 1 and to some extent characteristics of the digitizer.
3. Due to the above reasons values of average noise in time domain for acceleration, velocity and displacement of RESA V is more than their American counterparts. Perhaps, the optics of RESA V needs improvements and a more accurate digitizing table is required.
4. A method has been shown to choose cutoff frequency for records of RESA V which is based on signal to noise ratio of earthquake signal and noise. This ratio has been found in each bin frequency of Fourier transformation amplitude of uncorrected accelerogram and that of noise. However, such methods for choosing cut off frequencies require judgement which can vary from person to person.

Chapter 4

Band limited interpolation of nonuniform samples

Interpolation in a given sequence is a requirement which arises frequently while using and processing digital data. In the field of digital signal processing, such interpolations are generally done in a manner such that the frequency contents of original data do not change. However, in strong motion earthquake data processing, researchers mostly tend to use linear interpolation which invariably distorts the frequency contents of digital data. In this chapter, the necessity of using band limited interpolation while processing accelerograms is highlighted and a method is suggested to perform such interpolations for nonuniform samples.

The trace of most of the past earthquake records of analog accelerographs as reported in various reports/ papers were digitized on semi-automatic type digitizers, the kind of which are still employed at many places for this purpose. It is, therefore, obvious that data so obtained are not at a constant sampling interval and can be called nonuniform samples. All presently available methods of processing strong motion data convert such nonuniform samples into samples at constant time interval through linear interpolation which introduces frequencies from zero to infinity. Digital data which is always band limited, gets distorted by linear interpolation in the entire band upto Nyquist frequency due to effect of aliasing.

Another important question in this regard is related to interval at which the digitization should be performed so that mathematically sound information can be obtained in the desired band. The problem of sampling interval at which digitization should be performed is first addressed in this chapter by presenting the concept of stable sampling

set with regard to nonuniform samples. Then an iterative method is introduced for recovery of signal from nonuniform samples. The comparison of results of band limited interpolation of nonuniform samples with those of linear interpolation is done through study of Fourier spectra. A discussion on the band limited interpolation *vis a vis* linear interpolation is finally presented [52].

4.1 Digitization of analog records and stable sampling set

Semi-automatic digitizers require judgement of the operator to pick points on the trace (analog record on photographic paper or film) which is to be digitized. The question is how these points be picked up so that the signal can be recovered within the required frequency band. In this regard the concept of stable sampling set becomes important. Marvasti *et al.* [60] defined stable sampling set as follows:

A stable sampling set is a set of digital data that uniquely determines a band limited signal and satisfies the following inequality:

$$\int |x(t)|^2 dt \leq C \sum_{n=-\infty}^{\infty} |x(t_n)|^2 \quad (4.1)$$

where $x(t)$ is the signal and $x(t_n)$ is its n^{th} discrete sample. C is a parameter which represents nonuniformity of the samples.

It has been shown by Marvasti *et al.* [60] that the first condition of stable sampling set *ie.* a set of digital data from which the band limited signal can be determined uniquely, is achieved if the average sampling rate of the digital data is greater than Nyquist rate. However, such sampling set will be stable only when the sufficient condition of Inequality 4.1 is satisfied. They have also shown that one of the way to satisfy this condition is that all the samples should not be clustered in a finite interval but should be evenly distributed such that

$$|t_n - nT| < \frac{T}{4} \quad (4.2)$$

where t_n is the instant of n^{th} nonuniform sample and T is the sampling interval which should be less than or equal to sampling interval corresponding to Nyquist rate.

The same authors have presented an iterative scheme to recover signal from stable sampling set of nonuniform samples (discussed in next section). They have also shown

that if in a nonuniform sequence, average sampling rate is higher than Nyquist rate but the Inequality 4.2 is not satisfied then the convergence of iteration to recover the signal is possible but is slower in comparison to stable sampling set. Also if Inequality 4.2 is not satisfied and the average sampling rate is exactly equal to the Nyquist rate the convergence of iteration is not guaranteed. However, if the average sampling rate of the sequence is less than the Nyquist rate then the iteration will not converge. Thus the following can be concluded in relation to the digitization of the trace of an analog accelerogram.

1. If frequencies upto 25 Hz are required to be recovered then average sampling rate should be atleast 50 samples per second (SPS) which is the Nyquist rate. This means that the number of total samples digitized should be at least 50 times the duration of record in seconds. This is a necessary condition to get the desired results. In case the number of digitized samples are less than this value then the maximum frequency that is possible to be recovered from such data will also reduce accordingly.
2. The sampling points should be as evenly distributed as possible and clustering of sampling points around a finite duration should not be done. It will be desirable to have the distribution of most of the sampling points satisfy Inequality 4.2. Picking out peaks and troughs, which is the usual practice in digitizing traces of records of analog accelerographs, is not as important as distributing the sampling points evenly.
3. Although, the condition of digitizing with average sampling rate greater than Nyquist rate is an essential requirement, however, digitization to satisfy Inequality 4.2 is only a desirable requirement as it increases the speed of convergence. It should be appreciated that it will be impractical for an operator to pick samples during digitization strictly in a manner so as to satisfy Inequality 4.2.

4.2 Method of interpolation

Once the digitized data of analog trace is obtained, the next operation is to use calibrations of time mark and tilt sensitivity of accelerometer to get uncorrected accelerogram at nonuniform sample intervals. The signal now is required to be recovered from given sequence of nonuniform interval in such a way so as to retain the same frequency content. The word recovery of signal in this study refers to getting digital data at comparatively

large sampling points at constant interval. In this work, the signal is recovered at 200 *SPS*.

Marvasti *et al.* [60] have shown that for nonuniform samples given by

$$x_s(t) = \sum_i x(t_i)\delta(t - t_i) \quad (4.3)$$

where $\{t_i\}$ is a stable sampling set, the following iterative method shall recover the original band limited signal $x(t)$ from $x_s(t)$

$$x_{k+1}(t) = \lambda PS(x(t)) + (P - \lambda PS)x_k(t) \quad (4.4)$$

where λ is a convergence constant whose value should be between 0.5 and 1, $x(t)$ is the original signal and $x_k(t)$ is the signal obtained after k^{th} iteration. P is a band limiting operator (a low pass filter) and S is ideal nonuniform sampling operator or a staircase function operator. The band limiting operator P is self adjoint which means $P(x_k(t)) = x_k(t)$. The staircase function operator in this case assumes zero order hold of nonuniform samples and converts the nonuniform samples into a staircase form at a constant interval with 200 *SPS*. $PSx(t)$ in Eq. 4.4 is low passed signal of staircase nonuniform samples which is known before the start of iterations. Marvasti *et al.* [60] have also proved that there exists a range of values of λ for which the process of Eq. 4.4 will converge i.e.

$$\lim_{k \rightarrow \infty} x_k(t) = x(t) \quad (4.5)$$

4.2.1 The S Operator

The S operator in iteration of Eq. 4.4 requires construction of staircase from the nonuniform samples. The flow chart for obtaining staircase from nonuniformly sampled data is given in Fig. 4.1. The staircase is obtained by making a sequence at 200 *SPS* with each sample equal to last available nonuniform sample. Making stair case from a given nonuniform sample really means getting a zero order sample and hold signal. In fact the logic of recovering a signal from nonuniform samples through the staircase function is quite similar to the practice of constructing a band limited analog signal from a given digital data through sample and hold.

4.2.2 The P Operator

The P operator in Eq. 4.4 is called as band limiting operator which is essentially a low pass filter. Butterworth filter is used for performing the low pass operation. The

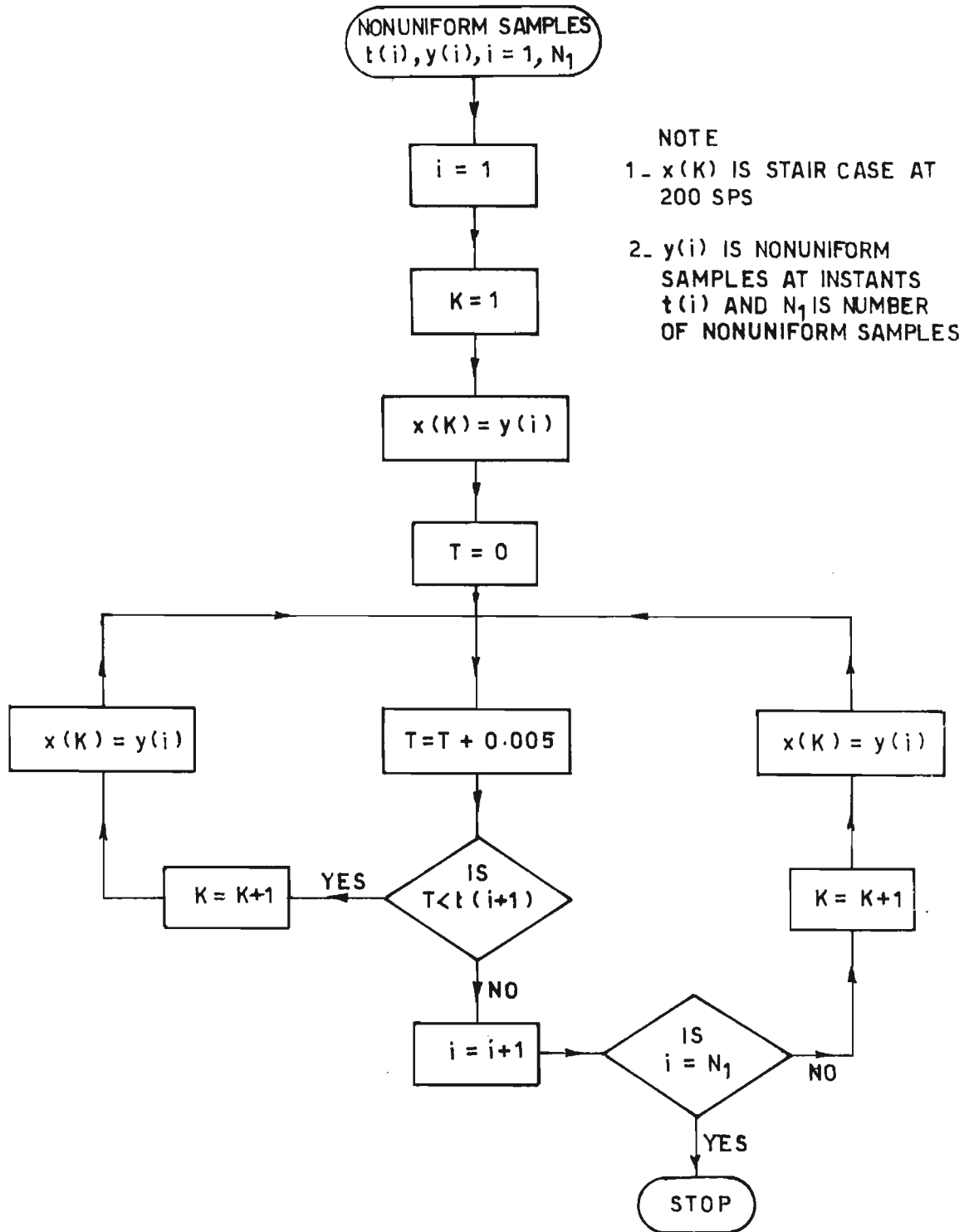


Figure 4.1: Flow chart for obtaining Staircase from nonuniform samples

filtering is performed in frequency domain. The filtering operation is performed by first finding FFT of the signal which is to be filtered. The bin frequency interval (Δf) at which the FFT of the signal is determined is given by

$$\Delta f = \frac{SPS}{N} \quad (4.6)$$

where SPS denotes samples per second which is 200 SPS in this case and N is the number of data points of the sequence which is lengthened by inserting zeros so that the sequence has exactly 2^j (where j is an integer) data points. For example, if sequence has 3910 data points then N is made 4096 (which is 2^{12}) by inserting 186 zeros at the end of the sequence. At the above bin frequency intervals, transfer function $|H(j\omega)|^2$ of Butterworth filter, which is given by the equation below (Lam [54]), is determined from DC to the Nyquist frequency.

$$|H(j\omega)|^2 = \frac{1}{1 - (\frac{\omega}{\omega_c})^{2n}} \quad (4.7)$$

where ω is the frequency at which the function is determined, ω_c is the cutoff frequency and n is the order of filter. It is quite obvious that cutoff frequency of the lowpass filter should be less than half average sampling rate of the nonuniformly sampled data. The order of the filter (n) determines the sharpness or the roll off of the filter function. A higher order filter provides steeper cut off or smaller roll off frequency. However, a very large order of filter introduces Gibbs phenomena particularly near cut off frequency. In this study, it has been found that a filter order of 6 provides a filter function which is sufficiently accurate for our work.

Convolution is then performed between the FFT of the signal and the transfer function of the filter. As the transfer function of filter has only real part, convolution in frequency domain means simple multiplication of real and imaginary parts of the signal with the filter function at the corresponding bin frequencies. Inverse FFT is then performed to get the low passed signal in time domain.

4.2.3 Iteration

Figure 4.2 gives flow chart of the software developed to perform the iteration of Eq. 4.4. The algorithm first converts nonuniform samples into staircase at 200 SPS . FFT of the staircase function is then found and $|H(j\omega)|^2$ of Butterworth filter is used to convolute the signal for low pass filtering in frequency domain. An inverse FFT is then performed to get $PS(x(t))$ which is also the signal for the first iteration. Iteration is performed next by adding to the $PS(x(t))$, the difference between the recovered signal of earlier

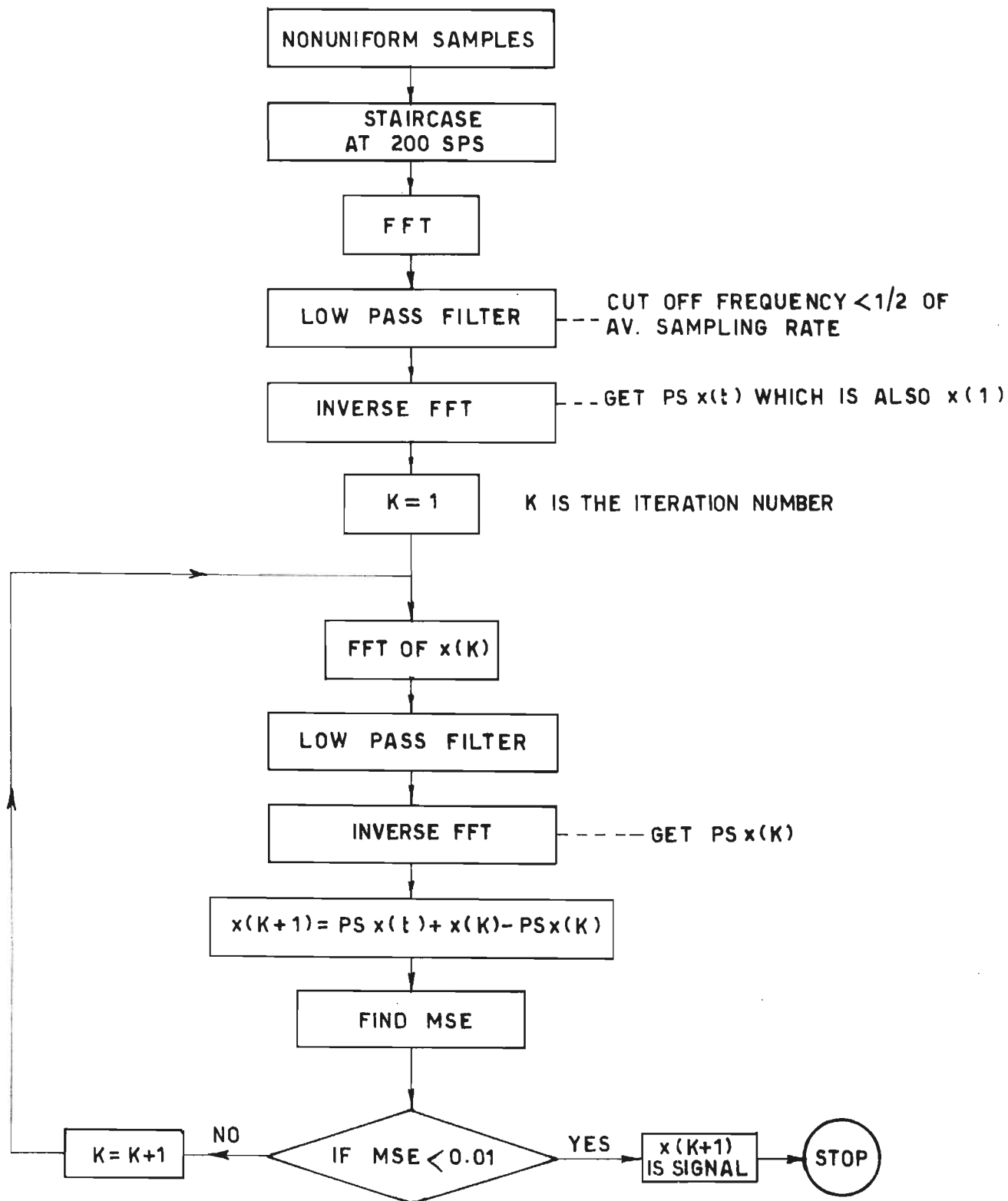


Figure 4.2: Flow chart of iteration for recovery of signal from nonuniform samples

iteration and its band operated signal. After each iteration mean square error (MSE) between x_{k+1} and x_k is determined. MSE is defined as :

$$MSE = \frac{\sum_i (\epsilon^i - \bar{\epsilon})^2}{N - 1} \quad (4.8)$$

where i is sample points and

$$\epsilon = x_{k+1} - x_k \quad (4.9)$$

and

$$\bar{\epsilon} = \frac{\sum_i \epsilon^i}{N} \quad (4.10)$$

The desired signal is assumed to be achieved and the iteration is deemed to have converged when value of MSE becomes less than 0.01. The computer program developed for this algorithm is interactive in nature and is quite flexible with regard to the choice of various characteristics like cutoff frequency, number of poles of filter, maximum number of iterations to be used etc.

4.3 Examples on recovery of sine waves

The algorithm and the computer program discussed in the earlier sections is used to recover sinewaves of different frequencies. For the sake of consistency with processing of accelerograms, the sine waves are assumed to have acceleration units (cm/sec^2 or *gals*) and thus the Fourier magnitudes determined have units of velocity (cm/sec). The frequency domain figures plotted in this section are between frequency and Fourier magnitudes converted into dB using the following relation:

$$dB = 20 \log F_a \quad (4.11)$$

where F_a is the Fourier magnitude in cm/sec .

The reason of plotting these figures with dB as ordinate is to highlight the comparison of smaller values of the signal or noise which may otherwise show almost zero values in a linear plot. Firstly sine waves of different frequencies defined at stable sample set are recovered and subsequently sine waves defined at random locations are recovered.

4.3.1 With Stable Sample Set

The sine waves are first defined by nonuniform samples at an average sampling rate of 50 *SPS* and these nonuniform samples are distributed so as to satisfy Inequality 4.2

which is a requirement for a stable sample set. The distribution of samples within the range of Inequality 4.2 is done randomly by generating random numbers. The program is then used to recover the single sinewaves of 1.02539 Hz (to be referred as 1 Hz), 10.05859 Hz (to be referred as 10 Hz) and 20.11719 Hz (to be referred as 20 Hz). The exact frequencies of the sinewaves are next higher bin frequency of 1 Hz , 10 Hz and 20 Hz . The exact bin frequencies are chosen so that computational leakage during calculation of FFT can be avoided. The recovery took 2 iterations for 1 Hz , 25 iterations for 10 Hz and 35 iterations for 20 Hz signals. Figure 4.3 gives time history of 10 Hz sinewave recovered using the proposed method along with linearly interpolated and exact sinewave. The proposed band limited interpolation clearly performs better in comparison to linear interpolation, although the sinewave recovered from the proposed method shows a slight phase shift. Similar results in time domain are obtained for other sinewaves also.

A comparison in frequency domain is then performed between the exact, band limited and linearly interpolated signal. Figure 4.4 shows FFT of the three signals plotted one over the other for 1 Hz sinewave, Fig. 4.5 shows the same comparison for 10 Hz sinewave and Fig. 4.6 shows it for 20 Hz sinewave. Table 4.1 gives maximum value of Fourier magnitude in cm/sec and in dB of the exact, band limited and linearly interpolated sinewaves along with duration of the record. These maximum values really indicate the strength of the recovered sinewaves.

Table 4.1: Comparison of Results for Recovery of Single Sine Waves from Stable Sample Set

Frequency (Hz)	Duration (Sec)	Max. Fourier Magnitude			Max. Fourier Magnitude		
		Exact (cm/sec)	Banded (cm/sec)	Linear (cm/sec)	Exact (dB)	Banded (dB)	Linear (dB)
1.025	39.980	1999.20	1997.70	1996.10	66.02	66.01	66.00
10.059	9.640	482.18	447.85	416.06	53.66	53.02	52.38
20.117	4.625	231.15	146.49	112.66	47.28	43.32	41.03

Figures 4.4 to 4.6 clearly indicate that the linear interpolation introduces high frequency noise although, in low frequency the noise content in the linearly interpolated data is slightly less than the noise content of the data obtained from the proposed method. From Table 4.1 it is seen that the sinewaves recovered using the proposed method is stronger and their maximum magnitudes are closer to the maximum magni-

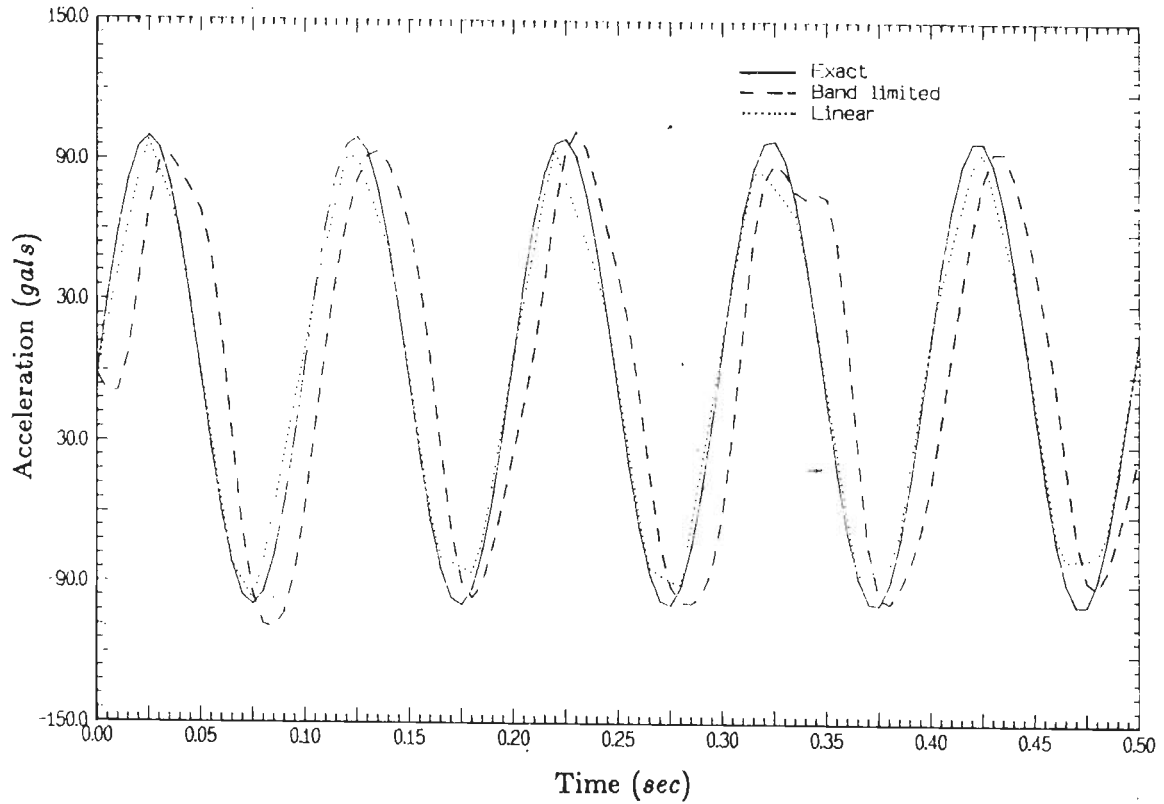


Figure 4.3: Time history of 10 Hz sine wave recovered through band limited interpolation of nonuniform samples (stable set) along with linearly interpolated and exact sine wave.

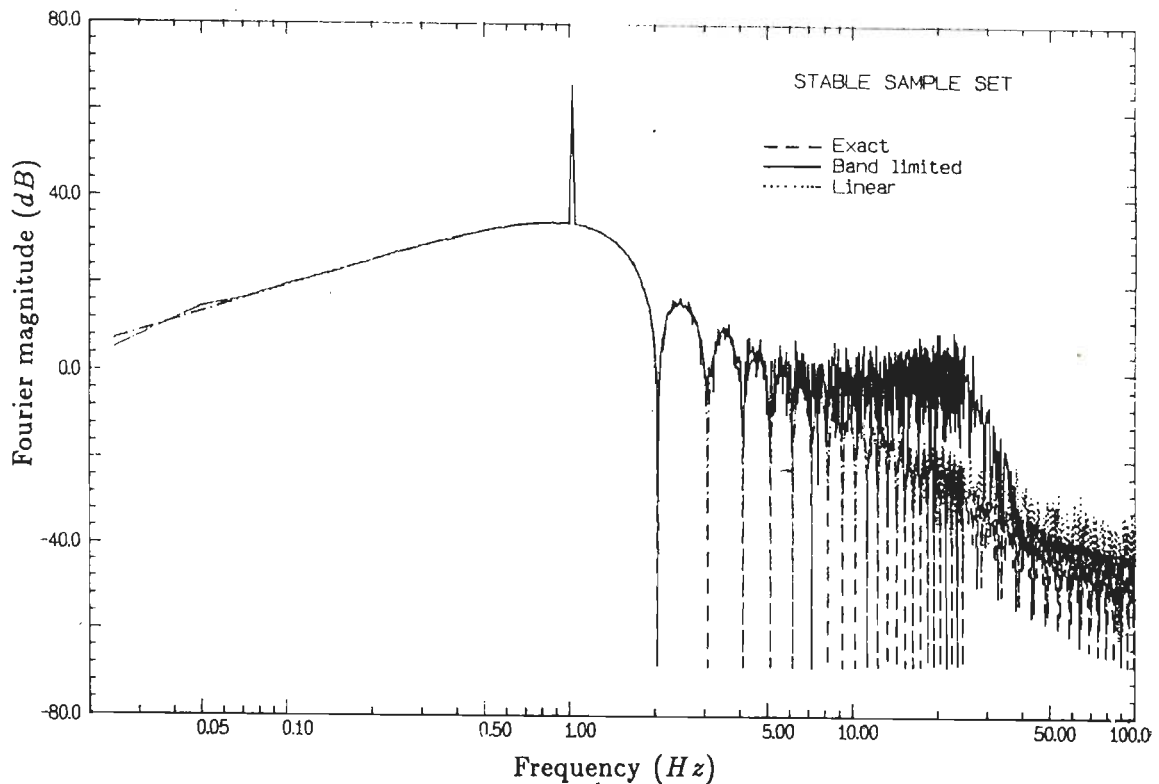


Figure 4.4: Fourier magnitude plots of 1 Hz sine wave recovered through band limited interpolation of nonuniform samples (stable set) along with linearly interpolated and exact sine wave.

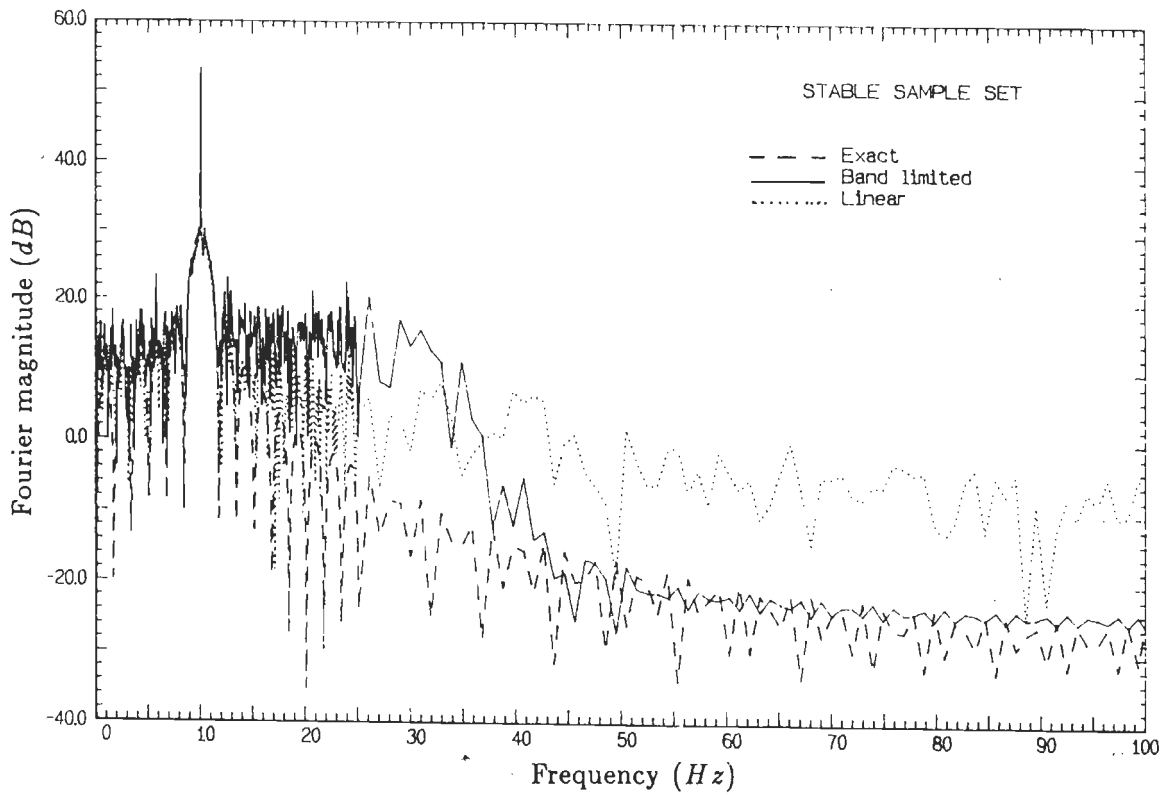


Figure 4.5: Fourier magnitude plots of 10 Hz sine wave recovered through band limited interpolation of nonuniform samples (stable set) along with linearly interpolated and exact sine wave.

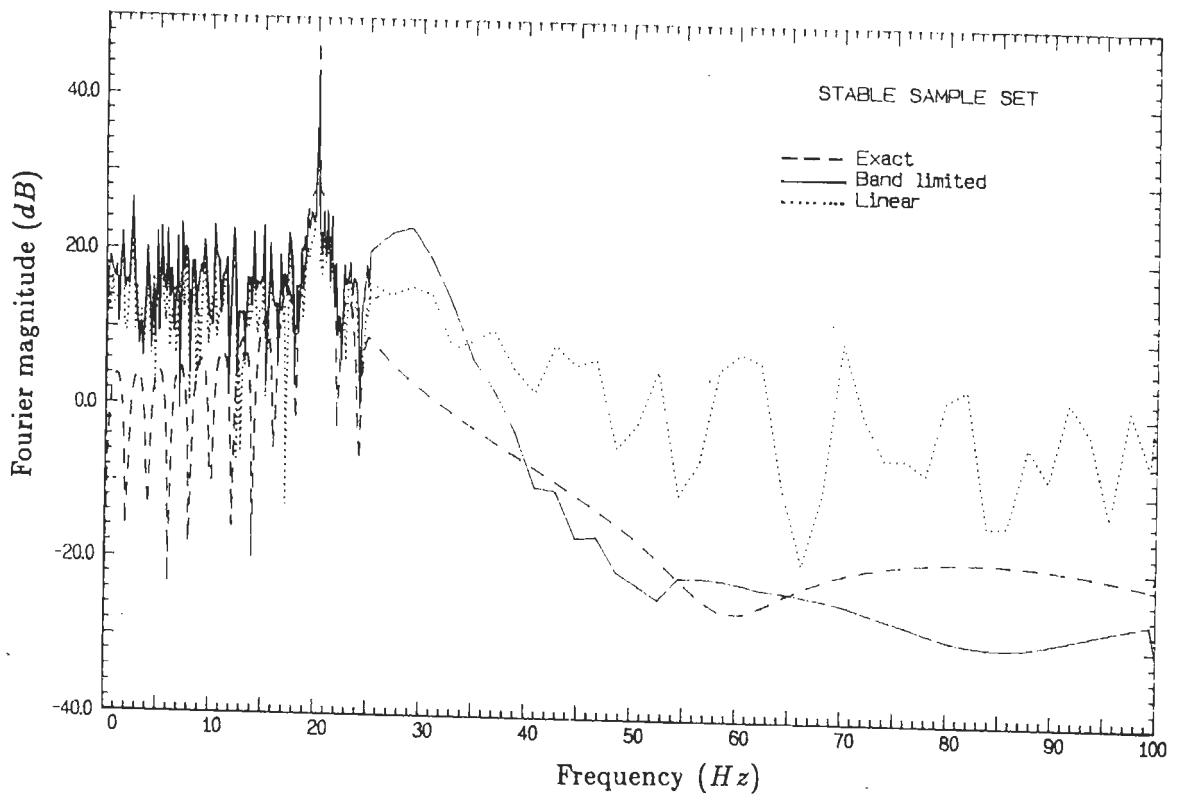


Figure 4.6: Fourier magnitude plots of 20 Hz sine wave recovered through band limited interpolation of nonuniform samples (stable set) along with linearly interpolated and exact sine wave.

tudes of the exact sine waves compared to those of the linearly interpolated sinewaves (this fact cannot be viewed in the figures as all the three spikes are at the same frequency thus making it difficult to read the maximum value of each peak). It may, however, be mentioned that inspite of slightly higher noise in the low frequency (pass band) of the proposed scheme, earthquake signals are bound to be recovered closer to the ideal case in comparison to the linear interpolation due to the fact that such signals cover the entire band upto Nyquist frequency and generally have high signal to noise ratio in this band.

To substantiate this point a combination consisting of 10 sine waves of different frequencies (0.0854 Hz, 2.637 Hz, 5.176 Hz, 7.727 Hz, 10.266 Hz, 12.817 Hz, 15.356 Hz, 17.908 Hz, 20.447 Hz and 22.998 Hz) with each frequency having the same amplitude and a random phase lag is recovered from nonuniform stable sampling set with an average sampling rate of 50 SPS. Exact and linearly interpolated signals are also determined. For the purpose of comparison the pass band is divided into ten segments such that each segment contains one of the defined frequency. The maximum value of the Fourier magnitude of the signal in each segment is determined in cm/sec and in dB and is given in Table 4.2.

Table 4.2: Recovery of Signal Made from 10 Sine Waves

Frequency Segment		Peak Fourier Magnitude			Peak Fourier Magnitude		
Begin (Hz)	End (Hz)	Exact (cm/sec)	Banded (cm/sec)	Linear (cm/sec)	Exact (dB)	Banded (dB)	Linear (dB)
0.000	1.367	3510.9	3511.0	3511.2	70.908	70.909	70.909
1.379	3.906	3505.9	3489.6	3472.3	70.896	70.856	70.812
3.918	6.458	3506.9	3449.2	3387.1	70.898	70.754	70.597
6.470	8.997	3507.8	3381.6	3246.9	70.901	70.582	70.229
9.009	11.548	3506.9	3283.7	3056.1	70.899	70.327	69.703
11.560	14.087	3508.3	3161.6	2822.0	70.902	69.998	69.011
14.099	16.638	3509.3	3019.0	2562.1	70.904	69.597	68.172
16.650	19.177	3508.4	2849.8	2273.2	70.902	69.096	67.133
19.189	21.729	3514.0	2667.4	1978.6	70.916	68.522	65.927
21.741	25.000	3514.3	2463.8	1677.7	70.917	67.832	64.494

Table 4.2 again show that the signal obtained through the band limited interpolation is stronger and closer to the exact signal than the signal obtained through linear interpolation in the entire pass band as all the ten spikes of sine wave of proposed

scheme show larger magnitudes than the spikes of linear interpolation.

To further substantiate the point, another signal is generated such that it contains any ten random frequencies between .075 and 23.5 *Hz*. The amplitude of the frequencies is kept smallest for the lowest frequency and is made to increase randomly for each higher frequency, keeping it fixed for 100 *gals* for the highest frequency. The generated signal is then amplitude modulated, to simulate the nonstationary property of an earthquake accelerogram, by a Horel function given by:

$$a(t) = \left(\frac{t}{t_m}\right)^\beta e^{(1-\frac{t}{t_m})^\beta} \quad (4.12)$$

where $a(t)$ is generated signal, t_m is the instant at which the signal reaches maximum and β is a constant which is greater than 0. The duration of the signal generated is 39.95 seconds and the maximum value of the signal is set at 12.5 *seconds*. The generated signal had following frequencies and the values given in the bracket are their amplitudes.

.0732 *Hz* (.00097 *gals*); 1.7456 *Hz* (0.5518 *gals*); 4.0039 *Hz* (2.9033 *gals*); 6.1768 *Hz* (6.9094 *gals*); 10.2051 *Hz* (18.8604 *gals*); 12.1948 *Hz* (26.9321 *gals*); 14.2700 *Hz* (36.8780 *gals*); 15.7471 *Hz* (44.9074 *gals*); 19.4214 *Hz* (68.3092 *gals*); 23.4985 *Hz* (100.00 *gals*).

This signal is defined at nonuniform stable sampling set and is recovered through the proposed scheme as well as through linear interpolation. Figure 4.7 gives Fourier magnitudes in *dB* of exact, linearly interpolated and band limited signal. In this type of signal, it is found that the noise in linearly interpolated data is higher in pass band as well as in the stop band. To provide the comparison in tabular form, the pass band is divided into ten segments such that each segment contains one of the frequency of the generated signal. The median of each segment is found which represents average noise in each segment. Table 4.3 presents this comparison.

From Table 4.3 and with other illustrative examples, it can be concluded that the proposed scheme recovers signals which are closer to the exact signal in comparison to linear interpolation.

4.3.2 With Random Sample Set

The proposed algorithm is next used to recover the sine waves which are again defined by nonuniform samples at an average sampling rate of 50 *SPS*. However, in this case nonuniform samples are distributed randomly without the restriction of Inequality 4.2. As in the earlier case, single sine waves of 1.02539 *Hz* (to be referred as 1 *Hz*),

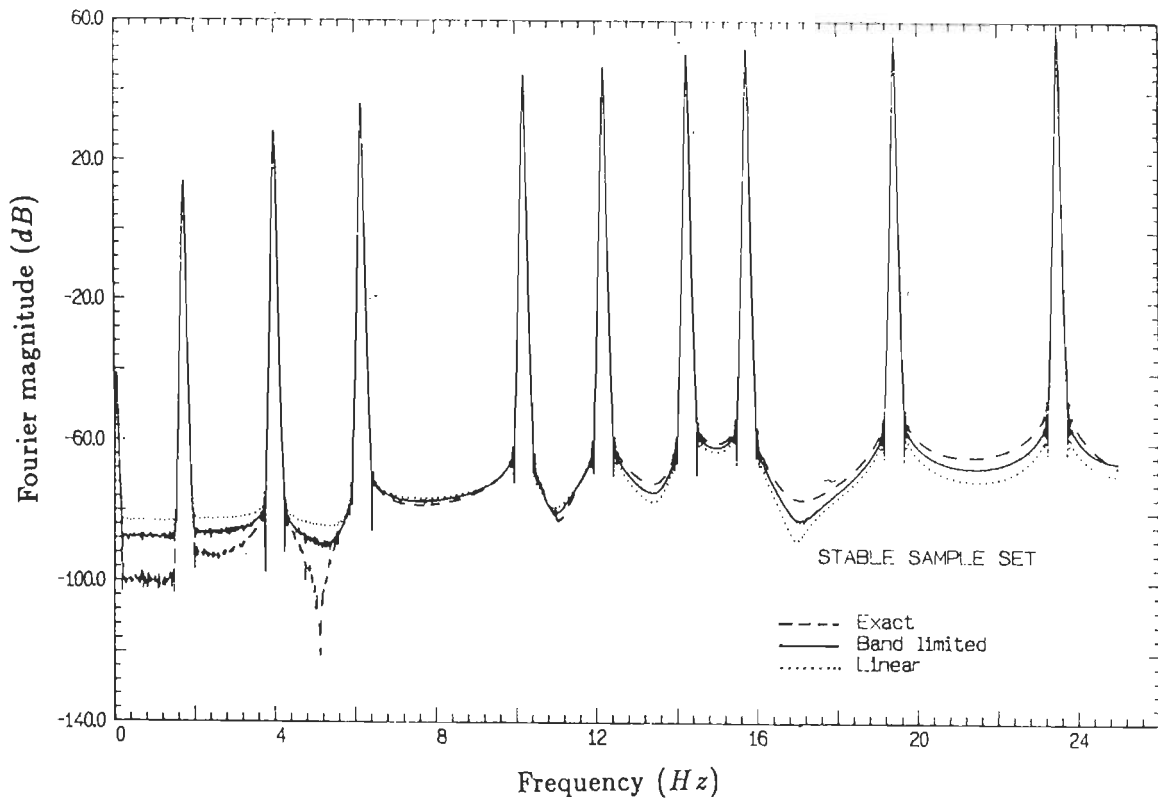


Figure 4.7: Fourier magnitude plots of enveloped history of combination of 10 sine waves recovered through band limited interpolation of nonuniform samples (stable set) alongwith linearly interpolated and exact sine waves.

Table 4.3: Recovery of Enveloped History

Frequency Segment		Median of Fourier Magnitude			Maximum of Fourier Magnitude		
Begin (<i>Hz</i>)	End (<i>Hz</i>)	Exact (<i>dB</i>)	Banded (<i>dB</i>)	Linear (<i>dB</i>)	Exact (<i>dB</i>)	Banded (<i>dB</i>)	Linear (<i>dB</i>)
0.000	0.916	-99.544	-87.564	-82.962	-41.091	-41.124	-41.152
0.928	2.881	-92.769	-86.404	-82.429	14.007	13.991	13.972
2.893	5.090	-87.867	-84.696	-81.598	28.428	28.342	28.341
5.103	8.191	-78.240	-77.046	-76.217	35.959	35.754	35.513
8.203	11.206	-73.858	-73.752	-73.628	44.682	44.115	43.452
11.218	13.232	-67.844	-68.945	-70.052	47.776	46.962	46.010
13.245	15.015	-60.214	-61.425	-62.745	50.506	49.382	48.069
15.027	17.590	-68.121	-70.272	-72.561	52.217	50.839	49.230
17.603	21.460	-63.399	-66.072	-69.000	55.860	53.721	51.229
21.472	25.000	-60.636	-63.402	-67.186	59.171	55.946	52.202

10.05859 *Hz* (to be referred as 10 *Hz*) and 20.11719 *Hz* (to be referred as 20 *Hz*) are recovered. The recovery took 5 iterations for 1 *Hz*, 30 iterations for 10 *Hz* and 38 iterations for 20 *Hz* signals. Figure 4.8 shows Fourier magnitudes of the three signals for 1 *Hz* sinewave, Fig. 4.9 shows the same comparison for 10 *Hz* sinewave and Fig. 4.10 shows it for 20 *Hz* sinewave. Table 4.4 gives maximum Fourier magnitudes of the recovered sine waves along with exact and linearly interpolated waves.

The comparisons yield similar conclusions as in the case of stable sample set. Thus it can be concluded that recovery of signals defined at nonuniform samples through the proposed band limited interpolation gives more accurate results than the linear interpolation for stable as well as random sample sets. However, when stable sample set is not used the convergence takes more number of iterations.

This computer program is then used to recover sine wave of 30 *Hz* which is defined by nonuniform samples with an average sampling rate of 50 *SPS* (less than the Nyquist sampling rate). As expected, the algorithm could not recover the sine wave because the iteration diverged. This is due to the fact that the signals which are sampled at less than Nyquist rate can not be recovered (Marvasti et al. [60]).

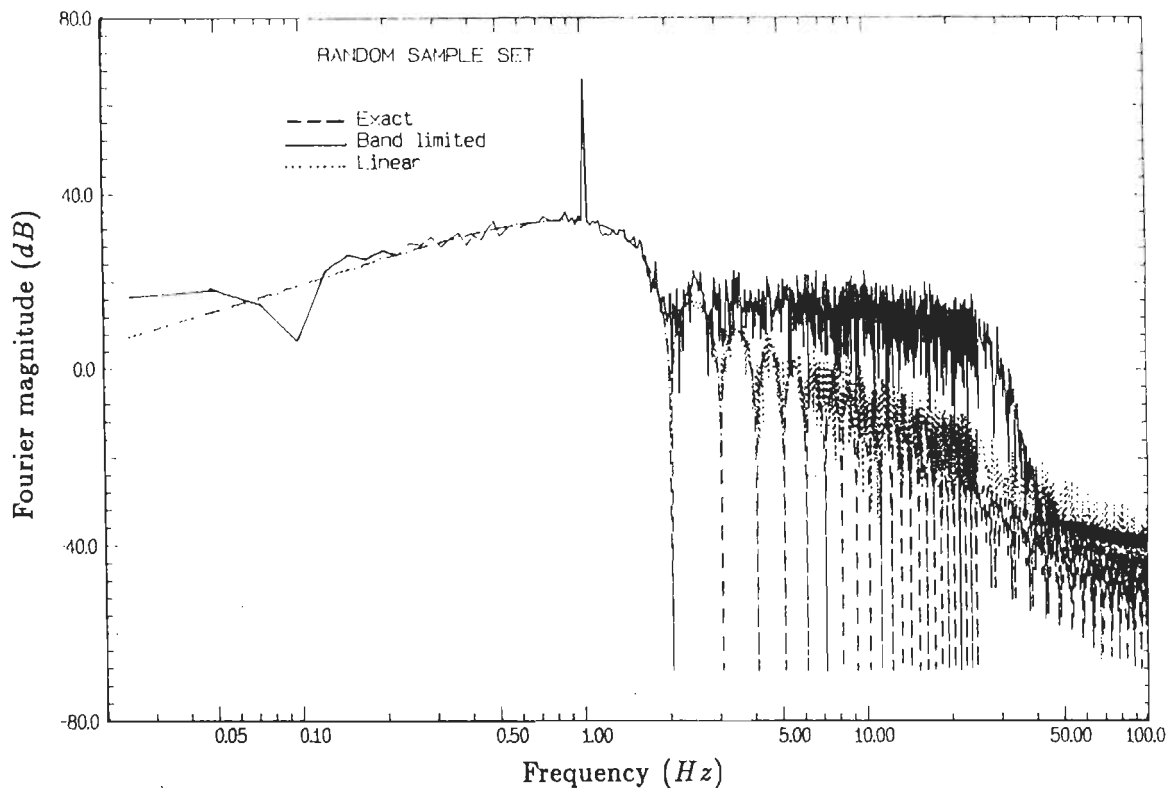


Figure 4.8: Fourier magnitude plots of 1 Hz sine wave recovered through band limited interpolation of nonuniform samples (random set) alongwith linearly interpolated and exact sine wave.

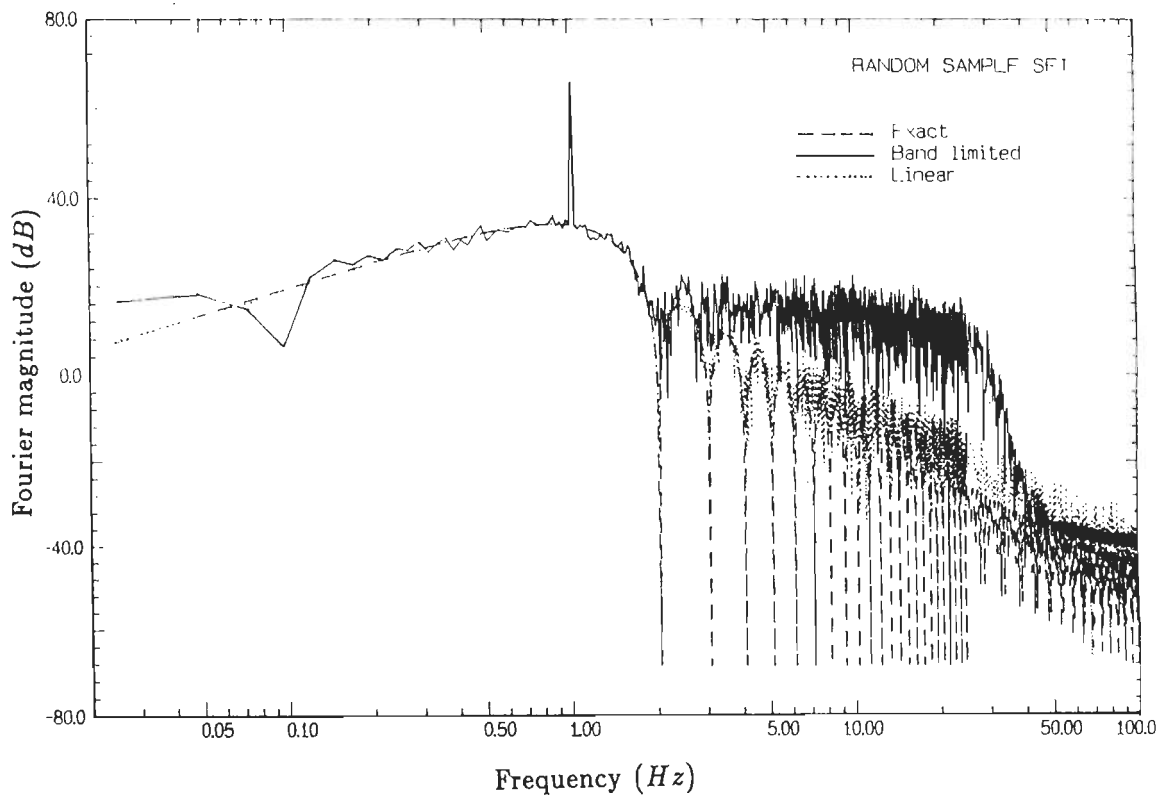


Figure 4.9: Fourier magnitude plots of 10 Hz sine wave recovered through band limited interpolation of nonuniform samples (random set) alongwith linearly interpolated and exact sine wave.

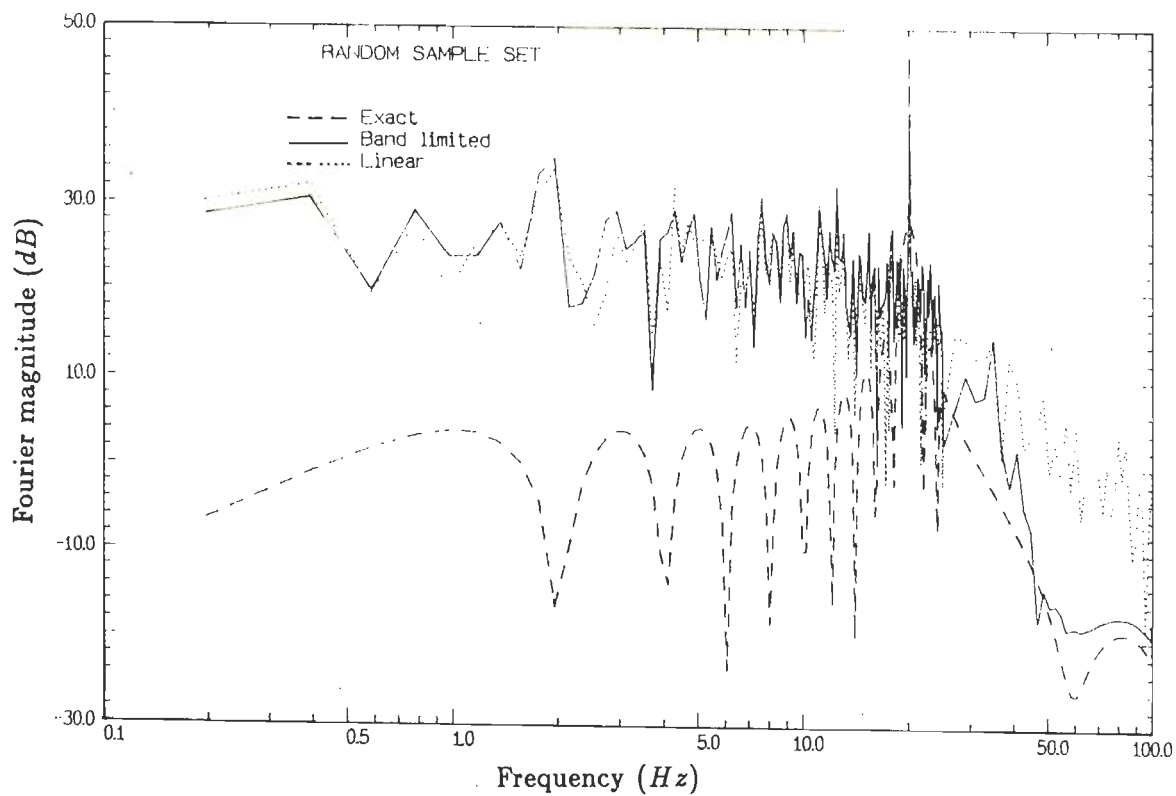


Figure 4.10: Fourier magnitude plots of 20 Hz sine wave recovered through band limited interpolation of nonuniform samples (random set) along with linearly interpolated and exact sine wave.

Table 4.4: Comparison of Results for Recovery of Single Sine Waves from Random Sample Set

Frequency (<i>Hz</i>)	Duration (<i>Sec</i>)	Max. Fourier Magnitude			Max. Fourier Magnitude		
		Exact (<i>cm/sec</i>)	Banded (<i>cm/sec</i>)	Linear (<i>cm/sec</i>)	Exact (<i>dB</i>)	Banded (<i>dB</i>)	Linear (<i>dB</i>)
1.025	39.980	1999.20	1995.30	1989.90	66.02	66.00	65.98
10.059	9.640	482.18	384.95	319.58	53.66	51.71	50.09
20.117	4.625	231.15	136.69	81.66	47.28	42.71	38.24

4.4 Examples on recovery of earthquake data

In this section, recovery of the signal from uncorrected earthquake accelerograms recorded on analog accelerographs and digitized at nonuniform samples on a semi-automatic digitizers is investigated. Uncorrected accelerogram recorded at El Centro (NS component) in Imperial valley earthquake of May 18, 1940, (EERL 70-20, file 1) [105], uncorrected accelerogram recorded at Cholame, Shandon (N05W component) during Parkfield earthquake of June 27, 1966 (EERL 70-21, file 40) [106], uncorrected accelerogram recorded at Taft Lincoln School Tunnel (N21E component) during Kern County California earthquake of July 21, 1952 (EERL 70-20, file 10) [105] and uncorrected accelerogram recorded at Uttarkashi (S72W component) during Uttarkashi earthquake of October 20, 1991 (Data obtained from INSMIN project of Department of Earthquake Engineering, University of Roorkee) are studied in detail. The band limited interpolation to recover the signal at 200 *SPS* is carried out for the nonuniform samples of uncorrected accelerograms of the four earthquakes mentioned above. The cutoff frequency in each case is taken less than half of average sampling rate. Table 4.5 gives details of uncorrected accelerograms, cutoff frequency used for recovery and number of iterations taken for recovery of signal (to get MSE less than 0.01).

Linear interpolation of the nonuniform samples of uncorrected accelerograms is also performed for the four earthquakes to get uniformly spaced data at 200 *SPS*. Fourier magnitudes of linear interpolated data and band limited data obtained through the proposed scheme are determined for the four accelerograms. Figures 4.11 to 4.14 give

Table 4.5: Details of Uncorrected Accelerograms and Recovery of Signals

Earthquake	Uncorrected Data			Recovery of Signal	
	Duration (Sec)	No. of Samples	Av. SPS	Cut off (Hz)	No. of iterations
El Centro	53.732	985	18.33	9.00	24
Parkfield	44.010	1010	22.95	11.00	11
Taft	54.360	958	17.62	8.50	14
Uttarkashi	37.135	2902	78.15	25.00	21

these plots for El Centro, Parkfield, Taft and Uttarkashi earthquakes respectively. These figures show that in passband, frequency contents of band limited data are quite different from those of linearly interpolated data. The studies performed on the recovery of sine waves provide enough reasons to conclude that the Fourier magnitudes in the pass band as recovered by the proposed method are more accurate than the Fourier magnitude of the linearly interpolated data. In stop band (which is nothing but noise), the frequency contents of band limited data as expected are very small whereas linearly interpolated data give substantial amount of high frequency noise. To understand and to illustrate the results in a statistical manner, the passband is divided into 10 equal segments while the stopband and the transition band are divided into six equal segments. For the four earthquakes mentioned earlier in this section, the mean value and coefficient of variation for each segment, for the whole passband and for the entire band upto Nyquist frequency is determined and is given in Tables 4.6 to 4.9. Mean values give a measure for comparison of signal recovered in each segment by the two schemes and coefficient of variation gives a measure of how reliable the observation can be taken as mean (a smaller coefficient indicates that the mean as an estimate of the observed value with high probability).

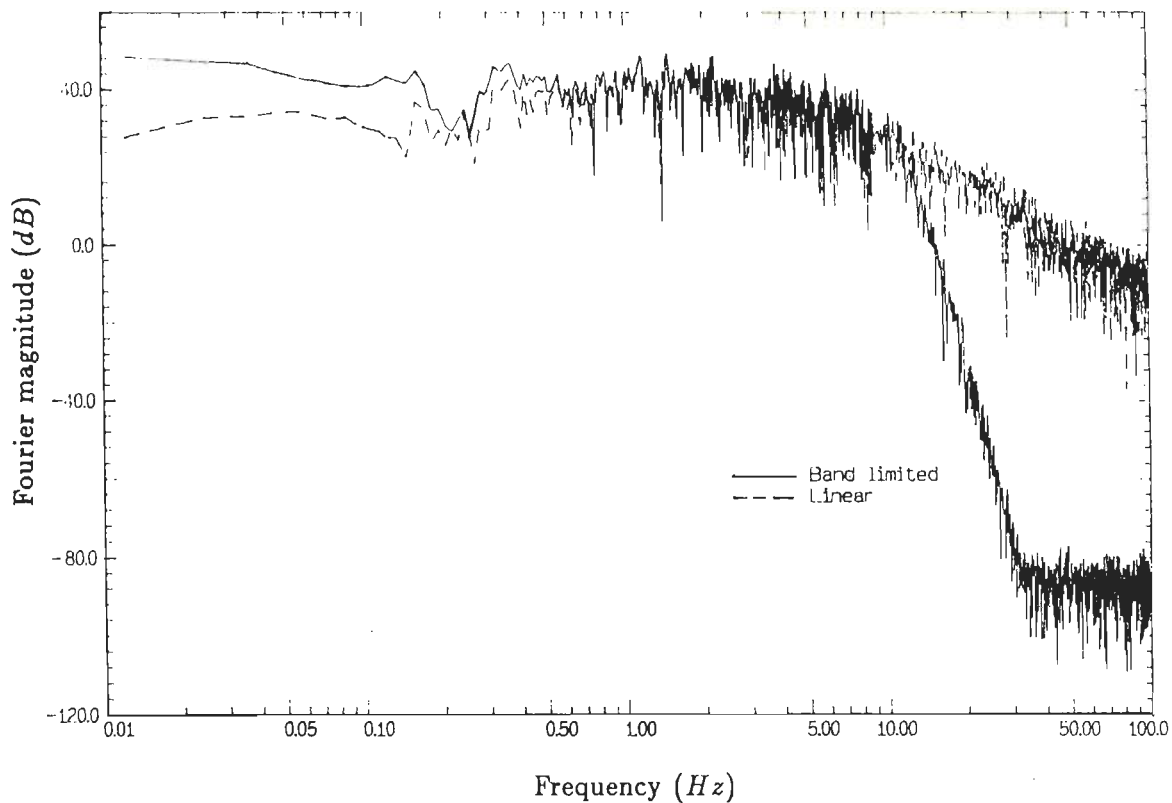


Figure 4.11: Fourier magnitude plots of uncorrected El Centro accelerogram recovered through band limited interpolation along with linearly interpolated.

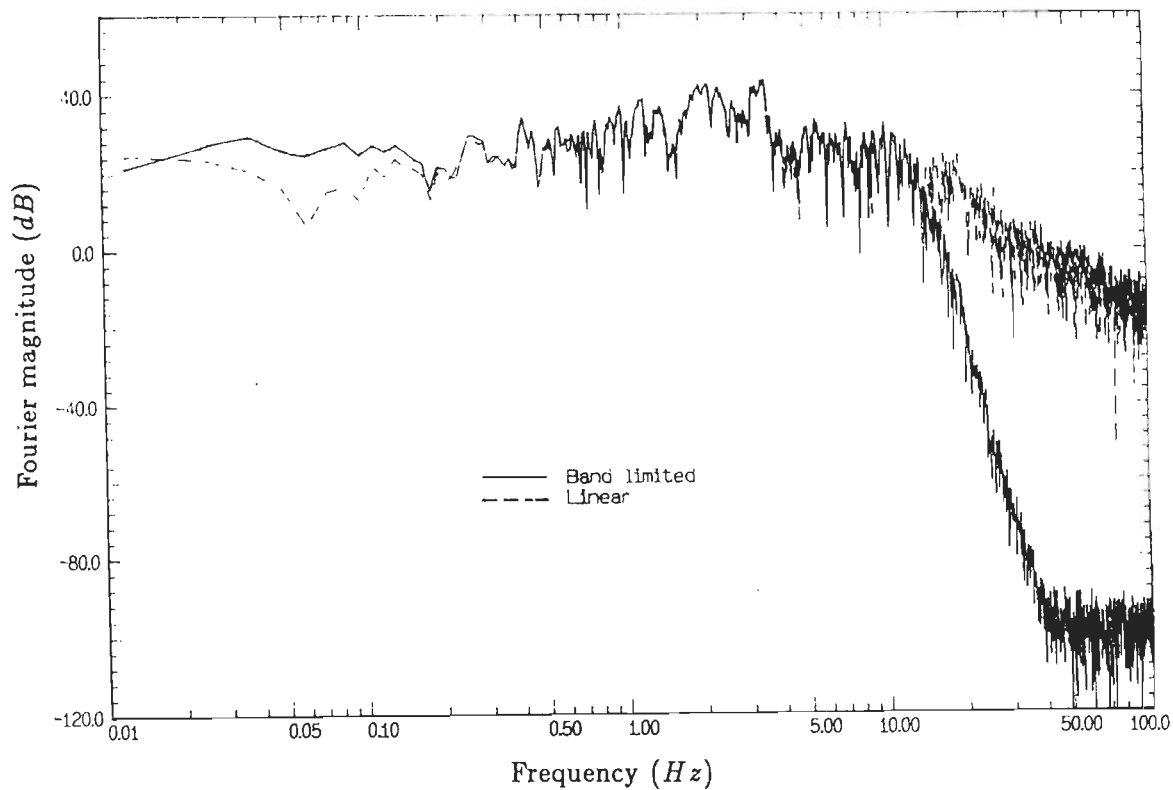


Figure 4.12: Fourier magnitude plots of uncorrected Parkfield accelerogram recovered through band limited interpolation along with linearly interpolated.

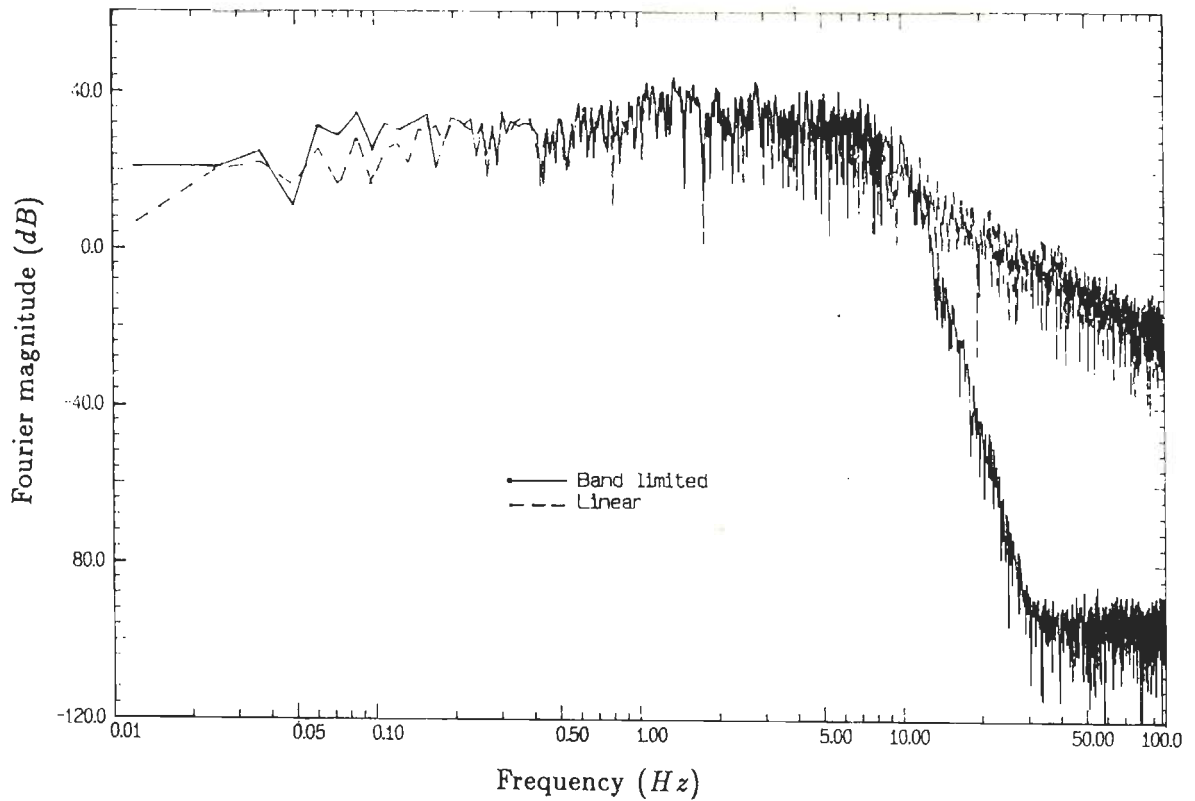


Figure 4.13: Fourier magnitude plots of uncorrected Taft accelerogram recovered through band limited interpolation alongwith linearly interpolated.

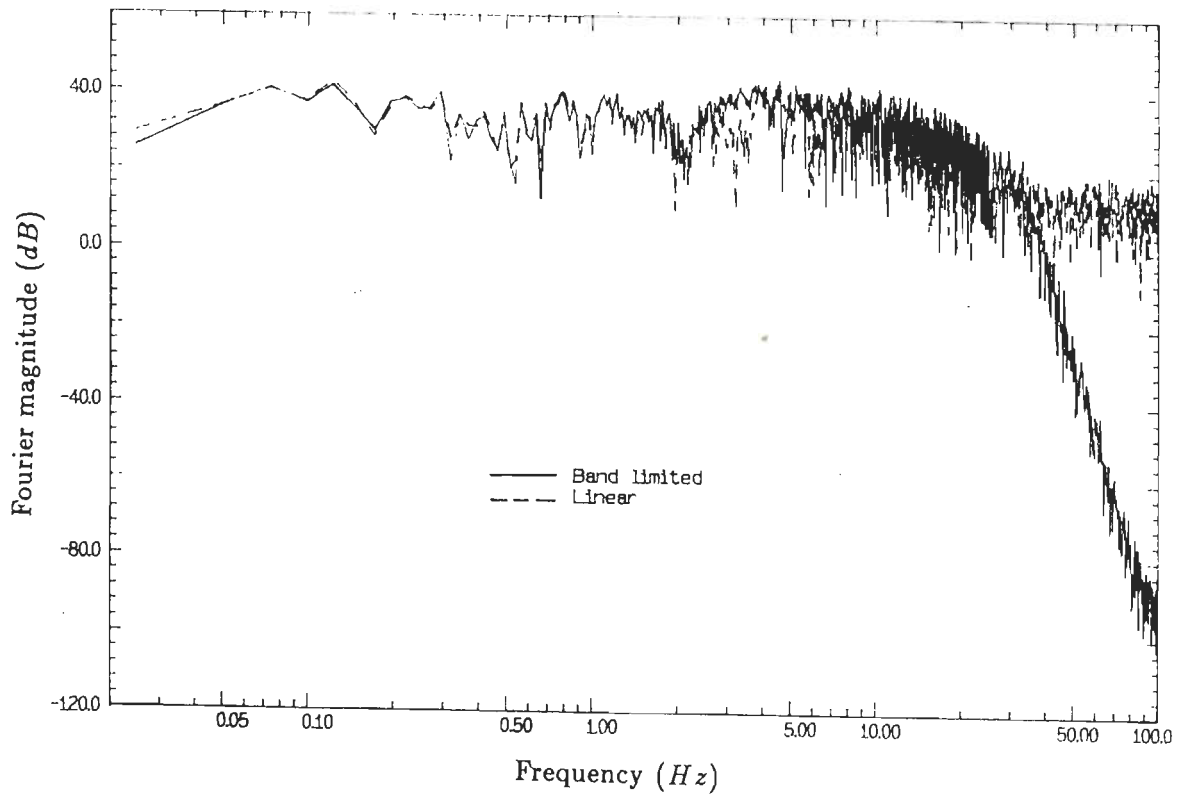


Figure 4.14: Fourier magnitude plots of uncorrected Uttarkashi accelerogram recovered through band limited interpolation alongwith linearly interpolated.

Table 4.6: Recovery of El Centro Accelerogram

Frequency Segment		Mean of Magnitude		Coefficient of variation	
Begin (Hz)	End (Hz)	Linear (dB)	Banded (dB)	Linear	Banded
0.000	0.879	36.512	41.326	0.566	0.457
0.891	1.770	41.725	41.704	0.492	0.484
1.782	2.661	40.868	41.368	0.486	0.472
2.673	3.552	36.558	36.611	0.491	0.492
3.564	4.443	37.763	38.937	0.529	0.538
4.456	5.334	35.500	35.814	0.474	0.435
5.347	6.226	33.387	34.738	0.592	0.657
6.238	7.117	32.679	33.221	0.429	0.490
7.129	8.008	33.058	34.628	0.382	0.430
8.020	8.899	28.076	28.601	0.581	0.578
0.000	8.997	36.384	37.486	0.697	0.681
8.911	24.072	21.442	16.328	0.707	1.891
24.084	39.246	9.356	-68.574	0.661	1.958
39.258	54.419	0.624	-86.313	0.531	0.545
54.431	69.592	-3.116	-86.215	0.517	0.525
69.604	84.766	-6.219	-86.194	0.476	0.529
84.778	99.939	-8.555	-86.394	0.503	0.528
9.009	100.000	9.149	0.568	1.852	5.209
0.000	100.000	18.639	17.747	2.723	3.449

Table 4.7: Recovery of Parkfield Accelerogram

Frequency Segment		Mean of Magnitude		Coefficient of variation	
Begin (Hz)	End (Hz)	Linear (dB)	Banded (dB)	Linear	Banded
0.000	1.086	27.010	27.946	0.635	0.537
1.099	2.185	36.174	36.145	0.541	0.566
2.197	3.284	36.665	36.414	0.442	0.422
3.296	4.382	33.799	33.937	0.933	0.905
4.395	5.481	24.821	26.429	0.495	0.429
5.493	6.580	27.143	27.407	0.352	0.427
6.592	7.678	25.046	25.990	0.395	0.442
7.690	8.777	22.641	23.284	0.432	0.511
8.789	9.875	22.745	24.908	0.401	0.486
9.888	10.974	24.614	25.729	0.567	0.592
0.000	10.999	29.717	30.127	0.969	0.900
10.986	25.806	16.982	9.886	0.728	1.993
25.818	40.637	2.268	-68.492	0.683	1.730
40.649	55.469	-4.086	-97.053	0.488	0.563
55.481	70.300	-7.003	-98.481	0.536	0.548
70.312	85.132	-11.936	-97.133	0.511	0.526
85.144	99.963	-13.407	-97.710	0.543	0.528
11.011	100.00	4.312	-5.816	1.962	5.371
0.000	100.000	13.683	12.016	2.840	3.512

Table 4.8: Recovery of Taft Accelerogram

Frequency Segment		Mean of Magnitude		Coefficient of variation	
Begin (Hz)	End (Hz)	Linear (dB)	Banded (dB)	Linear	Banded
0.000	0.830	30.098	30.494	0.580	0.530
0.842	1.672	37.149	37.418	0.458	0.486
1.685	2.515	33.437	34.152	0.519	0.546
2.527	3.357	35.481	36.001	0.446	0.487
3.369	4.199	31.049	32.549	0.495	0.464
4.211	5.042	31.353	33.843	0.565	0.563
5.054	5.884	29.651	33.353	0.442	0.489
5.896	6.726	28.021	32.045	0.474	0.367
6.738	7.568	28.174	32.362	0.469	0.421
7.581	8.411	22.189	27.712	0.554	0.486
0.000	8.496	31.469	33.321	0.691	0.587
8.423	23.669	11.490	11.315	0.925	2.138
23.682	38.928	-2.278	-81.824	0.586	1.698
38.940	54.187	-9.219	-95.234	0.578	0.538
54.199	69.446	-14.319	-95.584	0.555	0.546
69.458	84.705	-17.562	-95.001	0.518	0.514
84.717	99.963	-19.480	-95.089	0.544	0.546
8.508	100.000	-1.184	-4.559	2.183	5.772
0.000	100.000	12.007	13.034	3.217	3.430

For all the four earthquake accelerograms considered, it can be seen that the energy in band limited interpolation is more than in the linear interpolation in almost all the segments of the pass band as well as in the entire pass band. However, in the stop band, the energy in the band limited interpolation is substantially smaller than that for linear interpolation (in each segment as well as in the entire stop band). This is due to the fact that the linear interpolation introduces energy in the stop band at the cost of reducing energy from the required pass band. These results further confirm the need to perform band limited interpolation.



Table 4.9: Recovery of Uttarkashi Accelerogram

Frequency Segment		Mean of Magnitude		Coefficient of variation	
Begin (Hz)	End (Hz)	Linear (dB)	Banded (dB)	Linear	Banded
0.000	2.466	33.254	33.456	0.558	0.504
2.490	4.956	36.044	38.215	0.587	0.358
4.980	7.446	34.419	36.128	0.563	0.458
7.471	9.937	35.203	33.993	0.507	0.541
9.961	12.427	33.618	32.868	0.590	0.555
12.451	14.917	30.755	31.009	0.524	0.540
14.941	17.407	27.861	30.239	0.560	0.499
17.432	19.897	27.537	23.284	0.475	0.525
19.922	22.388	23.345	24.354	0.533	0.573
22.412	24.878	21.579	23.046	0.541	0.527
0.000	25.000	31.501	32.222	0.766	0.717
24.902	37.378	17.049	17.628	0.537	0.774
37.402	49.878	14.426	-7.155	0.521	1.135
49.902	62.378	13.791	-35.627	0.515	1.060
62.402	74.878	11.577	-59.107	0.522	0.907
74.902	87.378	12.206	-76.690	0.525	0.783
87.402	99.878	12.546	-87.129	0.573	0.593
25.024	100.000	13.777	2.416	0.591	2.764
0.000	100.000	23.323	20.991	1.558	2.030

4.5 Effect of convergence constant (λ) on recovery of earthquake data

In the Eq. 4.4 which really describes the process of iteration, the value of convergence constant (λ) was taken as 1 in the entire work described upto now. Here the effect of using different values of λ is studied. For this purpose the uncorrected El Centro accelerogram is recovered with $\lambda = 1.0$, $\lambda = 0.75$ and $\lambda = 0.5$ and their Fourier magnitudes are studied in detail. Table 4.10 gives details of mean and coefficient of variance of different segments of the band determined for the three values of λ . From this table it is quite clear that there is no difference in obtained data for different values of λ in the pass band and only a marginal difference in data in the stop band.

4.6 Discussion on interpolation of nonuniform samples

1. Based on the Nyquist theorem and definition of stable sampling set, guidelines may be provided to operators performing digitization of accelerograms on semi automatic digitizers as discussed in section 4.1.
2. Some of the published uncorrected accelerograms are reviewed and it is found that several of them have smaller number of sample points than required for recovering frequencies upto 25 Hz. In addition of El Centro, Parkfield and Taft accelerograms which are discussed earlier, in EERL Report no. 73-28 [107] record number 70.009 having duration of about 42 seconds had 1513 sample points for North-South component, 1594 sample points for East-West component and 1805 sample points for Vertical component. Thus, the average sampling rate was about 36 *SPS* for North-South component, 38 *SPS* for East-West component and 43 *SPS* for vertical component and therefore, the largest frequency which can be recovered from such data is 18 Hz for North-South component, 19 Hz for East-West component and 21.5 Hz for vertical component. There are several more similar examples in the published reports of uncorrected accelerograms of this earthquake as well as other earthquakes also. The point that has emerged is that because of prevalent practice of performing linear interpolation, the operators who digitize the records, consider it appropriate to pick only peaks and troughs of the record with few additional points in between which is likely to yield only limited information.

Table 4.10: Recovery of El Centro Accelerogram with different values of λ

Frequency Segment		Mean of Magnitude			Coefficient of variation		
Begin (Hz)	End (Hz)	$\lambda = 0.5$ (dB)	$\lambda = 0.75$ (dB)	$\lambda = 1.0$ (dB)	$\lambda = 0.5$	$\lambda = 0.75$	$\lambda = 1.0$
0.000	0.879	41.326	41.326	41.326	0.457	0.457	0.457
0.891	1.770	41.704	41.704	41.704	0.484	0.484	0.484
1.782	2.661	41.368	41.368	41.368	0.472	0.472	0.472
2.673	3.552	36.611	36.611	36.611	0.492	0.492	0.492
3.564	4.443	38.937	38.937	38.937	0.538	0.538	0.538
4.456	5.334	35.814	35.814	35.814	0.435	0.435	0.435
5.347	6.226	34.738	34.738	34.738	0.657	0.657	0.657
6.238	7.117	33.221	33.221	33.221	0.490	0.490	0.490
7.129	8.008	34.628	34.628	34.628	0.430	0.430	0.430
8.020	8.899	28.601	28.601	28.601	0.578	0.578	0.578
0.000	8.997	37.486	37.486	37.486	0.681	0.681	0.681
8.911	24.072	14.532	15.626	16.328	2.071	1.964	1.891
24.084	39.246	-74.243	-70.948	-68.574	1.954	1.956	1.958
39.258	54.419	-91.895	-88.511	-86.313	0.528	0.521	0.531
54.431	69.592	-91.916	-88.704	-86.215	0.535	0.534	0.525
69.604	84.766	-91.810	-88.522	-86.194	0.535	0.531	0.529
84.778	99.939	-91.989	-88.710	-86.394	0.535	0.523	0.528
9.009	100.000	-1.276	-0.151	0.568	5.628	5.378	5.209
0.000	100.000	17.535	17.660	17.747	3.524	3.480	3.449

3. An interactive computer program is developed to recover the band limited signal from nonuniform samples through performing iteration on Eq. 4.4.
4. The software is used to recover single sine waves of 1 Hz, 10 Hz and 20 Hz signal defined with average sampling rate of 50 SPS at nonuniform instants. Two cases of nonuniform samples are taken *viz.* nonuniform samples with stable sampling set and nonuniform samples at random instants. Signals consisting of combination of 10 sine waves of constant amplitude as well as combination of 10 sine waves of varying amplitudes with enveloped history is recovered. A comparison of signals recovered with proposed method and linear interpolation with exact signal indicate drawbacks of linear interpolation.
5. The software is then used to recover earthquake accelerograms digitized at random interval and the results were compared with linearly interpolated sequence in frequency domain. The comparison showed that distortions are more in linearly interpolated signals.
6. The paper speed of accelerograph becomes important in semiautomatic digitizers. A greater paper speed will make it easier for the operator to perform digitization with greater average sampling rate. For example the paper speed of 1 cm/sec available in some of commonly used accelerographs is not enough as digitizing average of 50 points in 1 cm is not an easy task. In this regard RESA V is better placed as it has a paper speed of 2 cm/sec.
7. Semiautomatic digitizers are nowadays getting replaced by automatic scanners which automatically perform digitization at constant time interval at sufficiently large sampling rate. However, the fact remains that large number of accelerograms recorded in the past have been digitized on semiautomatic digitizers and in India semiautomatic digitizers are still commonly used.

Chapter 5

Band limited interpolation of uniform samples

Most of the corrected accelerograms incorporate frequencies upto 25 Hz which can be obtained if the data is provided to the users at a sampling rate of 50 samples per second (*SPS*). This is the reason why most of the accelerograms are processed and made available at 50 *SPS* or at a duration of every 0.02 second. However, this time step may not be sufficiently small for seismic analysis applications. For example, if seismic analysis of structures is done using direct integration methods in time domain, it may require a time step which is much smaller than the sampling interval at which the accelerogram has been provided. Another example is for nonlinear problems where it often becomes necessary to iterate within a time step to obtain a converged solution and it has been felt that it is better to reduce the time step rather than pushing iteration of nonlinear quantities within a time increment (Zienkiewicz *et al.* [104]). Similarly there can be other situations where the requirements of the time step of input accelerogram may be smaller than the interval at which the accelerograms are provided. This necessitates the need for interpolating the digital data of accelerogram, which is conventionally done by linear interpolation between samples. However, as the original digital accelerogram is essentially a band limited signal, linear interpolation modifies the frequency content of the data and introduces spurious high frequency components at the cost of reducing power in the low frequency range. High frequency insertion in input acceleration history, excites high frequency modes of the structure, thereby yielding a jittery response. This part of the work highlights the inadequacy of linear interpolation of uniform samples and suggests the use of an interpolation technique by virtue of which the band limited property is maintained. A part of this study was published also [7].

Band limited interpolation is done by zero packing the data to an extent required for analysis. This zero packed accelerogram is low-passed to recover the base band signal of interest and eliminate the unwanted image of components generated by sampling rate expander. Thus, the proposed interpolation technique maintains the band limited property in the interpolated data.

Some illustrative examples are taken in which single sine waves defined at equal interval are interpolated by the proposed method as well as through linear interpolation and are compared with exact sine waves in time as well as in frequency domain. The comparison shows the efficacy of the proposed band limited interpolation of uniform samples over the linear interpolation. Similar effects in interpolation of some of the available accelerogram are also demonstrated.

Simple classical systems are analysed for illustrating the usefulness of the scheme. These are analysed using both conventional linear interpolation and with the aid of the proposed band limited interpolation technique.

5.1 The need to interpolate

There can be several situations where the given design accelerogram may be required to be interpolated. However, here details of requirements of seismic analysis using direct integration schemes have been discussed. These schemes employ a ground acceleration history that is either recorded and processed or is synthetically generated. In either case these are digital values at equally spaced discrete time intervals. Most of the recorded corrected accelerograms are available at a sampling interval of 0.02 *sec*, which amounts to a Nyquist frequency of 25 *Hz*. In other words the highest frequency content of the accelerogram gets decided by the sampling interval. Synthetic accelerograms are often generated at 100 *SPS*, but are normally provided to the analyst at a sampling interval of 0.02 *sec*. This again implies a Nyquist frequency of 25 *Hz*.

In case of direct integration schemes and for conditionally stable schemes, stability considerations may require a time step $\Delta t \leq T_{min}/\pi$, where T_{min} is the smallest natural period of the structure (Owen and Hinton [73]). Unconditionally stable implicit schemes on the other hand may require a small Δt from the point of view of accuracy. It has been suggested that results are accurate when the time step is limited to $\Delta t/T \leq 0.01$ (Bathe and Wilson [8]; Owen and Hinton [73]), where T is the fundamental period of the structure. For the Newmark method ($\beta = 0.25$ and $\gamma = 0.5$) it has been shown (Bathe and Wilson [8]) that the period elongation for an undamped single

degree freedom system is less than 3% for $\Delta t/T \leq 0.1$ and the method does not decay response amplitudes.

The point that emerges from the above discussion is that the sampling interval at which the input accelerogram is available, may, in fact, be too large for direct integration.

5.2 Interpolation schemes

The present practice is to assume that ground acceleration varies linearly in the time interval. Here it is shown that linear interpolation introduces a high frequency content which is absent in the original record and thus yields a response with spurious high frequency jitters.

Let the earthquake accelerogram data, which is a band limited sequence of samples be available at interval T_1 . The fundamental frequency interval of this band is $f_s = 1/T_1$. For some reason it is required to interpolate the data to a smaller sampling interval $T_2 < T_1$.

The linear and band limited interpolation schemes are considered in detail in reference to the problem in the following subsections.

5.2.1 Linear Interpolation

The impulse response function $h(n)$ of a linear interpolation filter can be written as

$$h(n) = \begin{cases} 1 - \frac{|n|}{I} & ; n \in [-I, I] \\ 0 & ; \text{otherwise} \end{cases} \quad (5.1)$$

where I is a factor by which sampling rate has been increased. This function has a triangular shape and the frequency response can be obtained through Fourier transformation as

$$H(e^{j\omega}) = \frac{1}{I} \left(\frac{\sin \frac{\omega I}{2}}{\sin \frac{\omega}{2}} \right)^2 \quad (5.2)$$

The log magnitude of the frequency response for $I = 10$ is shown in Fig. 5.1. It can be seen that its peak side lobe attenuates only to 26 dB relative to the pass band. Consequently unless the original record is highly band limited (*i.e.* to a band $\ll 1/2IT_1$) it will fail to attenuate replicates of the spectrum and thus introduce jitters in the solution.

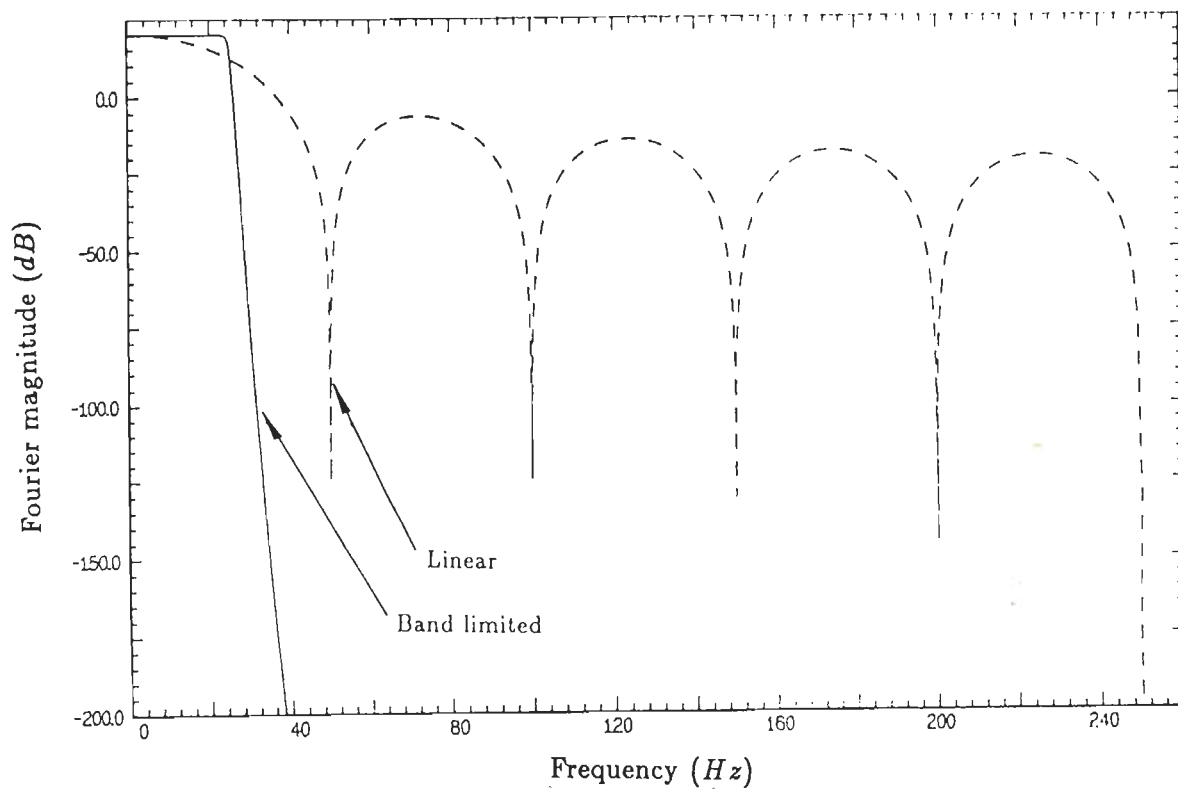


Figure 5.1: Frequency response of band limited and linear interpolation (initial sampling interval = 0.02 sec, interpolated sampling interval = 0.002 sec)

5.2.2 Band Limited Interpolation

Let the original accelerogram sampled at T_1 be $x(\cdot)$ and the interpolated accelerogram, interpolated by a factor I , which shall be assumed to be an integer, be $y(\cdot)$. If $h(\cdot)$ is the finite impulse response of the filter required for interpolation then the interpolated signal

$$y(n) = \sum_k h((k + \delta_n)T_1)x([n/I] - k) \quad (5.3)$$

where

$$[n/I] = \text{int}(n/I) \quad \text{i.e. integer part of } n/I$$

and

$$\delta_n = n/I - [n/I] \quad ; \quad \delta_n \in [0, 1]$$

From equation 5.3, it is clear that evaluation of $y(n)$ requires filter $h(\cdot)$ sampled at fractional delays of $\delta_n T_1$ from the sample. This makes the band limited interpolating filter a time varying system. However, the required time varying $h(\cdot)$ filter can be realized by I time invariant filters that are subsets of $h(\cdot)$. These time invariant filters operate at a low sampling rate and are known as polyphase filters (Bellenger *et al.* [12]). Equation 5.3 shows that the input sample is at time $[n/I] - I$ and the output at sample time n . The output can be written as

$$y(n) = \sum_k p_n(k)x([n/I] - k) \quad (5.4)$$

where $p_n(k) = h((k + \delta_n)T_1)$. Note $p_n(k)$ is periodic in n with period I . The term $[n/I]$ increases by one for every I samples. The $x(\cdot)$ enters at low sample rate f_s and $y(\cdot)$ is evaluated at sample rate If_s . Equation 5.4 can be written in polyphase structure as

$$y(nI + m) = \sum_k p_m(k)x(n - k) \quad (5.5)$$

where

$$p_m(k) = h(kI + m) \quad m = 0, 1, \dots, I - 1$$

If the lowpass filter $h(\cdot)$ has N taps and N is divisible by I , then each of the I polyphase subfilters will be identical in structure with N/I taps. Each input $x(\cdot)$ will generate one output for each of the polyphase subfilters as indicated by equation 5.5.

Since in our case the interpolation is not an on-line process, the interpolation becomes simpler and perhaps easier to understand. The interpolation is done by inserting $I - 1$ zeros in between two points. This results in the decrease of sampling interval to the desired value. This redefining of sample rate introduces I replicates of the spectrum

in the band of frequencies defined at this higher rate but the gain of the spectrum gets reduced by a factor I . However, the spectrum remains exactly periodic in $1/T_1$. The resulting data is low passed to eliminate the replicated copies with the gain of the filter in the pass band being taken as I . The task of this lowpass filter is to reject the spectral copies that occur at integer multiples ($< I$) of the input sampling frequency. Figure 5.1 compares frequency response of band limited interpolation and linear interpolation.

To further explain the whole process, let Fig. 5.2 be the Fourier magnitude plot of the given sequence having a sampling period of T_1 . Let it be assumed that this sampling period is required to be reduced by a factor of 4. Then, 3 zeros are required to be inserted between each sampling point of the given sequence. This zero packed data will now have a sampling period of T_2 which is equal to $\frac{T_1}{4}$. If Fourier magnitude plot of this zero packed data is taken then it will have 4 replicates of Fig. 5.2 and will look like Fig. 5.3. It may be noted that the Fourier magnitudes of the replicates will be exactly one fourth of the Fourier magnitude of Fig. 5.2. A low pass filtering with a cut off frequency of $\frac{1}{2T_1}$ and with gain of 4 in the pass band, rejects the replicates and preserves the frequency contents of the original data after the interpolation.

In such a situation any low pass filter with a cut off frequency equal to Nyquist frequency of original sampling rate can be used to reject the replicates of spectrum. However, an optimal Finite Impulse Response (FIR) filter can also be designed and a realisation algorithm can be made using the fact that out of I samples of zero packed data only one sample is nonzero to reduce computation.

The length N of such FIR lowpass filter can be chosen using the relation for transition band width of FIR antialiasing (Elliot [31]) filter as

$$\Delta f = K(A) \frac{f_s}{N} \quad (5.6)$$

where A is the minimum stopband attenuation and $K(A)$ is an attenuation related scale factor. $K(A)$ is bounded by

$$\frac{-20 \log(A)}{25} < K(A) < \frac{-20 \log(A)}{20} \quad (5.7)$$

From experience in filter design, the new two sided analysis band width is

$$2f_p = \frac{\alpha f_s}{I} \quad (5.8)$$

where α is a factor for alias free band width. The sampling rate, f_s required to obtain an alias free pass band down to a level $1/A$ satisfies the Nyquist theorem given by

$$f_s/I = 2f_p + \Delta f \quad (5.9)$$

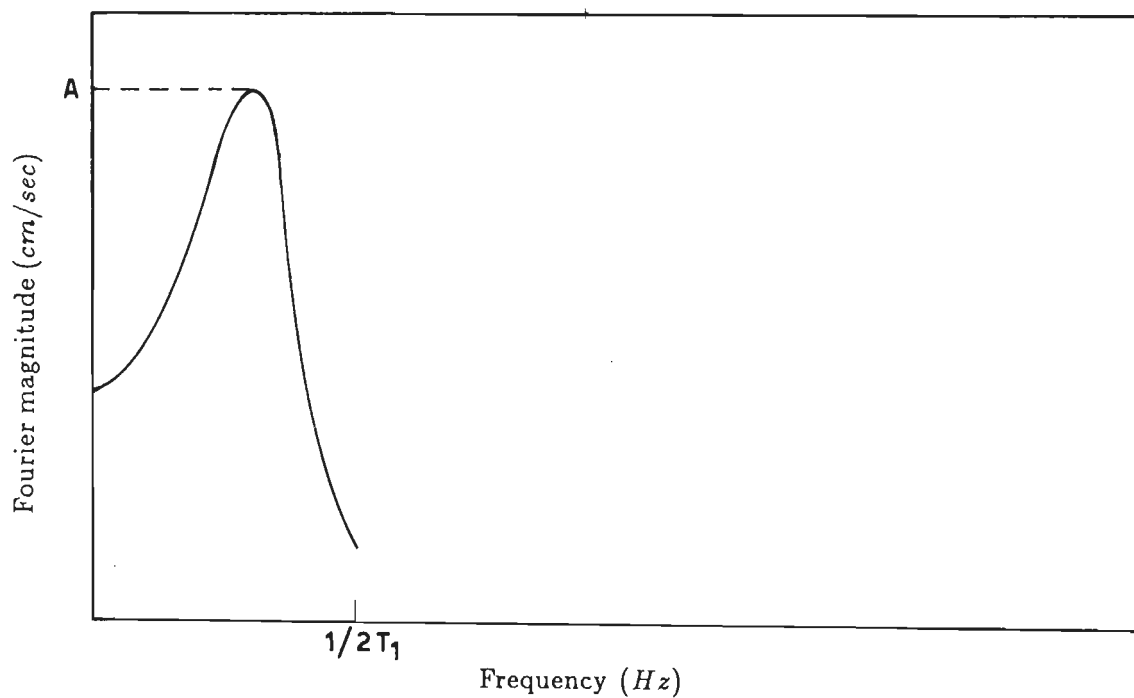


Figure 5.2: Fourier magnitude plot of an arbitrary sequence with sampling interval T_1

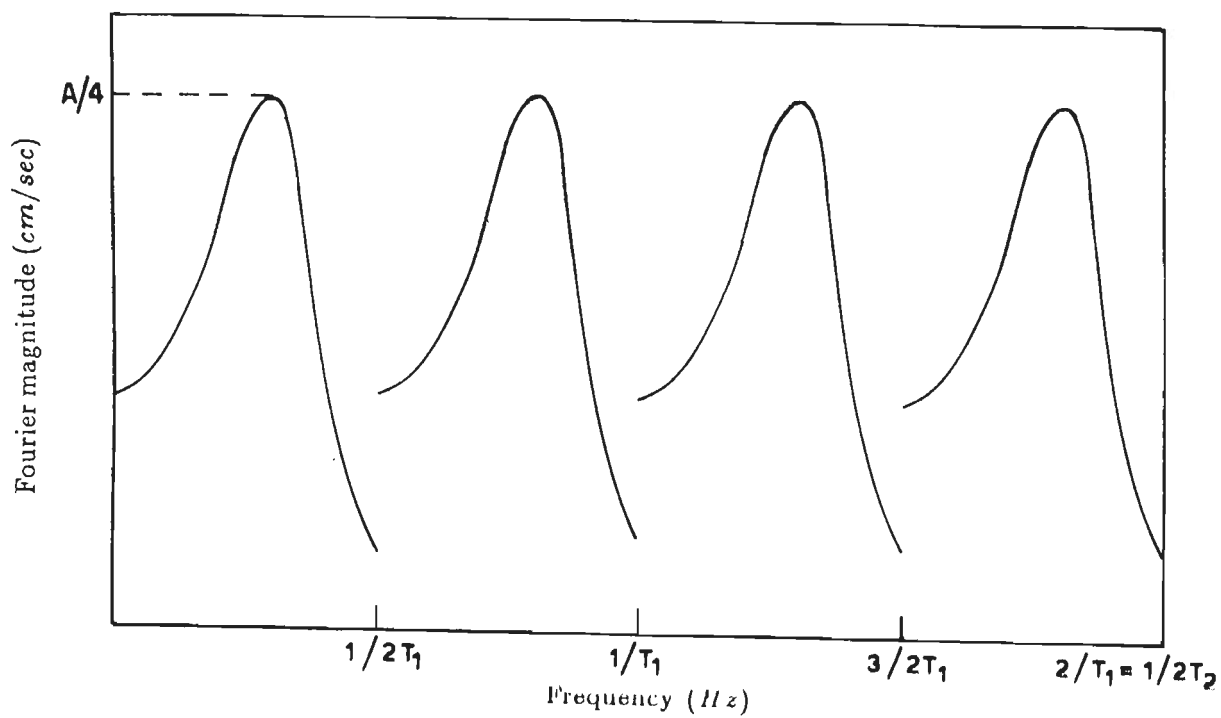


Figure 5.3: Fourier magnitude plot of zero packed sequence of Figure 5.2 for $I = 4$

By using equations 5.6 and 5.8 into 5.9 gives

$$N = I \frac{K(A)}{(1 - \alpha)} \quad (5.10)$$

Since for every I samples of zero packed data passed through the filter only one sample is nonzero, it reduces computation to N/I multiplications and additions per output data point. The impulse response function of the lowpass filter is partitioned into a collection of subfilters known as polyphase filters (Bellenger *et al.* [12]). The subset of filter coefficient needed to compute a given output point are those that intersect the nonzero data points in the span of filter's total impulse response. The nonzero data points avail different subset of the filter's impulse response needed to compute an output sample. In general identical structure of the subsets lead to N/I subsets. Oetken *et al.* [67] also give design of such an optimal filter for interpolation.

5.3 Details of band limited interpolation

The theory discussed in the earlier section is used to construct an algorithm for performing band limited interpolation of accelerograms to increase their sampling rate by integer multiples. The following are the steps of the algorithm:

1. Read number of data points (N_1) and sampling interval (T_1) of the original sequence and then read values of each sample.
2. Read the integer value (I) by which the sampling rate is required to be increased.
3. Insert $I - 1$ zeros between each of the two sample points of step 1. Now the total number of data points becomes N_2 which is

$$N_2 = (N_1 - 1) * I + 1 \quad (5.11)$$

and the duration between each sample becomes T_2 which is

$$T_2 = \frac{T_1}{I} \quad (5.12)$$

4. This zero packed data is then low passed with a cut off frequency equal to Nyquist frequency of original data of step 1 which is $(\frac{1}{2T_1})$. The gain of the filter is set as I in the pass band instead unity in the usual case. This low passed data is the desired interpolated data at a sampling interval of T_2 .

As it was pointed out in the earlier section, low pass filtering can be performed in the usual manner or an optimal FIR filter can be designed to reduce computation. In this work first a computer program given by Oetken *et al.* [67] is used to design an optimal filter to perform the low pass operation.

Next the operation of low pass filtering is attempted by using the transfer function $|H(j\omega)|^2$ of Butterworth filter, which is given by

$$|H(j\omega)|^2 = K \left(\frac{1}{1 - \left(\frac{\omega}{\omega_c}\right)^{2n}} \right) \quad (5.13)$$

where K is the gain of the filter, ω is the frequency at which the function is determined, ω_c is the cutoff frequency and n is the order of filter.

The process of low pass filtering is performed by convolution in the frequency domain, the details of which have already been discussed in Chapter 4 section 4.2.

It was found that although smaller computation time is required for the low pass operation by FIR optimal filter, the results obtained by both the methods are same for all practical purposes. Since in this work frequency domain filtering using $|H(j\omega)|^2$ of Butterworth filter has been very often used, it is decided to use the same in this part of the work also. This amounts to a slight compromise on the efficiency of the algorithm for the sake of using the same process of filtering and making the method simpler and perhaps easier to understand.

5.4 Illustrative examples on interpolation

5.4.1 Sine Waves

To understand the process of band limited interpolation of uniform samples, single sine waves of 1.02539 Hz (to be referred as 1 Hz), 10.05859 Hz (to be referred as 10 Hz) and 20.11719 Hz (to be referred as 20 Hz) are taken. In each case the sine waves are initially defined at a constant interval of 0.02 seconds (50 SPS). These sequences are then interpolated by the proposed method to get the sequences of the three single sine waves at an interval of 0.005 seconds (200 SPS). A linear interpolation of the 50 SPS data are also done for the three cases. Figure 5.4 gives time history of 200 SPS sequence of 20 Hz signal obtained through linear interpolation and proposed band limited interpolation alongwith exact sine wave. The plot clearly indicates closeness of the signal obtained through proposed method in comparison to linear interpolation. Figures 5.5, 5.6 and 5.7 gives plots of Fourier

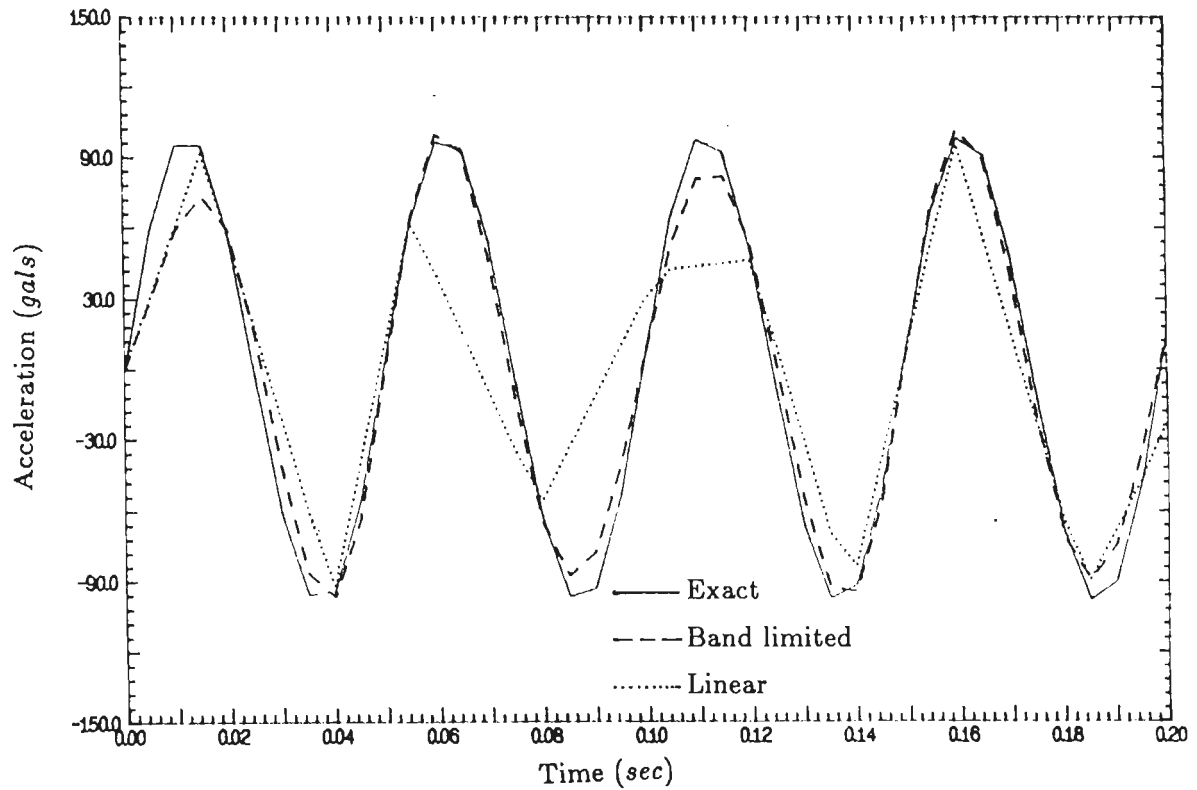


Figure 5.4: Time history of band limited interpolated 20 Hz signal along with linearly interpolated and exact sine wave.

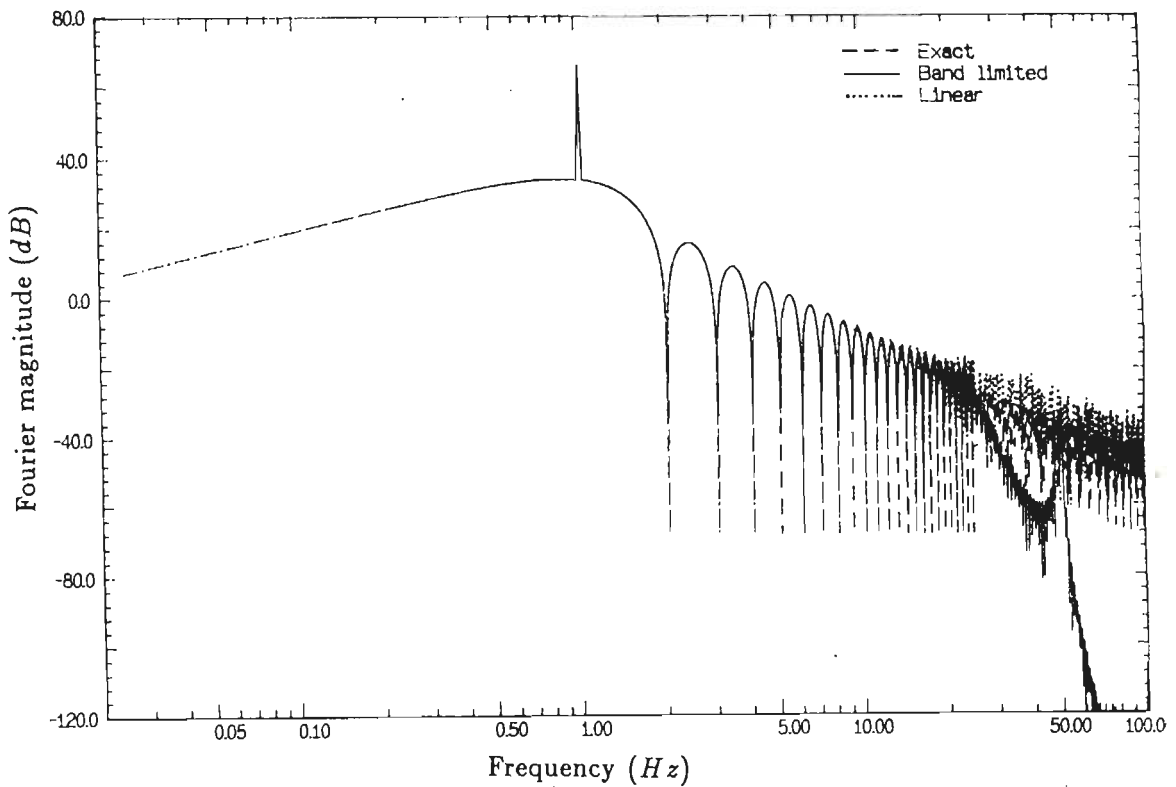


Figure 5.5: Fourier magnitude plots of 1 Hz sine wave obtained through band limited interpolation ($I = 4$) of uniform samples along with linearly interpolated and exact sine wave.

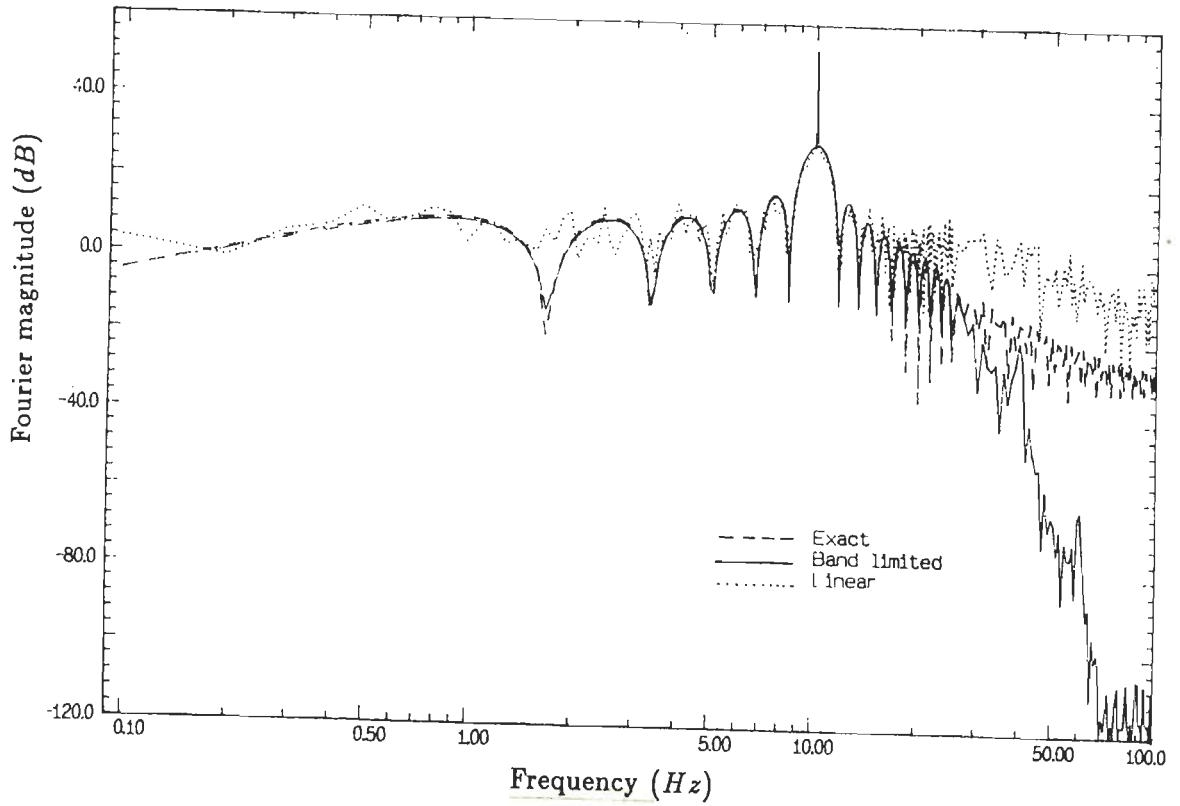


Figure 5.6: Fourier magnitude plots of 10 Hz sine wave obtained through band limited interpolation ($I = 4$) of uniform samples alongwith linearly interpolated and exact sine wave.

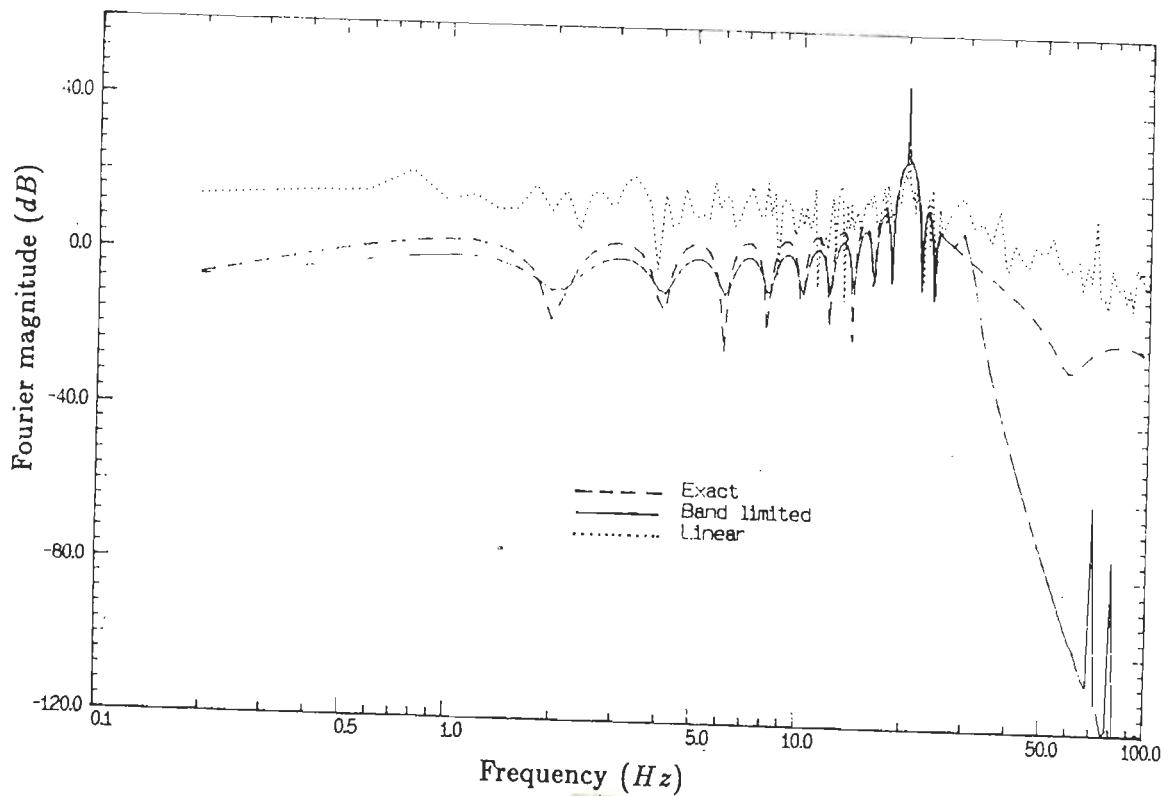


Figure 5.7: Fourier magnitude plots of 20 Hz sine wave obtained through band limited interpolation ($I = 4$) of uniform samples alongwith linearly interpolated and exact sine wave.

magnitudes determined for the 200 *SPS* data for 1 *Hz*, 10 *Hz* and 20 *Hz* signal in which exact, band limited and linearly interpolated Fourier magnitudes in *dB* are plotted one over the other. These figures highlight the high frequency jitters and the low frequency noise introduced in the linear interpolation. Table 5.1 gives maximum value of the spike of the Fourier magnitudes for the three cases in *cm/sec* and in *dB*. These values again prove that linear interpolation introduces high frequency noise in the stop band at the cost of reducing energy from the required pass band whereas band limited interpolation maintains the frequency contents of the original data.

Table 5.1: Comparison of Results of Interpolation of Single Sine Waves

Frequency (<i>Hz</i>)	Duration (<i>Sec</i>)	Max. Fourier Magnitude			Max. Fourier Magnitude		
		Exact (<i>cm/sec</i>)	Banded (<i>cm/sec</i>)	Linear (<i>cm/sec</i>)	Exact (<i>dB</i>)	Banded (<i>dB</i>)	Linear (<i>dB</i>)
1.025	39.98	1999.24	1999.24	1996.14	66.02	66.02	66.00
10.059	9.64	482.18	482.11	413.83	53.66	53.66	52.34
20.117	4.62	231.15	214.82	124.36	47.28	46.64	41.89

5.4.2 Earthquake accelerograms

An actual corrected earthquake accelerogram obtained from Parkfield earthquake of June 27, 1966 recorded in Cholame, Shandon (California Institute of Technology record no. IIB034, component N85E) is studied here. The above record is available at a sampling interval of 0.02 *second*. The Fourier magnitude spectrum of this record is given in Fig. 5.8 which is defined upto 25 *Hz* (half of the sampling rate). The sampling interval of this record is reduced from the given 0.02 *second* to 0.005 *second* ($I = 4$) by the proposed band limited interpolation as well as by linear interpolation. Figure 5.9 shows the variation of Fourier magnitudes of the interpolated accelerograms. It can be seen that the linearly interpolated record contains considerable spurious high frequency components. For the sake of statistical comparison between the two interpolated signals, the entire band upto the Nyquist frequency of the interpolated signal (100 *Hz* in this case) is divided into sixteen segments. The pass band upto 25 *Hz* is divided into ten equal segments and the remaining transition and stop bands are divided into six equal segments. Mean and coefficient of variation of each of the segment, of pass band, of stop band and of the entire band is determined and is given in Table 5.2.

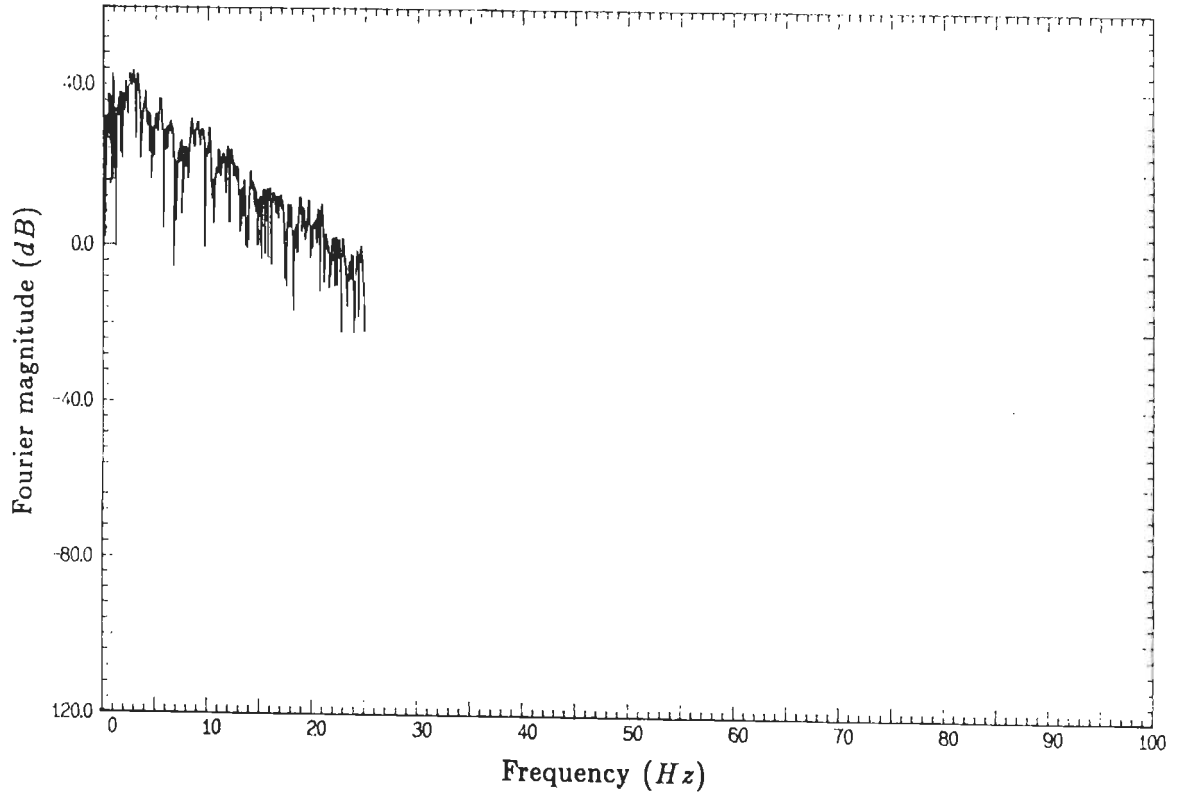


Figure 5.8: Fourier magnitude plot of original corrected Parkfield accelerogram defined at 50 SPS.

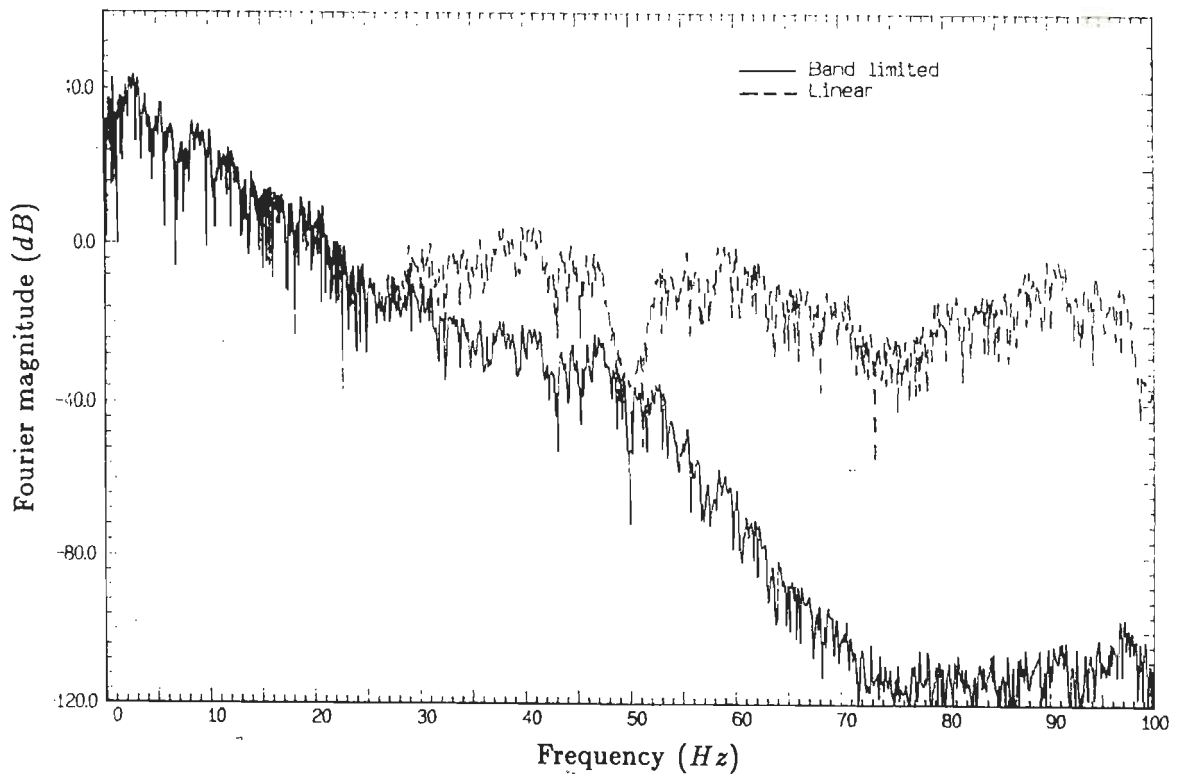


Figure 5.9: Fourier magnitude plot of Parkfield accelerogram using band limited and linear interpolation

The table indicates the distortion caused by linear interpolation which exists in the pass band and is substantially high in the stop band.

Table 5.2: Interpolation of Parkfield Accelerogram

Frequency Segment		Mean of Magnitude		Coefficient of variation	
Begin (Hz)	End (Hz)	Linear (dB)	Banded (dB)	Linear	Banded
0.000	2.478	34.063	34.092	0.622	0.623
2.490	4.968	35.742	35.867	0.665	0.661
4.980	7.458	27.533	27.914	0.668	0.661
7.471	9.949	25.020	25.863	0.452	0.454
9.961	12.439	19.820	21.180	0.513	0.502
12.451	14.929	11.551	13.552	0.551	0.535
14.941	17.419	7.077	9.929	0.411	0.407
17.432	19.910	2.228	5.905	0.483	0.485
19.922	22.400	-2.361	1.631	0.570	0.574
22.412	24.890	-10.873	-7.949	0.496	0.530
0.000	25.000	24.649	25.079	1.585	1.515
24.902	37.402	-7.129	-17.364	0.569	0.701
37.415	49.915	-4.805	-28.243	0.786	0.660
49.927	62.427	-9.366	-48.726	0.712	1.331
62.439	74.939	-16.918	-92.909	0.708	1.375
74.951	87.451	-18.897	-112.927	0.652	0.530
87.463	99.963	-13.275	-107.029	0.733	0.647
25.012	100.000	-10.317	-30.599	0.975	2.153
0.000	100.000	13.064	13.083	3.413	3.471

5.5 Effect of interpolation on SDF systems

Here some examples are considered to illustrate the points that have been made. The examples considered are of elastic damped and undamped single degree freedom (*SDF*) systems subjected to base excitation in the form of an acceleration time history. Direct integration is carried out using Newmark method (Bathe and Wilson [8]) with constants $\beta = 0.25$ and $\gamma = 0.5$.

5.5.1 Sinusoidal excitation

An undamped *SDF* system with natural frequency of 34.8 Hz is subjected to a base acceleration of the form

$$\ddot{y}(t) = a_1 \sin 2\pi f_1 t + a_2 \sin 2\pi f_2 t + a_3 \sin 2\pi f_3 t$$

with

$$a_1 = 10.0$$

$$a_2 = 5.0$$

$$a_3 = 3.0$$

$$f_1 = 3.91$$

$$f_2 = 9.77$$

$$f_3 = 15.26$$

The excitation is generated in a digital form at an interval 0.02 sec. This is then interpolated using linear and band limited interpolation with $I = 10$, which gives a record at 0.002 sec. These interpolated accelerograms are used as base acceleration ($\Delta t/T \approx 1/14$). Subsequent to direct integration from which the absolute acceleration response of the *SDF* system is obtained a Fourier analysis is carried out. Figure 5.10 shows the variation of Fourier amplitudes expressed in *dB* with frequency for the two interpolation schemes. For such an excitation it is also possible to find a closed form solution which is also shown in Fig. 5.10. Clearly the response at excitation frequencies is accurately predicted by both interpolation schemes. However in the high frequency range the response due to linear interpolation is jittery showing a presence of high frequencies that did not exist in the original signal. At the structural frequency too linear interpolation overestimates the response.

5.5.2 Parkfield Earthquake

An actual corrected earthquake accelerogram obtained from Parkfield earthquake of June 27, 1966 recorded in Cholame, Shandon (California Institute of Technology record no. IIB034, component N85E) was used as input excitation. The above record was available at a sampling interval of 0.02 sec and was interpolated by both the methods to obtain acceleration values at 0.002 sec ($I = 10$).

A *SDF* system with frequency 40 Hz and damping of 2% of critical was subjected to these "interpolated earthquakes" ($\Delta t/T = 1/12.5$). Fourier spectra of the absolute acceleration response is shown in Fig. 5.11. Once again it is seen that the linearly interpolated record overestimates the response in the high frequency range. Moreover, linear interpolation yields a jittery and thereby unreliable response as compared to band limited interpolation.

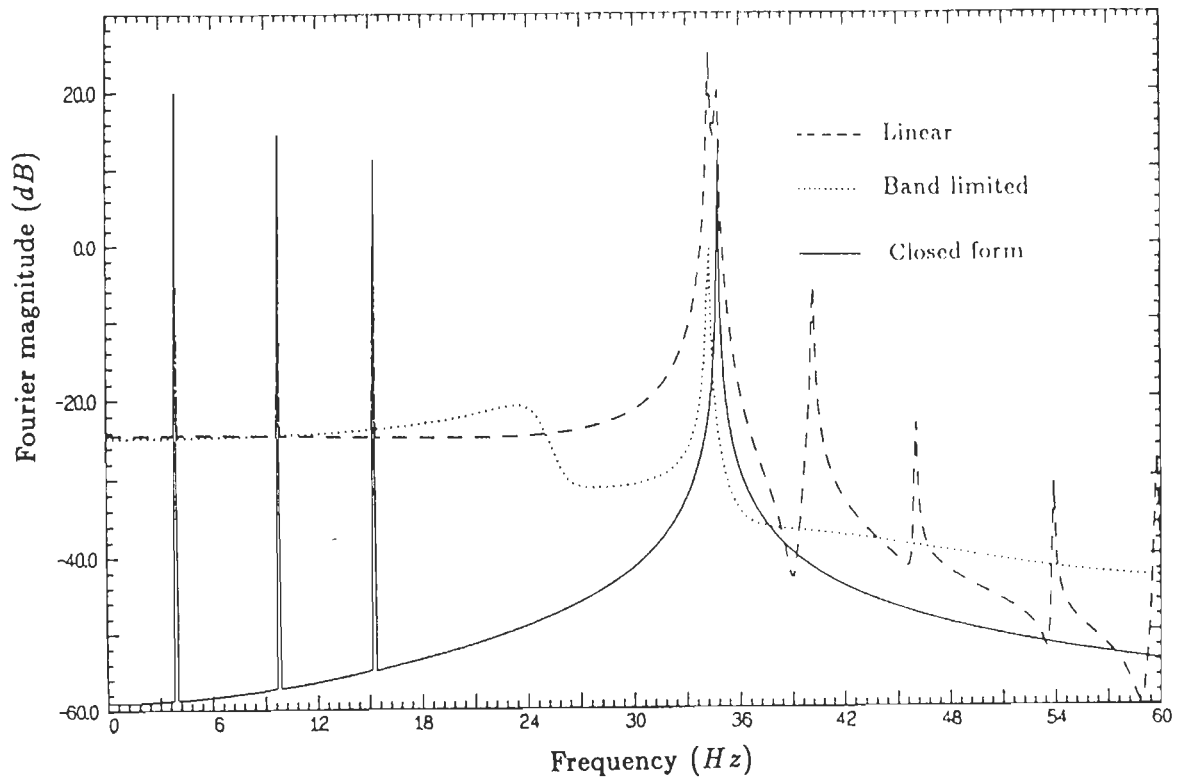


Figure 5.10: Fourier spectra of response of an undamped SDF system (natural frequency = 34.8 Hz) subjected to sinusoidal input consisting of three frequencies

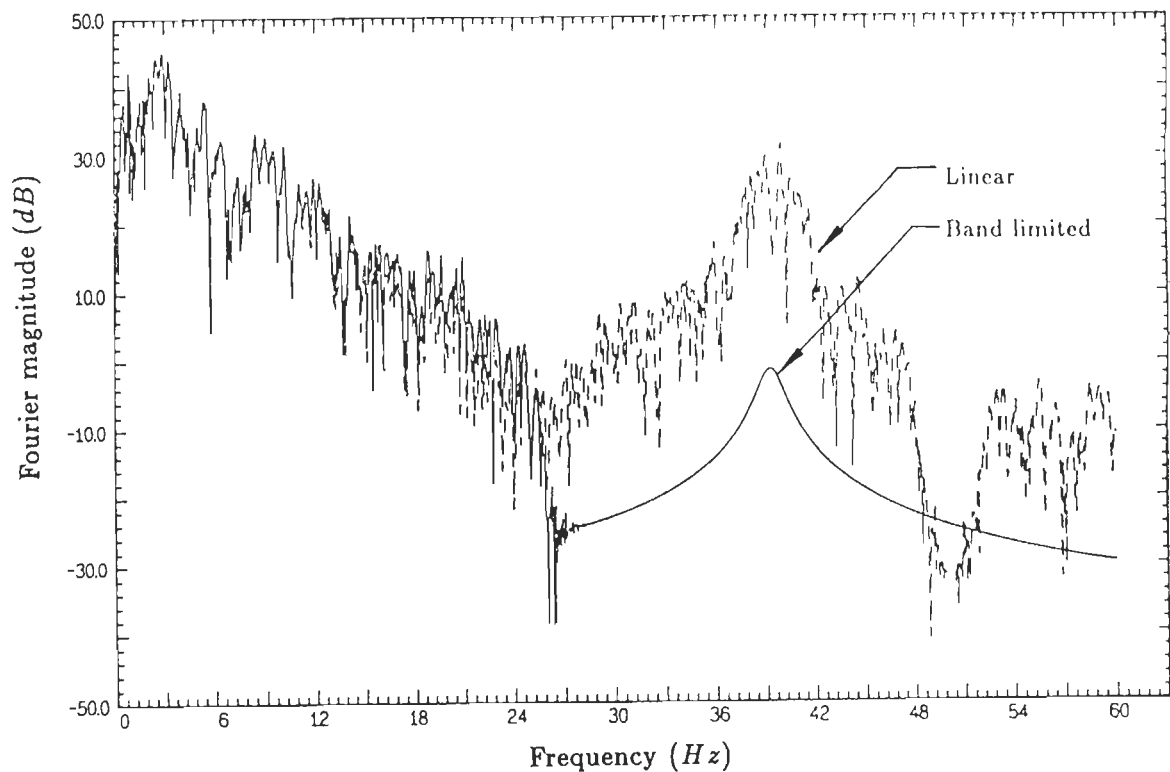


Figure 5.11: Fourier spectra of response of a SDF system (natural frequency = 40 Hz, damping = 2%) subjected to Parkfield earthquake

Chapter 6

Proposed correction scheme for records of analog accelerograph

Based on the study carried out by the author as reported in Chapter 4 and 5 on band limited interpolation of nonuniform and uniform samples, a new correction scheme for processing records of analog accelerographs is proposed. This scheme first converts the digitized data into time *vs.* acceleration values using the calibrations to get an uncorrected accelerogram. If the uncorrected accelerogram has nonuniform samples, then band limited interpolation is performed to recover the data at 200 *SPS*. The data is then decimated to 100 *SPS* in such a way as to preserve the frequency content upto the new Nyquist frequency (50 *Hz*). The instrument correction is applied in frequency domain by assuming the accelerometer to be a single degree of freedom system. The signal is then band-pass filtered in frequency domain using transfer function of the Butterworth filter thus obtaining the corrected accelerogram. The velocity and displacement histories are obtained by integrating the corrected accelerogram in frequency domain. In case the accelerogram is required at higher sampling rate, the band limited interpolation as discussed in the previous chapter is employed. Figure 6.1 gives flow chart of the proposed correction scheme and various steps of the flow chart are discussed in detail. Some of these steps are examined by imparting white noise input and comparing its output with an ideal situation. It may be mentioned that the proposed scheme comprises of steps as discussed above and some of the steps may not be required for a particular case and therefore can be dropped. A judgement in this regard will have to be taken by the users. However, for the purpose of discussion in this chapter the scheme is assumed to be comprising of all the steps.

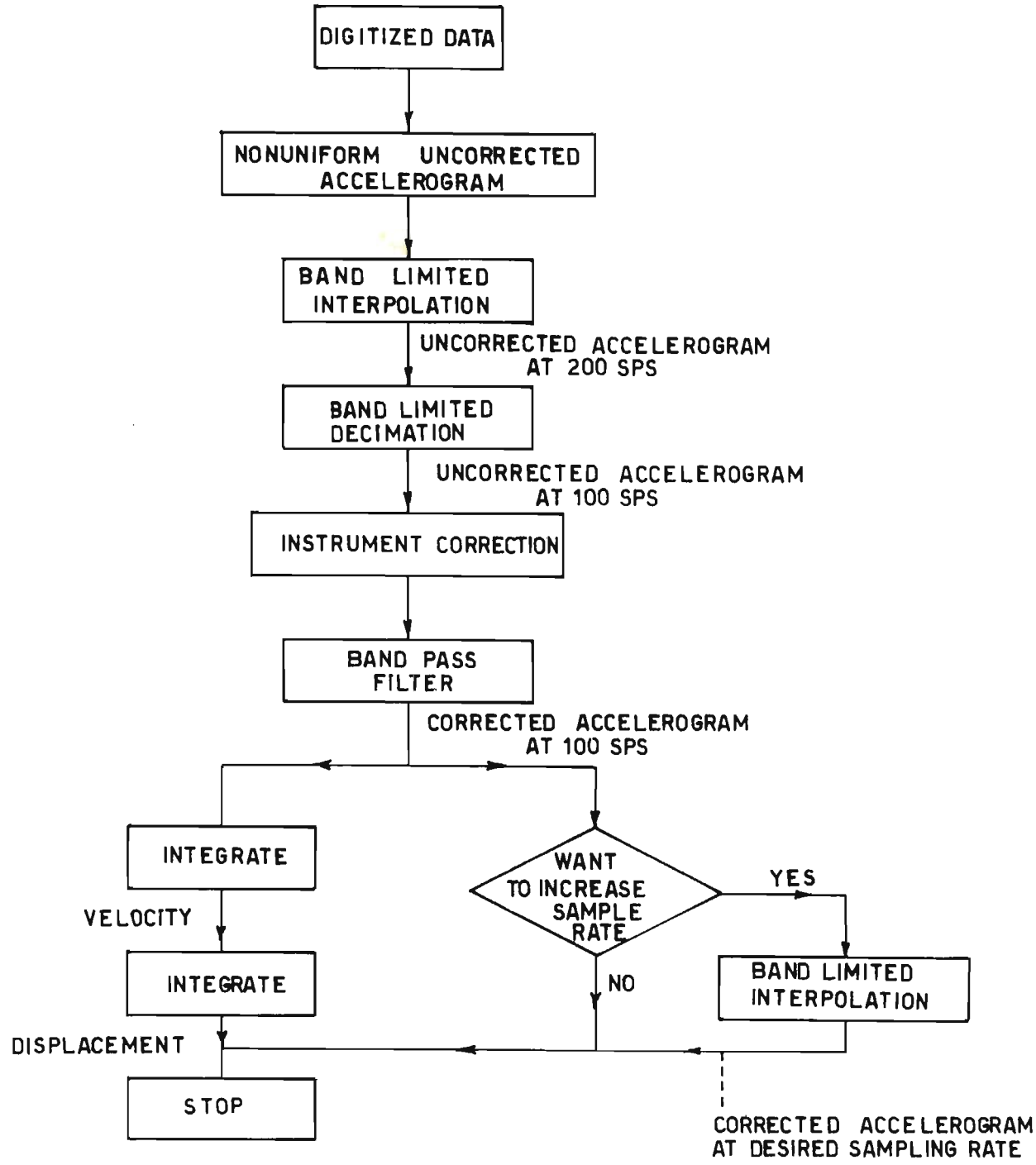


Figure 6.1: Flow chart of the proposed correction scheme

6.1 The uncorrected accelerogram

An earthquake record of an analog accelerograph generally has six traces. Three of these are records of longitudinal, transverse and vertical components of ground acceleration while two traces are from mirrors rigidly attached to the accelerographs frame. These fixed traces are used to neutralize the low frequency noise caused in the accelerograms due to paper (or film) distortion, motion of the film in the drive mechanism etc. The sixth trace is of quarter second OFF and quarter second ON time mark spots which provide the time axis of the record. The time mark spots are essential as the photographic paper may not have a completely uniform and constant speed. Thus, when an earthquake record of an analog accelerograph is digitized on a digitizing table, the operator generates six different files — one each for the six traces. Obviously, processing of the record is done separately for each of the three components of ground acceleration. For processing of each of the components; the time mark file, one of the fixed trace file (generally one which is nearest to the component) and the file of the concerned component, is used. All these files provide abscissa and the ordinate of points digitized.

The first step in processing the digitized record is to fit a least square line through the fixed trace to determine the angle from the abscissa of digitizing table. This is required as the accelerogram and table axes may not be exactly parallel. A correction for the rotation of the coordinates is then applied to all the three files. Subsequently, the ordinates of earthquake file are subtracted from the corresponding ordinate at the same abscissa of the fixed trace file. The corresponding ordinate at the same abscissa of fixed trace file is found through linear interpolation. Next a least square line is fitted in the above processed earthquake file which provides the ordinate of the origin of the new coordinate system. The abscissa of this origin is the abscissa of the first point of the earthquake record. The developed earthquake file is then translated to the new coordinate system. This provides the uncorrected accelerogram with both axes having the units of *thou*. The abscissas are converted into time in seconds by using time mark file, using linear variation within a pair of OFF and ON spot (1/2 second). The ordinates are converted into acceleration values by the tilt sensitivity calibration data which is provided for each component. This gives uncorrected accelerogram at nonuniformed sampling interval. Figure 6.2 gives flow chart for getting uncorrected accelerogram from the digitized data.

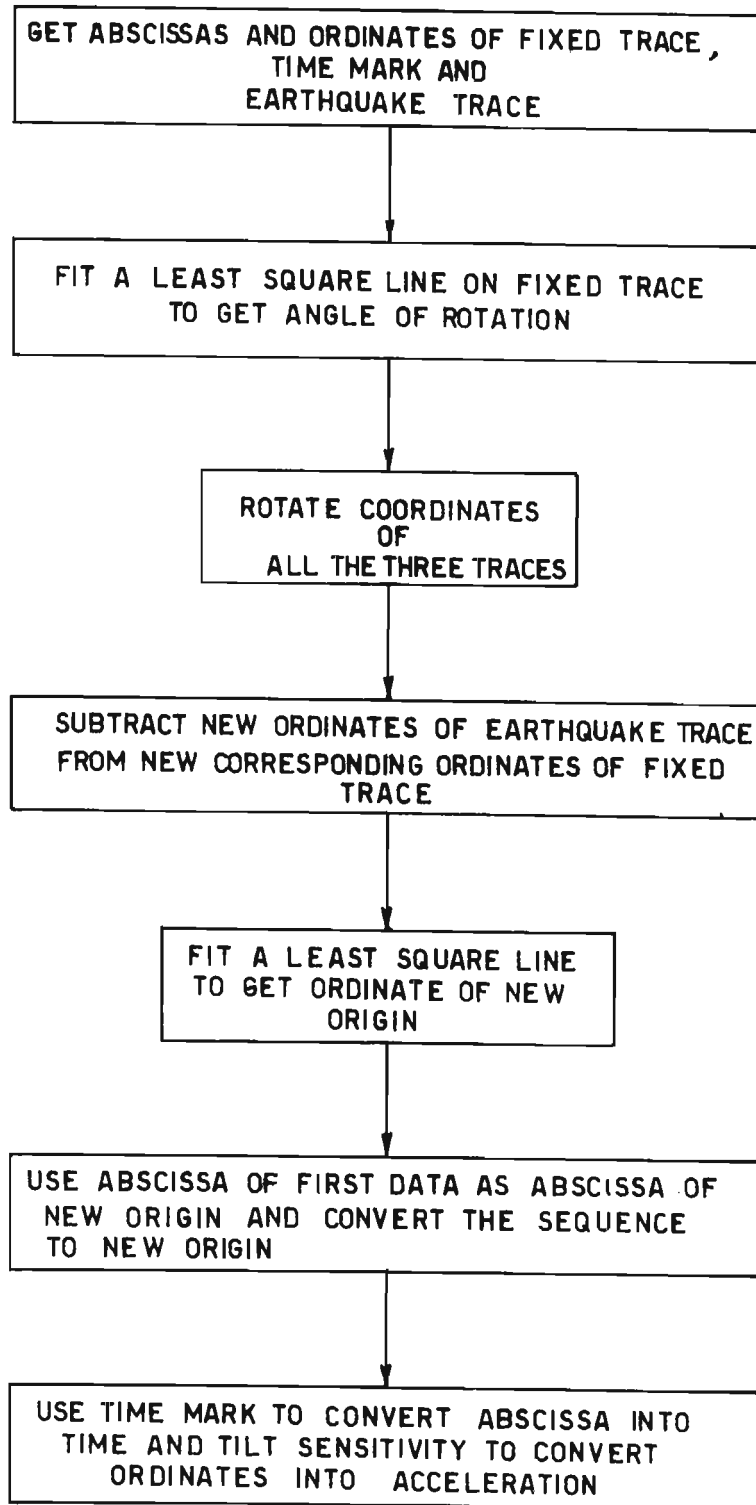


Figure 6.2: Flow chart for getting uncorrected accelerogram from the digitized data

6.2 Recovery of signal from nonuniform samples

This step is used if the digitization is performed on semi-automatic digitizer from which the sequence is obtained at nonuniform interval. However, if the digitization is performed in an automatic scanner then this step is not required. Uncorrected accelerogram at nonuniform sample interval is interpolated to 200 *SPS* using band limited interpolation of nonuniform samples discussed in detail in Chapter 4. The cutoff frequency used in the interpolation is half of average sampling rate of uncorrected accelerogram or 25 *Hz* whichever is lower. The interpolation is done using convergence constant $\lambda = 1$. Mean square error (MSE) determined between results of two consecutive iterations is used as convergence criterion and the iteration is assumed to have converged when MSE becomes less than 0.01. The value of MSE after each iteration is taken as output on the terminal to monitor the convergence.

6.3 Decimation

The band limited uncorrected data which is recovered at 200 *SPS* as described in Section 6.2 or which has been obtained directly at uniform sampling rate through Section 6.1 (in case of records digitized through automatic scanner) are decimated to 100 *SPS* data. The decimation is performed in a manner such that during the process of decimation, the frequency contents upto the new Nyquist frequency are preserved. To achieve this requirement, FFT of the 200 *SPS* signal is taken (Nyquist frequency 100 *Hz*). The new Nyquist frequency is determined by dividing the old Nyquist frequency by the factor by which the sampling rate is required to be reduced. Thus in this case the new Nyquist frequency becomes 50 *Hz*. From the FFT of 200 *SPS* data, the real and imaginary parts from DC to new Nyquist frequency only are kept. The real parts from new Nyquist frequency to twice the new Nyquist frequency are taken as mirror image of real part from DC to new Nyquist frequency whereas the imaginary parts from new Nyquist frequency to twice of new Nyquist frequency are taken as negative of mirror image of imaginary part from DC to new Nyquist frequency. A Fourier inversion of this set of real and imaginary data yields decimated history which preserves the frequency contents of the original signal upto the new Nyquist frequency. It may be noted that decimation reduces the total number of samples by the same factor by which the sampling rate decreases. Thus, after decimation the bin frequency of the FFT remains the same but the total number of points in frequency domain as well as in time domain reduces by the factor by which the sampling rate is reduced. In this work, the algorithm developed

for the decimation works well when the reduction factor is a power of 2. The proposed band limited decimation should be performed with care in case digitization of data is done on an automatic scanner, as it may introduce Gibb's phenomenon. Therefore such data should be first low pass filtered with a cutoff frequency of maximum 50 Hz before performing the decimation. But, in case the 200 SPS data is obtained from band limited interpolation of nonuniform samples, the proposed band limited decimation works well since such data is already low pass filtered.

6.4 Instrument correction

Instrument correction of uncorrected accelerogram is an important requirement. From the basic theory of seismic pickups it can be proved that the relative displacement of mass of a single degree of freedom (SDF) spring-mass-dashpot system is proportional to the ground acceleration if the natural frequency of the SDF system is much higher than the frequency of excitation. It is this simple principle, based on which the uncorrected accelerogram is derived and the tilt calibration is done. This uncorrected accelerogram may not require correction for instrument if the natural frequency of pendulum of accelerometer is substantially higher (about twice) than the largest frequency content of earthquake (generally assumed as 25 Hz) and the damping is fixed at 70% of critical (to get linear phase shift with respect to frequencies). However, the natural frequency of accelerometers used in the analog accelerographs cannot have a such high value as it will drastically reduce the sensitivity of instrument. The natural frequency of accelerometers of analog accelerographs varies from 18 Hz to 25 Hz. It is also impractical to set damping of accelerometers to be exact 70% of critical. The damping values in the accelerometers generally vary between 50% to 70% of critical. With this background, it becomes essential to perform instrument correction so that the recorded motion can be deconvoluted, to obtain ground excitation. This deconvolution in the present scheme is performed in the frequency domain.

Let ω_n be the natural frequency in *radians/sec* and ζ be the fraction of critical damping of accelerometer. Let $x(t)$ be the relative displacement of the pendulum and $a(t)$ be the ground acceleration. Then equation of motion of the pendulum of accelerometer can be written as

$$\ddot{x}(t) + 2\omega_n\zeta\dot{x}(t) + \omega_n^2x(t) = -a(t) \quad (6.1)$$

where \dot{x} and \ddot{x} are the first and second derivatives of relative displacement of the pendulum. It may be mentioned that the values of acceleration in the uncorrected accelerogram

grams are really $-\omega_n^2 x(t)$ which has been assumed to be equal to the ground acceleration $a(t)$. In other words, while deriving uncorrected accelerogram, the effect of first two terms of Eq. 6.1 are neglected. To get the frequency domain description from the given time domain sequence, let

$$x(t) = X(\omega)e^{j\omega t} \quad (6.2)$$

and

$$a(t) = A(\omega)e^{j\omega t} \quad (6.3)$$

where ω is the frequency contents of the signal in *radians/second* and $X(\omega)$ and $A(\omega)$ are the complex functions comprising real and imaginary parts of the Fourier transforms of $x(t)$ and $a(t)$ respectively. By using Eqs. 6.2 and 6.3 into 6.1 one obtains

$$-\omega^2 X(\omega) + 2j\omega_n \zeta \omega X(\omega) + \omega_n^2 X(\omega) = -A(\omega) \quad (6.4)$$

The above equation can be rewritten in the form

$$A(\omega) = -\omega_n^2 X(\omega) \left[1 - \left(\frac{\omega}{\omega_n} \right)^2 + 2j\zeta \frac{\omega}{\omega_n} \right] \quad (6.5)$$

$-\omega_n^2 X(\omega)$ on the right hand side of Eq. 6.5 is the Fourier transform of uncorrected accelerogram and let

$$u(\omega) = \Re\{-\omega_n^2 X(\omega)\} \quad (6.6)$$

and let

$$v(\omega) = \Im\{-\omega_n^2 X(\omega)\} \quad (6.7)$$

where \Re is real part and \Im is the imaginary parts of the discrete Fourier transform of $-\omega_n^2 x(t)$. In the right hand side of Eq. 6.5, the term inside the large bracket is the transfer function of the process of instrument correction and let this transfer function be called $H(\omega)$ and let

$$p(\omega) = \Re\{H(\omega)\} = 1 - \left(\frac{\omega}{\omega_n} \right)^2 \quad (6.8)$$

and let

$$q(\omega) = \Im\{H(\omega)\} = 2\zeta \frac{\omega}{\omega_n} \quad (6.9)$$

then $A(\omega)$ can be written as

$$A(\omega) = [u(\omega) + jv(\omega)][p(\omega) + jq(\omega)] \quad (6.10)$$

Equation 6.10 above will yield

$$\Re\{A(\omega)\} = u(\omega)p(\omega) - v(\omega)q(\omega) \quad (6.11)$$

and

$$\Im\{A(\omega)\} = u(\omega)q(\omega) + v(\omega)p(\omega) \quad (6.12)$$

An inverse Fourier transformation of the real and imaginary parts of $A(\omega)$ gives the instrument corrected data from uncorrected accelerogram. For the sake of clarity this process of instrument correction is summarized as follows:

1. Find FFT of uncorrected accelerogram (which is now available at 100 *SPS*) to get $u(\omega)$ and $v(\omega)$. The bin frequency interval at which the real and imaginary parts of the FFT are determined will be equal to $100/N$ where N is the total number of sample points which is made equal to 2^k (where k is an integer) by inserting required number of zeros at the end of the sequence.
2. At the above bin frequency interval, determine the real and imaginary parts of the transfer function $H(\omega)$ i.e. $p(\omega)$ and $q(\omega)$. Determine these values upto the Nyquist frequency (upto bin number $\frac{N}{2} + 1$). For bin numbers $\frac{N}{2} + 2$ to N , take $p(\omega)$ as mirror image of $p(\omega)$ determined upto Nyquist frequency. For bin numbers $\frac{N}{2} + 2$ to N , take $q(\omega)$ as negative of mirror image of $q(\omega)$ determined upto Nyquist frequency.
3. Find real and imaginary parts of $A(\omega)$ from Eqs. 6.11 and 6.12.
4. Take inverse FFT which will give time history of ground acceleration.

6.4.1 Response to White Noise

A white noise whose Fourier magnitude plot is a horizontal straight line with a magnitude of unity is generated at a sampling rate of 100 *SPS*. The white noise generated has 2048 data points i.e. it has a duration of 20.48 seconds. With FFT algorithm and availability of generation of random numbers in computer, generation of white noise is a simple matter. For a white noise of 2048 data points, any random number between -1 and 1 is picked up as the real part. Its corresponding imaginary part is found such that the magnitude is 1. Similarly 1025 pairs of real and imaginary parts corresponding to first 1025 bin frequencies (upto Nyquist frequency) are found. For bin numbers 1026 to 2048, real parts are found by taking mirror image of real part of the set upto Nyquist frequency and imaginary parts are found by taking negative of mirror image of imaginary parts of the set upto Nyquist frequency. Inverse FFT is then performed on these 2048 pairs of real and imaginary parts which yields the desired white noise.

This white noise is used as input for the instrument correction. The natural frequency of the accelerometer is taken as 20 *Hz* and damping is taken as 60% of critical. FFT of the instrument corrected history is then determined. Figure 6.3 shows

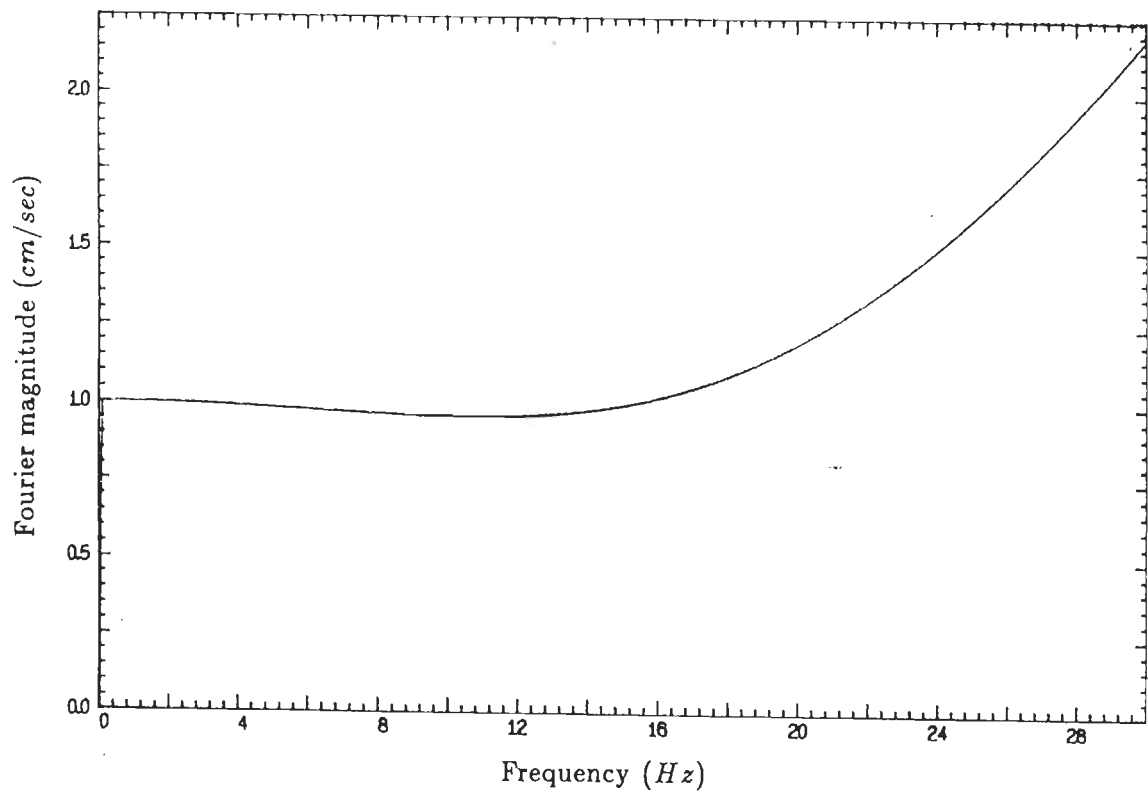


Figure 6.3: Response of proposed instrument correction scheme to white noise input.

the Fourier magnitude plot upto 30 Hz of the instrument corrected history. This Fourier magnitude plot matches exactly with the ideal plot in the entire range upto the Nyquist frequency. This test shows the superiority of performing the instrument correction in the frequency domain.

6.5 Bandpass filter

The next operation in the correction scheme is to perform the band pass filtering to remove low frequency and high frequency noise from the available sequence. Most of the high frequency noise has already been removed while recovering the signal during band limited interpolation of nonuniform samples (or at the time of decimation in case of data obtained from automatic scanners). However, to remove some of the high frequency noise which may have amplified during instrument correction, the low pass operation is performed again. High pass operation to remove low frequency noise has still not been performed and is, therefore, required to be done. Both these operations are done simultaneously by designing a band pass filter function corresponding to $|H(j\omega)|^2$ of Butterworth filter.

The filtering operation is performed by first finding FFT of the signal which is to be filtered. The bin frequency interval (Δf) at which the FFT of the signal is determined is given by

$$\Delta f = \frac{SPS}{N} \quad (6.13)$$

where SPS is the sampling rate which is 100 SPS in this case and N is number of data points of the sequence which is lengthened by inserting zeros so that the sequence has exactly 2^j (where j is an integer) data points. For example if sequence has 3910 data points then N is made 4096 (which is 2^{12}) by inserting 186 zeros in the sequence. At the above bin frequency intervals and upto the Nyquist frequency, transfer function $|H_1(j\omega)|^2$ of Butterworth filter for low pass operation, which is given by the equation below, is determined.

$$|H_1(j\omega)|^2 = \frac{1}{1 - \left(\frac{\omega}{\omega_l}\right)^{2n}} \quad (6.14)$$

where ω is the frequency at which the function is determined, ω_l is the cutoff frequency of low pass filter and n is the order of filter. It is clear that cutoff frequency of the lowpass filter should be less than half of average sampling rate of the original nonuniform sampled data or 25 Hz whichever is smaller.

Similarly for high pass operation, transfer function $|H_2(j\omega)|^2$ of Butterworth filter is determined at all the bin frequencies upto Nyquist frequency. However, now the

transfer function will be given by

$$|H_2(j\omega)|^2 = \frac{1}{1 - \left(\frac{\omega_A}{\omega}\right)^{2n}} \quad (6.15)$$

The net transfer function of the band pass filter $|H(j\omega)|^2$ at each bin frequency is determined by

$$|H(j\omega)|^2 = |H_1(j\omega)|^2 |H_2(j\omega)|^2 \quad (6.16)$$

Transfer function of the band pass filter from Nyquist frequency to twice of Nyquist frequency is found by taking the mirror image of the transfer function from DC to Nyquist frequency.

Convolution is then performed between the FFT of the signal and the transfer function of the filter. As the transfer function of filter has only real part, convolution in frequency domain means simple multiplication of real and imaginary parts of the Fourier transform of the signal with the filter function at the corresponding bin frequencies. Inverse FFT is then performed to get the band passed signal in time domain which gives the corrected accelerogram at 100 *SPS*.

Again to check the performance of this band pass filter, its response for white noise input of 100 *SPS* is determined. The cutoff frequency for the low pass filter is taken as 25 *Hz* and for high pass filter is taken as 0.1 *Hz*. The Fourier magnitude of the band pass filtered white noise is plotted and is shown in Fig. 6.4 . In this figure, the tapering of high pass operation is not properly seen. This is plotted by zooming Fig. 6.4 and is shown in Fig. 6.5.

6.6 Band limited interpolation to increase sampling rate

The proposed procedure provides the corrected accelerogram at a sampling rate of 100 *SPS*. This sampling rate may not be sufficient for a particular application and in this situation the corrected accelerogram may be required to be interpolated to obtain the desired sampling rate. In the proposed correction scheme this interpolation is done such that the frequency contents of the data do not change. This is achieved by performing the band pass interpolation, the details of which were discussed in Chapter 5.

To study the response of the entire scheme, a white noise at 200 *SPS* is generated. This white noise is used as uncorrected accelerogram to the scheme (starting from

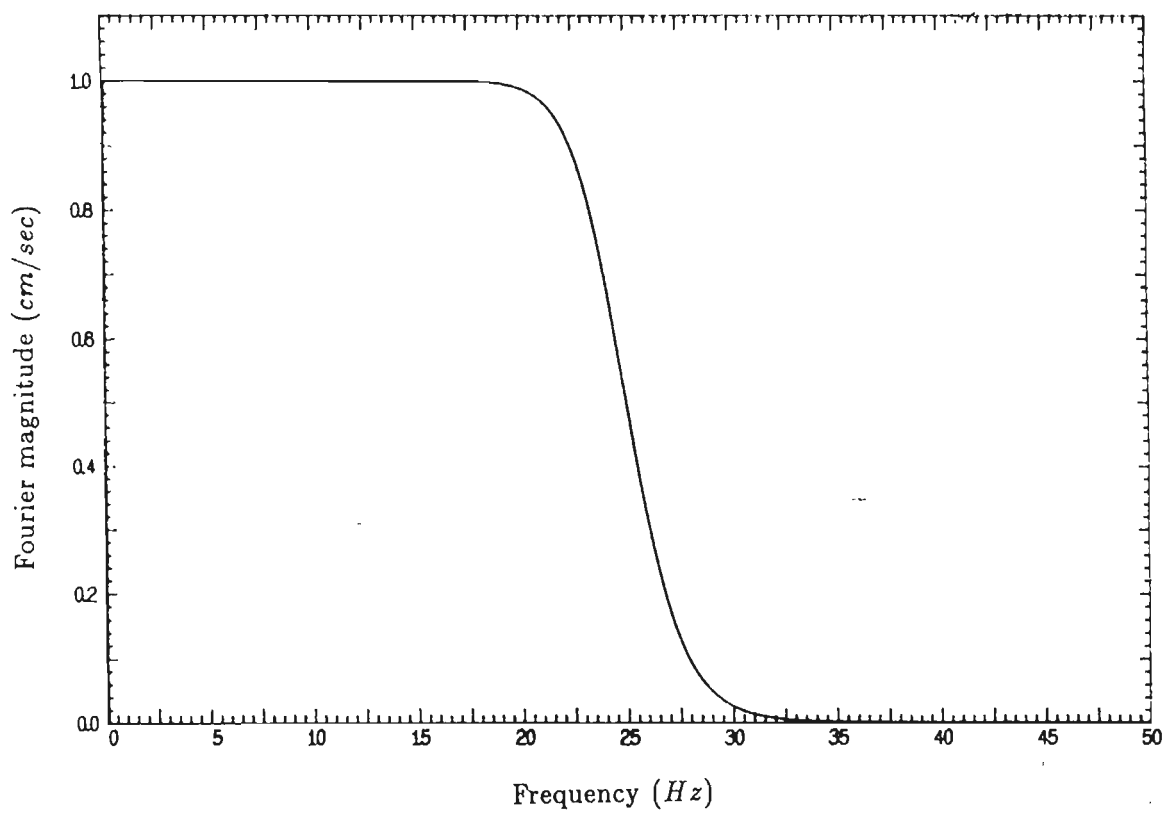


Figure 6.4: Response of proposed band pass filter to white noise input.

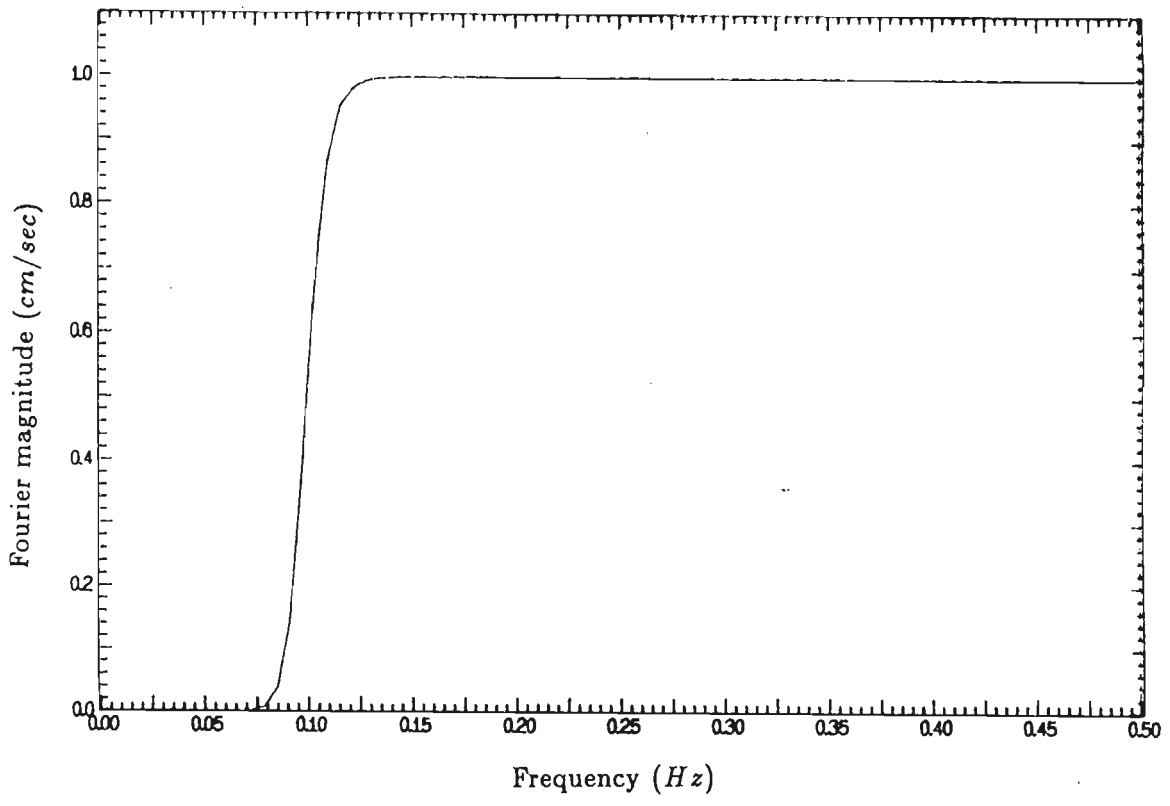


Figure 6.5: Zoomed Figure 6.4 to show response of high pass portion of band pass filter.

Section 6.3). The natural frequency of transducer is assumed to be 20 Hz and the damping is assumed to be 60% of critical. The corrected data at 100 SPS is band limited interpolated to get a sampling rate of 200 SPS. The Fourier transformation of this sequence is taken and Fig. 6.6 gives the Fourier magnitude plot of the response of the entire correction scheme to white noise.

6.7 Integration for velocity and displacement

Determination of ground velocity and ground displacement histories from the records of analog accelerographs will perhaps always remain questionable. This is due to the fact that some of the low frequency signals which predominantly effect the process of integration get overshadowed by the low frequency noise and, therefore, have to be removed through high pass filter. Also the initial conditions of zero displacement and zero velocity do not hold true for records of analog accelerographs which get triggered when the ground acceleration exceeds some threshold value. Nevertheless, integration of corrected accelerogram is performed with zero initial conditions to get the velocity and displacement histories. In the present scheme the integration is performed in the frequency domain.

Let $x_c(t)$ be the corrected accelerogram and let $X_c(\omega)$ be its Fourier transform and let $r(\omega)$ and $s(\omega)$ be the real part and imaginary parts respectively of $X_c(\omega)$, then

$$X_v(\omega) = \frac{X_c(\omega)}{j\omega} \quad (6.17)$$

where $X_v(\omega)$ is the Fourier transformation of velocity. In other words if $b(\omega)$ and $c(\omega)$ respectively are the real and imaginary parts of $X_v(\omega)$ then, Eq. 6.17 means

$$b(\omega) = \frac{s(\omega)}{\omega} \quad (6.18)$$

and

$$c(\omega) = -\frac{r(\omega)}{\omega} \quad (6.19)$$

With Eqs. 6.18 and 6.19, the real and the imaginary parts of the Fourier transformation of the ground velocity are found which on inversion yields time history of ground velocity. To account for the zero initial condition, $b(\omega)$ and $c(\omega)$ are taken as zero for $\omega = 0$ (at the first bin frequency).

To check the performance of this integration process, a white noise of 100 SPS with 2048 data points is generated. This white noise is integrated with the above

process. The Fourier transformation of this integrated signal is then taken. Figure 6.7 gives the Fourier magnitude plot of this integration process. The plot matches with the transfer function of an ideal integrator.

6.8 The computer program

The computer program developed for this correction scheme is comprehensive and interactive in nature. It demands from the terminal all the input and output file names. The input file names demanded are the time mark, the fixed trace and the earthquake files which are made by the digitizers. The names of the output files which the computer programme generates are also taken through the terminal. These files are uncorrected accelerogram at nonuniform sampling rate, uncorrected accelerogram at 200 *SPS*, corrected accelerogram at 100 *SPS*, corrected accelerogram at the desired sampling rate, velocity history and displacement history. The program also demands from the terminal, the various parameters of the process like natural frequency of accelerometer, damping of accelerometer, value of λ of iteration for recovery of signal from nonuniform samples, maximum number of iterations, cutoff frequency of low pass and high pass filters, the order of the filter and the number by which the sampling rate of the corrected accelerogram is desired to be increased. The options available with the computer program is to prepare a documentation file which prepares in the tabular form the acceleration, velocity and displacement histories with a header which specifies the details of earthquake, name of station, component orientation, cut off frequencies etc. The other options are preparation of response spectra and Fourier spectra of corrected accelerogram. A comprehensive terminal file can be prepared which provides all the inputs of the program in a sequential manner.

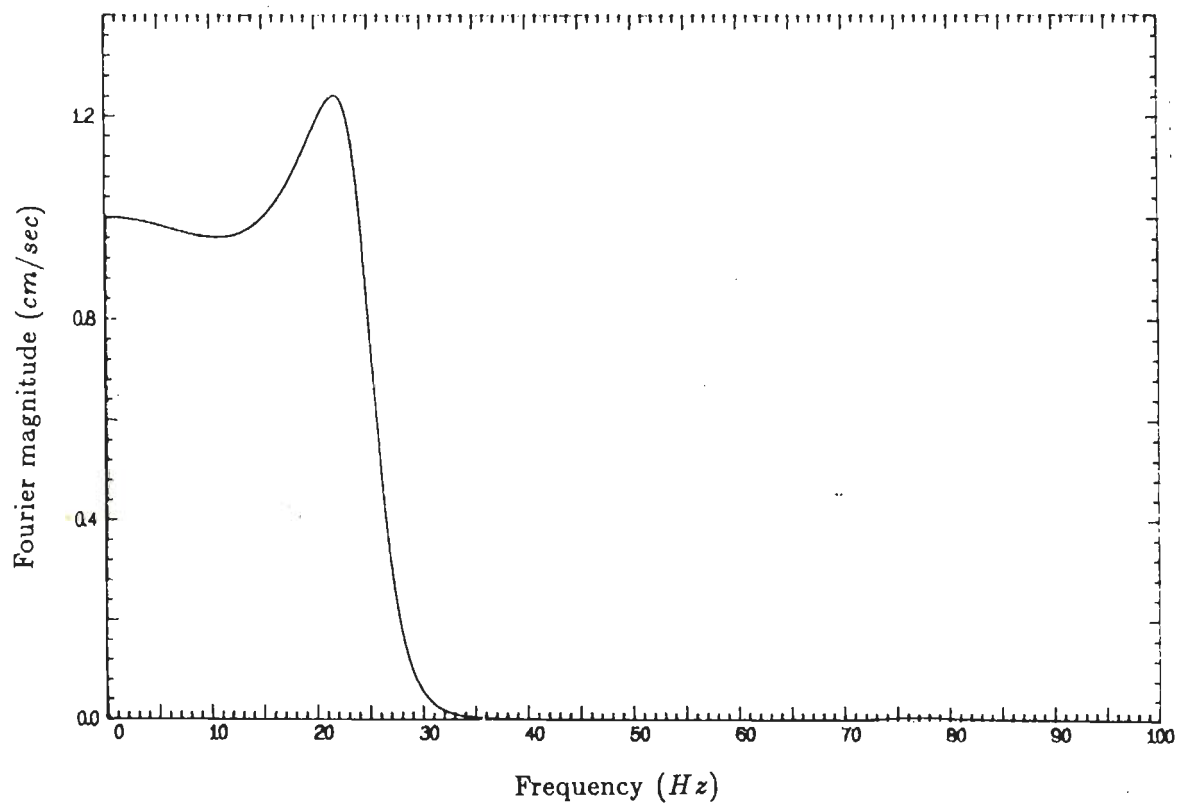


Figure 6.6: Response of the proposed correction scheme to white noise input.

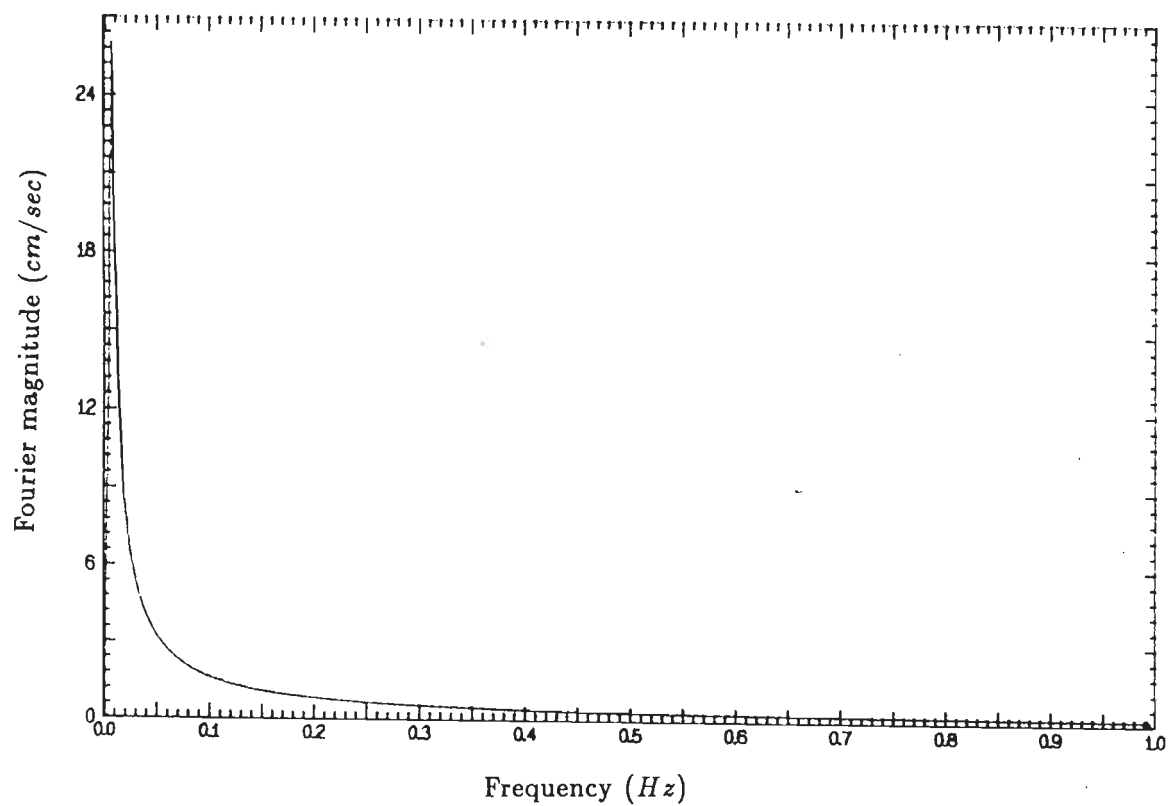


Figure 6.7: Response of integration process to white noise input.

Chapter 7

Comparison of proposed scheme with other schemes

A study is made to compare the proposed scheme (Chapter 6) with three other schemes, namely those of Lee and Trifunac [56], Erdik and Kubin [32] and Khemici and Chiang [50]. Schemes of Lee and Trifunac (referred as Trifunac's scheme) and of Erdik and Kubin (referred as Erdik's scheme) are in time domain whereas the scheme of Khemici and Chiang (referred as Khemici's scheme) is in frequency domain. In what follows a brief description is given about the correction procedure adopted by above mentioned three schemes and their response are studied for white noise input. Then characteristics of instrument correction and band pass filter algorithms of the three schemes mentioned above and that of the proposed scheme are compared through the Fourier magnitude of their response to white noise. Another comparison of the four schemes is performed by plotting one over the other, the Fourier transformation of the response of the entire correction schemes to the white noise input. Uncorrected accelerograms of El Centro, Parkfield, Taft and Uttarkashi are taken and corrected accelerograms are obtained from four schemes. Maximum values of acceleration, velocity and displacement and the time of their occurrence obtained for the above mentioned records are compared. Fourier transformation of these corrected accelerograms obtained by the four schemes are compared by dividing the band upto Nyquist frequency into sixteen segments and taking mean of each of the segment. Response spectra of the corrected accelerogram obtained from the proposed procedure is determined and is plotted over the response spectra determined through the Trifunac's scheme.

7.1 Scheme of Trifunac and Lee

Trifunac's scheme also known as Caltech data correction scheme was perhaps the first comprehensive scheme developed for processing accelerograms. This scheme is well documented and was quite popular till early eighties. Large number of accelerograms obtained in the past earthquakes have been processed with this scheme and are documented in several volumes of reports published by Earthquake Engineering Research Laboratory (EERL) of California Institute of Technology. These corrected accelerograms, response spectra and Fourier spectra have become a valuable data and which are used by research workers for different applications in the field of Earthquake Engineering. It is because of this reason that Trifunac's scheme is being chosen to be used in this work for the purpose of comparison. The computer code in FORTRAN is available for this scheme in Report no. 79-15 Volumes I and II of University of Southern California [56]. The computer program of Volume II is used here with minor modification particularly in handling input and output files.

Although the entire correction scheme is quite intricate, the salient points of the scheme is being described briefly in following steps.

1. Firstly, uncorrected accelerogram is made from the digitized data of the earthquake record, time mark and fixed trace, almost in the similar manner as is described for the proposed scheme in Chapter 6.
2. This uncorrected accelerogram is linearly interpolated to get the sequence at a uniform interval at 200 *SPS*.
3. This uncorrected accelerogram is low pass filtered using Ormsby filter in time domain. The filter weights of the Ormsby filter are found by a standard formulation. Number of filter weights are dependent upon the roll off of the filter and the sampling interval. If f_r is the roll off of the required filter and if T is the sampling interval then the number of filter weights N_w required by the Ormsby filter is

$$N_w = \frac{1}{f_r T} \quad (7.1)$$

In this scheme, the cut off frequency of the low pass filter is taken as 25 *Hz* with roll off of 2 *Hz*. With the sampling period of 0.005 *second* (200 *SPS*), the number of filter weights required will be 100. A time domain convolution is performed between the uncorrected accelerogram and unit impulse response function of the Ormsby filter as defined by its weights, to get the low passed accelerogram.

4. Instrument correction is then performed on this 200 *SPS* low passed data to estimate ground acceleration from the approximate accelerations of uncorrected accelerogram. If ω_n is the natural frequency and ζ is the fraction of critical damping of the pendulum of the accelerometer and if $a(t)$ is the true ground acceleration then the equation of motion of accelerometer is given by

$$\ddot{x}(t) + 2\omega_n\zeta\dot{x}(t) + \omega_n^2x(t) = -a(t) \quad (7.2)$$

where $x(t)$ is the relative displacement of the pendulum, $\dot{x}(t)$ is the first derivative and $\ddot{x}(t)$ is the second derivative of relative displacement of the pendulum. It may be mentioned that the values of acceleration in the uncorrected accelerograms are really $-\omega_n^2x(t)$. The true acceleration $a(t)$ is found by determining $\dot{x}(t)$ and $\ddot{x}(t)$ from the known $-\omega_n^2x(t)$ and putting these values in Equation 7.2. In this scheme the differentiation is performed using second order central difference approximation.

5. The instrument corrected sequence at 200 *SPS* is decimated to 50 *SPS* sequence by keeping only every fourth sample.
6. This data is then high pass filtered to remove low frequency noise using Ormsby filter with cutoff frequency generally 0.07 *Hz* and roll off of 0.05 *Hz*. For a roll off of 0.05 *Hz* and sampling rate of 50 *SPS*, the number of weights required in Ormsby filter will be 1000 as per Equation 7.1. To reduce computational work, the convolution is performed after decimating the signal to 5 *SPS* (sampling period of 0.2 *second*) thus reducing the number of weights of Ormsby filter to 100. The convoluted signal is then linearly interpolated to get the sequence at 50 *SPS* which when subtracted from the original sequence (which is also convoluted with a rectangular window) yielded the high pass filtered sequence which is the corrected accelerogram at 50 *SPS*.
7. The velocity and displacement sequences are obtained by integration using trapezoidal rule and zero initial conditions. These sequences are also high pass filtered as in step 6.

To evaluate the performance of this scheme, a white noise of 200 *SPS* and having 2048 data points is assumed as uncorrected accelerogram obtained from step 2. This is processed with the above scheme assuming natural frequency of accelerometer as 20 *Hz* and damping of 60% of critical. The cutoff frequency of low pass filter is taken as 25 *Hz* with a roll off of 2 *Hz* and the cutoff frequency of high pass filter is taken as 0.07 *Hz* with a roll off of 0.05 *Hz*. The corrected acceleration sequence at 50 *SPS* after step 6

is determined and Fourier transformation of this sequence is taken. Figure 7.1 gives the Fourier magnitude plot of the response of the scheme to white noise. In comparison to the proposed scheme (Fig. 6.6) it can be seen that the response of Trifunac's scheme has jitters in the pass band.

7.2 Scheme of Erdik and Kubin

The basic steps of this correction scheme are as follows:

1. Nonuniform sampled uncorrected accelerogram is linearly interpolated to get uniform sampled sequence at 100 *SPS*.
2. This uncorrected accelerogram is low pass filtered in time domain using Ormsby filter in the same way as in the Trifunac's scheme.
3. Data is then linearly interpolated to 200 *SPS* and instrument correction is performed a manner as in the case of Trifunac's scheme. This data is decimated back to 100 *SPS* data by dropping every alternate points.
4. A least square line is fitted in the instrument corrected sequence and the values of accelerations are adjusted accordingly.
5. The resulting acceleration is integrated in time domain through trapazoidal rule to obtain the velocity sequence assuming zero initial condition.
6. Cut off frequency of high pass filter is found by assuming that the Fourier magnitude of actual ground signal have a slope of -1 in the low frequency end. A plot of Fourier magnitude of uncorrected accelerogram is then used to recognise the frequency below which the Fourier magnitude spectrum deviates from the above property which is used as the cutoff frequency of the high pass filter to remove low frequencies.
7. The velocity sequence obtained from step 5 is high pass filtered with a cutoff frequency determined in step 6. A second order Butterworth filter is used in time domain to perform this high pass filtering. To avoid the nonlinear phase shift during the filtering, the sequence is filtered again with reverse time. This output when again reversed in time give high passed velocity sequence without any phase shift. This actually amounts to using $|H(j\omega)|^2$ of second order Butterworth filter.

8. A straight line is least square fitted to the velocity sequence obtained from step 7 and values of velocity are adjusted accordingly.
9. This velocity sequence is integrated to obtain the displacement sequence assuming zero initial condition.
10. A straight line is least square fitted to the displacement sequence obtained from step 9 and values of displacement are adjusted accordingly to obtain corrected displacement data.
11. The slope of the straight line of step 10 is added to the velocity sequence obtained after step 8 to get the corrected velocity data.
12. The corrected velocity is differentiated to get acceleration by using the FIR type linear phase digital differential filter as given by McClellan *et al.* [62]. The details of the digital filter designed in the present work to perform the required differentiation in this scheme is as follows:

$$\begin{aligned}
 \text{Filter length} &= 9 \\
 \text{Upper band edge} &= 0.30 \\
 \text{Peak relative error} &= 0.0032
 \end{aligned}$$

The impulse response factors obtained for above design are as following

$$\begin{aligned}
 h(1) &= -0.29521044E - 02 = -h(9) \\
 h(2) &= 0.15048594E - 01 = -h(8) \\
 h(3) &= -0.53063691E - 01 = -h(7) \\
 h(4) &= 0.14027159E + 00 = -h(6) \\
 h(5) &= 0.0
 \end{aligned}$$

where $h(1)$ to $h(9)$ are the weights of the FIR differentiator.

13. The obtained acceleration sequence is low pass filtered using Ormsby filter with the same filtering limits as of step 2. This yields corrected accelerogram.

To evaluate the performance of this scheme, a white noise of 100 *SPS* and having 1024 data points is assumed as uncorrected accelerogram obtained from step 1. This is processed with the above scheme with the same accelerometer and filter specifications as used for Trifunac's scheme. The corrected acceleration sequence after step 13 at 100 *SPS* is determined. Fourier transformation of this sequence is taken. Figure 7.2 gives the Fourier magnitude plot of the response of the scheme to white noise. In comparison to Trifunac's scheme it can be seen that the response of this scheme is quite

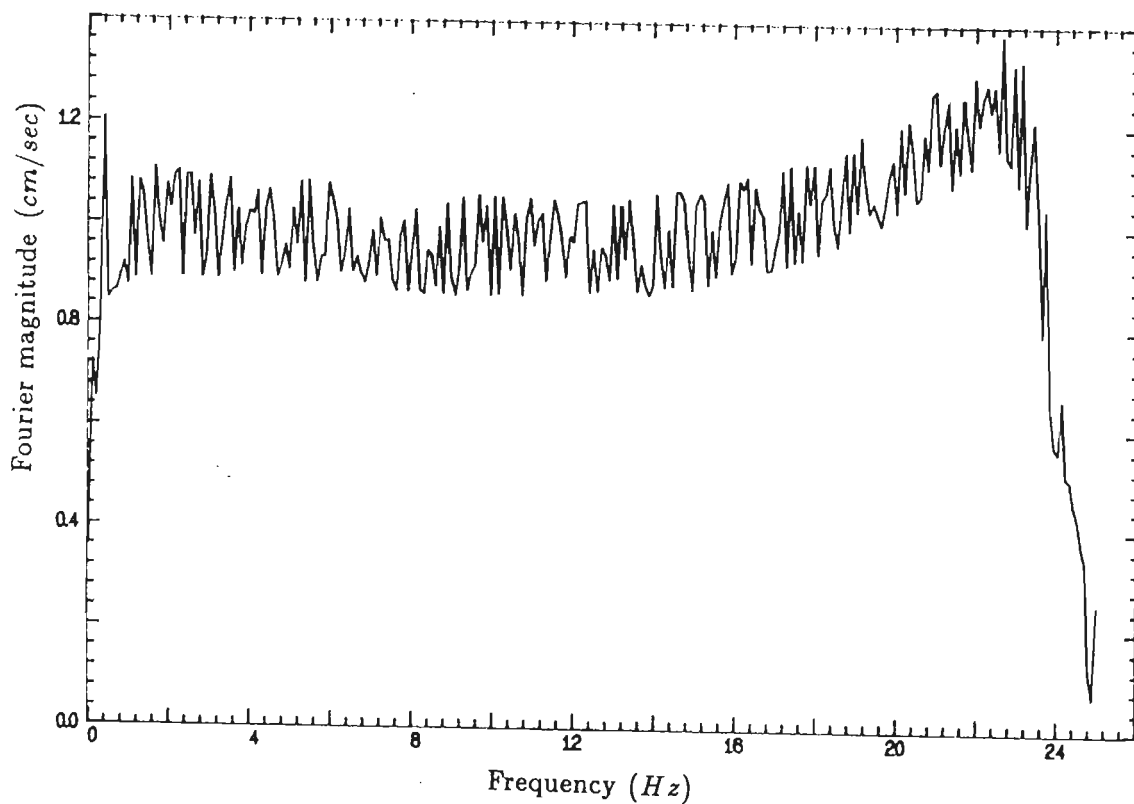


Figure 7.1: Fourier magnitude plot of Response of Trifunac's scheme to white noise input

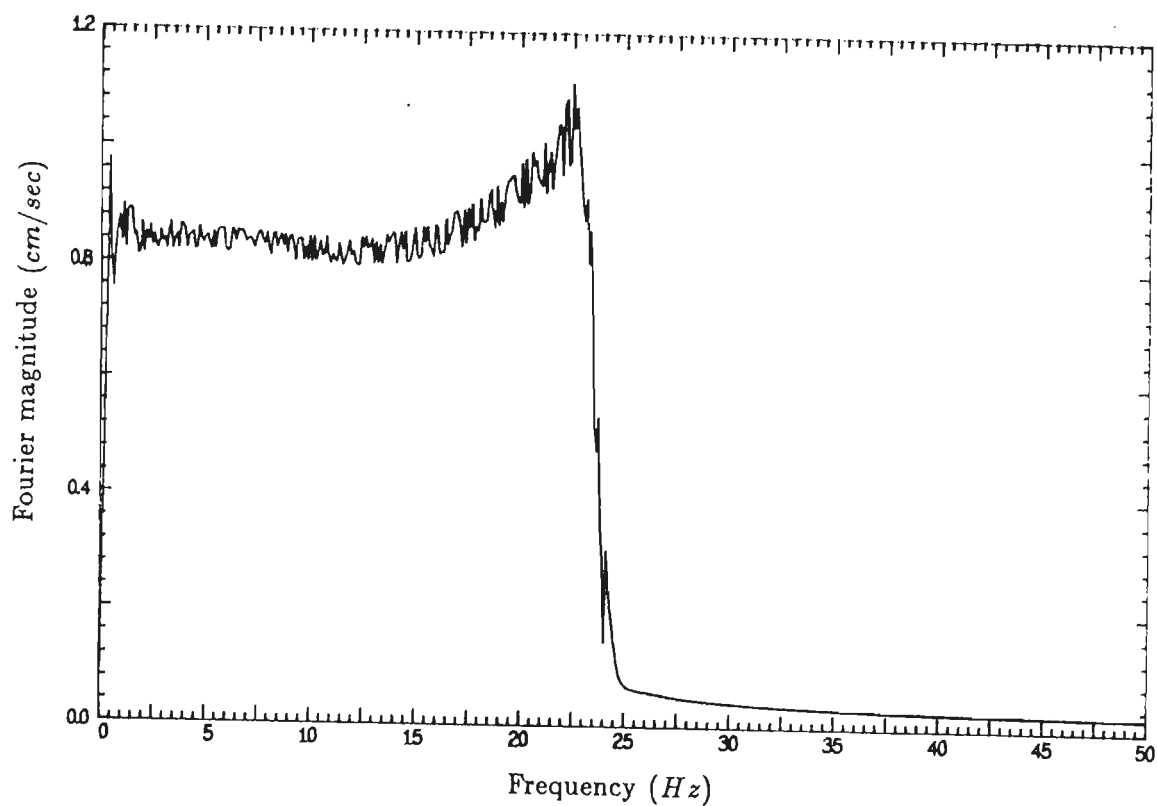


Figure 7.2: Fourier magnitude plot of Response of Erdik's scheme to white noise input

similar with jitters in the pass band. However, the jitters are smaller because the entire processing in this scheme is done at 100 *SPS* whereas it is done at 50 *SPS* in the Trifunac's scheme. However, in comparison to the response to the proposed scheme (Fig. 6.6) the response of this scheme is jittery in the pass band.

7.3 Scheme of Khemici and Chiang

The scheme of Khemici and Chiang which they refer as Stanford Accelerogram Correction Procedure (SACP) is in frequency domain and the proposed scheme described in Chapter 6 is quite similar to this scheme in several aspects. However, the Khemici's scheme has not suggested any method to interpolate the nonuniformly and uniformly spaced samples so that the frequency contents of the data do not change after the interpolation. The scheme of Khemici and Chiang starts with uniformly spaced uncorrected accelerogram. The instrument correction is performed in frequency domain in exactly the same fashion as discussed for the proposed scheme in the Chapter 6. The band pass filtering is performed by using a filter function which has unit gain in pass band, half cosine tapering in the transition bands and zero gain in the stop band. This filter function has only real values and therefore the filtering operation doesnot introduce any phase shift. The transfer functions of instrument correction and that of band pass filter are multiplied to obtain the overall transfer function of the scheme. The Fourier transformation of uncorrected accelerogram is found which on convolution with the transfer function of the scheme gives the Fourier transformation of the corrected accelerogram, an inverse Fourier transform of which yields corrected accelerogram. Integration of corrected accelerogram to get velocity and displacement are performed in frequency domain.

To check the performance of this scheme, a white noise input at 100 *SPS* in the similar manner as it is given in the earlier section is imparted in this scheme with same accelerometer and filter specifications. The Fourier magnitude plot of the corrected sequence obtained is given in Fig. 7.3. It can be seen that the response of this scheme is similar to the proposed scheme with no jitters in the pass band. It may, however, be noted that the similarity between this scheme and the proposed scheme exists only in response of instrument correction and band pass filter to white noise. However, the effect of band limited interpolation of nonuniform samples as suggested in the proposed scheme could not be studied here due to the fact that white noise with nonuniform samples could not be generated. Similarly, the effect of band limited interpolation of the uniform samples to increase the sampling rate of the corrected accelerogram as

suggested in the proposed scheme in comparison to the prevalent linear interpolation, has not been studied here. This part will be discussed in the next Section of this Chapter.

7.4 Comparative study of schemes to white noise

Some important sections of the schemes are studied separately to compare their performance for white noise input. In this regard the instrument correction and low pass filter are studied.

A white noise of 200 *SPS* with 2048 data points is generated. The instrument correction of this white noise is performed in time domain (as per scheme of Trifunac and also the scheme of Erdik) assuming natural frequency of accelerometer to be 20 *Hz* and damping to be 60% of critical. Similarly instrument correction of this white noise is performed in frequency domain (as per the proposed scheme and also the scheme of Khemici) for the same specifications of accelerometer. The Fourier spectra of the instrument corrected data by the two methods are determined and their Fourier magnitudes are plotted one over the other as shown in Fig. 7.4 (plotted upto 50 *Hz*). The plot shows that the frequency domain instrument correction matches exactly with the ideal instrument correction process. Whereas, the time domain correction process using central difference scheme is jittery and also drops down at higher frequencies in comparison to ideal case.

Similarly performance of low pass filter of different schemes to 200 *SPS* white noise with 2048 data points are studied next. The two time domain schemes use Ormsby filter as low pass filter, whereas, the proposed scheme uses Butterworth filter (order 6) and Khemici's scheme uses half cosine tapering. The convolution with white noise of filter of the proposed scheme as well as the scheme of Khemici is done in frequency domain. The low passed sequence of all the three filters for white noise input are found. The Fourier magnitudes of these schemes are plotted one over the other and is shown in Fig. 7.5. All the three low pass filters performs more or less similarly except that the response of the Ormsby filter shows jitters in the pass band whereas the response of Butterworth filter and half cosine filters show smooth pass band as well as transition band. This confirms the draw back of convolution in time domain which causes jitters.

Next a white noise input is given as uncorrected accelerogram to all the four schemes which are under study and with same accelerometer specifications as used earlier. The cut off frequency of high pass filter is taken as 0.1 *Hz* with roll off of

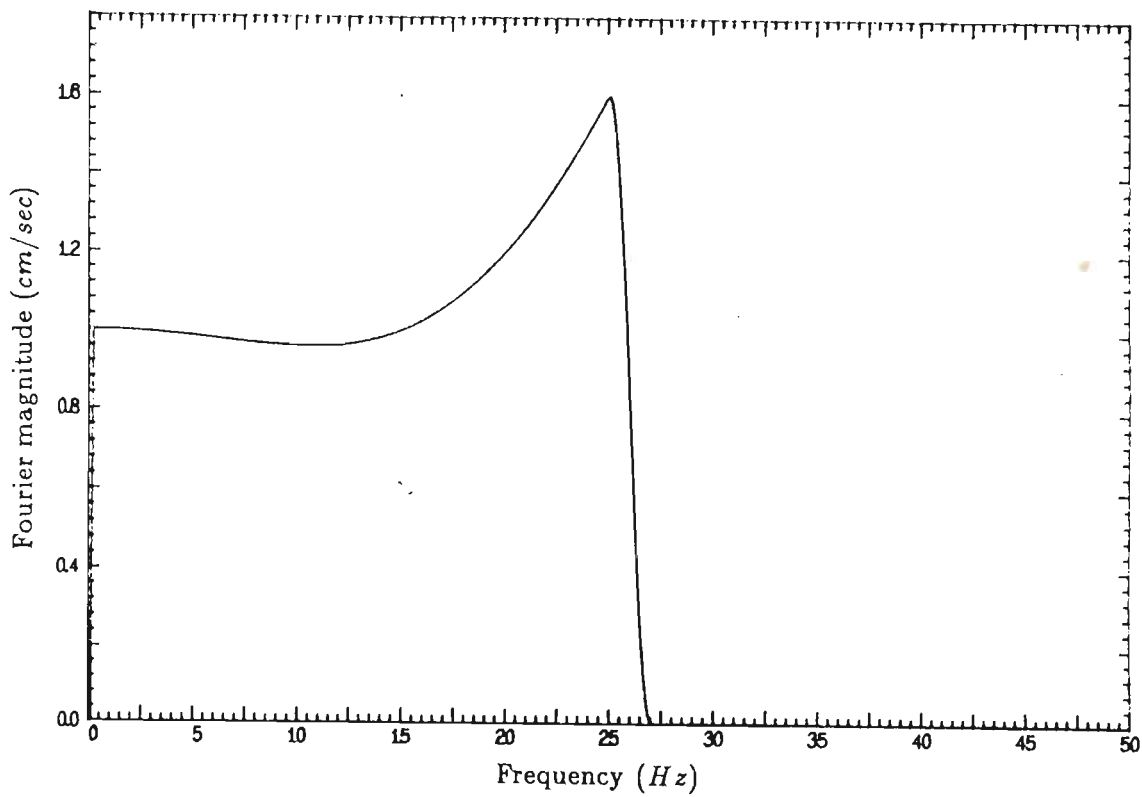


Figure 7.3: Fourier magnitude plot of Response of Khemici's scheme to white noise input

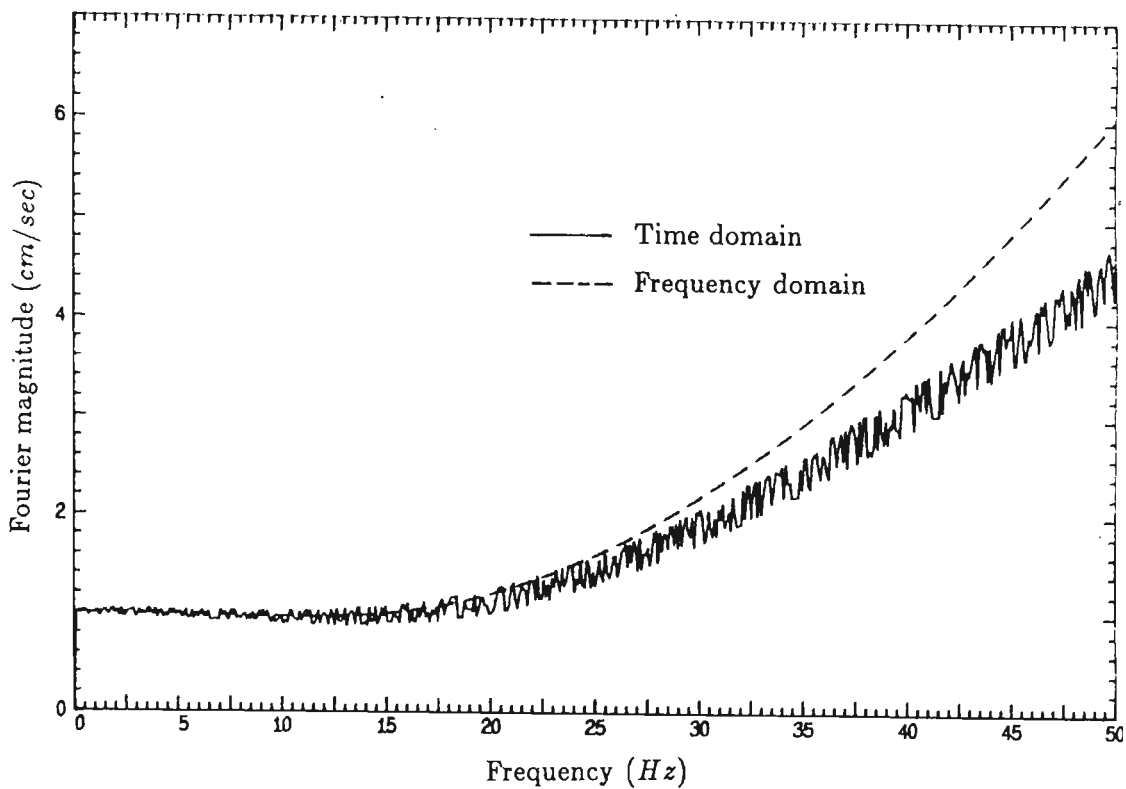


Figure 7.4: Comparison of response to white noise between instrument correction in time domain and frequency domain

0.02 Hz (if required) and cut off frequency of low pass filter is taken as 25 Hz with a roll off of 2 Hz (if required). The Trifunac's scheme determines the corrected sequence at 50 *SPS* whereas the proposed scheme, the Erdik's scheme and the Khemici's scheme determine the corrected sequence at 100 *SPS*. It is assumed that the user of the accelerogram is requiring the data at 200 *SPS*. The corrected sequence obtained from the proposed scheme is band limited interpolated using method described in Chapter 5 to double the sampling rate. The corrected sequence obtained from Trifunac's scheme is linearly interpolated to increase the sampling rate by four times. The corrected sequence obtained from Erdik's scheme and Khemici's scheme is linearly interpolated to double the sampling rate. Fourier spectra of 200 *SPS* sequence thus obtained for four schemes as described above are determined. Fourier magnitude spectra of all the four sequences are plotted one over the other and is shown in Fig. 7.6. This plot indicates the effect of linearly interpolating the sequence. The three schemes which are linearly interpolated have lost substantial amount of energy from the original frequency band and instead have high frequency replicates. The worst effected is Trifunac's scheme where the the sampling rate was increased four times as it has now three additional replicates in high frequency at the cost of lowering the contribution of the original frequency content. The Khemici's scheme and Erdik's scheme in which the sampling rate is doubled, show one additional replicate at the higher frequency at the cost of lowering the contribution of frequency contents of the original data. In fact the Khemici's scheme which had no jitters in the pass band before the interpolation has jitters now in the pass band. In contrast, the proposed scheme show a perfect and ideal overall performance and preserves frequency contents of the data.

7.5 Comparative study of schemes to earthquake signal

In this part of the work, four uncorrected accelerograms are corrected by the three schemes described in this chapter as well as by the proposed scheme described in Chapter 6. The uncorrected accelerograms are N-S component Imperial valley earthquake of May 18, 1940 recorded at El Centro (EERL 70-20, file 1) [105]; N05W component of Parkfield earthquake of June 27, 1966 recorded at Cholame, Shandon (EERL 70-21, file 40) [106]; N21E component of Kern County California earthquake of July 21, 1952 recorded at Taft Lincoln School Tunnel (EERL 70-20, file 10) [105] and S72W component of Uttarkashi earthquake of October 20, 1991 recorded at Uttarkashi (Data obtained from INSMIN project of Department of Earthquake Engineering, University

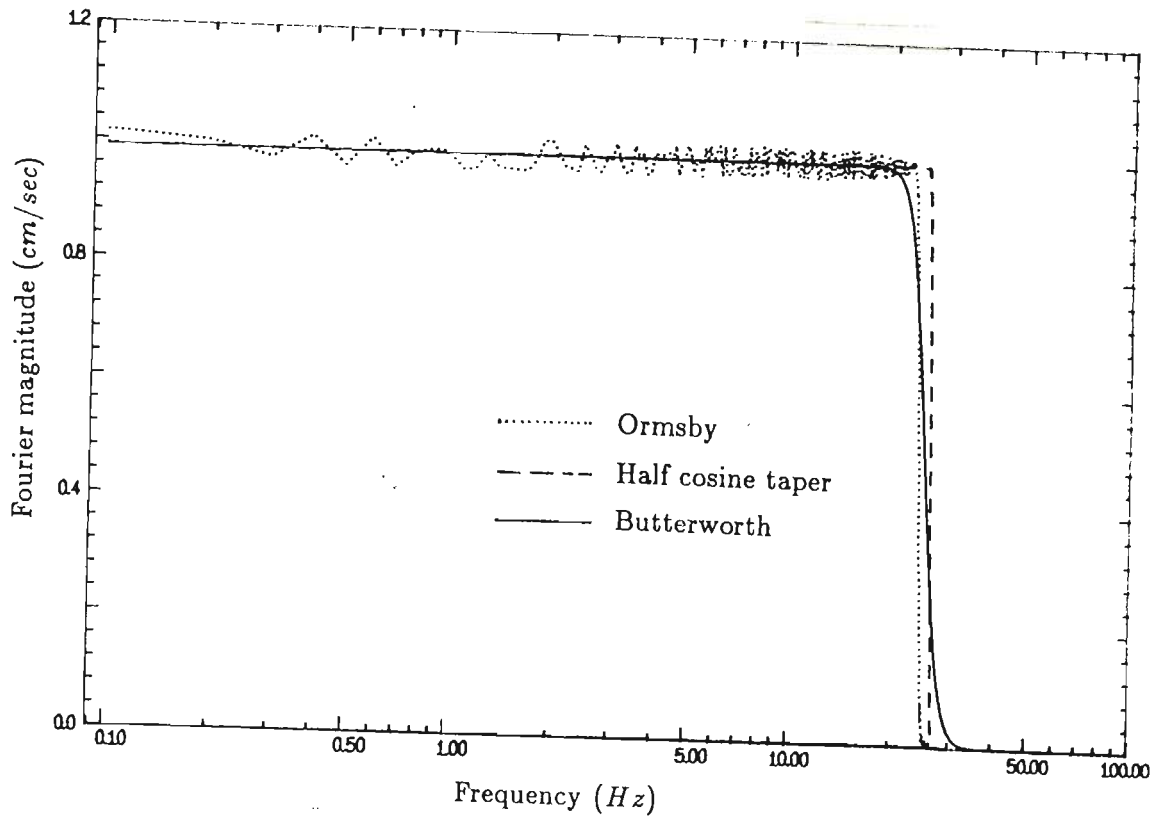


Figure 7.5: Comparison of response to white noise between Ormsby, half cosine taper and Butterworth low pass filters

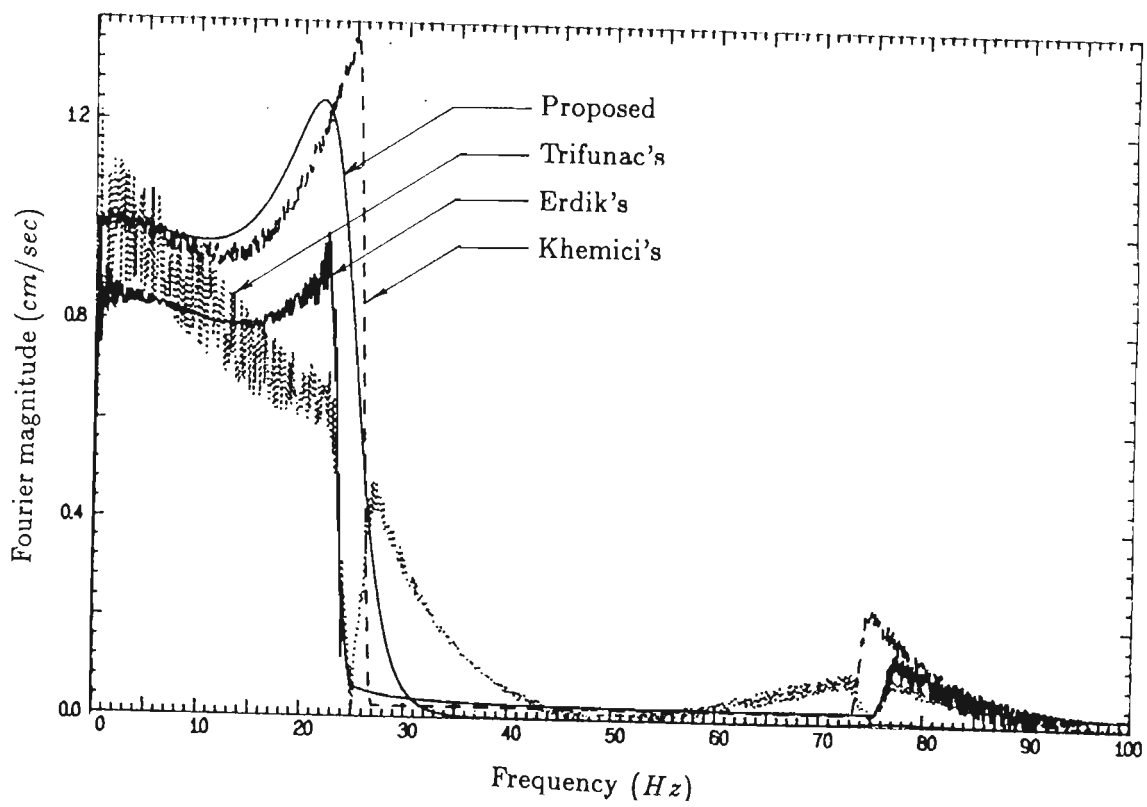


Figure 7.6: Comparison of response to white noise between proposed, Trifunac's, Erdik's and Khemici's schemes for corrected sequence of 200 SPS

of Roorkee). The corrected accelerograms of all the schemes are obtained at 200 *SPS*. Table 7.1 summarizes the methods of interpolations and the cut off frequencies used by different schemes.

Table 7.1: Summary of Type of Interpolation and Cut off Frequencies Used by Different Schemes

Scheme	Interpolation of Nonuniform Samples	Cut Off Frequencies (Hz) (roll off if required)		Sampling Rate Expander (Initial SPS, Final SPS)
		High Pass	Low Pass	
Proposed	Band Limited	0.07	< 0.5 (Av. <i>SPS</i>)	Band Limited (100,200)
Khemici	Linear	0.07 (0.05)	25.00 (2.00)	Linear (100,200)
Trifunac	Linear	0.07 (0.05)	25.00 (2.00)	Linear (50,200)
Erdik	Linear	0.07	25.00 (2.00)	Linear (100,200)

Table 7.2 gives details of accelerometer specifications and cut off frequency of low pass filter (ω_L) used in the proposed correction scheme for different earthquakes.

Table 7.2: Cut off Frequency of Low Pass Filter of the Proposed Scheme & Accelerometer Specifications

Earthquake	ω_L (Hz)	Accelerometer Specifications	
		ω_n (Hz)	ζ (% of critical)
El Centro	9.00	10.00	55.2
Parkfield	11.00	19.65	37.0
Taft	8.50	12.35	57.4
Uttarkashi	25.00	24.50	59.0

The maximum values of the acceleration, velocity and displacement as well as the time of their occurrence are compared in a tabular form for the four earthquakes. The Fourier magnitudes of corrected accelerograms of all the four schemes are determined and are compared for the four corrected accelerograms. Response spectra for 2% damping for the four earthquakes are computed for the proposed scheme and for Trifunac's scheme and are plotted one over the other for comparison.

7.5.1 Comparison of Maximum Motion

Tables 7.3 to 7.6 give the values of maximum acceleration, velocity and displacements alongwith time of its' occurence determined through four schemes for El Centro, Parkfield, Taft and Uttarkashi earthquakes respectively. These tables show that the maximum value of acceleration and its' time of occurence determined through all the four schemes match quite well. However, there are differences in derived maximum velocity and its' time of occurence and there are substantial differences in the derived maximum displacements and its' time of occurence. The differences in maximum velocity and maximum displacements have occurred due to the fact that the cutoff frequency of high pass filter has not been properly selected after viewing the frequency contents of uncorrected accelerogram. If the cutoff frequency of high pass filter is increased then the results of maximum velocity and maximum displacements from the four schemes comes out to be the same. However, neither of the two yield true velocity or displacement due to the simple fact that at very low frequency, noise is more than the signal and in integration the very low frequency contents dominate. Thus increasing cutoff frequency of high pass filter may give uniform results of maximum velocity and displacement for four schemes but these results will not be realistic.

Table 7.3: Maximum Motion for El Centro Accelerogram

Scheme	Max. Acceleration		Max. Velocity		Max. Displacement	
	Value (<i>gals</i>)	Instant (<i>sec</i>)	Value (<i>cm/sec</i>)	Instant (<i>sec</i>)	Value (<i>cm</i>)	Instant (<i>sec</i>)
Proposed	352.96	2.18	63.06	2.24	78.09	2.77
Khemic	399.07	2.24	39.83	2.23	22.37	1.11
Trifunac	394.60	2.14	44.54	2.20	53.93	53.74
Erdik	355.18	2.44	36.71	2.18	17.91	8.60

7.5.2 Comparison in Frequency Domain

A frequency domain comparison of the corrected accelerograms at 200 *SPS* obtained from four different schemes is also done. For this purpose, Fourier transformation of the corrected accelerograms is taken. The entire band upto 100 *Hz* (Nyquist frequency) is divided into 16 segments. Frequency band upto 25 *Hz* is divided into 10 equal segments and frequency band between 25 *Hz* and 100 *Hz* is divided into 6 equal segments. Mean Fourier magnitude in each band for the four schemes is determined and is presented in

Table 7.4: Maximum Motion for Parkfield Accelerogram

Scheme	Max. Acceleration		Max. Velocity		Max. Displacement	
	Value (<i>gals</i>)	Instant (<i>sec</i>)	Value (<i>cm/sec</i>)	Instant (<i>sec</i>)	Value (<i>cm</i>)	Instant (<i>sec</i>)
Proposed	352.05	7.43	21.50	7.53	12.05	1.17
Khemici	359.34	7.41	22.17	7.52	6.38	10.66
Trifunac	360.92	7.42	23.39	7.52	5.18	10.66
Erdik	313.82	7.40	23.04	7.50	4.88	5.84

Table 7.5: Maximum Motion for Taft Accelerogram

Scheme	Max. Acceleration		Max. Velocity		Max. Displacement	
	Value (<i>gals</i>)	Instant (<i>sec</i>)	Value (<i>cm/sec</i>)	Instant (<i>sec</i>)	Value (<i>cm</i>)	Instant (<i>sec</i>)
Proposed	198.68	9.19	21.11	9.55	16.75	2.96
Khemici	172.16	9.14	14.62	3.44	13.44	53.44
Trifunac	169.80	9.12	16.39	3.42	7.53	49.26
Erdik	146.16	9.10	15.87	3.41	7.86	49.28

Table 7.6: Maximum Motion from Uttarkashi Accelerogram

Scheme	Max. Acceleration		Max. Velocity		Max. Displacement	
	Value (<i>gals</i>)	Instant (<i>sec</i>)	Value (<i>cm/sec</i>)	Instant (<i>sec</i>)	Value (<i>cm</i>)	Instant (<i>sec</i>)
Proposed	508.00	5.15	31.56	5.05	42.86	30.47
Khemici	498.19	5.13	24.84	24.10	40.77	22.67
Trifunac	518.80	5.12	31.52	5.04	51.09	35.84
Erdik	481.50	5.10	29.45	5.02	37.49	30.55

Tables 7.7 to 7.10 for El Centro, Parkfield, Taft and Uttarkashi earthquakes respectively.

For El Centro, Parkfield and Taft accelerograms, in all the frequency segments which are above the cut off frequency of low pass filter (ω_L) of the proposed scheme (Table 7.2), the Fourier magnitude of proposed scheme is much smaller than the Fourier magnitude of the other three schemes. For these earthquakes, in most of the segments of frequencies less than, (ω_L) the mean Fourier magnitude is more in the proposed scheme in comparison to other three schemes. For Uttarkashi earthquake the cut off frequency of low pass filter is same (25 Hz) for the proposed scheme and the remaining three schemes. For this earthquake also, in most of the frequency segments less than 25 Hz the mean Fourier magnitude obtained from the proposed scheme is more than that of other schemes and also for most of the frequency segments greater than 25 Hz the mean Fourier magnitude of the proposed scheme is less than those of other three schemes. These results, thus clearly prove superiority of the proposed scheme over other schemes, as other schemes have larger energy in stop band at the cost of reducing energy from the pass band.

Table 7.7: Comparison of Schemes for El Centro Accelerogram

Frequency Segment		Mean of Magnitude			
Begin (Hz)	End (Hz)	Trifunac (dB)	Khemici (dB)	Erdik (dB)	Proposed (dB)
0.000	2.478	40.093	39.838	38.608	41.073
2.490	4.968	36.674	36.625	35.427	37.233
4.980	7.458	32.367	32.567	31.399	33.550
7.471	9.949	28.678	29.230	28.139	26.063
9.961	12.439	25.722	26.808	25.789	8.735
12.451	14.929	25.489	27.248	25.929	-14.610
14.941	17.419	25.603	27.999	26.771	-17.458
17.432	19.910	24.009	27.297	26.013	-18.667
19.922	22.400	23.370	27.824	26.104	-19.682
22.412	24.890	18.237	28.050	22.559	-20.514
0.000	25.000	30.435	31.590	30.117	28.158
24.902	37.402	14.976	5.829	12.266	-22.295
37.415	49.915	-0.150	-33.581	7.564	-25.672
49.927	62.427	-4.932	-35.489	5.393	-36.699
62.439	74.939	3.746	-9.942	4.330	-54.242
74.951	87.471	2.335	7.496	7.605	-68.327
87.463	99.963	-8.742	-8.130	3.023	-33.833
25.012	100.00	4.756	-1.769	7.214	-31.187
0.000	100.000	19.656	20.094	19.768	16.148

Table 7.8: Comparison of Schemes for Parkfield Accelerogram

Frequency Segment		Mean of Magnitude			
Begin (Hz)	End (Hz)	Trifunac (dB)	Khemici (dB)	Erdik (dB)	Proposed (dB)
0.000	2.478	33.783	33.631	32.368	33.689
2.490	4.968	32.783	32.711	31.482	32.860
4.980	7.458	25.606	25.746	24.581	26.637
7.471	9.949	21.086	21.618	20.445	22.300
9.961	12.439	20.682	21.624	20.471	16.841
12.451	14.929	13.300	14.902	13.629	-6.617
14.941	17.419	11.438	13.909	12.404	-35.432
17.432	19.910	12.157	15.774	13.830	-42.130
19.922	22.400	5.129	9.726	7.607	-43.565
22.412	24.890	0.131	9.790	1.717	-44.663
0.000	25.000	23.419	23.914	22.542	22.522
24.902	37.402	-0.226	-13.279	-21.011	-46.825
37.415	49.915	-6.225	-40.875	-25.631	-50.454
49.927	62.427	-11.019	-42.756	-27.807	-61.504
62.439	74.939	-10.818	-28.184	-29.030	-78.852
74.951	87.471	-12.504	-8.014	-10.952	-78.117
87.463	99.963	-14.798	-14.273	-15.185	-38.700
25.012	100.00	-7.770	-17.005	-18.988	-49.445
0.000	100.000	12.071	12.108	10.719	10.490

Table 7.9: Comparison of Schemes for Taft accelerogram

Frequency Segment		Mean of Magnitude			
Begin (Hz)	End (Hz)	Trifunac (dB)	Khemici (dB)	Erdik (dB)	Proposed (dB)
0.000	2.478	34.135	33.956	32.696	34.346
2.490	4.968	32.623	32.578	31.342	34.023
4.980	7.458	27.925	28.095	26.907	31.684
7.471	9.949	20.139	20.637	19.458	21.001
9.961	12.439	15.812	16.850	15.612	-3.964
12.451	14.929	11.930	13.776	12.390	-25.539
14.941	17.419	9.862	12.450	11.037	-27.378
17.432	19.910	7.905	11.419	9.838	-28.758
19.922	22.400	7.402	11.884	10.210	-29.865
22.412	24.890	2.641	12.171	6.367	-30.773
0.000	25.000	23.377	23.851	22.492	23.647
24.902	37.402	-0.669	-9.119	-5.653	-32.654
37.415	49.915	-7.930	-31.376	-10.411	-36.095
49.927	62.427	-12.147	-34.636	-12.617	-47.130
62.439	74.939	-11.742	-24.961	-13.808	-64.621
74.951	87.471	-13.214	-8.052	-9.051	-78.542
87.463	99.963	-16.226	-15.717	-12.828	-38.089
25.012	100.00	-8.689	-15.743	-10.286	-40.544
0.000	100.000	11.965	12.082	11.032	11.625

Table 7.10: Comparison of Schemes for Uttarkashi accelerogram

Frequency Segment		Mean of Magnitude			
Begin (Hz)	End (Hz)	Trifunac (dB)	Khemici (dB)	Erdik (dB)	Proposed (dB)
0.000	2.478	33.069	33.079	31.550	33.276
2.490	4.968	35.806	35.772	34.567	38.159
4.980	7.458	33.851	34.326	32.841	35.967
7.471	9.949	34.096	35.020	33.466	33.731
9.961	12.439	31.860	32.873	31.702	32.484
12.451	14.929	28.204	30.127	28.598	30.569
14.941	17.419	24.438	27.041	25.433	29.861
17.432	19.910	23.188	26.609	25.244	27.412
19.922	22.400	18.125	23.077	21.614	23.714
22.412	24.890	12.191	22.293	18.740	20.635
0.000	25.000	29.918	31.149	29.659	31.899
24.902	37.402	12.314	0.168	9.402	5.700
37.415	49.915	4.267	-28.396	4.673	-32.115
49.927	62.427	-1.048	-31.198	2.508	-43.533
62.439	74.939	1.970	-15.769	1.441	-32.855
74.951	87.471	0.149	4.739	5.396	-24.138
87.463	99.963	-4.485	-3.585	1.595	-30.177
25.012	100.00	4.005	-4.602	4.620	-9.586
0.000	100.000	19.110	19.529	18.971	20.081

7.5.3 Comparison of Response Spectra

Response spectra for 2% damping is found from corrected accelerogram of the proposed and that of Trifunac's scheme for all the four earthquakes discussed above. The response spectra are found using algorithm of Nigam and Jennings [65]. Figure 7.7 shows this comparison for El Centro accelerogram, Figure 7.8 shows this comparison for Parkfield whereas Figs. 7.9 and 7.10 show this comparison for Taft and Uttarkashi accelerograms respectively. In the low period side (high frequency) comparison for El Centro, Parkfield and Taft (Figs. 7.7, 7.8 & 7.9) show the effect of using wrong cut off frequency of low pass filter in Trifunac's scheme (which more or less represents all the scheme for response spectra). The differences in high frequency are thus caused by effect of aliasing particularly during linear interpolation in the processing scheme of Trifunac. This effect has resulted into higher spectral acceleration in El Centro and Parkfield accelerogram but has resulted into smaller value in case of Taft accelerogram. In higher periods, El Centro, Taft and Uttarkashi response spectra show good amount of difference but Parkfield accelerogram show surprisingly a very good matching. It can be concluded that in case band limited properties of the data is not properly preserved throughout the processing then the final effect on the response spectra obtained can be deceptive.

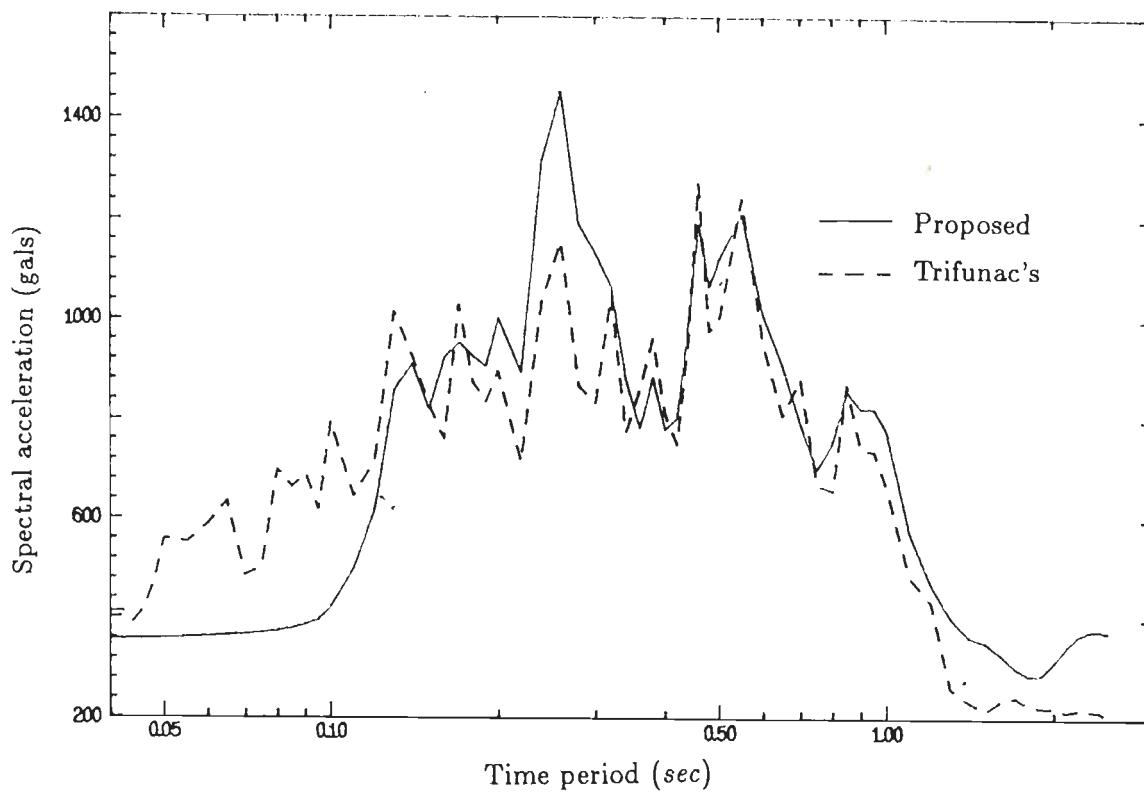


Figure 7.7: Comparison of response spectra (2% damping) determined from corrected accelerogram of the proposed scheme and that from Trifunac's scheme for El Centro motion

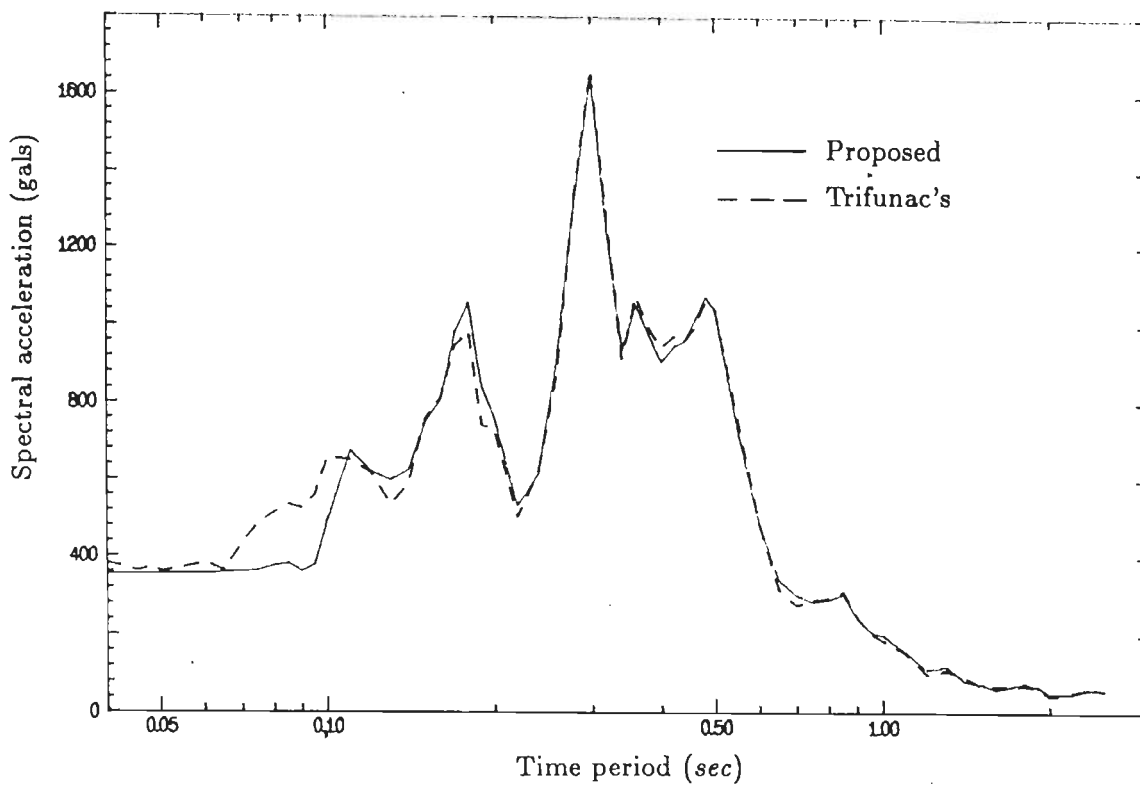


Figure 7.8: Comparison of response spectra (2% damping) determined from corrected accelerogram of the proposed scheme and that from Trifunac's scheme for Parkfield motion

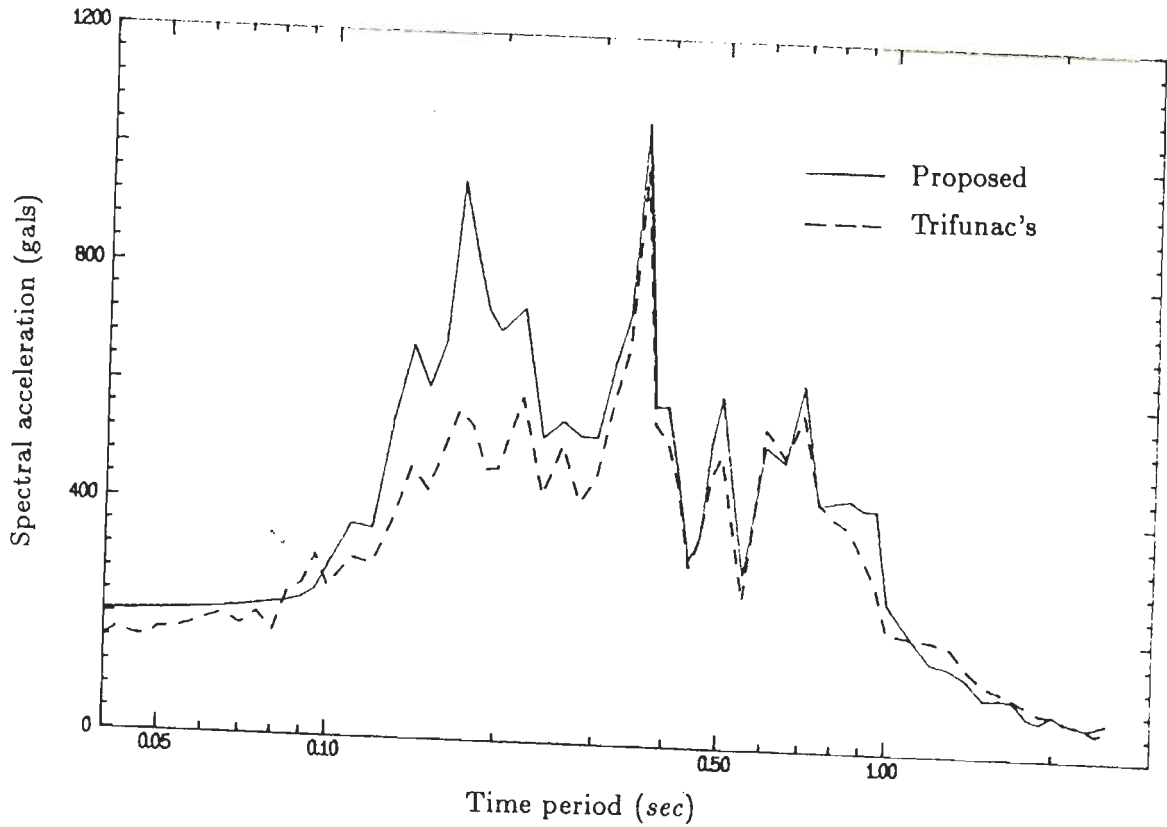


Figure 7.9: Comparison of response spectra (2% damping) determined from corrected accelerogram of the proposed scheme and that from Trifunac's scheme for Taft motion

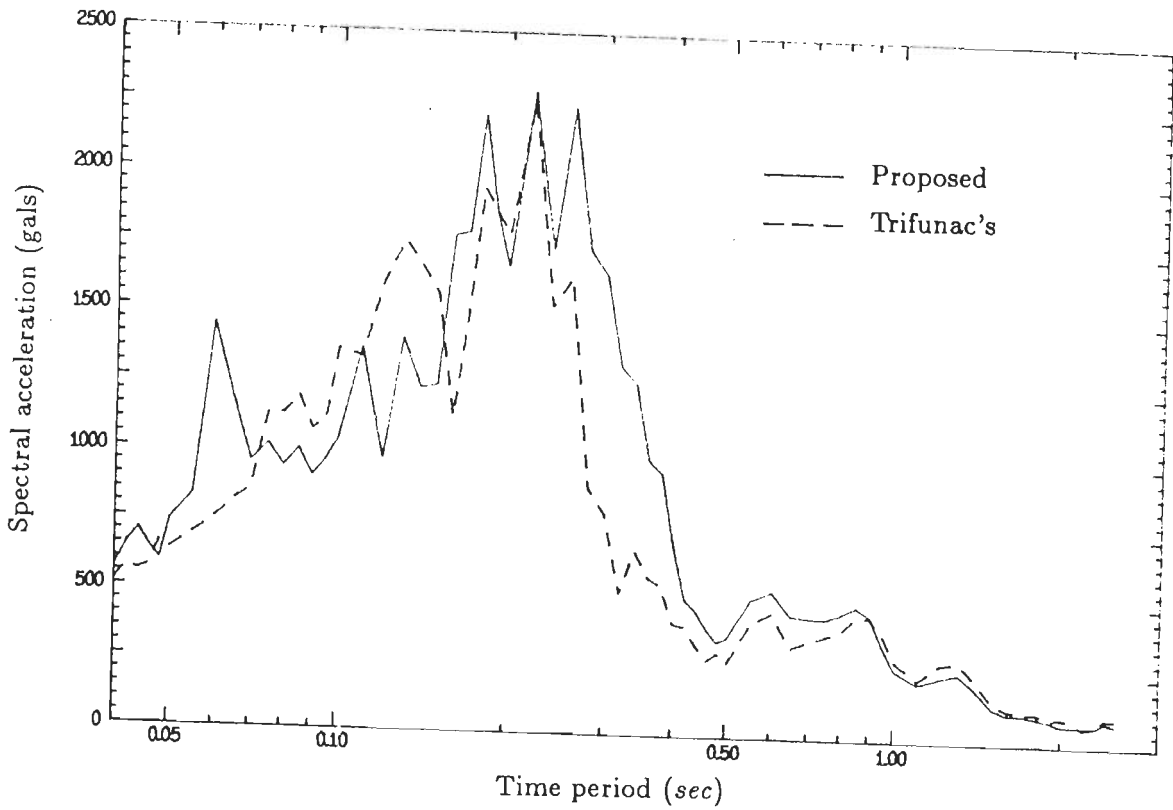


Figure 7.10: Comparison of response spectra (2% damping) determined from corrected accelerogram of the proposed scheme and that from Trifunac's scheme for Uttarkashi motion

Chapter 8

Problems of analog accelerograph & an ideal accelerograph

In this chapter, various aspects of analog accelerographs and the processing of its records is discussed. Analog accelerographs are viewed in regard to their design, operation and maintenance and problems associated in this regard are presented. In light of the work presented in chapters 4 to 7, a detailed review is done on the drawbacks of results obtained from the records of these instruments. Based on these discussions, requirements of an ideal accelerograph are outlined and specifications of a practical and economically feasible accelerograph are presented.

8.1 Design, operation & maintenance

Almost all analog accelerographs work on the principle as outlined for RESA V in Chapter 3. These accelerographs have stiff torsional pendulums which act as sensors and deflections of these pendulums are recorded on photographic paper or film through a suitably designed optics. The pendulums are damped through permanent magnets. The pendulums are carefully designed in such a way that except the fundamental torsional mode, all other modes of vibrations have higher frequencies so that their effects on the record remains small. However, the effect of the higher mode particularly that of bow string vibration of pendulum is bound to be present in the signature. The angular deflection of the torsional pendulum is recorded as linear deflection of the spot through optical amplification. Although, for all practical purposes, the small angular deflection of pendulum can be considered as proportional to the recorded linear deflection of the

spot but theoretically the effect of curvature is ignored. The control over the damping of the accelerometers is also approximate as it is achieved through permanent magnets. Although, these points may have only marginal effect on the final record but with ever increasing demand of higher accuracy in recording, such effects may become important.

Another important drawback in design of analog accelerograph is its recording through camera. Such recordings introduce low frequency noise due to misalignments in drive and pressure rollers of the camera which may cause wading of the recording paper. Fixed traces in the accelerographs provide only limited solution to this problem and the low frequency noise so introduced can not be eliminated with the help of fixed traces. One more problem of the camera is that its speed during the record particularly in the initial part is not constant and even with the time marks which provide segments of half seconds (generally calibrated through manual stop clocks) in the record, the time axis of the accelerogram may inherit errors. The design problems discussed above, are mainly due to the presence of one or more moving parts which introduce errors.

Analog accelerographs get triggered by a starting mechanism which is entirely independent of the sensors (accelerometers). This starting mechanism triggers the instrument at an approximately preset ground acceleration values. The threshold acceleration of the trigger can not be very exact due to characteristics and approximate calibration of triggering mechanism. But perhaps the biggest drawback of analog accelerographs is their incapability to record pre event. In fact such instruments start recording after almost 100 milliseconds of the trigger. Thus, some crucial part of the record before and after the trigger is invariably lost. Another problem associated with operation and recording from such instruments is thickness of the trace of the record which is thicker for small deflections and becomes thinner as the deflection increases.

Analog accelerographs require routine maintenance which should be carried out atleast once in 3 to 4 months. This includes checking of batteries, replacing photographic paper/film if required, checking the spots of accelerometers, fixed spots and time mark spots and adjusting them if required and some other carefully drawn out exercises to ensure proper working of the instrument. Obviously, such maintenance requires frequent visits to site by trained personnel and is time consuming and costly. In spite of this maintenance, problems of failure of power supply, jamming of camera, obstructions in the free movements of the accelerometer pendulums, failure of the photographic paper to enter inside the cassette, failure of the starting mechanism, shifting of the spot from the slit and other similar problems have been experienced. Most of these failures can be attributed again to mechanical troubles of the moving parts. Use of more reliable Ni-Cd batteries and solar cells have reduced the failure rate due to power problem, but still

10% to 15% of nonoperational analog accelerographs is quite common. Other problems of maintenance is that photographic paper/film used in such instruments have limited age and is necessarily required to be replaced immediately after its expiry even if it has not been fully used.

8.2 Development & digitization of records of analog accelerograph



The exposed photographic paper/film is brought in a cassette from the site to a dark room for development. Generally, this work is carried out at the headquarters where records from all the sites are brought for development. Several meters of photographic paper/film is needed to be developed for the record of each instrument. Thus, if an earthquake triggers few tens of accelerographs (30 to 40 is quite common) then retrieval and development of their records becomes a big exercise.

The developed records are then required to be digitized. Digitization is performed in either semi-automatic type digitizers or on automatic scanners, in which the former needs much more efforts. Some of the semi-automatic digitizers have inherent low frequency noise which gets added up with the digitized record. This can be found out by digitizing straight lines on these digitizers. However, this problem is not likely to be present in the automatic scanners. Digitization on semi-automatic digitizers is dependent on judgement of the operator who is required to pick the point on the record which is to be digitized by manually placing the hairline cursor. Automatic scanners give grey code of pixels of the screen. A judgement is thus required here also (which may be inherently built in the computer program) to pick the required pixels to form the record. It may be mentioned that due to thickness of the trace, more than one pixels in a vertical line will show a larger grey code and a logic is needed to pick one of them for the record. Semi-automatic digitizers provide samples at unequal interval whereas automatic scanners provide samples at constant interval and with quite high sampling rate. Semi-automatic type digitizer mostly have resolution of one thousandth of an inch. Automatic scanners are available from 600 dots per inch to 1500 dots per inch and thus have resolution of almost the same order as that of semi-automatic digitizers. With above discussions, advantages of using automatic scanner over conventional semi-automatic digitizers is apparent and thus semi-automatic type digitizers are now getting replaced by automatic scanners to perform digitization of records from large number of existing installations of analog accelerographs. However, large number of past records

of analog accelerographs were digitized on semi-automatic digitizers and in India such digitizers are not yet been replaced.

8.3 Processing of accelerograms

Digitized accelerogram are then required to be processed to obtain corrected accelerogram. This part has been discussed in detail in chapters 4 to 7. Chapter 4 presents a method to recover band limited signal from nonuniform samples if the record is digitized on a semi-automatic digitizer. Chapter 6 presents a scheme to process the accelerogram in frequency domain. The scheme proposed in this study preserves the band limited property of the data.

The processing procedure first passes the uncorrected uniformly spaced data through a low pass filter with a cut off frequency of half of average sampling rate of the raw digitized accelerogram or 25 *Hz* whichever is lower. The speed of the photographic paper as well as trace thickness of records do not permit resolution of the record more than this frequency. Thus, cut off frequency of maximum of 25 *Hz* is well in order.

This low passed data is then instrument corrected the details of which were discussed in Chapters 6 and 7.

All records of analog accelerographs have low frequency noise which creeps into the data during the process of recording and/or digitization. This noise exceeds signal or becomes comparable to signal at very low frequencies. It ,therefore, becomes essential to remove very low frequencies from the data where noise exceeds the signal or is comparable to the signal. This is achieved by performing high pass filter operation. This high passed data gives corrected accelerogram. Although, the value of a small change in the cut off frequency of the high pass filter does not have significant effect on the accelerogram but it has lot of effect on the derived velocity history and even greater effect on the derived displacement history. In fact, the derived velocity and displacement histories from records of analog accelerographs cannot be reliable if the low frequency noise is more than or is comparable to the low frequency signal which perhaps cannot be avoided in records of analog accelerographs. Other important reason for this conclusion is the fact that initial velocity and initial displacement, which are required during integration are assumed to be zero whereas actually analog accelerographs trigger at a preset threshold acceleration and at that instant of time the values of velocity and displacement are not known and these are certainly not zero.

8.4 An ideal accelerograph

8.4.1 Range of Recording

According to Hudson [43], a *strong motion accelerograph* is an instrumentation system from whose output an accurate determination can be made of the acceleration, velocity and displacement of the ground versus time for destructive earthquake ground motions. The use of word "accelerograph" in this connection implies neither that the basic instrument measures ground acceleration directly, nor that ground acceleration itself is alone a quantity of dominant importance. Hudson expects accelerographs to provide accurate recording from 0.05 to 50 Hz and having a dynamic range of 1000 to 1 (60 dB). However, in the presently available technology, accurate recordings are possible from DC onwards and a dynamic range of 72 to 96 dB is quite easily attained in digital systems. Systems with digital recording on solid state memory have several advantages which overcome most of the drawbacks of analog accelerographs which were discussed in the earlier section. Thus, an ideal accelerograph will necessarily have to be digital.

Such accelerograph should be able to provide accurate time histories of ground acceleration, velocity and displacement for frequencies for DC to 50 Hz. The capability to accurately record upto DC is essential to obtain information on low frequency velocity and displacement including permanent displacement of an earthquake which may be crucial for underground structures and systems.

For engineering purposes, if the time history can provide resolution of 1 gal it should be considered accurate enough. Thus, if maximum expected acceleration to be recorded is assumed to be $\pm 2g$ (about ± 2000 gals) then the dynamic range of accelerograph should be 72 dB. However, if an accelerograph can provide a dynamic range of 96 dB then the same accelerograph can be used to record acceleration of 1/16 gals. If upper limit of recording is made $\pm 1g$ instead $\pm 2g$ then accelerations as small as 1/32 gals can be recorded. In that case the accelerographs can be used to record even microearthquakes (it may not be appropriate then to call it a *strong motion* accelerograph). Thus, an ideal accelerograph is the one which should not only cater the needs of engineers who look for strong ground motion but may also be able to record microearthquakes and thus may even replace seismographs. An accelerograph should be able to record three components of ground acceleration. As per requirements of the resolution, for 96 dB dynamic range, a 16 bit analog to digital converter (ADC) is required and for resolution of 72 dB, a 12 bit ADC is required.

8.4.2 Sensor

The sensors to be used in an accelerograph should have high natural frequency (above 100 Hz) so that a flat frequency response from DC to 50 Hz can be obtained. The damping of the accelerometer should be 70% of critical. The natural frequency and damping of the accelerometer should be accurately controlled. The dynamic range of the accelerometer should be above 96 dB. It implies that if the largest signal which the accelerometer can record is set at $\pm 1g$ then the accelerometer should be able to provide a noiseless signal for $1/32$ gals or in other words the noise content of the accelerometer should be much smaller than voltage corresponding to $1/32$ g. The design of the sensor should be such that there is no chance of effect of its higher modes. It is possible only if the mass is permitted to move as little as possible. Servo accelerometers which are popularly called as force balance accelerometer (FBA) satisfy these requirements. With the introduction of FBA, the philosophy of seismic instruments has undergone substantial changes. Among the conventional seismic sensors, an accelerometer can not be used to record the ground motion of microearthquakes for the simple reason that the system is too stiff to produce any measurable deflection of the mass. However, in FBA the feed back current which is the measure of the ground acceleration, can be amplified and measured quite accurately. Thus the scenario has now shifted from mechanical measurement of the conventional sensors to electronic control and measurements employing force balance sensors.

The commonly used FBAs do not have phase advancing network which has advantages of getting feed back damping and a better balancing of forces on mass. Amini and Trifunac [4] have derived equation of motion and transfer function of FBA with phase advancing network which they attribute to technical notes and personal communications with Hudson. A schematic diagram of an FBA with phase advancing network is shown in Fig. 8.1. Here the basic sensor of the transducer is variable capacitance type. The output voltage of the sensor is amplified and through a phase advancing network fed to force generator which produces a force to balance the force caused by inertia force produced by ground acceleration. The voltage E_0 across resistance R of Fig. 8.1 is measured as output voltage. If $x(t)$ is the relative displacement of mass (M) in metre, then a voltage of $Dx(t)$ is fed to amplifier and phase shifting network where D is the sensitivity of capacitance sensor in volts/metre. The output voltage across resistance R is

$$E_0 = K_a D(x(t) + r\dot{x}(t)) \quad (8.1)$$

where K_a is the amplification of the amplifier, and r is the amplification of the phase

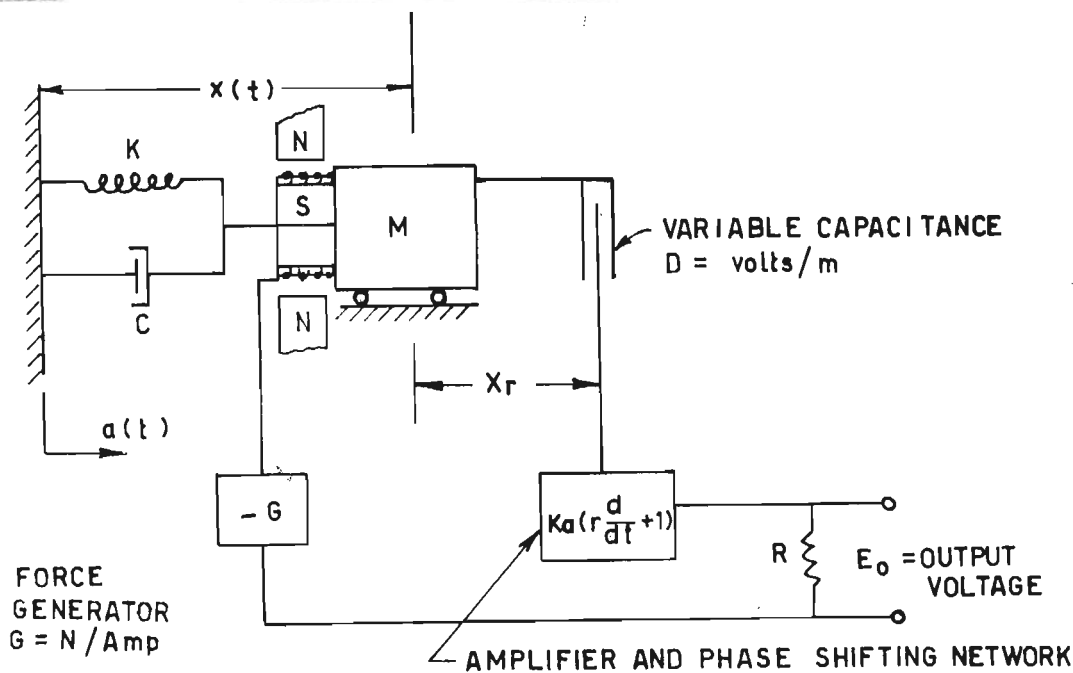


Figure 8.1: Schematic diagram of a FBA with phase advancing network. (from Amini and Trifunac [4])

shifting network. The current i in the feed back loop will be

$$\frac{E_0}{R} = \frac{K_a D}{R} (x(t) + r\dot{x}(t)) \tag{8.2}$$

This feed back current in the force generator produces a balancing force Gi on the mass, where G is a constant of the force generator whose units can be in *Newtons/amp*. Figure 8.2 gives freebody diagram of forces acting on the mass. By having equilibrium of mass, the equation of motion of FBA can be written as

$$M\ddot{x}(t) + C\dot{x}(t) + Kx(t) + Gi = -Ma(t) \tag{8.3}$$

where C is the co efficient of viscous damping and K is spring constant of the spring mass dashpot system and $a(t)$ is the ground acceleration. By putting value of i from Eq. 8.2 to Eq. 8.3, the following equation can be obtained

$$M\ddot{x}(t) + C\dot{x}(t) + Kx(t) + \frac{K_a D G}{R} (x(t) + r\dot{x}(t)) = -Ma(t) \tag{8.4}$$

The above equation can be written in the form

$$\ddot{x}(t) + 2\zeta\omega_n\dot{x}(t) + \omega_n^2x(t) = -a(t) \tag{8.5}$$

where

$$2\zeta\omega_n = \frac{C}{M} + \frac{rDGK_a}{MR} \tag{8.6}$$

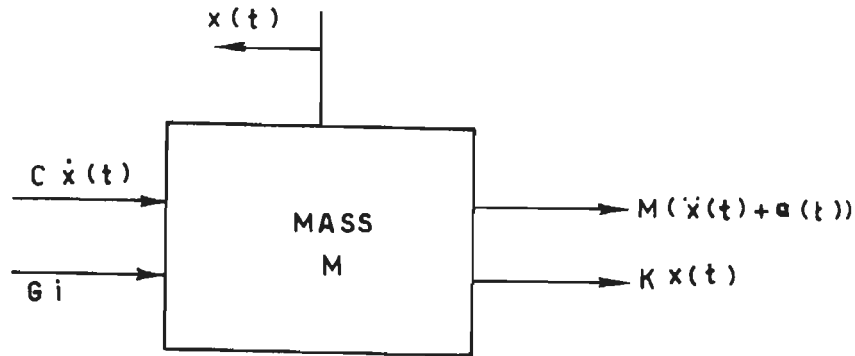


Figure 8.2: Free body diagram of forces acting on the mass of FBA

and

$$\omega_n^2 = \frac{K}{M} + \frac{DGK_a}{MR} \quad (8.7)$$

If the ground acceleration $a(t) = A \sin \omega t$ then the solution of Eq. 8.5 will be given by

$$x(t) = \frac{A}{\sqrt{(\omega_n^2 - \omega^2)^2 + (2\zeta\omega_n\omega)^2}} \quad (8.8)$$

In a FBA, mechanical damping $\frac{C}{M}$ of Eq. 8.6 and mechanical natural frequency $\frac{K}{M}$ of Eq. 8.7 are set much smaller than its electrical counterparts and can be ignored from Eqs. 8.6 and 8.7. If the value $x(t)$ from Eq. 8.8 is put on Eq. 8.1, then

$$E_0 = \left(\frac{MR}{G}\right)AY \sin(\omega t - \phi) \quad (8.9)$$

where

$$Y = \frac{\sqrt{1 + (2\zeta\frac{\omega}{\omega_n})^2}}{\sqrt{\{1 - (\frac{\omega}{\omega_n})^2\}^2 + \{2\zeta\frac{\omega}{\omega_n}\}^2}} \quad (8.10)$$

and

$$-\phi = \tan^{-1} \frac{2\zeta(\frac{\omega}{\omega_n})^3}{1 + (\frac{\omega}{\omega_n})^2(4\zeta^2 - 1)} \quad (8.11)$$

The magnitude of the transfer function between the output voltage E_0 and the ground acceleration A can be found from Eq. 8.9. The plot of the magnitude function gives a flat response from DC to about half of natural frequency for 70% damping and gives a linear phase shift for 70% damping for $\frac{\omega}{\omega_n}$ varying from zero to about 1.2. Thus the transfer function of this FBA is almost similar to transfer function of a conventional accelerometer. However, FBAs have several advantages over conventional accelerometer in which displacement of mass is converted into proportional voltage which is interpreted

in terms of acceleration. Internal displacement of mass in conventional accelerometers lead to inaccuracies and errors usually in the form of hysteresis, stickiness, nonlinearity and non repeatability. This is because of the fact that the sensing element is required to move over some distance to produce a measureable change in output. However, in FBA the output signal does not depend upon the displacement of mass and mass is permitted to move very little from its original position (typically less than one thousandth of an inch). Another advantage of FBA over conventional accelerometer is that in FBA, damping is controlled through electrical parameters and can be adjusted to precise value of 70% of critical, unlike in conventional accelerometers where damping is obtained through some viscous media and can not be controlled to precise value. Similarly, the natural frequency of FBA can be controlled precisely and varied with ease by selecting the values of components in circuit.

8.4.3 Other Specifications

An ideal accelerograph should have a recording capacity of 20 to 30 minutes which may be enough for 15 to 20 triggers. It should also have provision for recording pre event as well as absolute time of the trigger. There should be no drift in the clock (say less than 10 millisecond) which is possible only if the clock gets corrected continuously by radio time.

Since this accelerograph may be used for recording microearthquakes also, the trigger for the event should be selectable. There should be a provision to have trigger through STA/LTA (ratio of short term average and long term average) or through threshold acceleration as is usually done for accelerographs. An external trigger may also be there in the instrument so that if there are several instruments in a structural system or at a site then trigger of any one instrument may trigger all the instruments. This can also be made user selectable and a combination of triggers can be used for triggering the instrument.

The various control parameters of the accelerograph should be menu selectable. These parameters should be sampling rate, pre event time, post event time (to decide end of event) and decision on trigger algorithm. If trigger is to be done through threshold acceleration then the threshold values for start and end of event should be menu selectable. Similarly, if the trigger is to be done through STA/LTA then value of this ratio at which the trigger should take place and finish should be menu selectable.

The accelerograph should be battery operated with as small power requirement

as possible. The complete hardware should be in few PCBs which should be easily detached and fitted in the field. The complete accelerograph software should be permanently stored in EPROM so that there are no chances of its getting corrupted. The data retrieval including communication of the digital accelerograph with outside world for inspection, maintenance and operation should be done through a commonly used protocol like RS232C. The communication softwares and post processing softwares should be menu selectable and should be available in the computer to process the records. The computer used should be portable so that it can be taken to field and can be operated on battery. IBM compatible PCs are most suitable for this purpose as laptop and notebook type PCs are commonly available with RS232C ports. The accelerograph should have Modem facility so that it can be hooked up with telephone lines for remote communication. This will enable the users to communicate with the accelerograph from long distance and thus facilitate retrieval of earthquake records and inspection. At places where distances are large and where telephone facility is modern and reliable, the remote communication with accelerograph will be a cheaper and quicker method of inspection and data retrieval.

Chapter 9

Details of a digital accelerograph

In this chapter, some details of a digital accelerograph which was developed under a separate research scheme of which the author of this thesis was the Principal Investigator is discussed (Kumar *et al.* [53] and EQ Report [111]). This digital accelerograph uses a force balance accelerometer (FBA) transducer with a variable amplification signal conditioner having four pole Butterworth anti-aliasing filter. It is based on an INTEL 80C85 CMOS microprocessor with a 12 bit analog to digital converter (ADC). It has 512 KByte RAM which is sufficient to have a record of about 15 minutes at 100 *SPS*. Figure 9.1 gives block diagram of digital accelerograph instrumentation system. Various param-

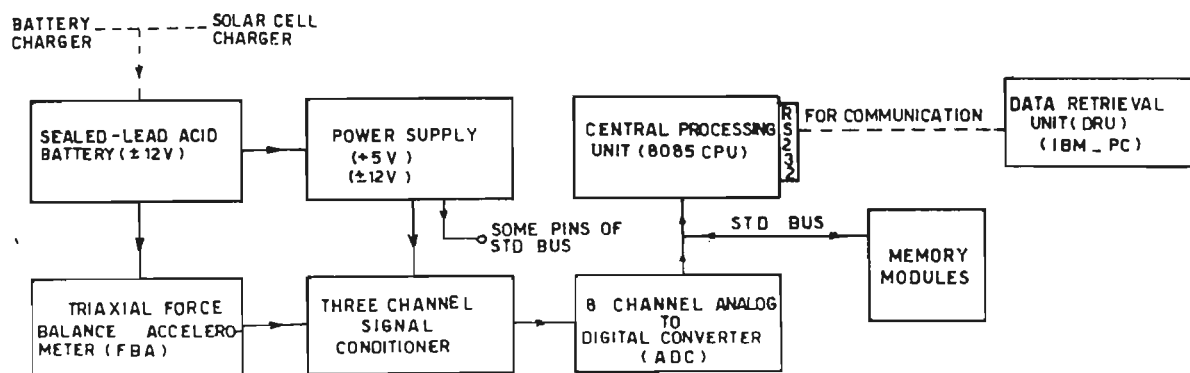


Figure 9.1: Block diagram of digital accelerograph instrumentation system

eters like sampling rate, pre-event time, post-event time, trigger threshold and end of

event threshold are menu selectable. Data retrieval is done on an IBM compatible PC through serial port. The communication between PC and digital accelerograph is done through a commercially available software. Two files are retrieved from digital accelerograph to PC. The first file named as the flag file has important information about the event to be processed, like trigger time, addresses of some important memory locations etc. and the second contains the data. An interactive software is developed in FORTRAN which reads the acquired files and give an output for the three components of time histories of recorded acceleration. The description of the instrument, its system software and hardware as well as post processing software is presented here. Table 9.1 gives detailed specifications of the digital accelerograph.

Table 9.1: SPECIFICATIONS OF DIGITAL ACCELEROGRAPH

ACCELEROMETER

- Triaxial force balance accelerometer (Columbia make SA-327TX)
- Full scale range: $\pm 2g$ (other ranges available)
- Damping: 0.70 of critical
- Calibration: through tilt test

DIGITAL RECORDER

- Resolution: 12 bits
- Signal Conditioner: Four pole Butterworth filter with variable gain
- Recording Bandwidth: 0.05 to 33 Hz.
- Processor: INTEL 8085
- Sample Rate: Menu selectable upto 200 SPS
- Trigger Mode: Signal derived from accelerometer
- Trigger Level: Menu selectable upto 0.03g
- Pre Event Memory: Menu selectable upto 10 seconds
- Post Event Memory: Menu selectable upto 20 seconds
- End of Event Level: Menu selectable upto 0.03g

- Memory: CMOS Ram (512 KByte)
- Battery Backup: Provided for memory card
- Recording Time: 15 minutes at 100 SPS for 3 channels
- Internal Clock: INTEL 5832 calendar chip

OTHER

- Data Retrieval: On IBM compatible PC
- Battery: 2 no. 12 volt 24 AH sealed lead acid battery
- Battery Charger: 220 Volts
- Weight: Approx. 15 Kg.
- Size: 370 × 370 × 200 mm

9.1 Transducer

A force balance accelerometer (FBA) is used as transducer in this instrument. FBAs have electrical feed back loop which is not there in conventional transducers. Most FBAs have variable capacitance type position detector whose output is amplified and is fed back. This electrical feed back loop produces an opposing force which is proportional to the feedback current and which balances the inertia force of mass caused by base acceleration. The schematic diagram of a typical FBA is given in Fig. 9.2. Amini and Trifunac [4] have shown that transfer function of such FBA are exactly same as the transfer function of a conventional transducer. However, the natural frequency and damping of FBA's are controlled by values of resistances and capacitances of the circuit. They have analyzed the transducer and derived its overall transfer function as well as natural frequency and damping in terms of values of capacitances and resistances of the circuit. The FBA which is currently used in the digital accelerograph is exactly similar to the one analyzed by Amini and Trifunac [4] and has the transfer function which is same as that of a conventional transducer.

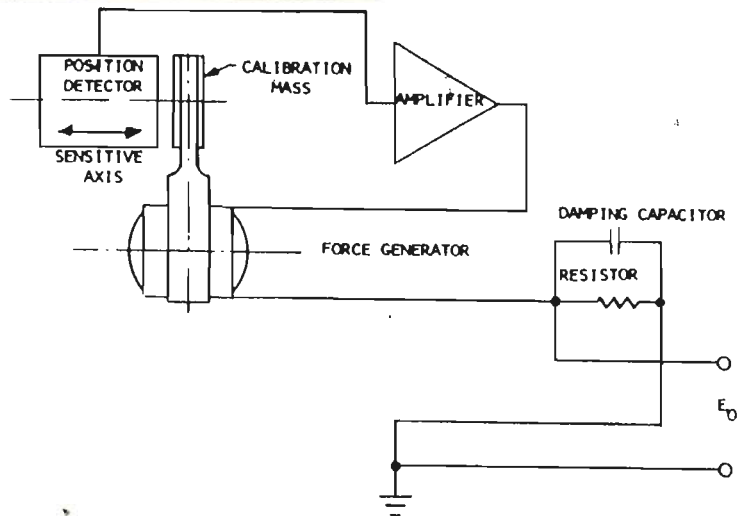


Figure 9.2: Schematic diagram of a force balance accelerometer

9.2 Signal conditioner

The signal conditioner developed for digital accelerograph performs two functions. Firstly, it amplifies the signal coming from the transducer. The amplification factor depends upon the maximum value of ground acceleration which is expected in an earthquake (range of record which is generally taken as $\pm 2g$), the sensitivity of accelerometer (volts/g) and the input to ADC which outputs all bits high (5 volt in this case). The amplification of the signal conditioner card is obtained by designing an operational amplifier circuit in which resistances can be varied through dip switches to get the desired amplification.

The second function performed by the signal conditioner is to filter high frequencies in order to eliminate affect of aliasing during digitization. In this setup four pole Butterworth low pass anti aliasing filter is designed to perform this function.

9.2.1 Design of Antialiasing Filter

To eliminate the effect of aliasing during the process of digitization in ADC, it is necessary that the analog signal fed to ADC is free from frequencies higher than half of sampling rate (Nyquist frequency) as otherwise these frequencies will distort the required frequency band. Thus, an analog online low pass filter with a cutoff frequency less than Nyquist frequency is an essential requirement of all digital recording systems.

In this case a four pole Butterworth analog filter is designed to perform this task. The filter is realized by cascading two second order filters. The second order transfer function is realized with RC elements and a single active device (Lam [54]). The transfer function of a normalised low pass four pole Butterworth filter is given by

$$H(s) = \prod_{k=1}^2 \frac{1}{(s^2 + b_k s + 1)} \quad (9.1)$$

where

$$b_1 = 0.7653668$$

$$b_2 = 1.84775907$$

Figure 9.3 give the circuit diagram of a second order low pass filter. Two such

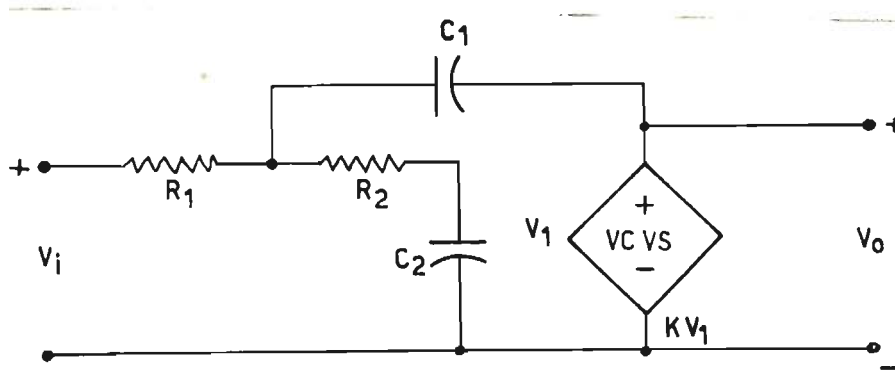


Figure 9.3: Circuit diagram of a standard second order low pass filter with RC elements and a single active device.

sections are cascaded and are designed according to following equations.

$$C_1 C_2 R_1 R_2 = 1 \quad (9.2)$$

and

$$C_1 R_1 + C_2 R_2 + R_1 C_2 - k C_1 R_1 = b \quad (9.3)$$

where C_1, C_2, R_1 and R_2 are values of resistances and capacitances as shown in Fig. 9.3 and k is the gain of the filter which is unity in this case. The value of b in Eq. 9.3 is to be taken as b_1 for the first section and is to be taken as b_2 for the second section. If the values of C_1 and C_2 are chosen then the values of R_1 and R_2 can be found from design Eqs. 9.2 and 9.3 and circuit diagram of low pass normalized filter where voltage controlled voltage source (VCVS) of Fig. 9.3 is replaced by a circuit of operational

amplifier with unit gain can be realized. If a cutoff frequency of 33 Hz is required which corresponds to 207.345 $radians/sec$ then the values of capacitance selected are divided by this number. An appropriate impedance scaling of the entire circuit is done to get suitable values of RC elements.

Both the sections of low pass second order Butterworth filter is similarly designed and are cascaded to get the Fourth order Butterworth filter.

9.3 Digital recorder

The digital recorder is based on 8085 microprocessor and the record is obtained on solid state memory. The output of signal conditioner is fed to 12 bit analog to digital converter (ADC). The ADC works in tandem with microprocessor and converts the analog signal into digital values at the desired sampling rate. Each digital value is then sent to the accumulator of the microprocessor which compares the value with the given threshold acceleration and determines whether the event has come or not. In case the event has not come, the digital data is fed to a set of memory locations (referred as ring storage). The number of memory locations in the ring storage are sampling rate multiplied by time for which pre-event data is required. The digital values of the output are stored in this ring storage till the event has not come. The moment the earthquake comes and the threshold ground acceleration exceeds the given value, the microprocessor start sending the digital values of the output to an open ended memory locations. The microprocessor also records the absolute time (month, day of week, day, hours, minute, second, mseconds) of occurrence of the earthquake in the flag of the software. The flag also stores other important informations of the event like starting address, end address, jump address of preevent etc. The data so recorded on solid state memory is retrieved on to a floppy or a hard disk of an IBM compatible PC.

9.3.1 Brief Description of Hardware

The hardware of digital recorder is divided in two cards. The first card which is called as CPU/ADC card consists of 80C85 microprocessor, Max162 ADC chip, 8253 timer, 8255 PPI, 1488, 1489 communication chips, 58167 calender chip with other supporting circuitry.

Max162 ADC chip has a resolution of 12 bits and its pin configuration is given in Fig. 9.4. Conversion in ADC is controlled by the \overline{CS} , \overline{RD} and HBEN digital inputs.

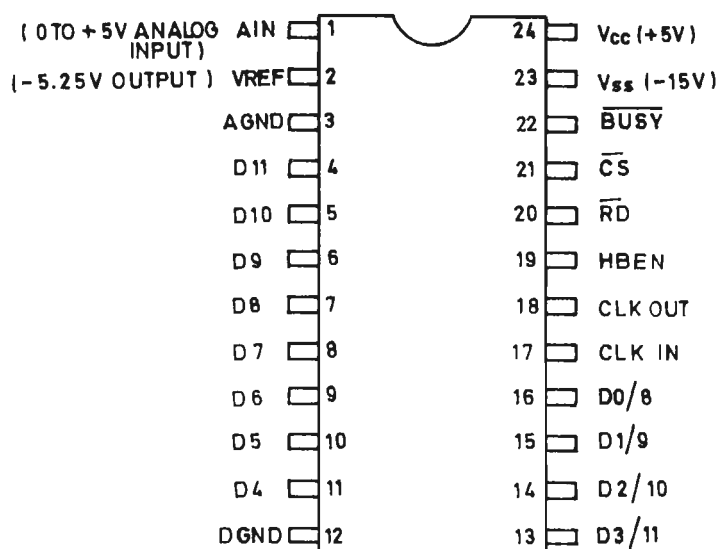


Figure 9.4: Pin configuration of Max162 ADC chip

A conversion starts at the falling edge of \overline{CS} and \overline{RD} while HBEN is low. The \overline{BUSY} output goes low as soon as the conversion starts. The 12 output bits are presented as two 8 bit words and data lines D7 to D0 are used. Byte selection is controlled by HBEN which multiplexes the data outputs. When HBEN is low, the lower 8 bits are presented as data output. When HBEN is high, the upper four bits are presented with leading four bits being low for lines D7 to D0. The control and timing diagram as well as data bus status on first, second and third read are given in Fig. 9.5 . A conversion is started with a READ operation with HBEN low. The data outputs present the 8 LSB's from the previous conversion and this data can be disregarded. Two more READ operations are needed to access the conversion result. The first read must be with HBEN high where the 4 MSB's with 4 leading zeros are accessed. The second READ is with HBEN low, which reads in the 8 LSB's and start a new conversion.

Timer 8253 is programmed to generate an interrupt after the interval at which sampling is required. This system is using a clock of 1.5 MHz and thus if the sampling rate is chosen as 100 SPS, then a hexadecimal equivalent of 15000 is required to be loaded on 8253. This number is read by the microprocessor from a menu string which enables the software to use the desired sampling rate. It may be noted that sampling rate should not be selected less than 66 SPS as in that case the anti aliasing filter will become ineffective.

The CPU/ADC card has 32KByte of memory capacity for addresses from 0000(H)

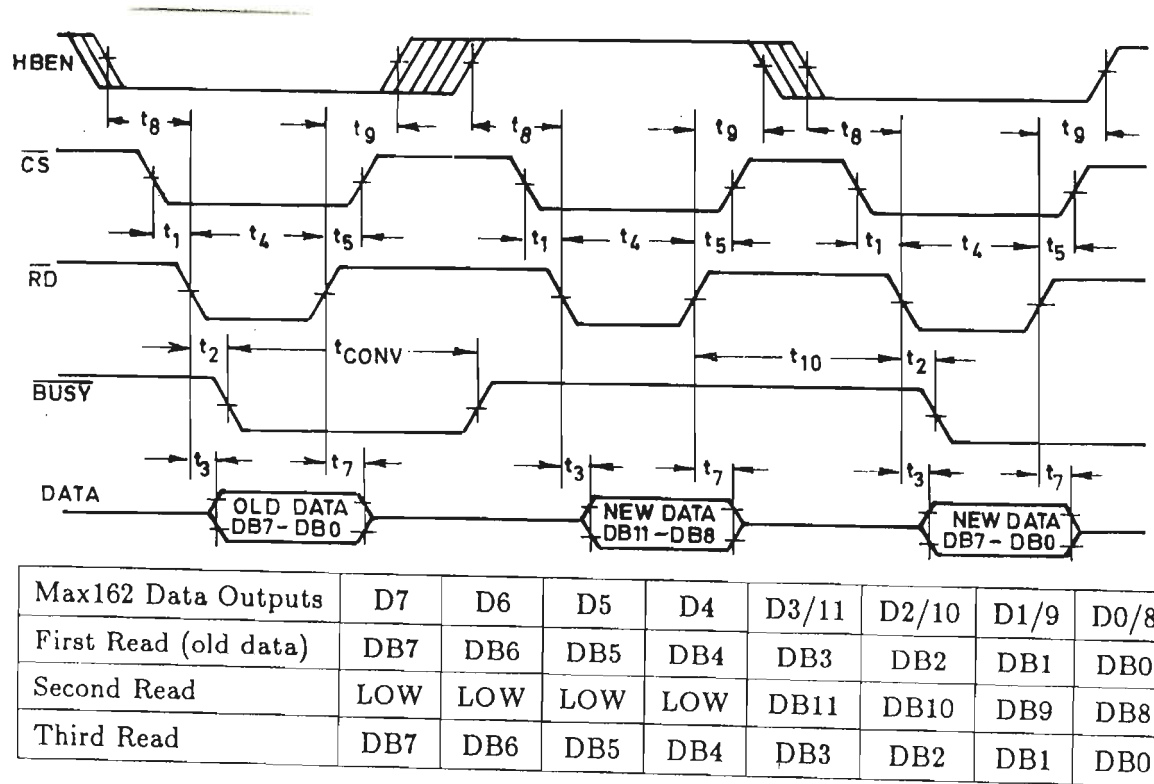


Figure 9.5: Control and timing diagram of ADC and data bus status on first, second and third READ

to 7FFF(H) in a suitable combination of EPROM/RAM. EPROM contains system monitor software for communication with outside world and for editing the data or program of the memory. This is stored at addresses from 0000(H) to 0FFF(H). Digital accelerometer program which will be discussed in the next subsection is also stored in EPROM at locations having addresses from 1000(H) to 1FFF(H). Memory locations of addresses 2000(H) to 2FFF(H) have RAM and is used for flags of the monitor program and similarly memory locations from 3000(H) to 3FFF(H) have RAM which is used for flags and menu string of digital accelerometer program. The memory mapping of the whole system is given in Fig. 9.6.

Support chip 8255 is programmed to give signal to an event indicator which glows on triggering. SID and SOD lines alongwith 1488 and 1489 chips are used to communicate with outside world via RS-232 port.

ADC, timer, support chip, memory bank and 58167 calendar chip are taken as I/O devices and each of them are assigned specific addresses and "IN" and "OUT" commands are used to input the data to the accumulator or to output the data from the accumulator. Table 9.2 gives the addresses assigned to these I/O devices.

The memory card of the digital accelerometer consists of 16 number of 62256 mem-

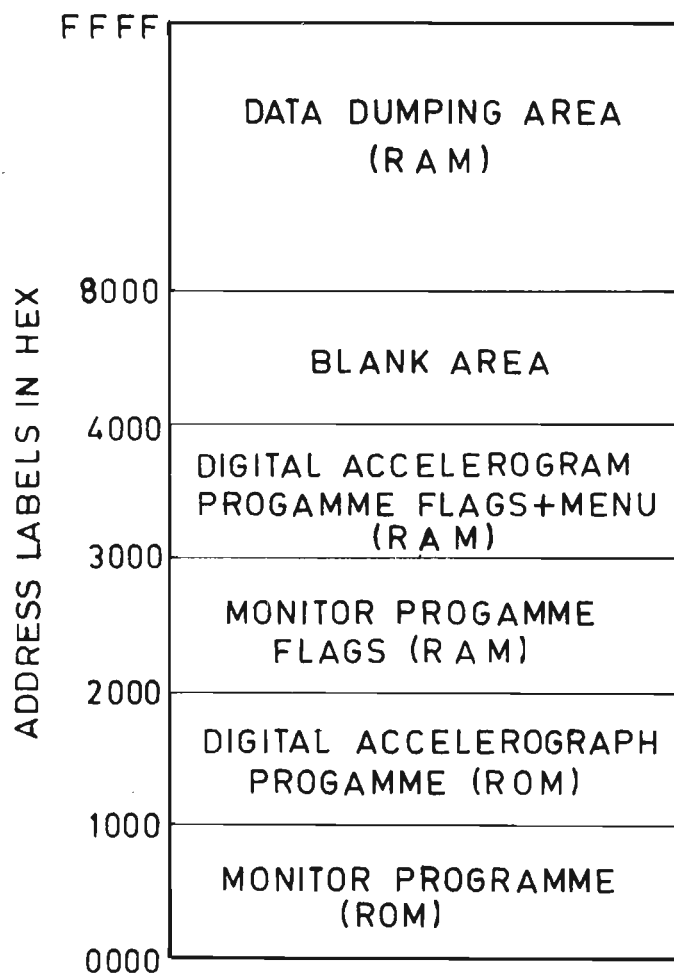


Figure 9.6: Memory mapping of digital accelerograph system

Table 9.2: Addresses of I/O Devices

Device	Port	Port Address (Hex)
8255 PPI	Port A	00
	Port B	01
	Port C	02
	Control Word	03
8253 Timer	Timer 0	10
	Timer 1	11
	Timer 2	12
	Control Word	13
Max 162 ADC	Channel select	A0
	Lower Byte	C0
	Upper Byte	C1
58167 Calender	10 Milli Sec.	E0
	100 Milli Sec.	E1
	Second	E2
	Minute	E3
	Hour	E4
	Day of Week	E5
	Date	E6
Month	E7	
Memory Bank		80

ory chips. Each of the 62256 memory chip consists of 32 KByte memory space. Thus, this memory card has 512 KByte memory space. Memory locations of each of the 16 memory chips have address from 8000(H) to FFFF(H). In case while recording, if one of the chip gets full then the software selects the next chip. For example the following commands will select chip number 7

```
MVI  A  07
      OUT 80
```

Where the memory bank has address 80.

9.3.2 Digital Accelerograph Software

The software is required to set parameters like sampling rate, upper and lower threshold level for trigger of event, upper and lower threshold levels for end of event, time of pre event memory and time for post event. For this purpose a menu string is developed which stores the relevent data.

The conditioned analog signals of three orthogonal components of ground acceleration are fed to different channels of CPU/ADC card. The 12 bit samples of each channel are taken to accumulator one by one at a desired sampling rate by the developed software. The flow charts of digital accelerograph software are shown in Figs. 9.7 to 9.12. In the main program (Fig. 9.7), various data and addresses for pre-event, earthquake event and post-event as well as timer are initialized. As discussed in the earlier section, the timer provides a hardware interrupt at an interval at which the sampling of the data is desired. On receiving an interrupt, the program jumps to vector location of interrupt (which is in ROM), the vector location is programmed to make the program counter jump to the starting address of interrupt service subroutine (ISS). Flow chart of ISS is shown in Fig. 9.8. First ISS checks whether Register E is 00(H) or not. Register E is used as trigger indicator and if it contains 00(H) then there is no event and in case of an event it contains 01(H). ISS then calls ADC subroutine (Fig. 9.9) and then compares the three samples for trigger. For this comparison, the limits of threshold values are read from the menu string. If the event has not occurred, ISS moves to store the pre event data in a ring storage. In the case of pre event, ISS calls subroutine COMPARE1 (Fig. 9.10) for detecting the event. If the acquired value of the any one of the three sample exceeds the threshold value, subroutine COMPARE1 moves to store absolute time of earthquake event and jump address at flag in a definite format. It also makes the event indicator

to glow in case of an event through 8255 support chip. In case of an earthquake event, ISS calls ADC and COMPARE2 subroutines. Flow chart of COMPARE2 is shown in Fig. 9.11. COMPARE2 checks whether an event has completed or not. The earthquake data is stored in an open ended memory and when COMPARE2 indicates the end of the event, then ISS calls REVALUE subroutine (Fig. 9.12) which makes the software ready for the next event.

9.4 Post processing

An IBM compatible personal computer (PC) is used as data retrieval unit of digital accelerometer. A commercially available software is used to communicate between digital accelerometer and PC. The monitor software of the microprocessor has the option of sending contents of required memory locations to the PC as Hexadecimal values of each memory in ASCII form in a specified format. First, the FLAG file is captured which is resident in memory locations 3000(H) to 35FF(H). The FLAG file provides complete information about various important details of the data recorded by the instrument. With the help of the FLAG file, the start address (along with chip number of the memory bank) and end address (along with chip number of memory bank) of each of the events are found and then for each event, a separate data file is captured. Two byte samples of the three channels are stored in a sequence and thus, six bytes are required for data of single instant.

An interactive computer program is developed in FORTRAN which takes the FLAG file and the data file as input files and asks for calibration values of three channels. The important task of the computer program is to read the jump address of the ring storage from the FLAG file and use it to cut and paste the ring storage to put the pre event memory in sequence to the main event. Another task of the program is to separate out three channels from the sequential data. The program then uses the calibration and gives three output files corresponding to three channels. Each file contain time vs. acceleration values. The header of output files give channel number, name of station (which is inputted to the program) and the trigger time.

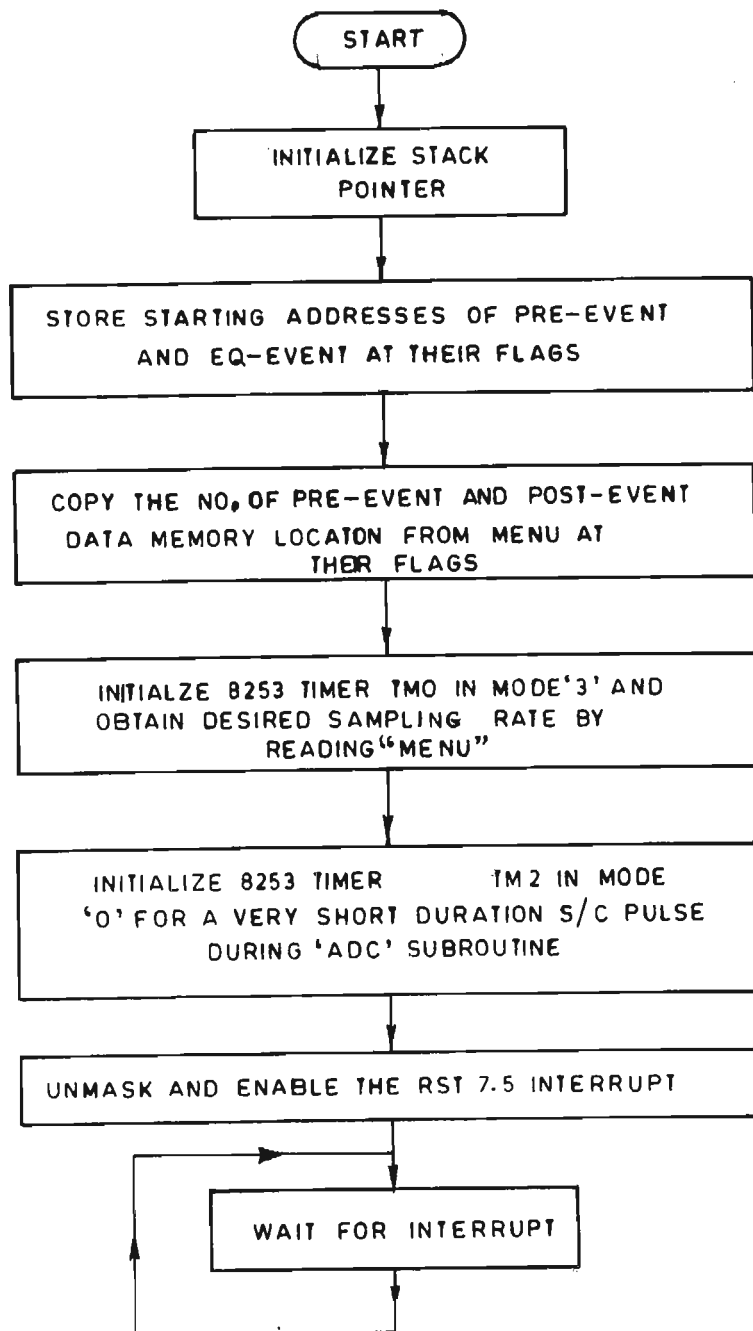


Figure 9.7: Flow chart of the MAIN program

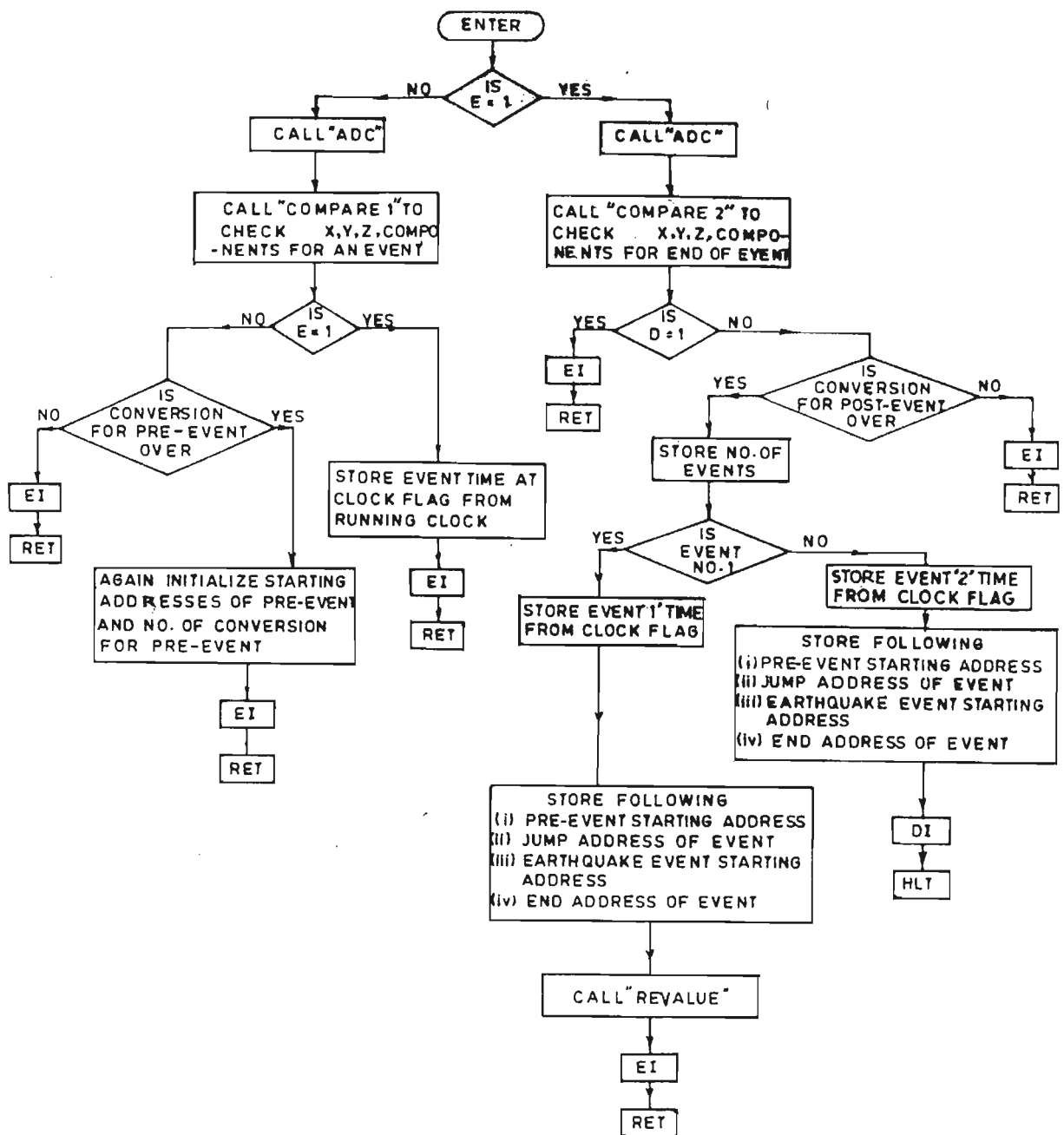


Figure 9.8: Flow chart of Interrupt service subroutine for two events

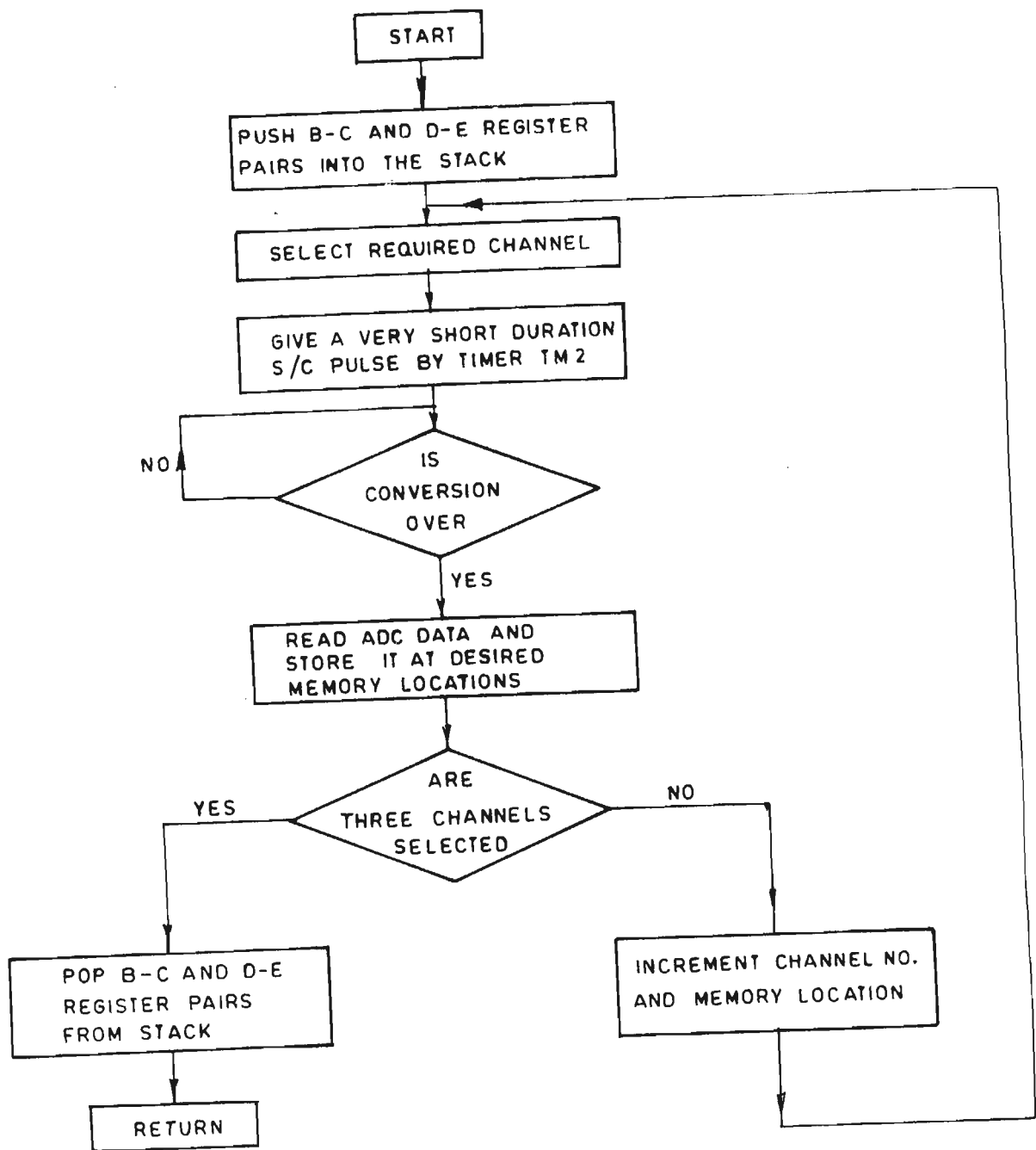


Figure 9.9: Flow chart of ADC subroutine

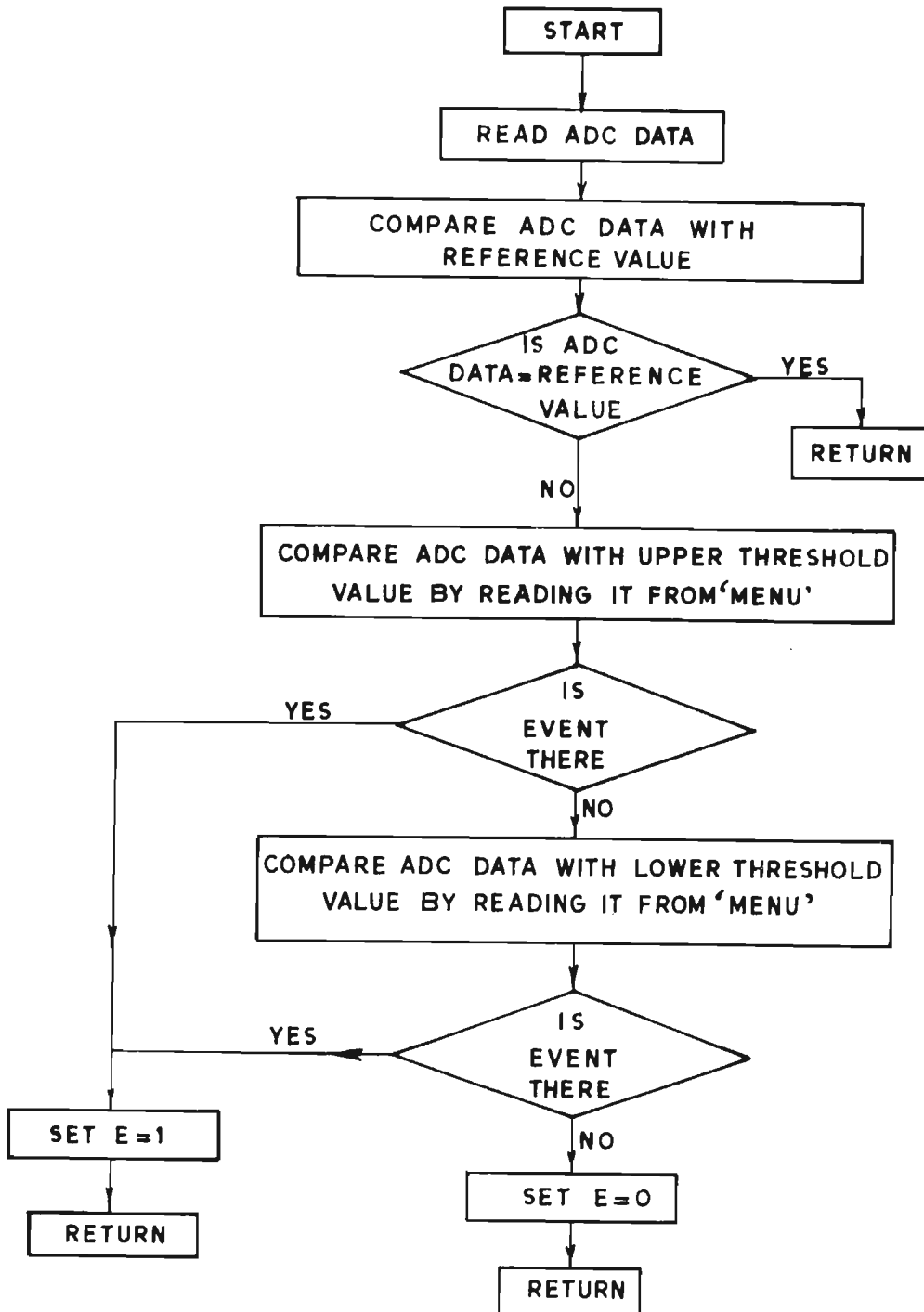


Figure 9.10: Flow chart of COMPARE1 subroutine

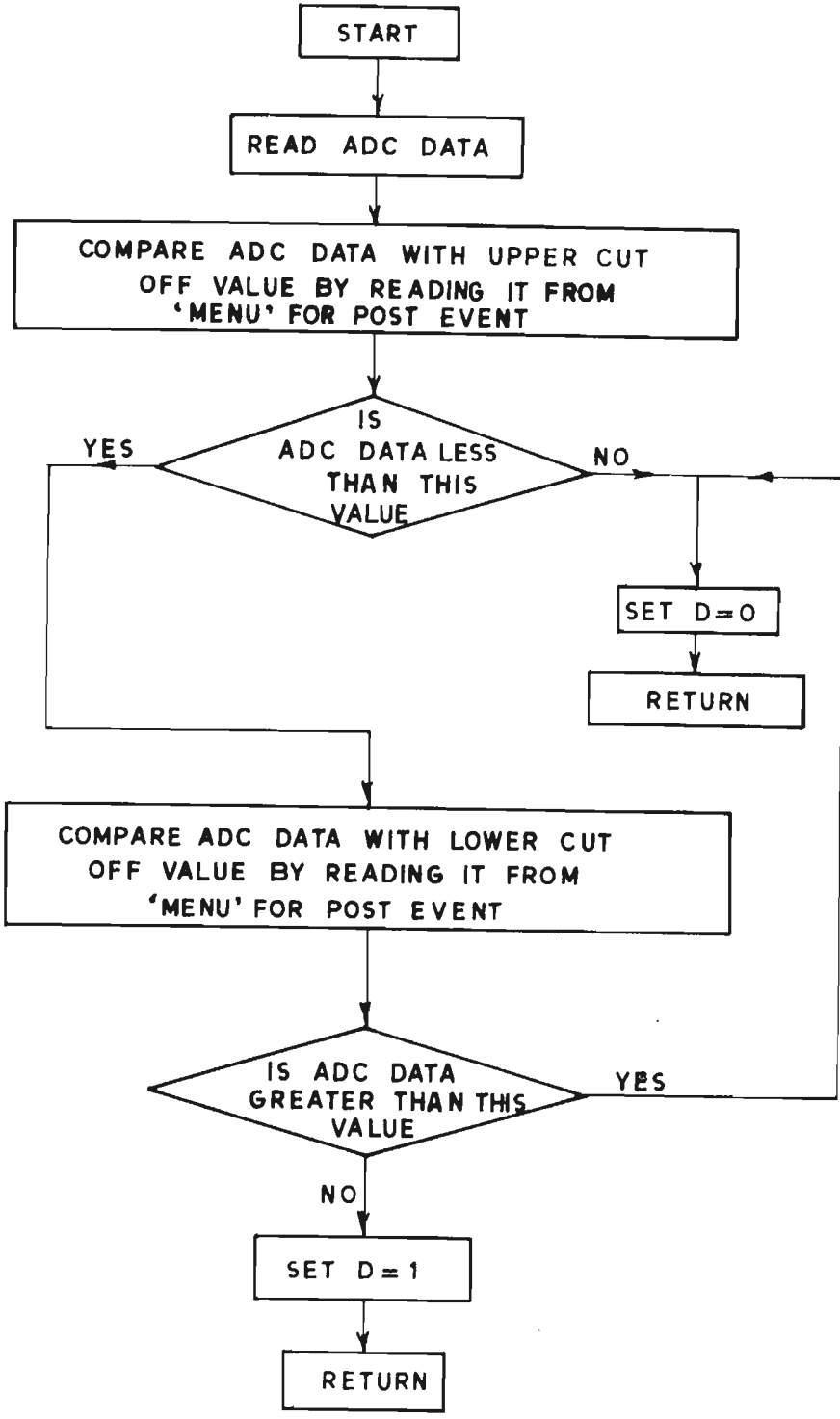


Figure 9.11: Flow chart of COMPARE2 subroutine

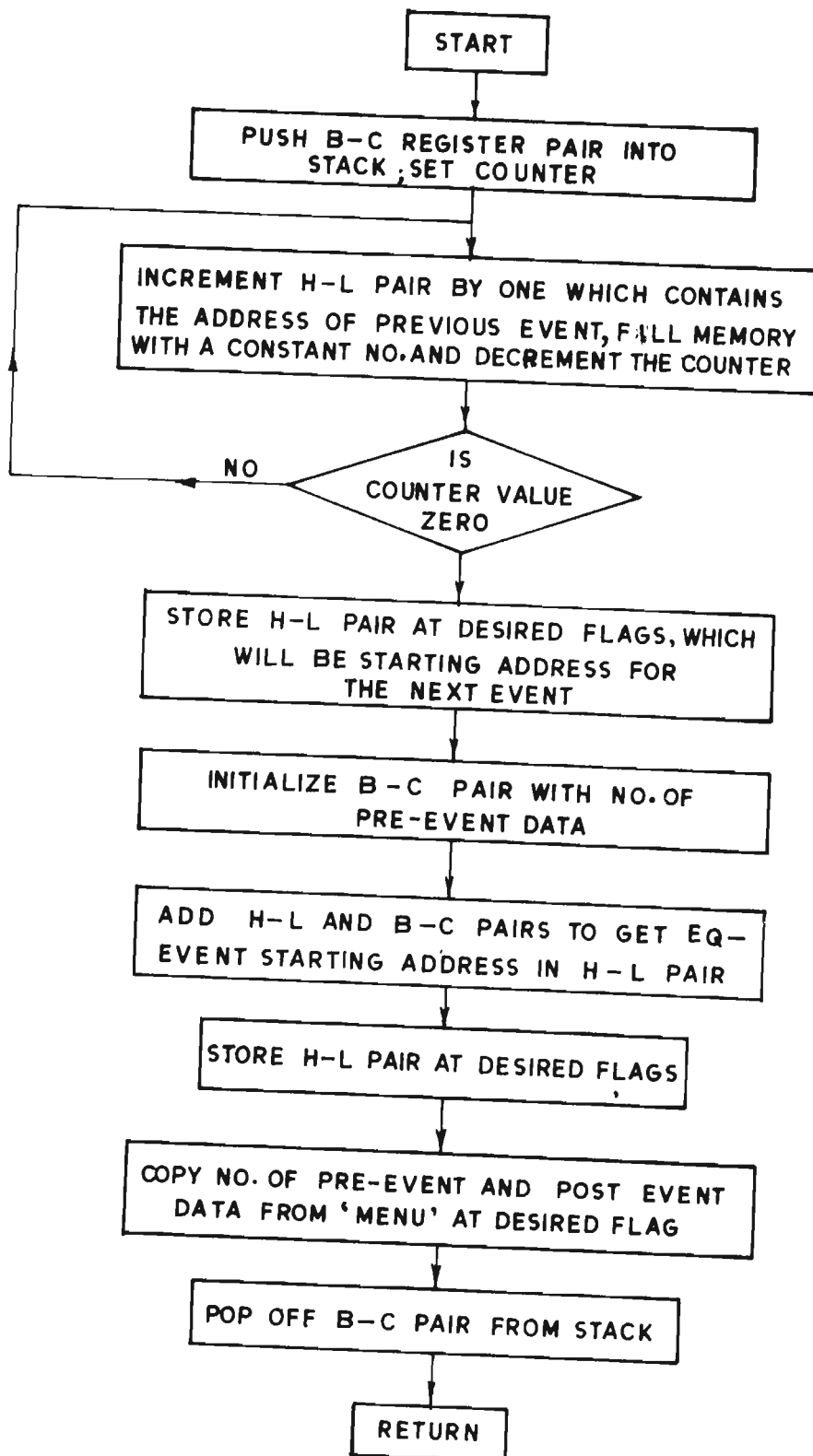


Figure 9.12: Flow chart of REVALUE subroutine

Chapter 10

Correction of data recorded from digital accelerographs

As mentioned in earlier chapters, data recorded from digital accelerographs have substantially smaller noise to signal ratio in the frequency range of recording as compared to analog accelerographs due to the fact that (a) such accelerographs have no moving parts as in analog instruments; (b) the data are free from human errors associated with digitization and (c) sensors of digital accelerographs (usually FBAs) are more accurate, have a higher natural frequency and larger dynamic range. Due to these reasons it may be assumed that each record of digital accelerographs have unique noise characteristics which can be determined. In this chapter a procedure based on adaptive filters is suggested which uses untriggered portion of the pre-event data to determine the noise characteristics of records. The transfer function of the noise so determined is used for noise cancellation for the event to obtain the corrected accelerogram. The philosophy of such a correction scheme can be derived taking a cue from the use of adaptive filters in modelling and cancellation of noise in various fields such as electrocardiogram, echo cancellers, adaptive line enhancers, speech synthesis etc [34]. However, the problem of correction of records of digital accelerographs is more complex.

10.1 Transformations and noise in digital accelerographs

Although the noise to signal ratio in the data recorded from digital accelerographs is far less than that in analog accelerographs [48], yet, noise creeps in the records of

digital accelerographs during transformations at various stages of recording. The first transformation takes place in the accelerometer where acceleration is converted into equivalent voltage. Closed form solution in frequency domain for transfer function of FBA are available [4]. This transfer function can be used to get the acceleration from the recorded voltage output through deconvolution. Another transformation takes place at the signal conditioner. Here the anti-aliasing filter removes high frequencies and the voltage signal is amplified to the required range. For example a four pole Butterworth filter is used with a cutoff frequency of 33 Hz in the digital accelerograph described in Chapter 9.

In spite of the fact that anti-aliasing filter is an essential requirement for any digital recording system, most analog filters like Butterworth produce nonlinear phase shift. Whereas these nonlinear phase shifts should not be of much consequence yet earthquake engineers have objections to these [55]. One of the method of removing this nonlinear phase shift is to design a digital filter having the same performance as of the analog anti-aliasing filter. This means that operation for $H(j\omega)$ takes place at analog stage and operation for $H(-j\omega)$ is performed for the recorded digital data to obtain zero phase shift.

In addition to the above transformations, the system continuously records some noise which may be either instrument noise or background noise. It is this noise which has been examined in detail and a procedure is suggested to remove this noise and obtain the corrected accelerogram. Although in some of the strong motion records this noise may not be of much concern but with the large dynamic ranges available today, it becomes important to analyse such noise and to develop an algorithm for its cancellation. The attempt for such noise cancellation should ultimately aim to incorporating these algorithms as part of hardware and software configuration of the digital accelerograph so that such noise cancellation takes place during the recording itself. Clearly this would help in employing such accelerographs record microearthquakes also successfully as the filtering of the background noise is an important requirement there. However, in this part of the work attention is confined to develop an algorithm which can identify the transfer function of noise from the pre-event record and affect noise cancellation in the recorded portion. The feasibility of incorporating the algorithm as part of hardware and software configuration of digital accelerograph (perhaps using DSP chips) are presently left out of consideration. However, while developing this algorithm, this requirement is constantly kept in mind. The procedure proposed for correction of records is as follows

- Analyse the noise of digital accelerograph and perform noise cancellation in the

following steps

1. Find the transfer function of the noise through an adaptive algorithm analysing the pre-event portion of the record assuming it to be an auto-regressive (AR) model.
 2. Perform noise cancellation of the event using the transfer function of the noise determined above.
- Perform $H(-jw)$ operation of the recorded data on the basis of order and type of anti-aliasing filter to get rid of nonlinear phase shift.
 - Perform instrument correction, if required.

To check the effectiveness of the correction scheme, the digital accelerograph described in Chapter 9 was made to record the motion of a biaxial (one horizontal and vertical) computer controlled shake table. The shake table was excited by a prescribed time history. The shake table motion had a duration of 10.24 seconds and had zero displacement at the end of the motion. The digital accelerograph was placed on the shake table so as to record one horizontal and vertical motion only and was set with the following parameters:

Sampling rate	=	100 SPS
Pre event time	=	5 sec
Trigger level	=	0.03g
Post event time	=	5 sec
End of event level	=	0.03g

The recorded vertical and horizontal components (channel 1 and channel 3 respectively) were used for further processing as discussed in the subsequent sections.

10.2 Analysis of noise and algorithm for noise cancellation

Digital accelerograms comprise samples of ground acceleration combined with environmental and instrument noise. The recorded data in the solid state memory is constitutes of two parts — the pre-trigger and the post-trigger samples. Let K be the number of samples of pre-trigger part and N be the number of samples of post-trigger part. Most of the first part of K samples of $x(n)$ are the samples of noise only which are recorded prior to the set trigger level. The following N samples include signal and noise.

Adaptive filters have been widely used for noise cancellation in various disciplines [34] for which statistical characteristics of the signal are not *a priori* known. These problems can be broadly divided into following two categories.

1. When the records of the observed signal (composed of actual signal corrupted with an additive noise) and of reference noise are available for the entire duration. The additive noise then is estimated from the reference noise and subtracted from the observed signal to estimate the actual noise free signal.
2. In the second class of problems, the signal and noise lie in different bands and only the corrupted signal is available. The adaptive algorithm then uses the properties of the signal and of the noise that lie in different bands. For example consider the signal to be wide band and noise to be narrow band. Since the noise band is narrow in comparison to the signal, the noise part of the sample will be highly correlated. The corrupted signal is delayed long enough to cause the actual signal components contained in it to be uncorrelated and the delayed corrupted signal is passed through an adaptive filter to linearly predict the noise.

However, in case of digital accelerographs, although a record with signal superimposed with noise is available, the categorization of the frequency contents of actual signal and noise can not be made as discussed above. A reference noise is available only in the pre-event portion of the record. This forces one to first examine if the noise can be modelled at all. Once this question is resolved, an adaptive filter algorithm can be developed to achieve noise cancellation from the recorded signal.

10.2.1 Noise analysis

In general, modelling and linear prediction of a stationary signal with zero mean requires an infinite set of parameters, since the prediction is based on an infinite past. However, if the reference noise $x(n)$ is a sample of an AR process, the model $1/A(z)$ is an all pole filter, where $A(z)$ is a polynomial representing a filter given by

$$A(z) = \sum_{i=0}^M a(i)z^{-i} \quad ; \quad a(0) = 1 \quad (10.1)$$

where z is complex and M is the length of the filter. The reference noise $x(n)$ can be generated by a white noise sequence $w(n)$. Thus

$$\sum_{i=0}^M a(i)x(n-i) = w(n) \quad (10.2)$$

and the optimal predictor

$$\hat{x}(n|n-1) = - \sum_{i=1}^M a(i)x(n-i) \quad (10.3)$$

Superscript $\hat{}$ means estimated value of the parameter and $(n|n-1)$ means estimated n^{th} sample from previous $(n-1)^{\text{th}}$ data.

In this case only the first $M+1$ parameters namely $\mathbf{a}^T = \langle 1, a(1), a(2), \dots, a(M) \rangle$ are nonzero in the infinite set of parameters required for stationary signal. The forward and the backward prediction error $u_M(n)$ and $v_M(n)$ respectively are defined by filtering $x(n)$ through the prediction error filter $\mathbf{a} = \langle 1, a(1), a(2), \dots, a(M) \rangle^T$ and $\mathbf{a}^R = \langle a(M), a(M-1), a(M-2), \dots, a(1), 1 \rangle^T$ as

$$u_M(n) = \sum_{i=0}^M a(i)x(n-i) \quad (10.4)$$

and

$$v_M(n) = \sum_{i=0}^M a(i)x(n-M+i) \quad (10.5)$$

respectively. Thus, the second moment of forward backward prediction error can be written as

$$E[u_M^2(n)] = E[v_M^2(n)] = \mathbf{a}^T \mathbf{R} \mathbf{a} \quad (10.6)$$

where E is expectation operator and \mathbf{R} is the autocorrelation matrix and

$$R(i, j) = R(i-j) = E[x(n+i-j)x(n)] = E[x(n+i)x(n+j)] \quad ; \quad i, j \in [0, M] \quad (10.7)$$

In the Burg's method [21] (also known as maximum entropy method), for extracting modelling parameters from a measured block K of reference noise $x(n)$, assuming ergodicity, the ensemble average is replaced by time average and the sum square of the forward and the backward prediction errors ε is minimized. This criterion can be written as

$$\varepsilon = \min \left[\sum_{n=M}^{K-1} \{u_M^2(n) + v_M^2(n)\} \right] \quad (10.8)$$

Thus the method does not assume anything about the reference noise $x(n)$ beyond the data block of K samples. An iterative method based on partial correlation (also known as reflection) coefficients is suggested by Burg [21] such that the prediction error filter is minimal phase. Since partial correlation coefficient γ_k can be determined from the

known prediction error filter of order $k - 1$ using Levinson recursion [29,57].

$$\begin{Bmatrix} 1 \\ a(1) \\ a(2) \\ \vdots \\ a(k-1) \\ a(k) \end{Bmatrix}_k = \begin{Bmatrix} 1 \\ a(1) \\ a(2) \\ \vdots \\ a(k-1) \\ 0 \end{Bmatrix}_{k-1} - \gamma_k \begin{Bmatrix} 0 \\ a(k-1) \\ a(k-2) \\ \vdots \\ a(1) \\ 1 \end{Bmatrix}_{k-1} \quad (10.9)$$

where $\{\}_i$ refers to order i of the prediction error filter. The lattice relationships of forward and backward prediction error are

$$u_k(n) = u_{k-1}(n) - \gamma_k v_{k-1}(n-1) \quad (10.10)$$

and

$$v_k(n) = v_{k-1}(n) - \gamma_k u_{k-1}(n-1) \quad (10.11)$$

and the best choice of γ_k can be made as

$$\frac{\partial \mathcal{E}}{\partial \gamma_k} = 2 \sum_{n=k}^{K-1} \left\{ u_k(n) \frac{\partial u_k(n)}{\partial \gamma_k} + v_k(n) \frac{\partial v_k(n)}{\partial \gamma_k} \right\} = 0 \quad (10.12)$$

both valid for $n \in [k, K-1]$. The solution gives

$$\gamma_k = \frac{2 \sum_{n=k}^{K-1} u_{k-1}(n) v_{k-1}(n)}{\sum_{n=k}^{K-1} \{ u_{k-1}^2(n) + v_{k-1}^2(n-1) \}} \quad (10.13)$$

Use of Schwarz inequality shows that the partial correlation coefficient γ_k has magnitude less than unity which ensures minimum phase property of prediction error filter. Defining zeroth order mean squared prediction error as

$$E_0 = \frac{1}{K} \sum_{n=0}^{K-1} x^2(n) \quad (10.14)$$

it can be shown that k^{th} order mean squared prediction error is

$$E_k = (1 - \gamma_k^2) E_{k-1} \quad (10.15)$$

for $k \in [1, M]$. Since higher order prediction error can be built from the knowledge of one stage lower prediction error filter, the parameters of prediction error filter can be generated by initializing zeroth stage forward and backward prediction error as the sample of reference noise. The schematic diagram of the lattice structure is shown in Fig. 10.1.

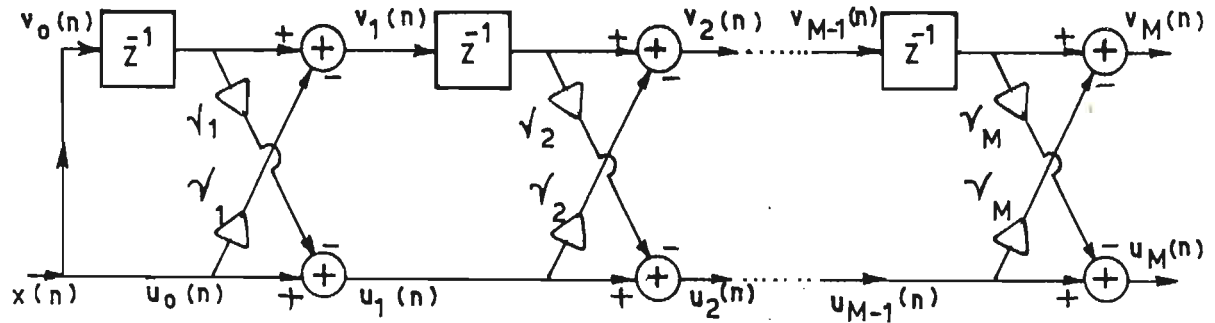


Figure 10.1: Schematic diagram of the lattice structure.

The power spectral density estimate of an autoregressive process is derived from the normal equation [33,59] and is given by

$$\hat{s}(\omega) = \frac{\hat{\beta}}{|\hat{A}(e^{j\omega})|^2} \quad (10.16)$$

where

$$\hat{\beta} = \frac{\hat{\epsilon}_{M-1}}{2(K-M)} \quad (10.17)$$

and

$$\hat{\epsilon}_{M-1} = \sum_{n=M}^{K-1} [u_{M-1}^2(n) + v_{M-1}^2(n-1)] \quad (10.18)$$

In the subsequent subsection power spectrum of the model of the pre-trigger portion is estimated using Eq. 10.16.

10.2.2 Model of pre-event data

Digital accelerogram obtained from shake table test was analysed as per the scheme shown in Fig. 10.1 to identify the possible model parameters. On studying the pre-event part of the record of the digital accelerograph carefully, it can be found that the first 474 samples (at 100 SPS) is noise. The estimated mean of this sequence of 474 samples is $\bar{x} = 0.1811$ gals. This mean is subtracted from the data for further analysis. The choice of parameter M is an important criteria in model selection. The choice is

dependent on the length of data and a measure of how close the data fits the model. The measure is the mean squared prediction error \hat{E}_M of the M^{th} order prediction error filter. As M increases, \hat{E}_M decreases and number of representative error samples decreases too. Moreover, for short data records spurious features get introduced. This is known as *bias versus variance dilemma*. Some of the proposals of order selection criteria for M are on final prediction error and can be given formally as

$$\min_M [(K + M + 1)\hat{E}_M / (K - M - 1)] \quad (10.19)$$

$$\min_M [\ln(\hat{E}_M) + 2M/K] \quad (10.20)$$

$$\min_M \left[\left(\sum_{j=1}^M 1/\hat{E}_j \right) / K - 1/\hat{E}_M \right] \quad (10.21)$$

due to Akaike [1,2], and Parzen [74] respectively. The plots of $M \in [0, 32]$ are shown in Fig. 10.2. All of them show a decreasing trend with increasing M . From this figure M was selected as 15 as ordinate of all the three curves of Fig. 10.2 beyond order 15 reduces little. The data is again analysed with $M = 15$ and power spectrum given by Eq. 10.16 is estimated. Direct estimate of power spectrum is also made. This is carried out by modifying the data $x(n)$ by a cosine taper window [15] weighting function

$$d(k) = \begin{cases} 1.0 & 0 \leq |k| \leq \alpha K/2 \\ 0.5 \left[1.0 + \cos \left\{ \pi \frac{k - \alpha(K/2)}{2(1-\alpha)(K/2)} \right\} \right] & \alpha K/2 \leq |k| \leq K/2 \end{cases} \quad (10.22)$$

where α is a window parameter. A value of $\alpha = 0.8$ is used in this analysis. The autocorrelation is estimated as

$$\hat{R}(k) = \frac{1}{K-k} \sum_{i=1}^{K-k} \left\{ x(k+i)d(k+i - \frac{K}{2}) \right\} \left\{ x(i)d(i - \frac{K}{2}) \right\} \quad (10.23)$$

for lag $k \in [0, 256]$. The double sided z-transform of the estimated autocorrelation gives the periodogram estimate. The cosine tapered data is also used to estimate power spectrum directly by using FFT in two ways. First, the autocorrelation is estimated for 16 lags using FFT which are modified by Hamming window to reduce the effect of truncation of autocorrelation and then FFT is used to estimate power spectra (modified periodogram method). The second way to estimate power spectra of the cosine tapered data was through Welch's method in which the modified periodogram with Hamming window is estimated with 50% overlap of data. These methods are well described in Rabiner and Gold [76]. Figure 10.3 shows the power spectral estimate of the model (Eq. 10.16), periodogram, using modified periodogram method and using Welch's method. The figure shows that the average trend of the data matches quite well. The

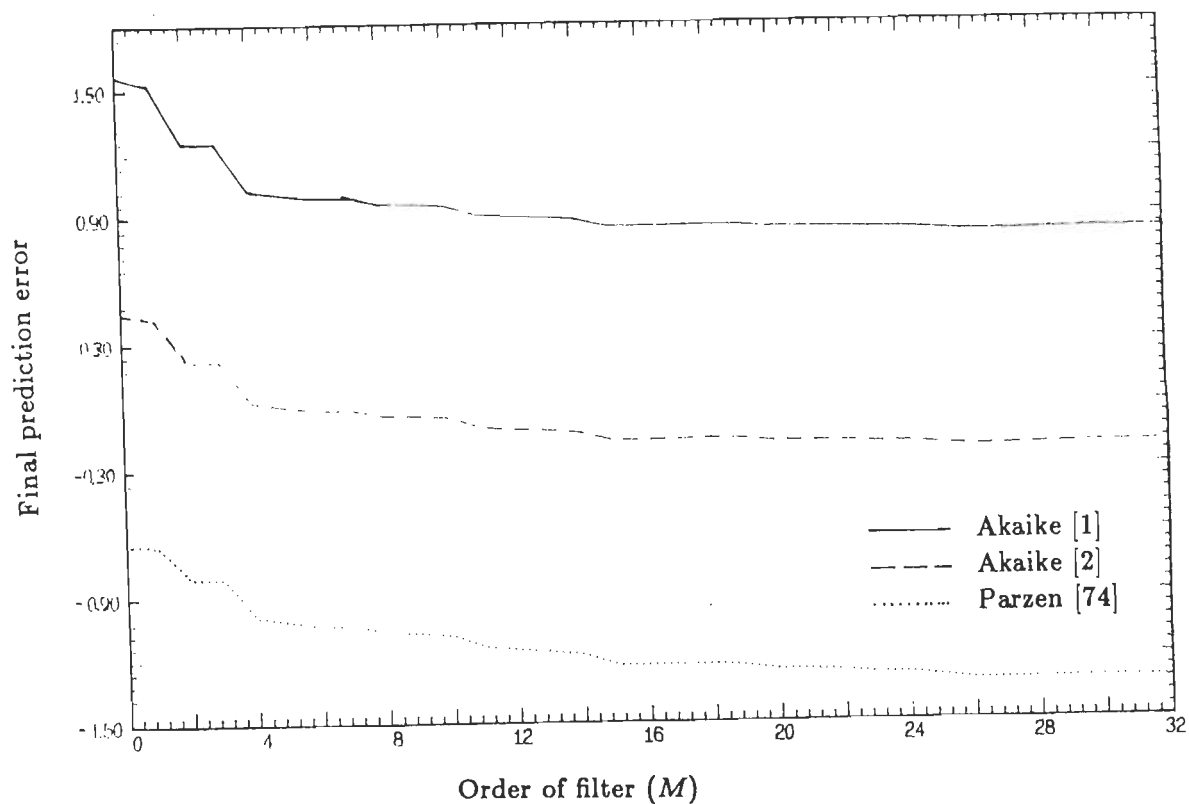


Figure 10.2: Final prediction error for selection of order of filter.

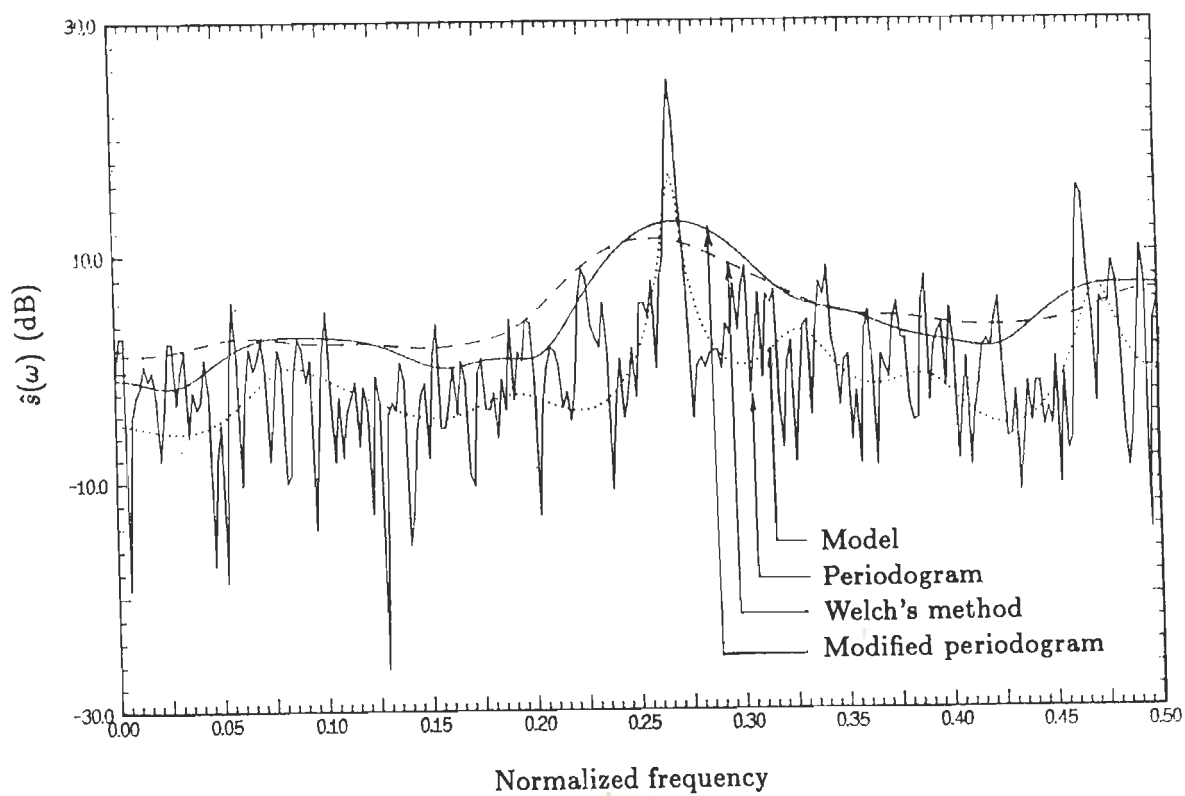


Figure 10.3: Comparison of power spectra of model with power spectral estimate by periodogram, modified periodogram method and Welch's method.

validation of the model was carried out by correlation analysis of estimated error given by

$$\hat{w}(n) = x(n) - \hat{x}(n|n-1) \quad (10.24)$$

and cross correlation analysis of pre-event $x(n)$ and estimated error $\hat{w}(n)$ [58]. Figure 10.4 shows autocorrelation of error with 95% confidence for white noise test. For a valid model, the autocorrelation except at zero lag should be within this limit. Figure 10.5 shows cross correlation of pre-event with error with 95% confidence band. This figure tests the independence between pre-event and error. However, Figure 10.5 shows some cross correlation exists both in the negative and positive lags. This shows that error and pre-event are not independent. However, the variation shown is not very significant and it can be reasonably taken that the pre-event can be modelled as coloured noise (AR process).

10.2.3 Time domain analysis of adaptive filter

The data of digital accelerograph contain reference noise signal only in the pre-event portion of the record. Beyond this part only the signal corrupted with noise is available. In the previous subsection it has been found that reference noise can be modelled as coloured noise (AR process). Objective thus is to use this information to cancel noise from the recorded event. Hence, the pre-event data can be analysed as given in Fig. 10.6. The output of this filter is $b(n)$. This output will be white noise if the length of the adaptive FIR predictive filter $H(z)$ is adequate. The output $c(n)$ will be estimated coloured noise. After the trigger, the adaptive filter designed prior trigger is considered as a fixed filter. When the signal and coloured noise pass through this fixed filter, the output $b(n)$ will be a broad band signal superimposed with white noise. The frequency contents of this broad band signal will be same as that of the post trigger part of the accelerogram with a change of amplitude. However, amplitude at this stage is not important. The output $b(n)$ of this stage is used as input to the second stage adaptive FIR filter to estimate optimum noise part of the signal (coloured noise) as shown in Fig. 10.7. As long as the optimum noise signal estimator is independent of the amplitude of the broad band signal, the filter will be good for estimation of coloured noise. The composite filter for the event is shown schematically in Fig. 10.8.

In the adaptive filtering problem, the filter length M has to be fixed *a priori*. For the sake of convenience, the length M of both the filters $H(z)$ and $G(z)$ are chosen to be identical. At the pre-event stage the output of filter is

$$b(n) = x(n) - c(n) \quad (10.25)$$

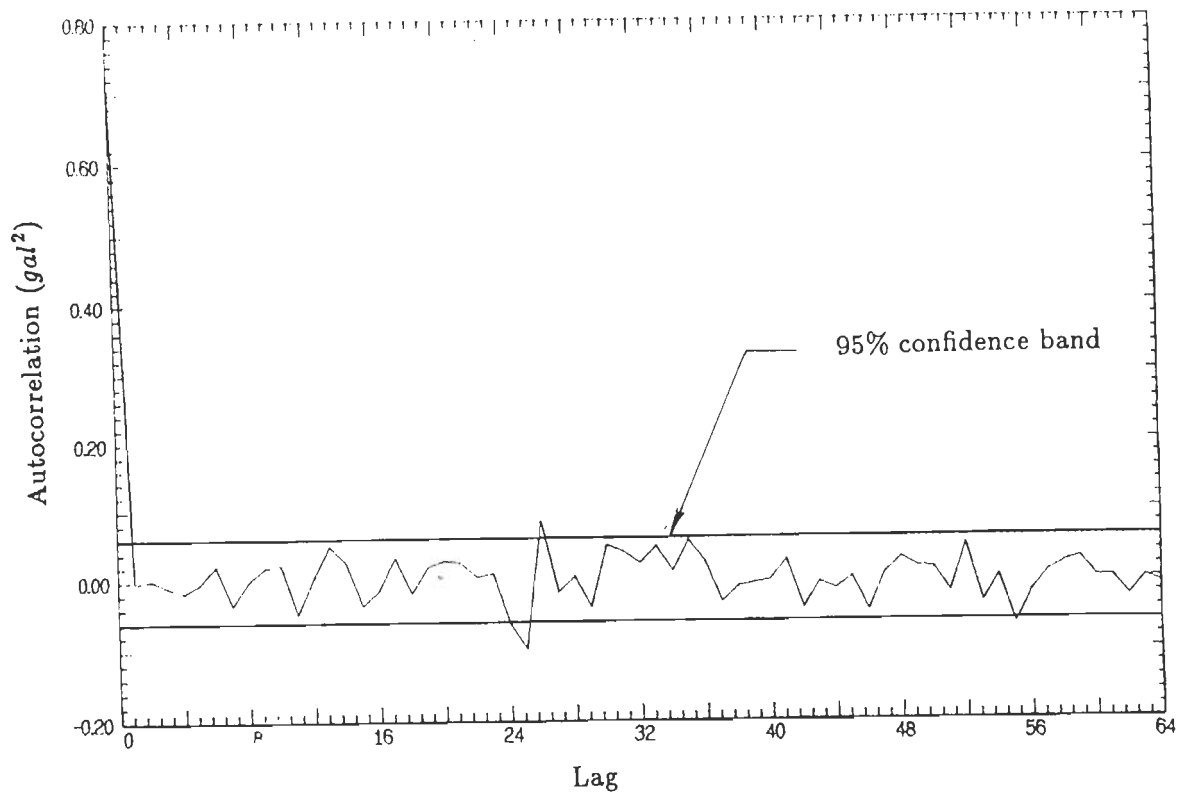


Figure 10.4: Autocorrelation of error with 95% confidence band for white noise test.

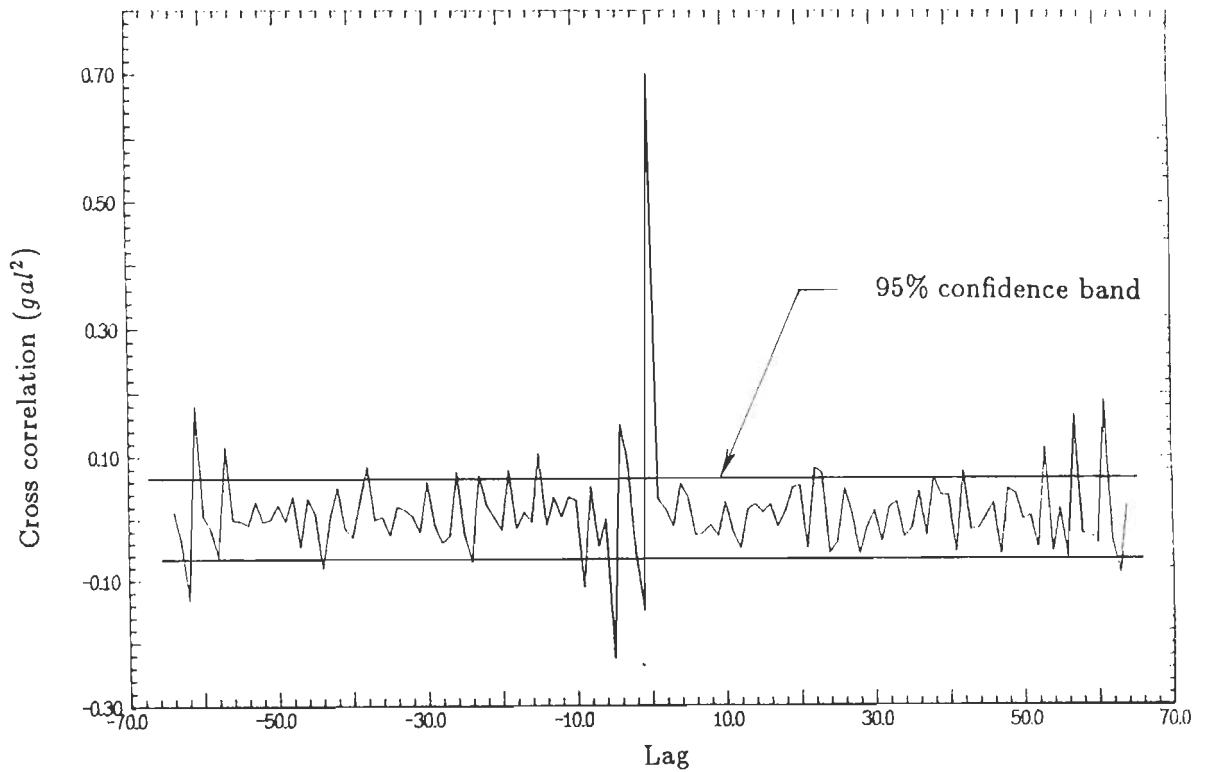


Figure 10.5: Cross correlation between signal and error with 95% confidence band.

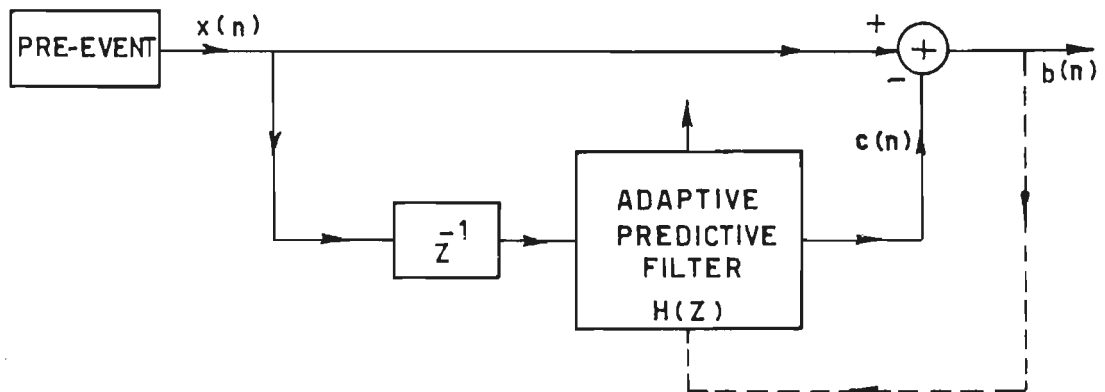


Figure 10.6: Adaptive filter for pre-event part of the record.

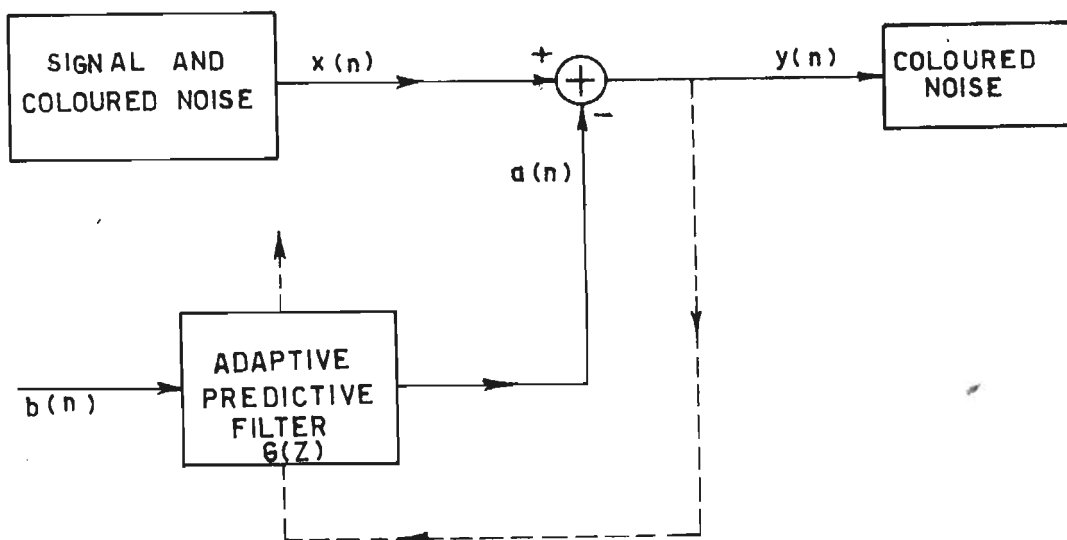


Figure 10.7: Second stage adaptive filter to estimate optimum coloured noise.

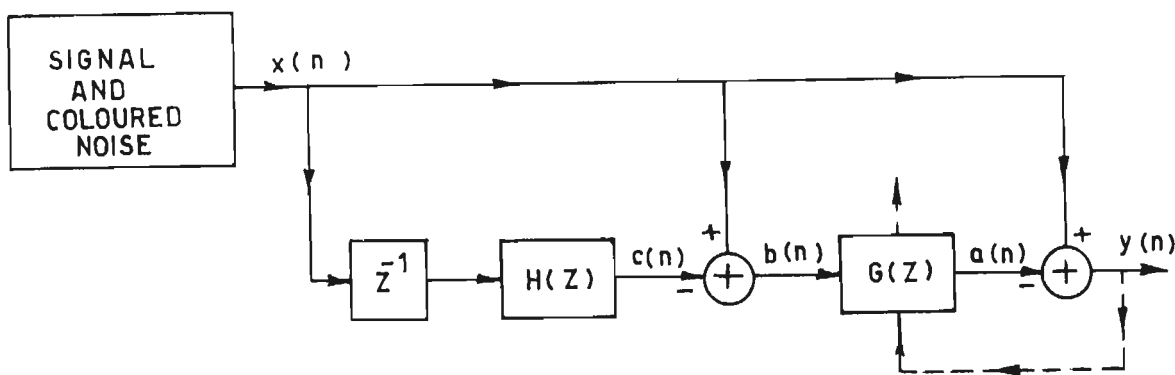


Figure 10.8: The composite filter for the event.

which can be written as

$$b(n) = x(n) - \sum_{i=1}^M h(i)x(n-i) \quad (10.26)$$

where $h(i)$, $i \in [1, M]$ are the filter coefficients and $c(n)$ is the coloured noise part estimated by the filter $H(z)$. The Equation 10.26 can be written as

$$B(z) = H'(z)X(z) \quad (10.27)$$

where $B(z)$ and $X(z)$ are the z-transform of $b(n)$ and $x(n)$ respectively and

$$H'(z) = 1.0 - H(z) \quad (10.28)$$

$$H(z) = \sum_{i=1}^M h(i)z^{-i} \quad (10.29)$$

After the event, output $b(n)$ of the first stage fixed filter is the input to the second stage adaptive filter. The output of the second stage can be written as

$$y(n) = x(n) - a(n) \quad (10.30)$$

where

$$a(n) = \sum_{i=1}^M g(i)b(n-i) \quad (10.31)$$

Equation 10.31 can be written in z-transform as

$$A(z) = G(z)B(z) \quad (10.32)$$

and

$$G(z) = \sum_{i=0}^{M-1} g(i)z^{-i} \quad (10.33)$$

The z -transform of Eq. 10.30 is

$$Y(z) = X(z) - A(z) \quad (10.34)$$

Using Eqs 10.27 and 10.32, it can be shown that

$$A(z) = G(z)H'(z)X(z) = F(z)X(z) \quad (10.35)$$

where the overall transfer function is given by

$$F(z) = \frac{A(z)}{X(z)} = G(z)H'(z) \quad (10.36)$$

and

$$Y(z) = \{1.0 - F(z)\}X(z) \quad (10.37)$$

The schemes described above are realised adaptively and the details are given in the following subsection.

10.2.4 Adaptive algorithm

The FIR filter described in the previous subsection can be designed adaptively through recursive least square (RLS) algorithm [34,58]. Since the noise can be reasonably represented as an AR process, the noise removal can be tried as direct form recursive filter. The algorithm can be conveniently described in matrix notation. A time index is used to denote recursion in time. Let at instant n , $\Theta_M(n)$ be the filter coefficient vector given as

$$\Theta_M(n) = \begin{Bmatrix} \theta(0, n) \\ \theta(1, n) \\ \theta(2, n) \\ \vdots \\ \theta(M-1, n) \end{Bmatrix} \quad (10.38)$$

Similarly the input vector to the filter is

$$\mathbf{X}_M(n) = \begin{Bmatrix} x(n) \\ x(n-1) \\ \vdots \\ x(n+1-M) \end{Bmatrix} \quad (10.39)$$

Let $y(n)$ be the desired output of the filter which is observed for a duration of N samples. The coefficient vector $\theta_M(n)$ is determined by minimizing a weighted sum of magnitude square errors

$$\varepsilon = \min \left[\sum_{n=1}^N \prod_{k=n+1}^N \lambda(k) e^2(n) \right] \quad (10.40)$$

where estimation error is

$$e(n) = y(n) - \hat{y}(n) = y(n) - \mathbf{X}_M^T(n) \boldsymbol{\Theta}_M(n) \quad (10.41)$$

The superscript T refers as transpose of matrix and $\lambda(k)$ is the time varying *forgetting factor* used to track the possible nonstationarity of the signal better and is given by

$$\lambda(k) = 1 - \lambda_0 + \lambda_0 \lambda(k-1) \quad (10.42)$$

By differentiating Eq. 10.40 with respect to the filter coefficients, the so called normal form of the equation is obtained as

$$\mathbf{R}_M(n) \boldsymbol{\Theta}_M(n) = \mathbf{r}_M(n) \quad (10.43)$$

where

$$\mathbf{R}_M(n) = \sum_{k=1}^n \prod_{i=k+1}^n \lambda(i) \mathbf{X}_M(k) \mathbf{X}_M^T(k) \quad (10.44)$$

and

$$\mathbf{r}_M(n) = \sum_{k=1}^n \prod_{i=k+1}^n \lambda(i) \mathbf{X}_M(k) y(k) \quad (10.45)$$

The solution of Eq. 10.43 is then

$$\boldsymbol{\Theta}_M(n) = \mathbf{R}_M^{-1}(n) \mathbf{r}_M(n) \quad (10.46)$$

However, in the adaptive implementation, it is impractical to solve the set of M linear equations at the arrival of each new signal component. The rank-one updating properties are used in adaptive RLS algorithm to arrive at a n^{th} stage solution from the known $(n-1)^{\text{th}}$ stage. The matrix $\mathbf{R}_M(n)$ and vector $\mathbf{r}_M(n)$ satisfy

$$\mathbf{R}_M(n) = \lambda(n) \mathbf{R}_M(n-1) + \mathbf{X}_M(n) \mathbf{X}_M^T(n) \quad (10.47)$$

and

$$\mathbf{r}_M(n) = \lambda(n) \mathbf{r}_M(n-1) + \mathbf{X}_M(n) y(n) \quad (10.48)$$

Since inverse of $\mathbf{R}_M(n)$ is needed for solution of Eq. 10.46, the algorithm only stores the same. Denoting

$$\mathbf{R}_M^{-1}(n) = \mathbf{P}_M(n) \quad (10.49)$$

and using matrix inversion lemma [38], the recursive computational form can be obtained as

$$\mathbf{P}_M(n) = \lambda^{-1}(n) \left[\mathbf{P}_M(n-1) - \frac{\mathbf{P}_M(n-1)\mathbf{X}_M(n)\mathbf{X}_M^T(n)\mathbf{P}_M(n-1)}{\lambda(n) + \mathbf{X}_M^T(n)\mathbf{P}_M(n-1)\mathbf{X}_M(n)} \right] \quad (10.50)$$

For computational convenience, a *a priori* estimate of $\hat{y}(n|n-1)$, estimation error $e(n|n-1)$ and Kalman gain factor $\mathbf{K}_M(n|n-1)$ are denoted as

$$\hat{y}(n|n-1) = \mathbf{X}_M^T(n) \boldsymbol{\Theta}_M(n-1) \quad (10.51)$$

$$e(n|n-1) = y(n) - \hat{y}(n|n-1) \quad (10.52)$$

$$\mathbf{K}_M(n|n-1) = \lambda^{-1}(n)\mathbf{P}_M(n-1)\mathbf{X}_M(n) \quad (10.53)$$

Thus, it can be seen that a *a priori* solution is the solution of the problem at instant $n-1$. If a scalar $\mu(n)$ is defined as

$$\mu(n) = \mathbf{K}_M^T(n|n-1)\mathbf{X}_M(n) \quad (10.54)$$

or

$$\mu(n) = \lambda^{-1}(n)\mathbf{X}_M^T(n)\mathbf{P}_M(n-1)\mathbf{X}_M(n) \quad (10.55)$$

The *posterior* Kalman gain vector $\mathbf{K}_M(n)$ can be given as

$$\mathbf{K}_M(n) = \frac{1}{1 + \mu(n)} \mathbf{K}_M(n|n-1) = \mathbf{P}_M(n)\mathbf{X}_M(n) \quad (10.56)$$

Thus Eq. 10.50 can be written as

$$\mathbf{P}_M(n) = \lambda^{-1}(n)\mathbf{P}_M(n-1) - \mathbf{K}_M(n)\mathbf{K}_M^T(n|n-1) \quad (10.57)$$

The filter coefficients of Eq. 10.46 with the use of rank-one updating property, Eqs. 10.47 and 10.48 reduces to

$$\boldsymbol{\Theta}_M(n) = \boldsymbol{\Theta}_M(n-1) + \mathbf{P}_M(n)\mathbf{X}_M(n) \left[y(n) - \mathbf{X}_M^T(n) \boldsymbol{\Theta}_M(n-1) \right] \quad (10.58)$$

Use of Eqs 10.51, 10.52 and 10.56 give

$$\boldsymbol{\Theta}_M(n) = \boldsymbol{\Theta}_M(n-1) + \mathbf{K}_M(n)e(n|n-1) \quad (10.59)$$

Using Eqs. 10.52, 10.55, 10.56 and 10.59, the *posterior* estimation error $e(n)$ and estimate $\hat{y}(n)$ respectively can be obtained as

$$e(n) = \frac{1}{1 + \mu(n)} e(n|n-1) \quad (10.60)$$

and

$$\hat{y}(n) = \mathbf{X}_M^T(n) \boldsymbol{\Theta}_M(n) = y(n) - e(n) \quad (10.61)$$

It should be noted that *posterior* solution is the solution of the filtering problem at stage n .

To start the recursion, $\mathbf{P}_M(0)$ will be needed which will be high and is generally taken as

$$\mathbf{P}_M(0) = \frac{\mathbf{I}_M}{\delta} \quad (10.62)$$

where \mathbf{I}_M is an identity matrix. However, the algorithm is insensitive to the value of δ and often used value is $\delta = 0.01$. The λ_0 defined in Eq. 10.42 is customarily taken as $\lambda_0 = 0.99$ and $\lambda(0) = 0.95$. The computation steps of adaptive RLS can be summarized as follows:

1. Initialize $\boldsymbol{\Theta}_M(0) = \boldsymbol{\Theta}_M$ where $\boldsymbol{\Theta}_M$ is assumed as the starting value and $y(n) = x(n) = 0.0$ for $n \leq 0$.

For $n \in [1, N]$ the steps will be the following

2. Compute forgetting factor as

$$\lambda(n) = 1 - \lambda_0 + \lambda_0 \lambda(n-1) \quad (10.63)$$

3. Compute *a priori* Kalman gain as

$$\mathbf{K}_M(n|n-1) = \lambda^{-1}(n) \mathbf{P}_M(n-1) \mathbf{X}_M(n) \quad (10.64)$$

4. Compute scalar $\mu(n)$ as

$$\mu(n) = \mathbf{K}_M^T(n|n-1) \mathbf{X}_M(n) \quad (10.65)$$

5. Compute *posterior* Kalman gain as

$$\mathbf{K}_M(n) = \frac{1}{1 + \mu(n)} \mathbf{K}_M(n|n-1) \quad (10.66)$$

6. Compute inverse of correlation matrix as

$$\mathbf{P}_M(n) = \lambda^{-1}(n) \mathbf{P}_M(n-1) - \mathbf{K}_M(n) \mathbf{K}_M^T(n|n-1) \quad (10.67)$$

7. Compute *a priori* estimate and estimation error as

$$\hat{y}(n|n-1) = \mathbf{X}_M^T(n) \boldsymbol{\Theta}_M(n-1) \quad (10.68)$$

$$e(n|n-1) = y(n) - \hat{y}(n|n-1) \quad (10.69)$$

8. Compute *posterior* error, estimate and update of filter coefficients

$$e(n) = \frac{1}{1 + \mu(n)} e(n|n-1) \quad (10.70)$$

$$\hat{y}(n) = y(n) - e(n) \quad (10.71)$$

$$\Theta_M(n) = \Theta_M(n-1) + \mathbf{K}_M(n)e(n|n-1) \quad (10.72)$$

In the analysis of the data by the scheme δ was taken as 0.01 and the parameter λ_0 and $\lambda(0)$ were taken as 0.99 and 0.95 respectively.

10.2.5 Noise cancellation using adaptive algorithm

Figure 10.9 gives recorded accelerogram of Channel 3 (horizontal motion) of the digital accelerograph obtained from a shake table test. The data is composed of 1525 samples out of which 501 samples are of pre-event and 1024 samples are post trigger. The pre-event part of the data is the reference noise which is proposed to be used to correct the event part as per scheme discussed in subsection 10.2.3. Figure 10.10 and Fig. 10.11 show the Fourier magnitude plot of pre-event and the event part respectively. From Fig 10.10 (for the pre-event) it can be seen that noise has peak around 27 Hz and 47 Hz. This noise is also reflected in the Fourier magnitude plot of the event in Fig. 10.11. The recorded data is analysed by the developed scheme described earlier with a filter length of 16. The corresponding filter coefficients are given in Table 10.1 at the trigger, at the 513th sample (mid-point) of the event and at the end of the event.

Figure 10.12 shows the magnitude plot of the adaptive filter at the trigger, at the mid point of the event and at the end of the event. This plot is between gain of the filter and normalized frequency defined as frequency divided by the sampling rate (100 SPS in this case). In this figure magnitude of $H'(z)$ of Eq. 10.28 is plotted at the trigger and magnitude of $F(z)$ is plotted for mid event and at the end of event. It can be seen from Fig. 10.12 that the gain of the developed adaptive filter is almost unity at most of the frequencies and it removes from the accelerogram, the coloured noise corruption of around 27 and 47 Hz. Figure 10.13 shows the accelerogram after the process of adaptive filter for Channel 3. Figure 10.14 show the Fourier magnitude plot of the event part of the processed accelerogram. A comparison between Figs. 10.11 and 10.14 clearly indicate that coloured noise peaks at around 27 and 47 Hz are removed in the processed record. Table 10.2 gives comparison of uncorrected accelerogram, corrected accelerogram and noise in frequency domain in 16 different frequency segments. From

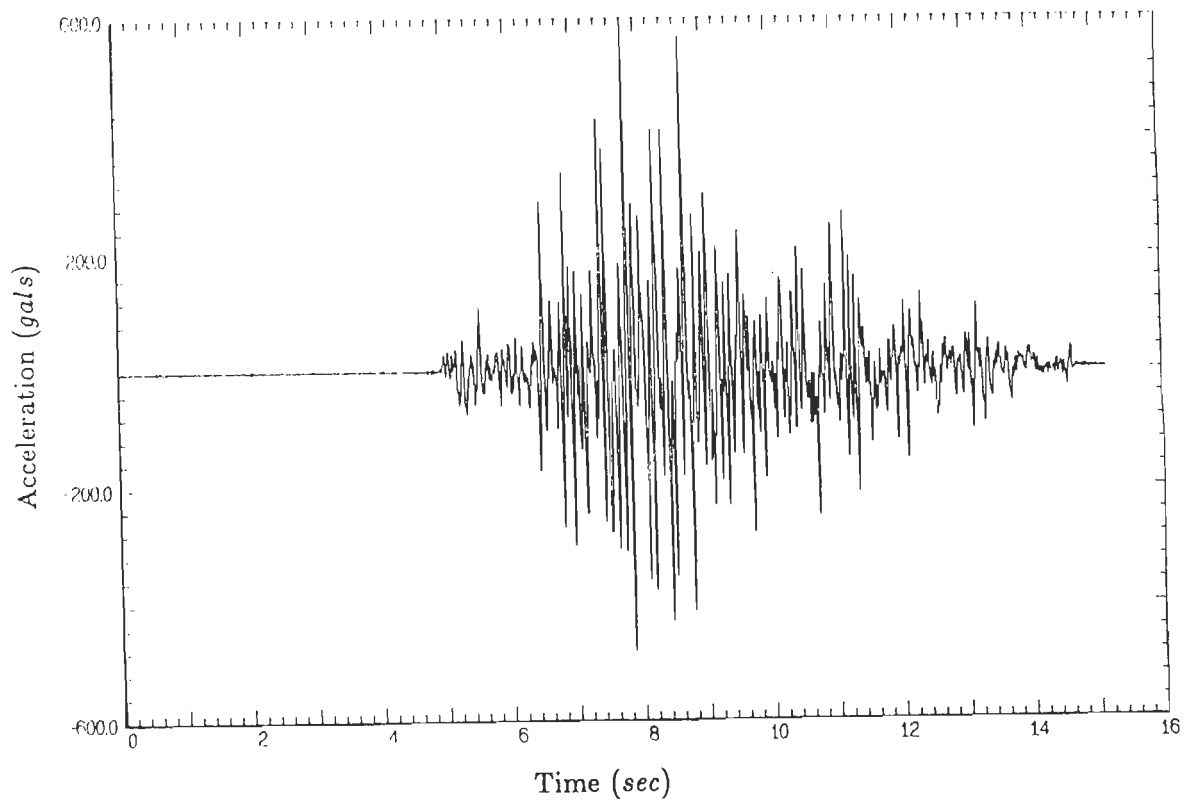


Figure 10.9: Recorded accelerogram (uncorrected) of horizontal motion of the shake table (channel 3).

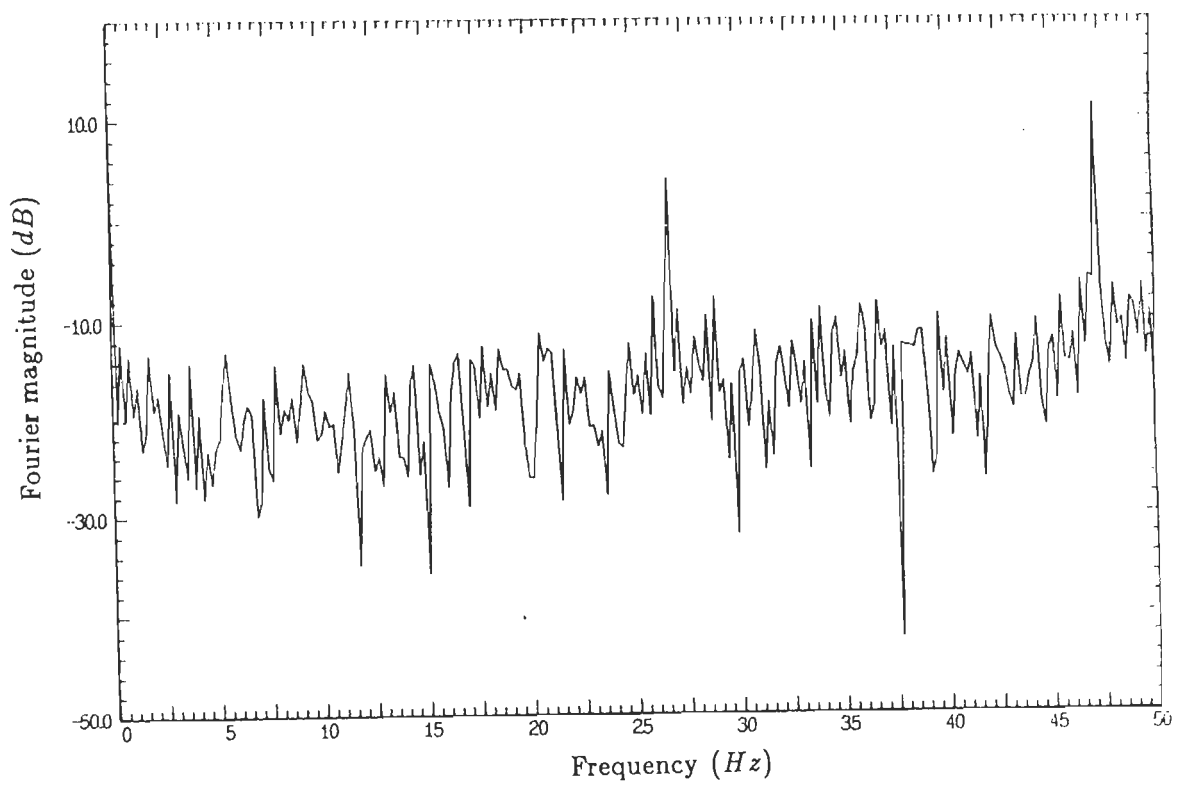


Figure 10.10: Fourier magnitude of pre-event of uncorrected accelerogram of channel 3.

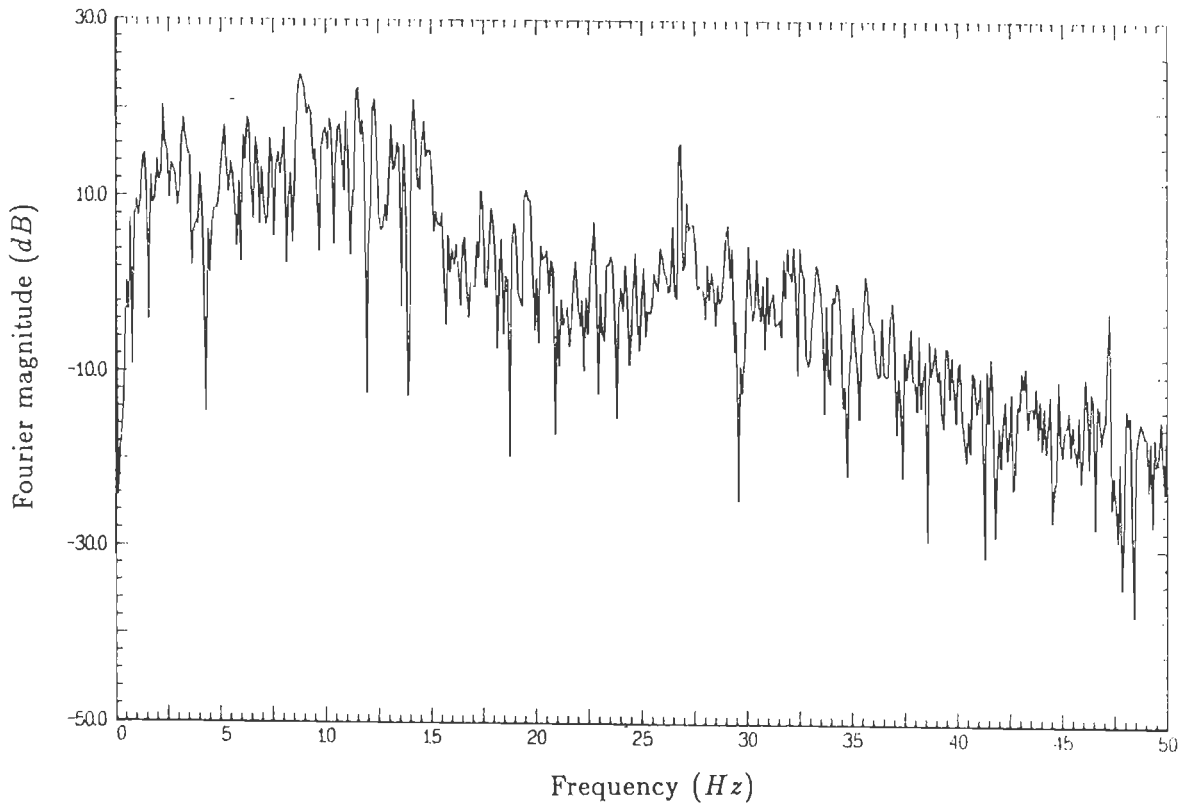


Figure 10.11: Fourier magnitude of event part of uncorrected accelerogram of channel 3.

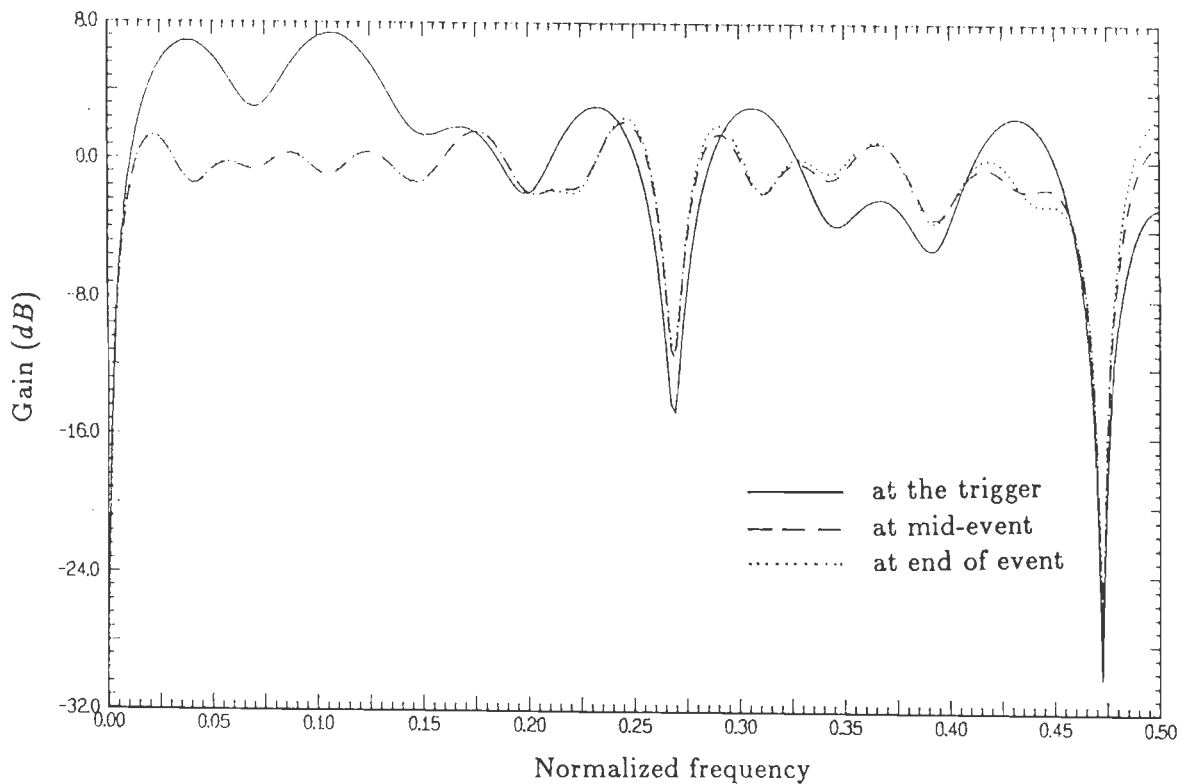


Figure 10.12: Magnitude of transfer function of adaptive filter of channel 3 at the trigger, at mid-event and at the end of event.

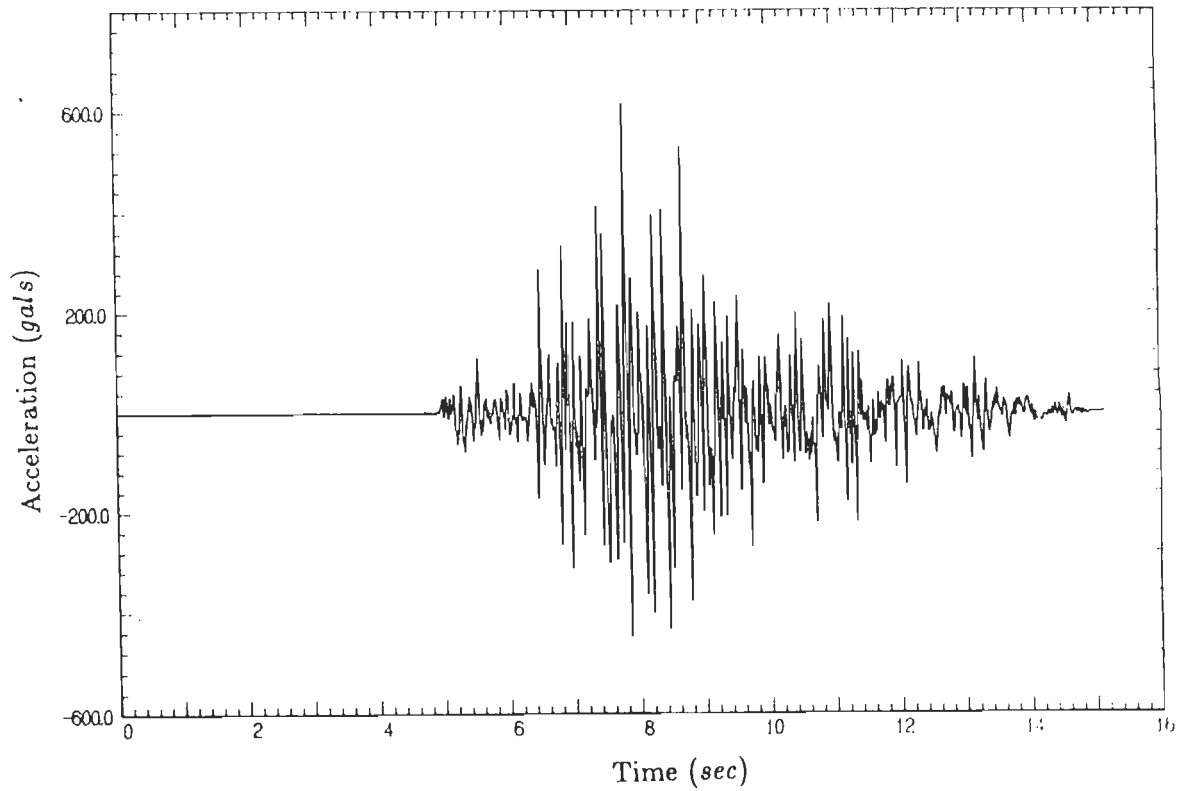


Figure 10.13: Accelerogram obtained after noise cancellation through adaptive filter for channel 3.

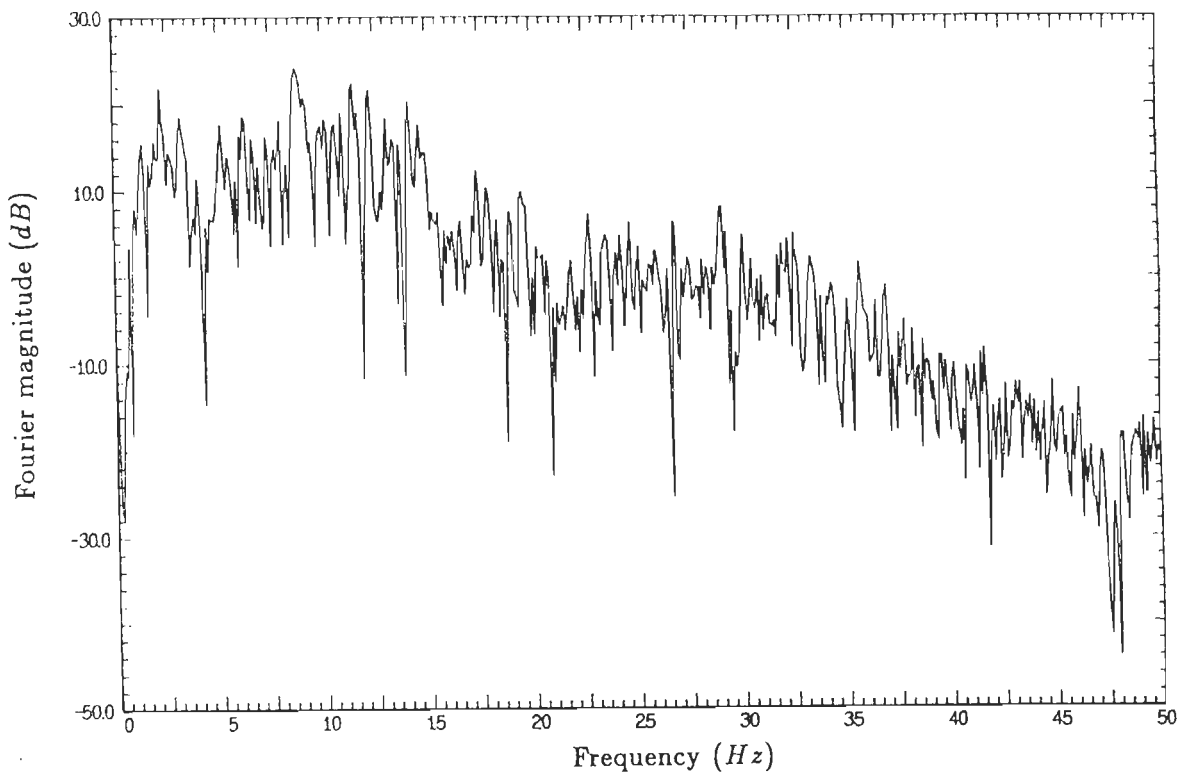


Figure 10.14: Fourier magnitude of event part of accelerogram obtained after noise cancellation through adaptive filter for channel 3.

Table 10.1: Filter Coefficients of Channel 3

Index (i)	$h(i)$ at trigger	$g(i)$ at mid event	$g(i)$ at end of event
1	-0.48058	0.84939	0.86304
2	-0.10905	-0.29713	-0.31795
3	-0.04464	-0.05998	-0.05198
4	0.22158	0.04907	0.04988
5	0.15222	0.06247	0.07810
6	0.22058	0.03756	0.01053
7	0.06202	0.09285	0.11163
8	0.19377	-0.10942	-0.12155
9	-0.06577	0.15652	0.17460
10	-0.08661	-0.18112	-0.20817
11	0.24126	0.03561	0.06015
12	0.09002	0.16850	0.15308
13	0.11050	0.02510	0.04858
14	0.04257	-0.06369	-0.10032
15	0.37203	0.06596	0.09439
16	0.04325	0.09378	0.08568

this table it can be seen that in the frequency ranges 26 to 29 Hz and also 44 to 50 Hz , mean Fourier magnitude of the corrected accelerogram is substantially smaller than that of uncorrected accelerogram. This is due to the fact that noise in the record was predominantly of about 27 and 47 Hz (Fig. 10.10) which is removed by the adaptive filter.

Table 10.2: Comparison of Correction in Frequency Domain for Channel 3

Frequency Segment		Mean			Coefficient of Variation		
Begin (Hz)	End (Hz)	Noise (dB)	Uncorr. (dB)	Corr. (dB)	Noise	Uncorr.	Corr.
0.000	3.125	2.226	10.298	10.653	0.801	0.710	0.828
3.223	6.348	-6.510	12.027	11.510	0.507	0.609	0.632
6.445	9.570	-8.106	15.548	15.622	0.437	0.644	0.676
9.668	12.793	-7.675	15.219	15.043	0.639	0.603	0.610
12.891	16.016	-6.940	12.395	11.849	0.663	0.664	0.647
16.113	19.238	-9.043	3.182	4.306	0.608	0.515	0.540
19.336	22.461	-11.800	1.376	0.125	1.068	0.743	0.737
22.559	25.684	-10.080	-0.506	0.824	0.629	0.494	0.451
25.781	28.906	-0.021	4.136	-0.668	1.070	0.851	0.473
29.004	32.129	-16.345	-0.536	-0.999	0.596	0.561	0.661
0.000	32.910	-6.032	9.198	8.913	1.209	0.996	1.039
32.227	35.059	-19.120	-2.663	-3.261	0.524	0.606	0.637
35.156	37.988	-22.105	-6.853	-6.834	0.662	0.535	0.561
38.086	40.918	-20.931	-10.854	-12.487	0.546	0.455	0.435
41.016	43.848	-22.109	-14.160	-15.296	0.404	0.487	0.489
43.945	46.777	-19.275	-15.926	-18.633	0.582	0.456	0.462
46.875	49.707	-19.784	-16.715	-22.285	1.314	0.984	0.568
33.008	50.00	-20.442	-10.555	-11.789	0.777	0.854	0.950
0.000	50.000	-8.840	6.025	5.694	1.460	1.318	1.373

Similar results are obtained for Channel 1 of the recorded motion. Figure 10.15 gives recorded accelerogram of Channel 1 (vertical motion). Figure 10.16 and Fig. 10.17 show the Fourier magnitude plot of pre-event and the event part respectively. From Fig 10.16 (for the pre-event) it can be seen that noise has peaks around 27 Hz and 47 Hz as in the case of horizontal motion. This noise is also reflected in the Fourier magnitude plot of the event in Fig. 10.17. The recorded data is analysed by the developed scheme described earlier with a filter length of 16. The corresponding filter co-efficients are

given in Table 10.3 at the trigger, at the 513th sample (mid-point) of the event and at the end of the event.

Table 10.3: Filter Coefficients of Channel 1

Index (i)	h(i) at trigger	g(i) at mid event	g(i) at end of event
1	-0.22407	0.96726	0.97295
2	-0.19393	-0.22226	-0.22714
3	-0.07094	-0.09914	-0.10197
4	0.14804	-0.04371	-0.04566
5	-0.15908	0.18039	0.18561
6	0.01193	-0.24049	-0.23072
7	0.05175	0.13863	0.10906
8	0.15895	-0.04890	-0.01877
9	0.01187	0.24129	0.21401
10	0.04250	-0.26006	-0.21962
11	0.22831	0.29488	0.24704
12	0.07874	-0.12248	-0.08006
13	0.05981	0.26557	0.24211
14	-0.09063	-0.28710	-0.28000
15	0.18301	0.15038	0.15245
16	-0.02389	0.01591	0.01521

Figure 10.18 show the magnitude plot of the adaptive filter at the trigger, at the mid point of the event and at the end of the event. Figure 10.19 shows the accelerogram after the process of adaptive filtering for Channel 1. Figure 10.20 show the Fourier magnitude plot of the event part of the processed accelerogram. A comparison between Figs. 10.17 and 10.20 indicates that coloured noise peaks at around 27 and 47 Hz are removed in the processed record. Table 10.4 gives comparison of uncorrected accelerogram, corrected accelerogram and noise in frequency domain in 16 different frequency segments. Similar results as discussed for channel 3 can be seen in this table also.

10.3 Low pass filter for phase correction

As was discussed earlier, the analog signal from accelerometer of digital accelerograph passes through an anti-aliasing filter which ensures that frequencies more than the Nyquist frequency do not exist in the analog signal which is fed to ADC. Most of

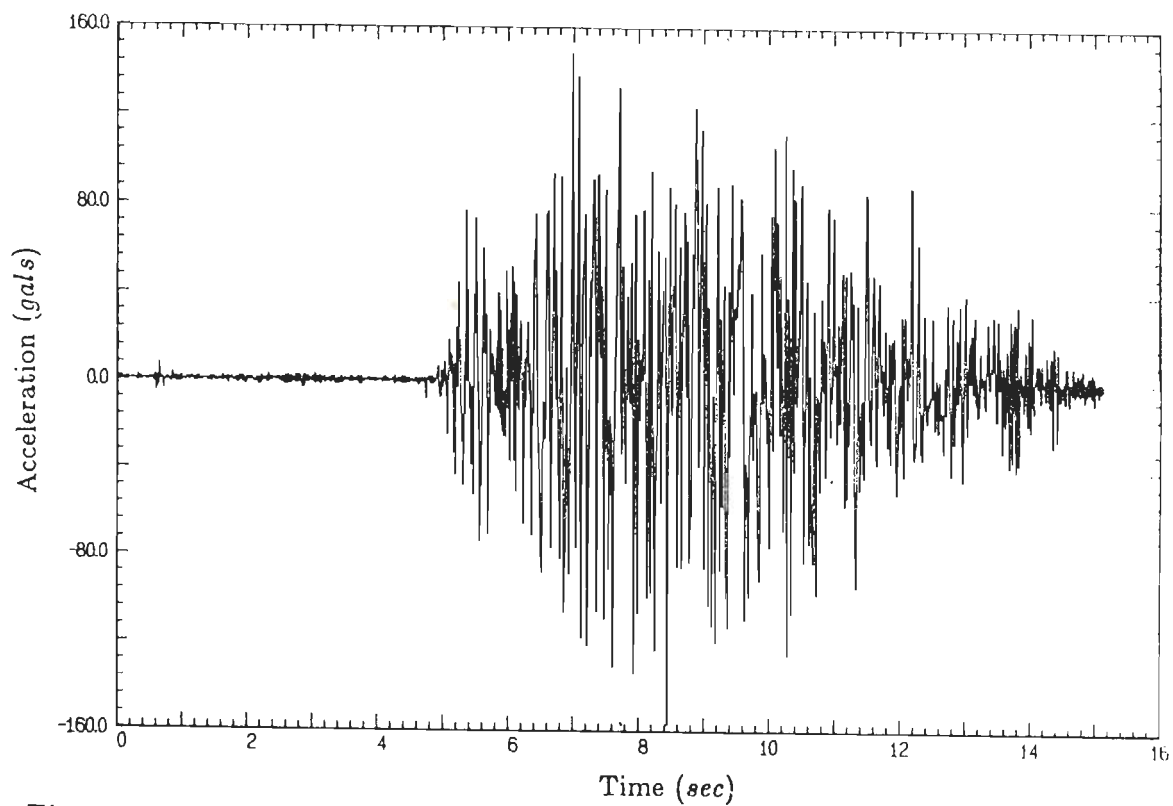


Figure 10.15: Recorded accelerogram (uncorrected) of vertical motion of the shake table (channel 1).

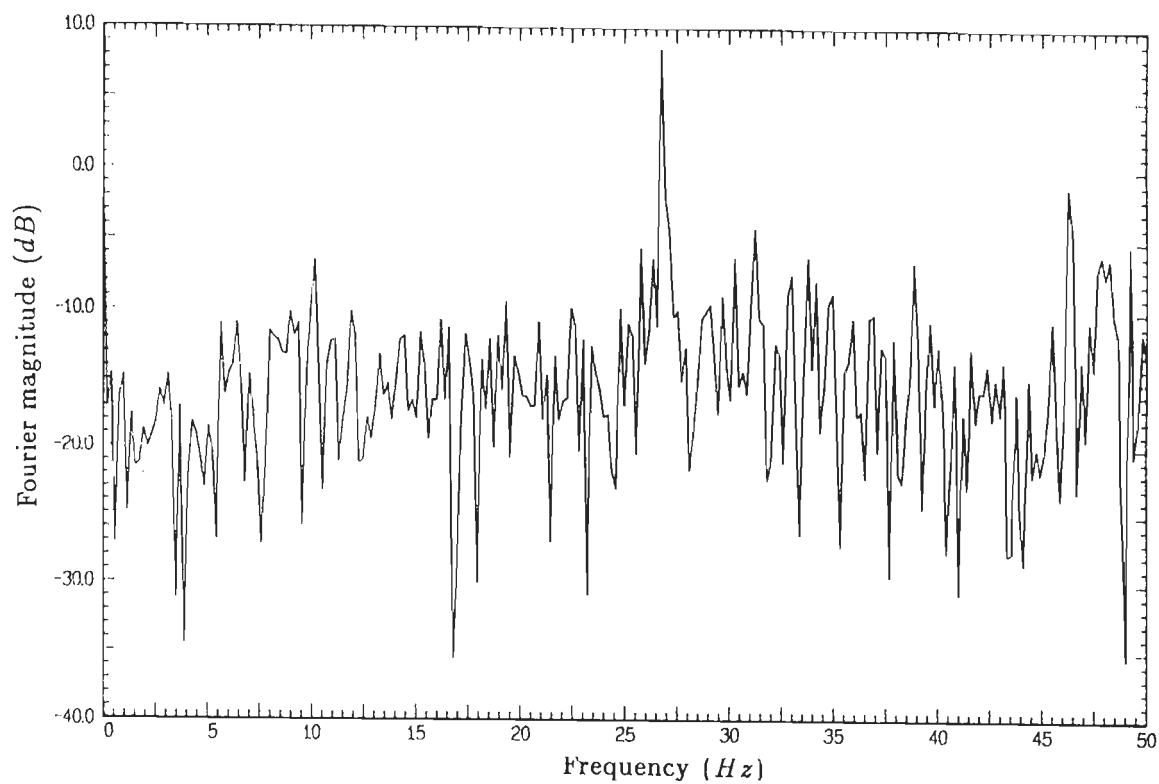


Figure 10.16: Fourier magnitude of pre-event of uncorrected accelerogram of channel 1.

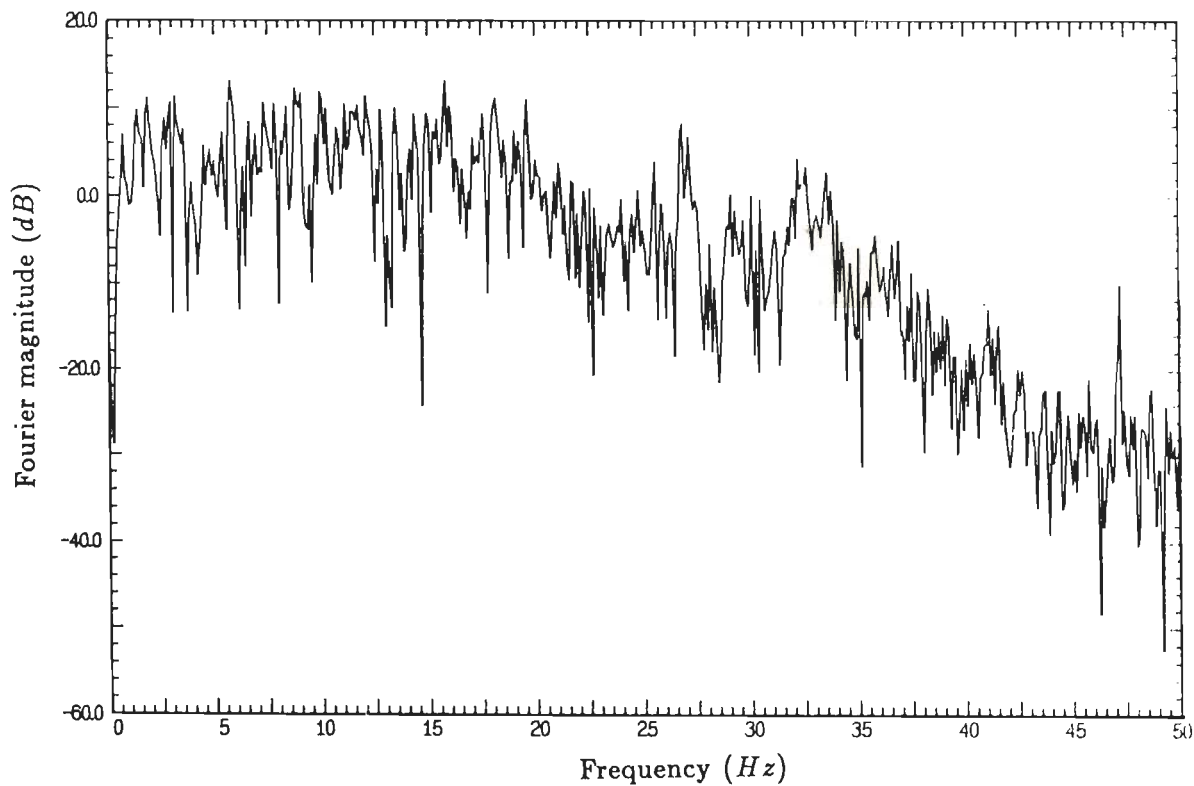


Figure 10.17: Fourier magnitude of event part of uncorrected accelerogram of channel 1.

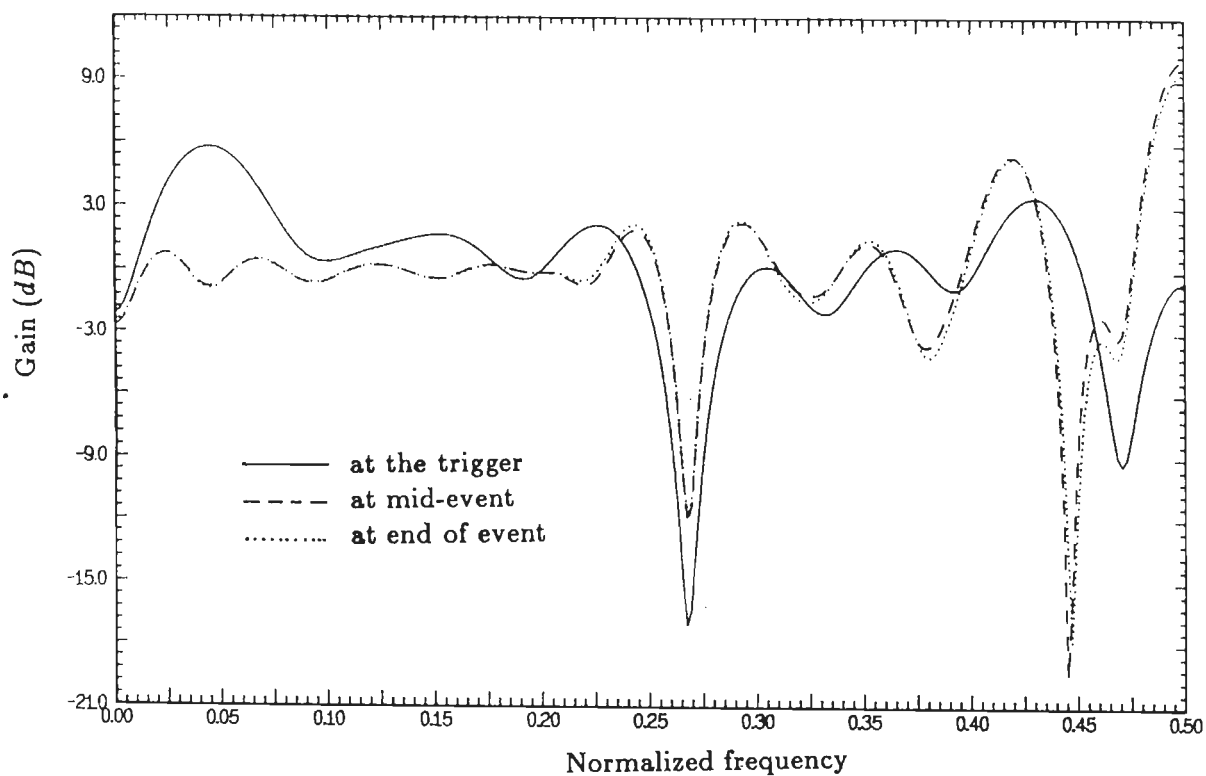


Figure 10.18: Magnitude of transfer function of adaptive filter of channel 1 at the trigger, at mid-event and at the end of event.

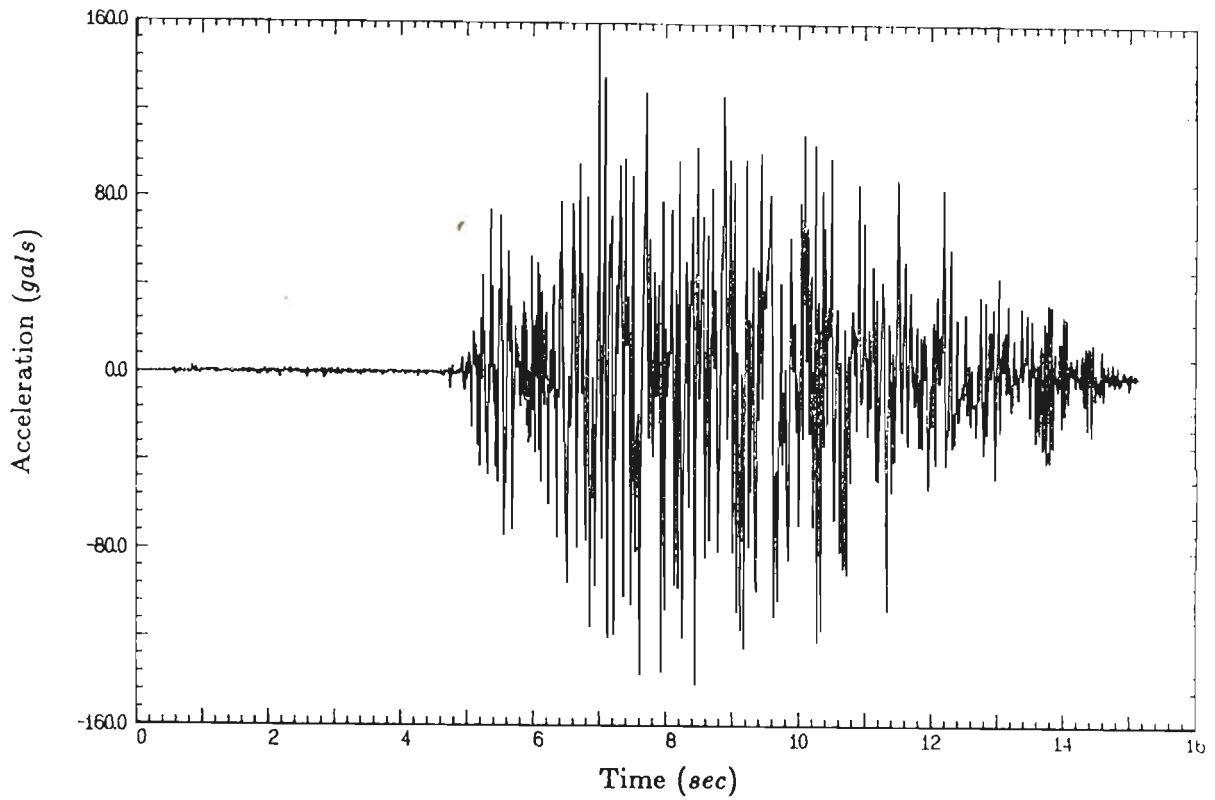


Figure 10.19: Accelerogram obtained after noise cancellation through adaptive filter for channel 1.

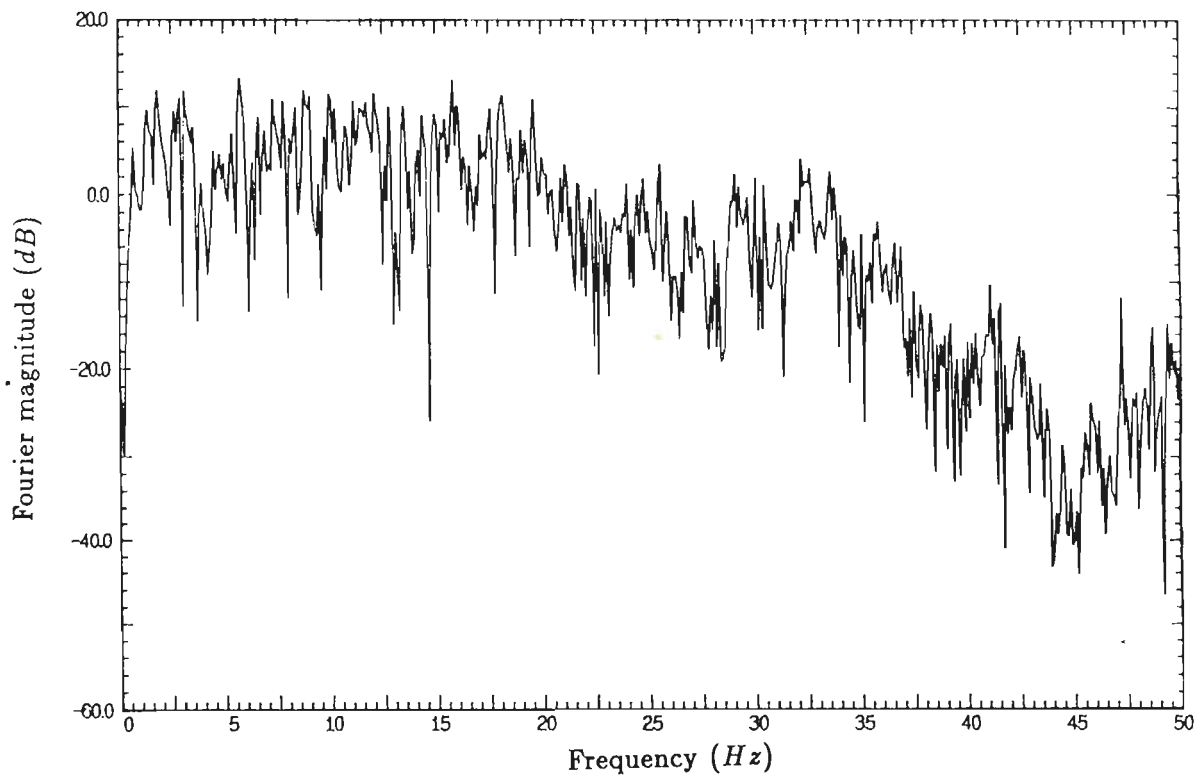


Figure 10.20: Fourier magnitude of event part of accelerogram obtained after noise cancellation through adaptive filter for channel 1.

Table 10.4: Comparison of Correction in Frequency Domain for Channel 1

Frequency Segment		Mean			Coefficient of Variation		
Begin (Hz)	End (Hz)	Noise (dB)	Uncorr. (dB)	Corr. (dB)	Noise	Uncorr.	Corr.
0.000	3.125	-12.140	4.193	4.255	0.666	0.671	0.712
3.223	6.348	-18.853	3.722	3.519	0.733	0.646	0.674
6.445	9.570	-21.612	5.431	5.316	0.635	0.576	0.572
9.668	12.793	-21.948	6.689	6.693	0.544	0.426	0.428
12.891	16.016	-23.337	4.826	4.631	0.548	0.618	0.618
16.113	19.238	-23.017	4.488	4.571	0.554	0.485	0.488
19.336	22.461	-22.567	0.313	0.039	0.526	0.636	0.653
22.559	25.684	-15.909	-4.343	-3.554	1.085	0.514	0.475
25.781	28.906	-6.849	-3.197	-7.925	1.043	0.916	0.580
29.004	32.129	-17.787	-5.660	-4.388	0.843	0.523	0.527
0.000	32.910	-16.719	2.541	2.374	1.415	0.735	0.751
32.227	35.059	-22.816	-2.953	-3.147	0.513	0.582	0.566
35.156	37.988	-25.265	-10.858	-10.683	0.492	0.527	0.576
38.086	40.918	-28.035	-18.797	-19.688	0.498	0.535	0.498
41.016	43.848	-26.574	-22.487	-20.500	0.442	0.691	0.754
43.945	46.777	-30.490	-28.557	-32.311	0.513	0.549	0.622
46.875	49.707	-24.913	-26.180	-22.865	0.896	1.141	0.782
33.008	50.00	-26.016	-15.429	-15.217	0.670	1.327	1.272
0.000	50.000	-18.924	-0.532	-0.676	1.543	1.044	1.054

these anti-aliasing filters are designed by using standard filter approximations of some commonly used IIR filter function. For example, the digital accelerograph described in Chapter 9 uses Butterworth function for filter approximation. In all such filters, the signal undergoes a nonlinear phase shift. Here a method is proposed through which the nonlinear phase shift occurred at the anti-aliasing stage can be neutralized. The method works on the assumption that the analytical function on which the anti-aliasing filter is based is known.

The output of anti-aliasing filter of the digital accelerograph of Chapter 9 has already undergone transformation corresponding to the four pole transfer function $H(s)$ of Butterworth filter which introduces nonlinear phase shift. This can be removed by performing $H(-s)$ operation on the signal at this stage. For a four pole Butterworth filter the transfer function is

$$H(s) = \prod_{k=1}^2 \frac{1}{(s^2 + b_k s + 1)} \quad (10.73)$$

where

$$\begin{aligned} b_1 &= 0.7653668 \\ b_2 &= 1.84775907 \end{aligned}$$

By replacing s of Eq. 10.73 by $-j\omega$ gives

$$H(-j\omega) = \prod_{k=1}^2 \frac{1}{(1 - \omega^2) - j b_k \omega} \quad (10.74)$$

This function is determined at each bin frequency and the filtering operation in the frequency domain is performed to get the corrected accelerogram.

The record obtained after noise cancellation through adaptive filter is thus low pass filtered with a cut off frequency of 33 Hz using Eq. 10.74. The instrument correction on this data was not performed as the natural frequency of the transducer was quite high (100 Hz) with a damping of 70% of critical. Figure 10.21 gives corrected accelerogram of Channel 3 whose Fourier magnitude applied with running mean window (weights: 0.25,0.50,0.25) is shown in Fig. 10.22. Figure 10.23 gives velocity history of the horizontal motion and Fig. 10.24 gives its displacement history. Similarly for Channel 1 (vertical motion), Fig. 10.25 gives corrected acceleration history, Fig. 10.26 gives Fourier magnitude applied with running mean window of corrected acceleration history, Fig. 10.27 gives velocity history and Fig. 10.28 gives displacement history of the vertical motion. The plots of velocity and displacement for both channels give almost zero values at the end of motion which is correct as the signal given to shake table had zero displacement at the end of the motion in horizontal as well as in vertical directions.

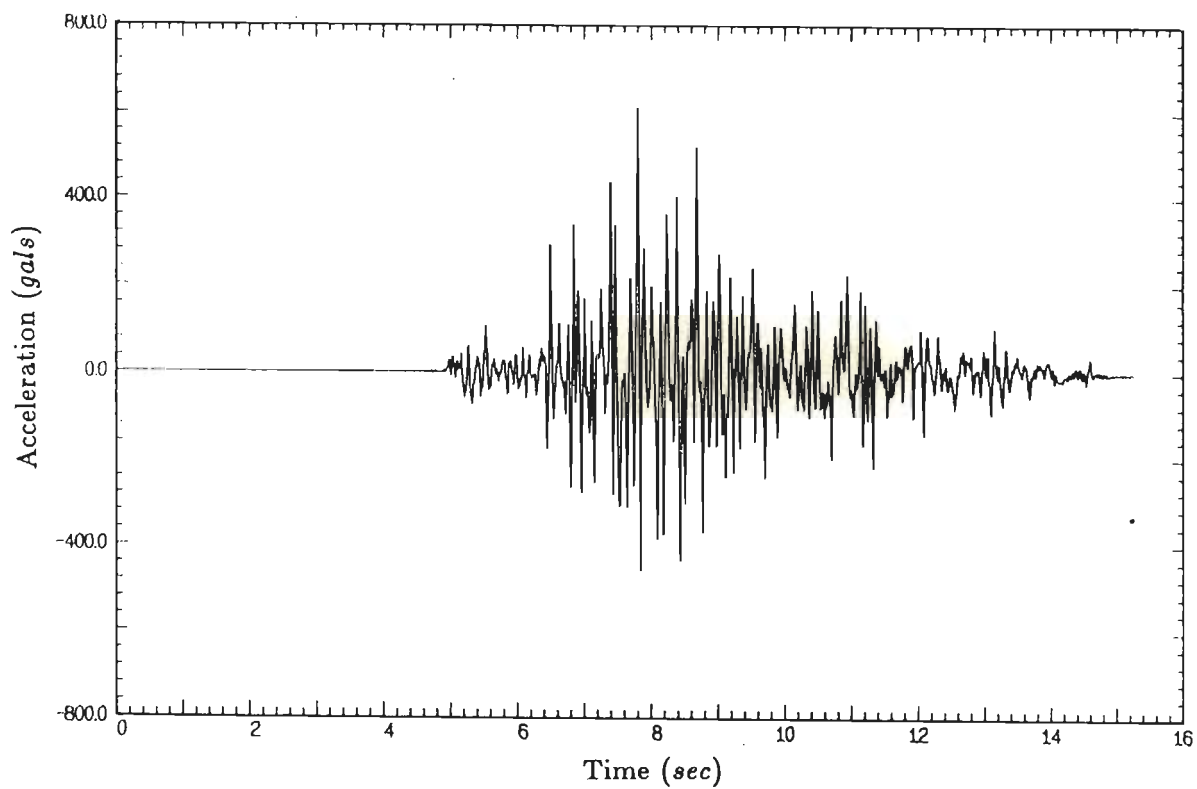


Figure 10.21: Corrected accelerogram of Channel 3.

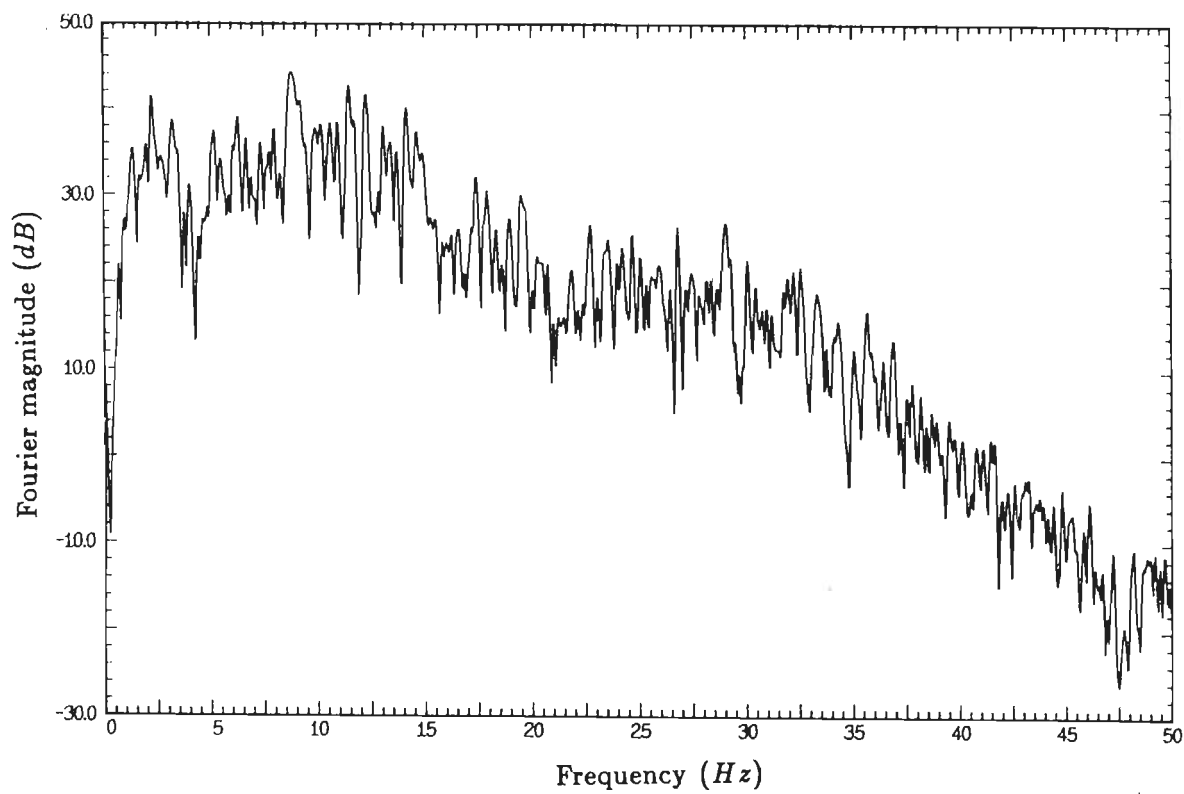


Figure 10.22: Fourier magnitude of corrected accelerogram of Channel 3.

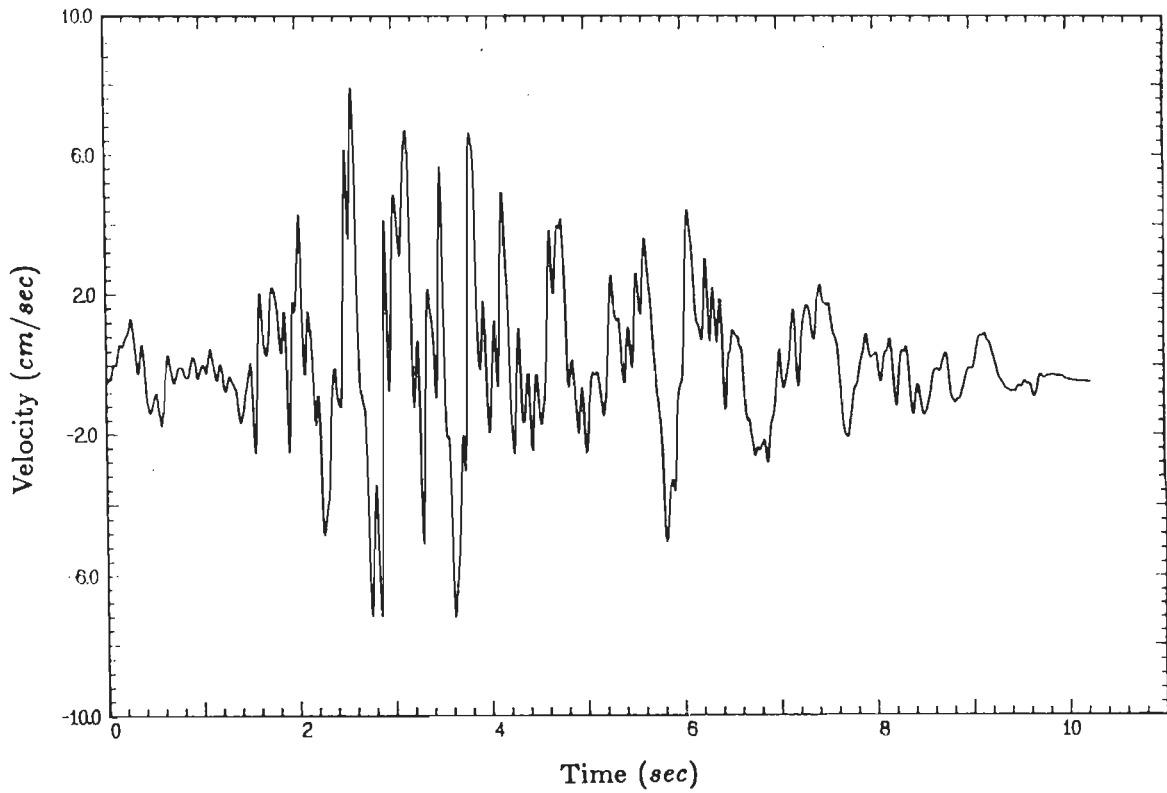


Figure 10.23: Velocity history obtained from corrected accelerogram of channel 3.

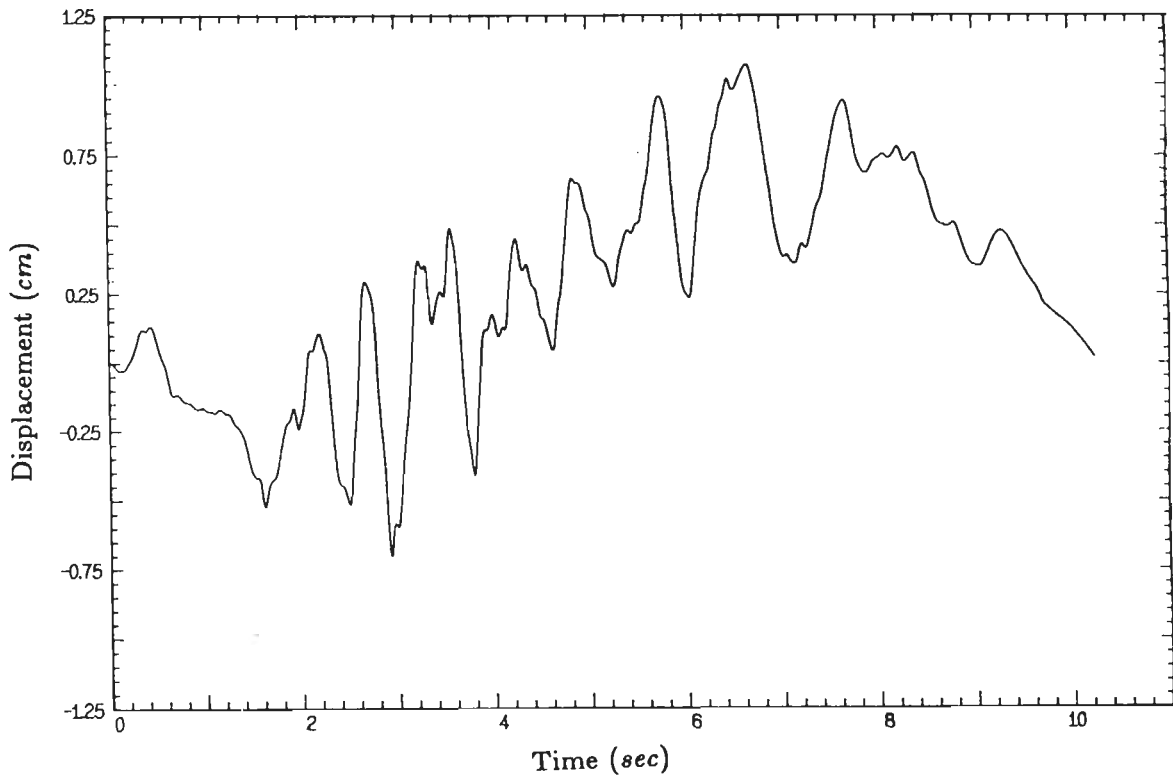


Figure 10.24: Displacement history obtained from corrected accelerogram of channel 3.

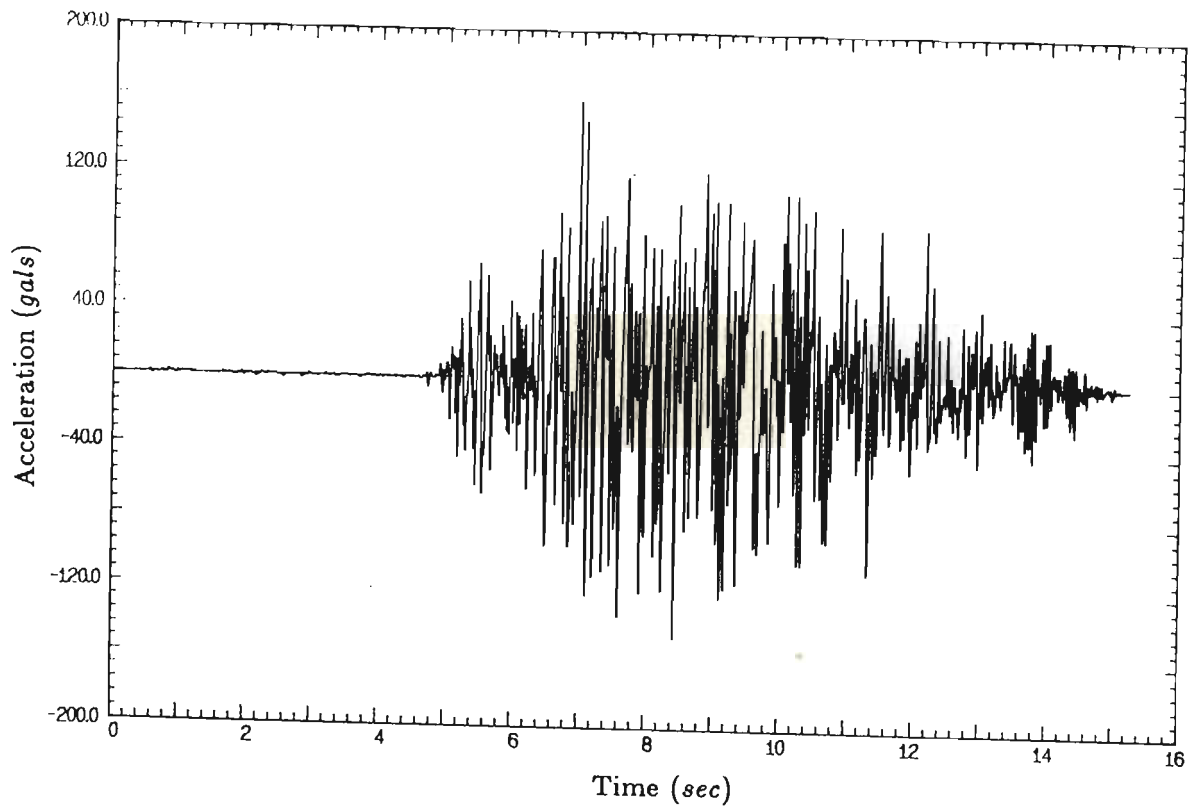


Figure 10.25: Corrected accelerogram of Channel 1.

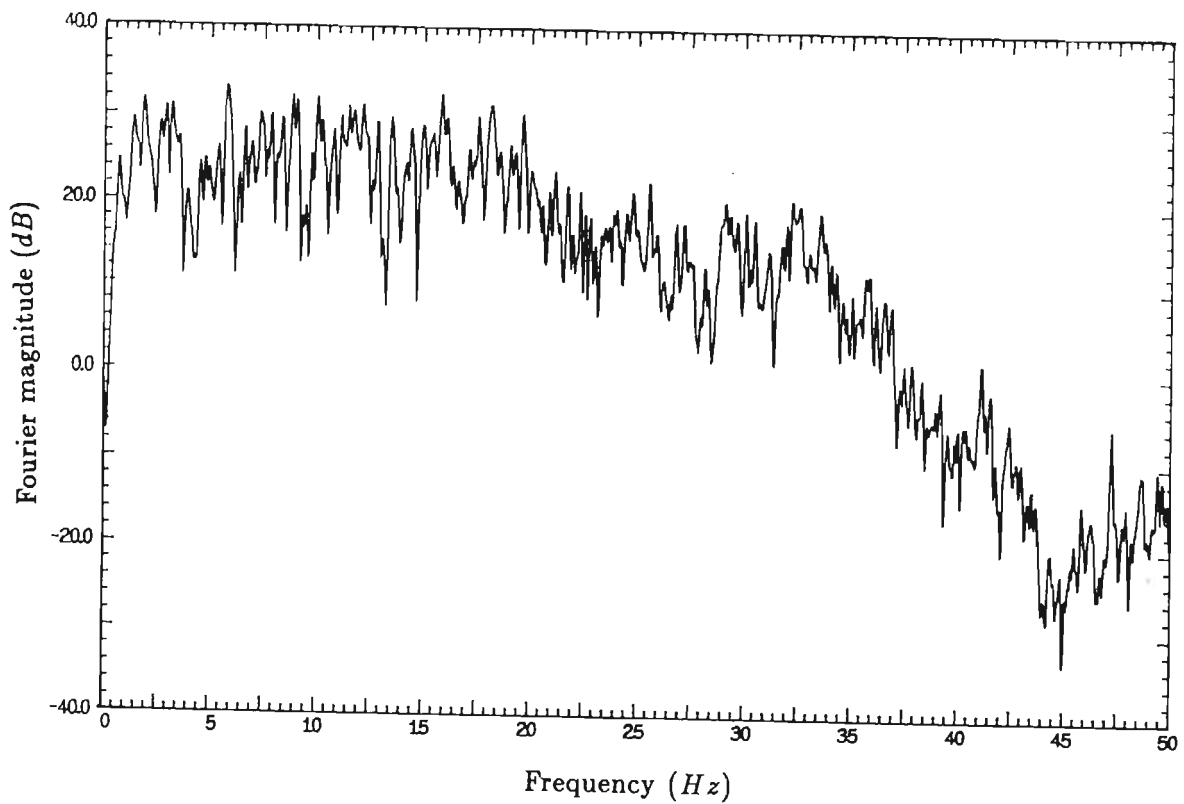


Figure 10.26: Fourier magnitude of corrected accelerogram of Channel 1.

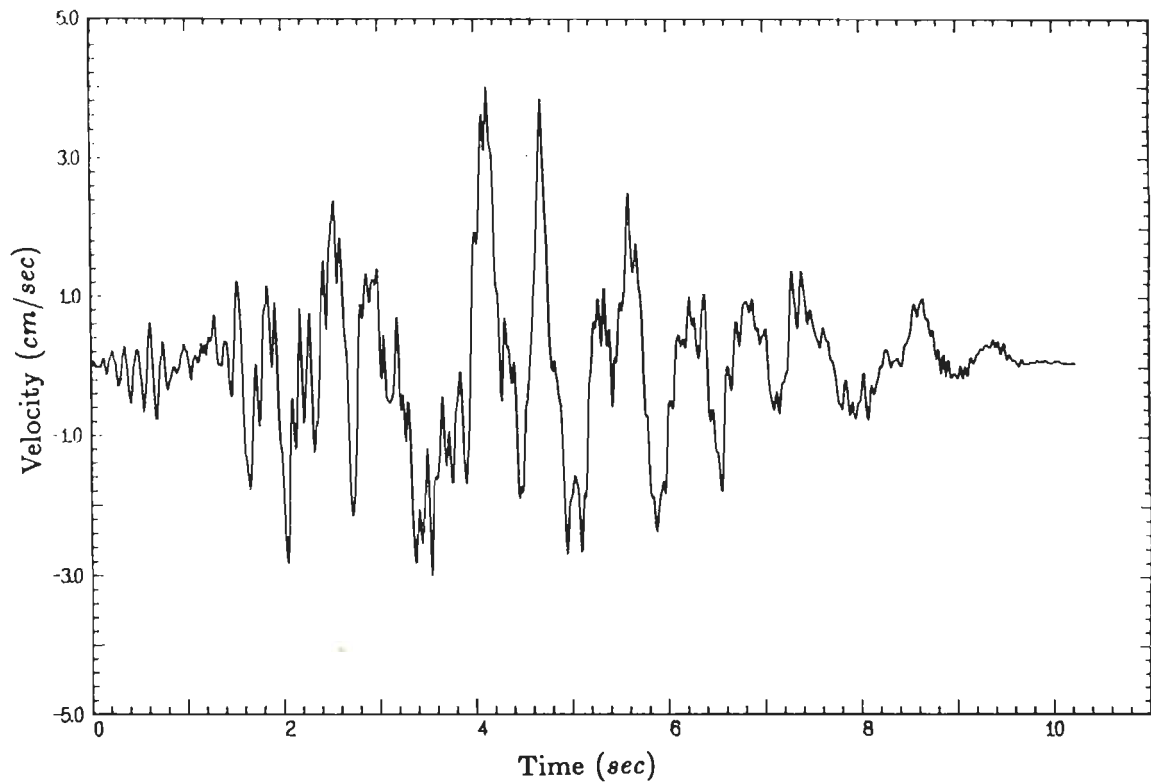


Figure 10.27: Velocity history obtained from corrected accelerogram of channel 1.

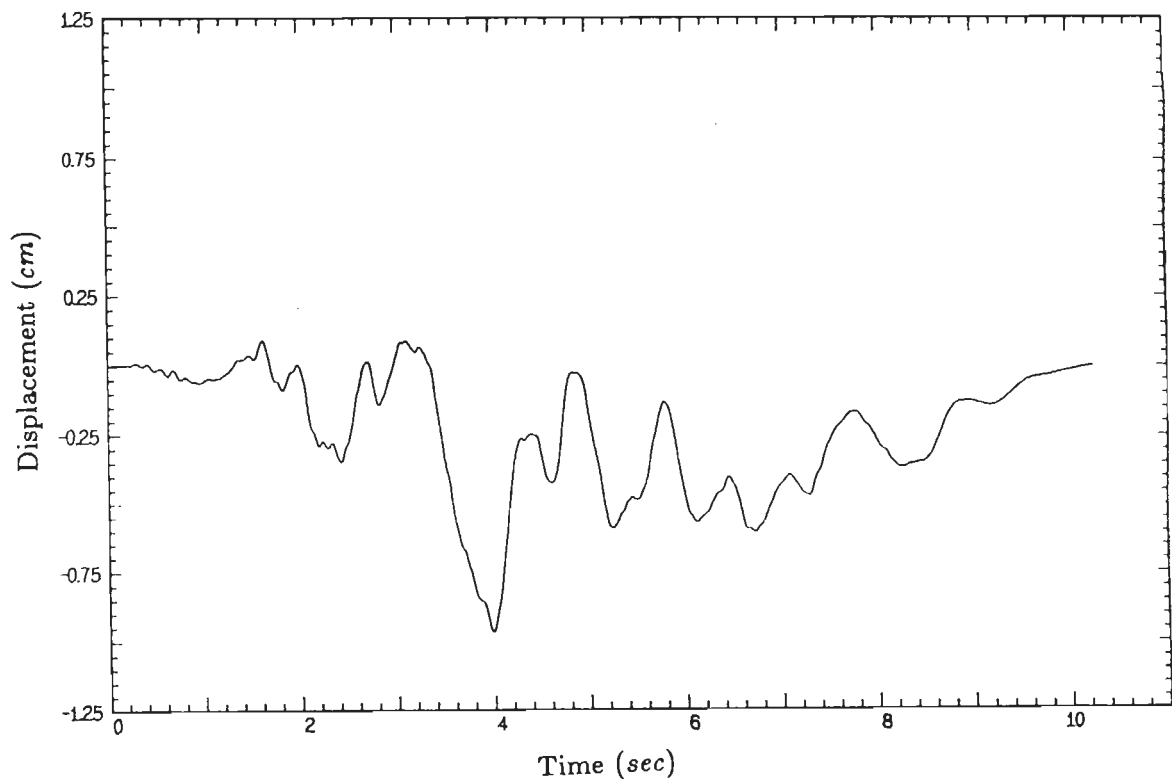


Figure 10.28: Displacement history obtained from corrected accelerogram of channel 1.

Chapter 11

Conclusions

This research work can be broadly divided in two parts. (a) A scheme for correcting records of analog accelerographs in which there is complete control on the frequency contents of the uncorrected accelerogram available at either nonuniform or uniform intervals and (b) a correction scheme for data obtained from digital accelerographs which uses pre-event portion of the record to simulate the noise contents in the record and perform noise cancellation through adaptive filtering technique. In the course of achieving the above objectives several useful results were obtained as described below:

1. Nonuniform samples of uncorrected accelerograms obtained from the records of analog accelerographs are till now linearly interpolated to perform further processing. In this work limitations of linear interpolation of such nonuniform sequences are highlighted. It is shown that linear interpolation introduce high frequency noise at the cost of reducing energy from the required pass band. It is brought out that the digital data cannot provide information about frequencies which are more than half of the average sampling rate of the initially digitized data. Any process which ignores this basic theory of digital signal processing will definitely distort the frequency content of original data due to effect of aliasing. Unfortunately, in the field of processing of strong motion data this aspect was being overlooked perhaps because methods to recover band limited data from nonuniform samples were not known. Some of the authors in their discussions about the processing schemes did mention this drawback but no serious efforts in this direction was reported. Based on the work of Marvasti et al. [60], an algorithm is developed here which recovers band limited data at 200 *SPS* from nonuniform samples of records of analog accelerographs obtained from semi automatic digitizers. A comprehensive comparison is made of exact solutions with several combinations of sine waves

defined at nonuniform samples and interpolated through proposed band limited method as well as linear interpolation. The results clearly establish superiority of the proposed interpolation scheme over the linear interpolation. It is shown that due to prevalent practice of linear interpolation, most of the past earthquake accelerograms have less number of digitized samples required to obtain information upto 25 Hz. It is recommended that such accelerograms should be processed and if possible digitized again keeping this aspect into consideration.

2. In the work reported herein it is shown that linear interpolation commonly employed to increase the sampling rate of uniformly spaced sequence (generally corrected accelerograms) introduces high frequency noise. It is suggested that for increasing the sampling rate, the sequence should be first zero packed with the required number of zeros between the two samples. These should then be low pass filtered with cut off frequency equal to Nyquist frequency of the original sequence and with gain of the filter increased in proportion to the sampling rate. With this, the frequency contents of the original sequence are preserved and a desired sampling rate is obtained. It is also shown that if linear interpolation of a sequence is done then the resulting response obtained for a single degree of freedom system will not be correct.
3. Based on the work done on interpolation of nonuniform and uniform sequences, a new correction scheme for processing accelerograms recorded from analog accelerographs is proposed. This correction scheme first performs band limited interpolation if required, then band limited decimation to get the sequence at 100 SPS. As in the case of band limited interpolation, the process of band limited decimation preserves the frequency contents of the sequence upto the new Nyquist frequency. The instrument correction in the proposed scheme is done in frequency domain and it is shown that this leads to exact deconvolution of the signal in the entire band upto the Nyquist frequency. Band pass filtering is finally done using Butterworth function to get corrected accelerogram. The process of the proposed band pass filtering does not introduce any phase shift of the frequency contents of the signal during the convolution in the frequency domain, as the filter function multiplies real and imaginary parts of the Fourier transform of the signal with a real value only. The proposed scheme also performs integration of corrected accelerogram in frequency domain using zero initial condition to get sequence of velocity and then displacement. It is argued that the velocity and displacement sequences derived from records of analog accelerograph give values which may not be realistic for two reasons. First, the process of integration is predominantly affected by the

low frequency contents of the sequence and in the very low frequency range, noise contents in the unprocessed data is more than or is comparable to signal. This necessitates filtering of low frequencies from the acceleration sequence, whose effect would have been significant on the velocity and displacement sequences. The second reason is that the zero initial conditions which are assumed for the integration are not true since the instrument triggers after the earthquake starts.

4. In this work it is shown that a correction scheme or its parts can be truly evaluated convincingly by using white noise input. The present practice of comparing performance of schemes by maximum values of history and the time of its occurrence is not sufficient as it provides no information about the manner in which the scheme changes the frequency contents of the signal. This is important since in any use of strong motion data it is the frequency contents of the data which play greater role than just the values of the peak acceleration and its instant.
5. The proposed scheme has also been compared with those of Trifunac & Lee, Erdik & Kubin and Khemici & Chiang. The performance of instrument correction and band pass filters of these schemes are evaluated with white noise input. It is shown that instrument correction done in time domain (in which the differentiation of equation of motion of the accelerometer is done through second order central difference approximation) gives inaccurate results at high frequency in addition to the fact that the response is jittery. In contrast, the instrument correction in frequency domain gives exact and smooth response for white noise input. It can, thus, be concluded that instrument correction in frequency domain certainly yields more accurate results than time domain instrument correction. Similarly, a comparison of frequency response of low pass filters of different schemes for white noise input show that filters performs more or less same but Ormsby filter shows some jitters in the pass band because it works in time domain, also, the type of the filter used does not have any appreciable affect on the process although frequency domain convolution yields smoother frequency response.

A comparison is also made of the overall frequency response of all the four schemes with white noise input. For the purpose of comparison it is assumed that the user of the data requires the sequence at 200 *SPS* and therefore in the proposed scheme, band limited interpolation of the corrected accelerogram as discussed in Chapter 5 is done whereas in other schemes linear interpolation is done. Fourier transformation of the corrected sequence of all the four schemes amply highlights the superiority of the proposed scheme in comparison to other schemes. It is shown that linear interpolation introduces noise in high frequency at the cost of

reducing energy from the pass band. This problem becomes even more serious for large increase in the sampling rate as is evident from the results of Trifunac's scheme.

A close look at the scheme of Erdik and Kubin has shown that this scheme performs high pass filter of the velocity sequence rather than of acceleration sequence as is commonly done. The philosophy of doing this is perhaps to get more accurate velocity and displacement sequences. However, in this process the performance of this scheme in regard to getting corrected acceleration sequence becomes poor and it is shown that the frequency magnitude plot of its response to white noise is around 0.82 whereas it should be around unity.

A comparison is made of response spectra of the corrected acceleration sequence of the proposed scheme with that of Trifunac's scheme for four different earthquakes. It is shown that two spectra for different earthquakes differs considerably. The difference is appreciable in frequencies more than half of average sampling rate where Trifunac's scheme overestimates the response due to linear interpolation. Response spectra at other frequencies for some of these earthquakes also gets distorted in Trifunac's scheme. These results further highlight that undesirable changes in the frequency contents which creeps in while processing of strong motion data cannot be ignored and the processing scheme should be such that there is complete control on the frequency contents. The proposed scheme satisfies these requirements quite well.

6. It is brought out that an ideal accelerograph can only be of digital type as features like pre-event memory, automatic digitization, larger dynamic range, higher signal to noise ratio cannot be incorporated in an analog accelerograph. Several other advantages of digital accelerograph are also presented. It is concluded that if properly designed, a digital accelerograph can also be used to record microearthquakes also.
7. It is shown in this work that pre-event portion of the record of a digital accelerograph can be effectively used to understand and analyse the noise contents of the record. It is concluded that the noise contents of digital accelerograph can be modelled as coloured noise and adaptive filter can be designed to cancel this noise. The adaptive filters are quite commonly used in echo cancelling, electrocardiogram etc. and it is shown here that it can be also be used in processing the records of digital accelerograph, although, it requires entirely different algorithm which is presented in this work. Future incorporation of such filter as part of hardware and software feature in the digital accelerograph can enable online processing of

the recorded data. This is perhaps the only way by which a digital accelerograph can be used to record microearthquakes where background noise may be of the same level as that of signal. In this work, a detailed study of the algorithm which should be used to design such filters are discussed. Some records obtained on a digital accelerograph through shake table tests were analysed and usefulness of the proposed scheme is established.

8. In addition to the above, the proposed scheme for processing the records of digital accelerograph features performing $H(-j\omega)$ operation on the digital data to neutralize the nonlinear phase shift of the signal which takes place at the anti-aliasing filter and perform instrument correction if required.
9. There is a great need to have further studies on feasibility of incorporating adaptive filters for online processing. The future work in this direction will involve development of suitable hardware and software for this purpose.

BIBLIOGRAPHY

1. Akaike, H. (1970) —On a Semi Automatic Power Spectrum Estimation Procedure. *Proceedings Third Hawaii International Conference on System Science, Part 2*, pp974–977.
2. Akaike, H. (1974) —A New Look at Statistical Model Identification. *IEEE Transaction on Automatic Control*, Vol. AC-19, December, pp716–723.
3. Alessandrini, B., Rovelli, A., Cocoo, M. and Mazza, S. (1990) —Computation of Ground Displacements from Strong Motion Accelerograms Using the Exact Deconvolution Technique. *Bulletin of Seismological Society of America*, Vol. 80, Part A, No. 6, pp.1753–1761.
4. Amini, A. and Trifunac, M.D. (1983) —Analysis of Feed Back Transducer. *Report of University of Southern California, Report no. 83-03*.
5. Amini, A. and Trifunac, M.D. (1985) —Analysis of Force Balance Accelerometer. *Soil Dynamics and Earthquake Engineering*, Vol.4, No.2, pp.82–90.
6. Basili, M. and Brady, A.G. (1978) —Low Frequency Filtering and the Selection of Limits for Accelerogram Correction. *Proceedings Sixth European Conference on Earthquake Engineering, Ljubljana, Yugoslavia*.
7. Basu, S., Pankaj and Kumar, A. (1992) —On the Importance of Band Limited Excitation in Direct Integration Analysis of Structures. *Proceedings Tenth World Conference on Earthquake Engineering, Madrid, Spain, Vol.7*, pp.3779–3785.
8. Bathe, K.J. and Wilson, E.L. (1978) — Numerical Methods in Finite Element Analysis. *Prentice Hall of India Private Limited, New Delhi*.
9. Beaudet, P.R. and Wolfson, S.J. (1970) —Digital Filter for Response Spectra. *Bulletin of Seismological Society of America*, pp.1001–1012.
10. Beck, J.L. and Dowling, M.J. (1988) —Quick Algorithm for Computing either Displacement, Velocity or Acceleration of an Oscillator. *Earthquake Engineering and Structural Dynamics*, Vol.16, Feb. 1988, pp.245–253.
11. Beck, J.L. and Park, H. (1984) —Optimal Algorithm for Calculating the Response of Linear Oscillator to Digitized Ground Acceleration. *Proceedings Eighth World Conference on Earthquake Engineering, San Francisco, USA, Vol. IV*, pp347–354.

12. Bellenger, M.G., Bonnerot, G. and Candreuse, M. (1976) — Digital Filtering by Polyphase Network: Application to Sample Rate Alteration and Filter Banks. *IEEE Transaction on Accoustics, Speech and Signal Processing*, Vol. AASP-24, pp109-114.
13. Berrill, J.B. and Hanks, T.C. (1974) —High Frequency Amplitude Errors in Digitized Strong-motion Accelerograms. *Report of Earthquake Engineering Research Laboratory, California Institute of Technology, Pasadena, Report no. 74-104, Vol. 4, Part Q.*
14. Bhaskar Rao, D.V. and Kung, S. (1984) —Adaptive Notch Filtering for the Retrieval of Sinusoidal Noise. *IEEE Transaction on Accoustics, Speech and Signal Processing*, Vol. AASP-32, pp791-802.
15. Bingham, C., Godfrey, M.D. and Tukey, J.W. (1967) —Modern Technique of Power Spectrum Estimation. *IEEE Transaction on Audio and Electroaccoustics*, Vol. AU-15, No.2, pp56-66.
16. Bolt, B.A. and Hudson, D.E. (1975) —Seismic Instrumentation of Dams. *Journal of the Geotechnical Engineering Divison, ASCE.*
17. Borchardt, D.R. (1984) —On Recent Advances in Strong Motion Data Acquisition Capabilities. *Proceedings Eighth World Conference on Earthquake Engineering, San Francisco, USA, Vol. II, pp63-70.*
18. Brady, A.G. and Mork, P.N. (1984) —Synthetic Accelerogram for Testing Processing Procedure. *Proceedings Eighth World Conference on Earthquake Engineering, San Francisco, USA, Vol. II, pp127-134.*
19. Brady, A.G. (1988) —Processing Digitally Recorded Seismic Strong Motion Accelerations. *Proceedings of the Second Workshop on Processing of Seismic Strong Motion Records, Tokyo, Japan, Vol.2, pp.15-23.*
20. Brune, J.N. (1970) —Tectonic Stress and the Spectra of Seismic Shear Waves from Earthquakes. *Journal of Geophysical Research, Vol. 75, pp.4997-5009.*
21. Burg, J.P. (1967) —Maximum Entropy Spectral Analysis. *Proceedings 37th Meeting of International Society of Exploration Geophysics, Oklahoma City.*
22. Burrus, C.S. and Park, T.W. (1985) —DFT/FFT and Convolution Algorithms. *John Wiley, New York.*

23. Chandra, B. and Kumar, A. (1992) —Development of Strong Motion Instruments in India. *Himalayan Seismicity, Memoir no. 23 of Geological Society of India, edited by G.D. Gupta.*
24. Chandrasekaran, A.R. (1987) —Measurement and Analysis of Strong Earthquake Ground Motion. *Bulletin of the Indian Society of Earthquake Technology, Vol. 24, no. 2, pp77-86.*
25. Chandrasekaran, A.R. and Das, J.D. (1990) —Strong Motion Arrays in India and Characteristics of Recent Recorded Events. *Bulletin of the Indian Society of Earthquake Technology, Vol. 27, no. 1, pp1-66.*
26. Converse, A.M. (1983) —AGRAM: A Series of Computer Programs for Processing Digitized Strong Motion Accelerograms. *USGS Open-File Report, USGS, Menlo Park, USA, Version 1.0, Report no. 83-276.*
27. Converse A.M., Brady, A.G. and Joyner, W.B. (1984) — Improvements in Strong Motion Data Processing Procedure. *Proceedings Eighth World Conference on Earthquake Engineering, San Francisco, Vol 2, pp 143-148.*
28. Diehl, J.G. (1985) —Implications of Accelerographs Features on Processing, Use and Application of Data. *Workshop on Investigation of Strong Motion Processing Procedures, Rome, pp.336-347.*
29. Durbin, J. (1960) —The Fitting of Time Series Models. *Review of International Statistical Institute, Vol. 28, pp233-244.*
30. Eisenberg, A. and McEvelly (1971) —Comparison of Some Widely Used Strong Motion Earthquake Accelerometers. *Bulletin Seismological Society of America, Vol.61, No.2.*
31. Elliot, D.F. (1987) —Handbook of Digital Signal Processing Engineering Applications. *Academic Press.*
32. Erdik, M. and Kubin, J. (1984) —A Procedure for the Accelerogram Processing. *Proceedings Eighth World Conference on Earthquake Engineering, San Francisco, USA, Vol. II, pp.135-139.*
33. Friedlander, B. (1982) —Lattice Method for Spectral Estimation. *Proceedings IEEE, Vol. 70, September, pp990-1017.*
34. Goodwin, G.C. and Sin, K.S. (1984) —Adaptive Filtering Prediction and Control. *Prentice Hall, Inc., Englewood Cliffs, N.J..*

35. Gray, A.H. and Markel, J.D. (1976) —A Computer Program for Designing Digital Elliptic Filters. *IEEE Transaction Acoustics, Speech and Signal Processing*, December.
36. Hanks, T.C. (1973) —Current Assessment of Long Period Errors, Strong Motion Earthquake Accelerograms— Digitized and Plotted Data. *Report of Earthquake Engineering Research Laboratory, Report no. EERL 73-52* California Institute of Technology, Pasadena, U.S.A.
37. Hanks, T.C. (1975) —Strong Ground Motion of the San Fernando Earthquake: Ground Displacement. *Bulletin Seismological Society of America*, Vol.65, No.1.
38. Householder, A.S. (1964) —The Theory of Matrices and Numerical Analysis. *Blaisdell, Waltham, Mass.*
39. Hudson, D.E. (1963) —The Measurement of Ground Motion of Destructive Earthquakes. *Bulletin Seismological Society of America*, Vol.53, No.2, pp419-437.
40. Hudson, D.E. (1970) —Ground Motion Measurements. *Chapter 6 of Earthquake Engineering ; Coordinating Editor R.L. Wiegel, Prentice Hall, Inc. Englewood Cliffs, N.J.*
41. Hudson, D.E. (1979) —Reading and Interpreting Strong Motion Accelerograms. *Earthquake Engineering Research Institute, Berkeley, C.A.*
42. Hudson, D.E. (1982) —Design of Strong Motion Instruments, Networks and Arrays. *Proceedings of the Seventh European Conference on Earthquake Engineering, Athens, Greece.*
43. Hudson, D.E. (1984) —Strong Motion Accelerograph Systems— Problems and Prospects. *Proc. Eighth World Conference on Earthquake Engineering, San Francisco, USA, Vol. II, pp.39-45.*
44. Hudson, D.E., Nigam, N.C. and Trifunac, M.D. (1969) —Analysis of Strong Motion Accelerograph Records. *Fourth World Conference on Earthquake Engineering, Santiago, Chile.*
45. Iai, S. (1988) —State of the Art: Processing of Analogue Strong Motion Seismic Record. *Proceedings of the Second Workshop on Processing of Seismic Strong Motion Records, Tokyo, Japan, Vol. I, pp.1-9.*

46. Iai, S., Kurata, E., Tsuchida, H. and Hayashi, S. (1980) —Integration of Strong Motion Accelerograms. *Proceedings of the Tenth Joint Panel Conference of the U.S.-Japan Cooperative Programme in Natural Resource, Wind and Seismic Effects*, H.S. Lew Ed., NBS, Special Publication 560, U.S. Department of Commerce/Nation Bureau of Standards, pp7-1 to 7-16.
47. Iai, S., Tsuchida, H., Kurata, E. and Noda, S. (1988) —Processing of Strong Motion Records by Port and Harbor Research Institute, Japan. *Proceedings of the Second Workshop on Processing of Seismic Strong Motion Records, Tokyo, Japan*, Vol.1, pp.51-67.
48. Iwan, W.D., Moser, M.A. and Peng, C.Y. (1985) —Some Observations on Strong Motion Earthquake Measurement Using a Digital Accelerograph. *Bulletin of Seismological Society of America*, Vol.75, No. 5, pp.1225-1246.
49. Katukura, H., Tanaka, T. and Watanabe, T. (1988) —Processing of Strong Motion Accelerograms Considering Causality of Seismic Waves. *Proceedings of the Second Workshop on Processing of Seismic Strong Motion Records, Tokyo, Japan*, Vol.1, pp.68-84.
50. Khemici, O. and Chiang, W.L. (1984) —Frequency Domain Corrections of Earthquake Accelerograms with Experimental Verification. *Proceedings Eighth World Conference on Earthquake Engineering, San Francisco, USA*, Vol. II, pp.103-110.
51. Kumar, A., Basu, S. and Chandra, B. (1992) — Correction of Data Obtained from Digital Accelerographs. *Proceedings Tenth World Conference on Earthquake Engineering, Madrid, Spain*, Vol. 1, pp187-193.
52. Kumar, A., Basu, S. and Chandra, B. (1992) —The Effect of Band Limited Interpolation of Nonuniform Samples on Records of Analog Accelerographs. *Bulletin of the Indian Society of Earthquake Technology*, Vol. 29, no. 4, pp53-67.
53. Kumar, A., Gupta, N.C., Basu, S., Panday, A.D., Bansal, M.K. and Verma, V.K. (1990) —Microprocessor Based Strong Motion Accelerograph. *Proceedings Ninth Symposium on Earthquake Engineering, University of Roorkee, Roorkee*, Vol. 1.
54. Lam H.Y.F. (1979) —Analog and Digital Filters: Design and Realization. *Prentice-Hall, Inc., Englewood, New Jersey 07632*.

55. Lee, V.W. (1984) —Recent Developments in Data Processings of Strong Motion Accelerograms. *Proceedings Eighth World Conference on Earthquake Engineering, San Francisco, USA, Vol. II*, pp.119–126.
56. Lee, V.W. and Trifunac, M.D. (1979) —Automatic Digitization and Processing of Strong Motion Accelerograms. *Report of Department of Civil Engineering, University of Southern California, U.S.A, Report no. 79-15, Vol. I and II*.
57. Levinson, N. (1947) —The Weiner RMS Criterion in Filter Design and Prediction. *Journal Mathematical Physics, Vol. 25, January*, pp261–268.
58. Ljung, L. (1978) —System Identification Theory for the Users. *Prentice Hall Inc., Englewood, Calif., N.J.*
59. Marple, S.L. (1980) —A New Autoregressive Spectrum Analysis Algorithm. *IEEE Transaction on Acoustics, Speech and Signal Processing, Vol. AASP-28, August*, pp441–454.
60. Marvasti, F., Analoui, M. and Gamshadzahi, M. (1991) —Recovery of Signals from Non Uniform Samples using Iterative Methods. *IEEE Transaction on Signal Processing, Vol. 39, No. 4*.
61. McLennan, G.A. (1969) —An Exact Correction for Accelerometer Error in Dynamic Seismic Analysis. *Bulletin of Seismological Society of America, Vol.59, No. 2*.
62. McClellan, J.H., Parks, T.W. and Rabiner, L.R. (1973) —A Computer Program for Designing Optimum FIR Linear Phase Filters. *IEEE Transaction on Audio Electroacoustics, Vol. AU-21, Dec.,* pp.506–526.
63. Mittal, A.V. (1991) —Comparison of Schemes for Correction of Accelerograms Obtained from Analog Accelerographs. *M.E Dissertation of Department of Earthquake Engineering, University of Roorkee, Roorkee*.
64. Newmark, N.M. (1973) —An Exact Correction for Accelerometer in Dynamic Analysis. *Bulletin of the Seismological Society of America, Vol. 59*, pp705–715.
65. Nigam, N.C. and Jennings, P.C. (1968) —Digital Calculation of Response Spectra from Strong Motion Earthquake Records. *Report of Earthquake Engineering Research Laboratory, California Institute of Technology, June, 1968*.

66. Nigam, N.C. and Jennings, P.C. (1969) —Calculation of Response Spectra from Strong Motion Earthquake Records. *Bulletin of the Seismological Society of America*, Vol. 59, No. 2, pp909–922.
67. Oetken, G., Parks, T.W. and Schussler, H.W. (1975) —New Results in the Design of Digital Interpolators. *IEEE Transactions on Acoustics, Speech and Signal Processing*, Vol. ASSP–23, No. 3.
68. Ohta, T. (1988) —Strong Motion Data File No. 5 and Simultaneous Records by Means of Velocity and Displacement Meters. *Proceedings of the Second Workshop on Processing of Seismic Strong Motion Records, Tokyo, Japan*, Vol. I, pp.10–15.
69. Okada, S., Goto, W. and Ohta, Y. (1984) —Experiments onto Renewal of Strong Motion Observation Instruments. *Proceedings Eighth World Conference on Earthquake Engineering, San Francisco, USA*, Vol. II, pp.71–78.
70. Omote, S., Ohta, T., Hiehata, S. and Ikeura, T. (1988) —Data Processing Method for Acceleration Records and its Application Results. *Proceedings of the Second Workshop on Processing of Seismic Strong Motion Records, Tokyo, Japan*, Vol.1, pp.119–135.
71. Oppenheim, A.V. and Schafer, R.W. (1975) —Digital Signal Processing. *Prentice Hall, Inc. Englewood Cliffs, N.J.*.
72. Ormsby, J.F.A. (1961) —Design of Numerical Filters with Application to Missile Data Processing. *Association of Computing Machinery Journal*, Vol. 8.
73. Owen, D.R.J. and Hinton, E.(1980) — Finite Elements in Plasticity: Theory and Practice. *Pineridge Press, Swansea*.
74. Parzen, E. (1974) —Some Recent Advances in Time Series Modelling. *IEEE Transaction on Automatic Control*, Vol. AC–19, December, pp724–730.
75. Pauley, S.E. (1984) —Strong Motion Accelerograph Selection. *Proceedings Eighth World Conference on Earthquake Engineering, San Francisco, USA*, Vol. II, pp.47–54.
76. Rabiner, L.R. and Gold, B. (1988) —Theory and Application of Digital Signal Processing. *Prentice Hall of India Private Ltd., New Delhi*.
77. Rabiner, L.R., McClellan, J.H. and Parks, T.W. (1975) —FIR Digital Filter Design Techniques Using Weighted Chebyshev Approximation. *Proceedings IEEE*, Vol.63, No.4, April.

78. Rojahn, C. and Borchert, D. (1982) —On the Status of In-Situ Strong Ground Motion and Structural Response Investigations. *Proceedings Third International Earthquake Microzonation Conference*, pp329–363.
79. Schuessler, H.W. and Ibler, W. (1974) —Digital Filters for Integration. *European Conference on Circuit Theory and Design, Institution of Electrical Engineers, Conference publication no. 116*.
80. Shakal, A.F. and Ragsdale, J.T. (1984) —Acceleration, Velocity, and Displacement Noise Analysis for the CSMIP Accelerogram Digitizing System. *Proceedings Eighth World Conference on Earthquake Engineering, San Francisco, USA, Vol. II*, pp. 111–118.
81. Shyam Sunder, S. (1980) —On the Standard Processing of Strong Motion Earthquake Signals. *Ph.D Thesis of Department of Civil Engineering, School of Engineering, Massachusetts Institute of Technology, USA*.
82. Shyam Sunder, S. and Connor, J.J. (1982) —A New Standard Processing Scheme for Strong Motion Earthquake Signals. *Bulletin of Seismological Society of America, Vol. 72, No. 2, 1982*, pp.643–661.
83. Singhal, D.K. (1991) —Performance of Digital Accelerograph by Shake Table Testing. *M.E Dissertation of Department of Earthquake Engineering, University of Roorkee, Roorkee*.
84. Stagner, J.R.,(1970) —Applications to the Bi Linear Z-Transform Method to the Ground Motion Studies. *Bulletin of Seismological Society of America*, PP 809–817.
85. Toki, K. and Sawada, S. (1988) —A Method for Correction of Accelerograms. *Proceedings of the Second Workshop on Processing of Seismic Strong Motion Records, Tokyo, Japan, Vol.1*, pp.183–199.
86. Tribolet, J.M. (1977) —A New Phase Unwrapping Algorithm. *IEEE Transactions on Acoustics, Speech and Signal Processing, Vol. 25, No. 2*.
87. Tribolet, J.M. (1979) —Seismic Applications of Homomorphic Signal Processing. *Prentice Hall, Inc. Englewood Cliffs, N.J.*
88. Trifunac, M.D. (1971) —Zero Base Line Correction of Strong Motion Accelerogram. *Bulletin Seismological Society of America, Vol. 61*, pp1201–1211.

89. **Trifunac, M.D. (1972)** —A Note on Correction of Strong Motion Accelerograms for Instrument Response. *Bulletin of Seismological Society of America*, Vol. 62, pp.401–409.
90. **Trifunac, M.D. (1976)** —Preliminary Empirical Model for Scaling Fourier Amplitude Spectra of Strong Ground Motion Acceleration in Terms of Earthquake Magnitude, Source to Station Distance, and Recording Site Conditions. *Bulletin of the Seismological Society of America*, Vol. 65, No. 4, pp1343–1373.
91. **Trifunac, M.D. (1977)** —Uniformly Processed Strong Earthquake Ground Acceleration in the Western United States of America for the Period from 1933–1971: Pseudo Relative Velocity Spectra and Processing Noise. *Report University of Southern California*, Report no. CE 77–04.
92. **Trifunac, M.D. and Hudson, D.E. (1970)** —Laboratory Evaluation and Instrument Corrections of Strong Motion Accelerographs. *Report of EERL, California Institute of Technology*, Report no. EERL70–04.
93. **Trifunac, M.D. and Lee, V.W. (1973)** —Routine Computer Processing of Strong Motion Accelerograms. *Report Earthquake Engineering Research Laboratory*, Report no. EERL 73–03, California Institute of Technology, Pasadena.
94. **Trifunac, M.D. and Lee, V.W. (1974)** —A Note on Accuracy of Computed Ground Displacements from Strong Motion Accelerograms. *Bulletin of Seismological Society of America*, 1974, pp1209–1219.
95. **Trifunac, M.D. and Lee, V.W. (1978)** —Uniformly Processed Strong Earthquake Ground Acceleration in the Western United States of America for the Period from 1933–1977: Corrected Acceleration, Velocity and Displacement Curves. *Report University of Southern California*, Report no. CE 78–01.
96. **Trifunac, M.D., Udawadia, F.E. and Brady, A.G. (1971)** —High Frequency Errors and Instrument Corrections of Strong Motion Accelerograms. *Report of EERL, California Institute of Technology*, Report no. EERL 71-05.
97. **Trifunac, M.D., Udawadia, F.E. and Brady, A.G. (1973)** —Analysis of Errors in Digitized Strong Motion Accelerograms. *Bulletin of Seismological Society of America*, Vol. 63 No. 1.

98. Widrow, B., Glover, J., McCool, J., Kannitz, J., Williams, C., Hearn, R., Zeidler, J., Dong, E. and Goodline, R. (1975) —Adaptive Noise Cancelling: Principles and Applications. *Proceedings IEEE*, Vol. 63, No. 12, pp1692–1716.
99. Widrow, B. and Hoff, M. (1960) —Adaptive Switching Circuits. *IRE Wescon Convention Records, Part 4*, pp96–104.
100. Widrow, B. and Stearns, D. (1985) —Adaptive Signal Processing. *Prentice Hall, Englewood Cliffs, N.J.*
101. Wiegel, R.L. (1970) —Earthquake Engineering. *Prentice Hall, Englewood Cliffs, N.J.*
102. Wiener, N. (1949) —Extrapolation, Interpolation, and Smoothing of Stationery Time Series. *John Wiley, New York*.
103. Wong, H.L. and Trifunac, M.D. (1977) —Effects of Cross Axis Sensitivity and Misalignments of the Response of Mechanical Optical Accelerographs. *Bulletin of Seismological Society of America*, Vol. 67 No. 3.
104. Zienkiewicz, O.C., Wood, W.L., Hines, N.W. and Taylor, R.L. (1984) — A Unified Set of Single Step Algorithms , Part 1: General Formulation and Applications. *International Journal on Numerical Methods in Engineering*, Vol.20, pp1529—1552.
105. —(1970) Strong Motion Earthquake Accelerograms; Vol.I Uncorrected Accelerograms. *Report of Earthquake Engineering Research Laboratory, California Institute of Technology, Report no. EERL 70–20, Vol. I, Part A.*
106. —(1970) Strong Motion Earthquake Accelerograms; Vol.I Uncorrected Accelerograms. *Report of Earthquake Engineering Research Laboratory, California Institute of Technology, Report no. EERL 70-21, Vol. I, Part B.*
107. —(1973) Strong Motion Earthquake Accelerograms; Vol.I Uncorrected Accelerograms. *Report of Earthquake Engineering Research Laboratory, California Institute of Technology, Report no. EERL 73-28, Vol. I, Part W.*
108. —(1978) Strong Motion Earthquake Instrument Array. *Proceedings International Workshop on Strong Motion Earthquake Instrument Arrays, Honolulu.*
109. —(1988) *Proceedings of the Second Workshop on Processing of Seismic Strong Motion Records, Tokyo, Japan, August, 1988.*

110. —(1988) Uniform Building Code. *International Conference of Building Officials, Whittier, USA.*
111. —(1990) Development of Digital Accelerograph. *Report of Department of Earthquake Engineering, University of Roorkee No. EQ. STUDIES 90-02.*